Investigating the regulation of Th17 cell fate and function at mucosal surfaces

by

VERONIKA MATEI-RASCU

A thesis submitted to the University of Birmingham for the Degree of

DOCTOR OF PHYLOSOPHY

Institute of Immunology and Immunotherapy

College of Medical and Dental Sciences

University of Birmingham

May, 2022

ABSTRACT

T helper 17 cells, characterised by interleukin-17 production, are crucial to appropriate mucosal immunity but, when dysregulated, are known causative agents of a multitude of inflammatory disorders. Thus, Th17 cell regulation is highly relevant to human health. However, the design and development of therapies targeted at the modulation of Th17 cell responses is impeded by gaps in the available understanding of the control of Th17 cell function and fates and a paucity of experimental systems appropriate for the comprehensive study of mucosal immune responses. Here, I took multiple interconnected approaches to begin to address some of the outstanding questions regarding mucosal Th17 cell regulation including the extent to which CD4 T cell subsets of the mucosal compartment transdifferentiate into one another, the role of costimulation and transcriptional networks in the control of these processes, and the effects of Th17 cell plasticity on memory formation. Throughout this thesis I have shown that Th17 cells do not maintain their characteristic cytokine profile but instead readily transdifferentiate into both suppressive Treg and proinflammatory Th1-like cells. By assessing the transcriptional regulation of Th17 cell function using animal models I show that three key lineage-defining transcription factor networks are integrated to control Th1-like exTh17 cell differentiation. Through characterisation of these models I show that Th17 cell effector functions, as well as development, are supported by the transcription factors RORγt and RORα. Conversely, T-bet expression within Th17 cells was found to be indispensable for complete loss of Th17 cell-associated functions but, strikingly, not for the acquisition of Th1 cell characteristics. Furthermore, I show that these novel models enable segmentation of exTh17 cell differentiation into better-defined stages, thus aiding detailed studies of this process. Moreover, I present initial characterisation of an exciting new experimental model that enables the identification and long-term tracking of CD4 T cells responding to mucosal infections, including memory T cells. Collectively these data reveal new insight into transcriptional control of Th17 cell differentiation and establish a robust experimental platform for investigating Th17 cell fate and memory formation.

ACKNOWLEDGEMENTS

First and foremost, I would like to thank Prof David Withers for being a wonderful PhD supervisor. Dave not only provided guidance and scientific input but also created a fun and supportive lab environment. I have really enjoyed the past 4 years working in this group.

Thank you to all the Withers lab members for always being ready to help and provide advice. Special thanks to Claire Willis and Isaac Dean for keeping me going and creating so many great memories during long hours in the lab. I would also like to thank the whole of 4th floor IBR for creating a great environment and making my PhD a really enjoyable experience.

Finally, I would like to thank my family and friends, especially my wonderful husband Mihai, for supporting me throughout this whole experience. It wouldn't have been possible without you.

TABLE OF CONTENTS

LIST OF FIGURES

LIST OF TABLES

LIST OF ABBREVIATIONS

$^{-/-}$	knockout
($^{v}/_{v}$)	volume per volume
($^{w}/_{v}$)	weight per volume
2LT	secondary lymphoid tissue
µg	microgram
AhR	aryl hydrocarbon receptor
aLN	axillary lymph nodes
AMP	antimicrobial peptide
APC	antigen presenting cell
Bcl6	B cell lymphoma 6
BCR	B cell receptor
bLN	brachial lymph nodes
BMSU	University of Birmingham Biomedical Services Unit
CaLP	caecum lamina propria
CFU	colony forming units
CI	confidence interval
CLP	colon lamina propria
CP	caecal patch
CRS	cryptdin-related sequence
CTLA-4	cytotoxic lymphocyte-associated antigen-4
D	day
DAMP	danger-associated molecular pattern
DC	dendritic cell
DKO	OX40/CD30 double knockout
DPBS	Dulbecco's phosphate buffered saline
dsRNA	double-stranded ribonucleic acid
EAE	experimental autoimmune encephalomyelitis
EDTA	ethylenediaminetetraacetic acid
Eomes	eomesodermin

eYFP	enhanced yellow fluorescent protein
FBS	foetal bovine serum
^{fl}, floxed	LoxP-flanked
FoxP3	Forkhead box protein P3
g	gram
G-CSF	granulocyte colony stimulating factor
HBSS	Hanks' balanced salt solution
hNGFR	human nerve growth factor receptor
hr	hours
Id2	Inhibitor of DNA binding 2
IEC	intestinal epithelial cell
IEL	intraepithelial lymphocyte
IESC	intestinal epithelial stem cell
IFNγ	interferon-gamma
Ig	immunoglobulin
IL-XX	interleukin-XX
IL-XXR	interleukin-XX receptor
ILC	innate lymphoid cell
ILC1	group 1 ILC
ILC2	group 2 ILC
ILC3	group 3 ILC
iLN	inguinal lymph nodes
pTreg	induced peripheral regulatory T cell
JAK	Janus tyrosine kinase
L/D	Live/Dead viability dye
LB	lysogeny broth
Lgr5	leucine-rich repeat-containing G-protein coupled receptor 5
^{lo}	low (expression of protein)
loxP	locus of crossover [x] in P1
Lti	lymphoid tissue inducer
M	molar

MALT	mucosal associated lymphoid tissue
M cells	microfold cells
mFI	median fluorescence intensity
mg	milligram
MHC	major histocompatibility complex
MHCI	class I MHC
MHCII	class II MHC
min	minutes
ml	millilitre
mLN	mesenteric lymph node
NGFR	nerve growth factor receptor
NK	natural killer
NLR	NOD-like receptor
nMFI	normalised median fluorescence intensity
NOD	nucleotide-bind and oligomerisation domain
OX40L	OX40 ligand
p:MHC	peptide:MHC
PAMP	pathogen-associated molecular pattern
PBS	phosphate buffered saline
pLN	pooled peripheral lymph nodes
PMA	phorbol-12-myristate 13-acetate
PP	Peyer's patch
PRR	pattern recognition receptor
rcf	relative centrifugal force
RAG	recombination-activating gene
REG	regenerating islet-derived protein
RELM-β	resistin-like molecule-β
RNA	ribonucleic acid
RORα	RAR-related orphan receptor alpha
RORγt	RAR-related orphan receptor gamma 2
RPMI	Roswell Park Memorial Institute 1640 medium

RT	room temperature
Runx1	Runt-related transcription factor 1
s	seconds
SB	staining buffer
SD	standard deviation
SFB	segmented filamentous bacteria
sIgA	secretory IgA
SILP	small intestine lamina propria
STAT	signal transducers and activators of transcription
T-bet	T-box expressed in T cells
Tcm	central memory T
TCR	T cell receptor
tdRFP	tandem-dimer red fluorescent protein
tdTomato	tandem-dimer tomato
Teff	effector T
Tem	effector memory T
TF	transcription factor
Tfh	T follicular helper
TGF	transforming growth factor
Th1	T helper 1
Th2	T helper 2
Th17	T helper 17
TMR	Toll-like receptor
TNF	tumour necrosis factor
TNFR	tumour necrosis factor receptor
TNFRSF	tumour necrosis factor receptor superfamily
Treg	regulatory T
Trm	tissue resident memory T
Wnt	Wingless-Int
WT	wild type

CHAPTER 1: INTRODUCTION

1.1 THE IMMUNE SYSTEM

The human body is constantly exposed to a barrage of environmental antigens and must mount appropriate responses – tolerance against harmless triggers and protection from pathogens and noxious stimuli. The immune system evolved to recognise and respond to threats or damage to the body through multiple layers of protection. Cells of the innate immune system mount rapid but broad responses following direct sensing of pathogens or indirect recognition of the damage caused by their invasion. Adaptive immune responses, on the other hand, take days to develop but are highly specific to and effective against certain antigens. The innate and adaptive immune systems carry out their functions in cooperation with stromal cells. Barrier site epithelial cells exposed to environmental antigens play an especially important role in the recognition of both innocuous and pathogenic microbes, and the activation of immune responses.

1.1.1 Innate immunity

Maintenance of homeostasis requires rapid reactions to any signs of danger. The innate immune system comprises myeloid and lymphoid cells that share the ability to recognise conserved pathogen- or danger-associated molecular patterns (PAMPs and DAMPs). PAMP and DAMP recognition trigger rapid activation of innate immune functions that aim to eliminate or, should this fail, contain the threat. Innate immune cells include granulocytes (eosinophils, basophils, neutrophils and mast cells), dendritic cells (DCs) and macrophages (Janeway & Medzhitov, 2002). Further immune cell populations, such as innate lymphoid cells (ILCs), were more recently described as crucial parts of the innate immune system. ILCs are subdivided into three main groups based on their effector functions upon activation. These ILC subsets are group 1 ILCs (ILC1s) that include natural killer (NK) cells, group 2 ILCs (ILC2s) and group 3 ILCs (ILC3s) that include lymphoid tissue inducer (Lti)-like cells. ILCs are

especially important in barrier site immune responses and are enriched at these locations (Aparicio-Domingo et al., 2015; Campbell et al., 2019; Hepworth et al., 2015; Satoh-Takayama et al., 2008).

Innate sensing of danger relies on evolutionarily conserved germline-encoded pattern recognition receptors (PRRs) that trigger broad and potent responses upon activation (Janeway & Medzhitov, 2002). A multitude of PRRs with diverse functions exist reflecting the wide range of threats organisms must be able to recognise. Viral infection is detected primarily by PRRs that recognise viral genetic material such as double-stranded ribonucleic acid (dsRNA) in the cytoplasm (Clemens & Elia, 1997; Sun et al., 2013). The resulting signalling cascades drive anti-viral cytokine expression in a nuclear factor-κB and mitogen-activated protein kinase pathway-dependent manner (Williams, 1999). A further defence mechanism triggered by viral RNA sensing is the PRR signalling-mediated apoptosis of infected host cells (Kumar & Carmichael, 1998). The most-studied cytosolic PRRs are the nucleotide-binding and oligomerisation domain (NOD) like receptors (NLRs). NLRs respond to intracellular stress and cytosolic PAMPs resulting in the formation of inflammasomes and the eventual secretion of pro-inflammatory cytokines interleukin (IL)-1β and IL-18 (Broz & Dixit, 2016; Lamkanfi & Dixit, 2014). NLR signalling can further drive pyroptosis, a form of inflammatory cell death (Jorgensen et al., 2017). Membrane-bound PRRs are responsible for detecting PAMPs and DAMPs within the extracellular space, when expressed at the cell surface, or intracellular compartments such as the ER and lysosomes, when internalised (Latz et al., 2004). The most widely studied members of this group are the Toll-like receptors (TLRs). TLRs were first described in *Drosophila melanogaster* (fruit flies) and shown to be protective against fungal infections (Lemaitre et al., 1996). Vertebrates possess a range of TLRs that recognise further PAMPs and DAMPs including bacterial products such as lipopolysaccharide, cell wall components, flagellin and microbial genetic material (Ahmad-Nejad et al., 2002; Latz et al., 2004; Matsumoto et al., 2003; Poltorak et al., 1998). TLRs possess a Toll/Interleukin-1 receptor domain (Akira & Takeda, 2004) that is responsible for driving TLR signalling following activation through the recruitment of adaptor proteins (Horng et al., 2002; Yamamoto et al., 2002). Especially important in the integration of TLR-derived signals and downstream expression of pro-

inflammatory cytokines is the myeloid differentiation primary response protein MyD88 (Adachi et al., 1998).

The inflammatory response induced by the innate immune system is, on occasion, successful in eliminating the cause of activation. However, most often innate immune activation serves to contain the source of danger and activate or modulate specialised adaptive immune responses (Fearon & Locksley, 1996).

1.1.2 Adaptive immunity

Unlike innate immune cells, cells of the adaptive immune system each express a single antigen receptor assembled from rearranged gene segments to give highly specific recognition at the individual cell level but broad coverage when considered at the population level. B cells are marked by B cell receptor (BCR) and T cells by T cell receptor (TCR) expression. Unlike PRRs, these antigen receptors are not able to inherently sense the nature of the threat facing the organism. Therefore, the adaptive immune system relies on innate immune cell-derived signals to communicate the context of activation (Jain & Pasare, 2017). DCs activated by PRR signalling are uniquely adapted to interact with naïve adaptive immune cells within secondary lymphoid tissues (2LT) such as lymph nodes, the spleen and mucosal associated lymphoid tissues (MALTs). DCs provide a number of specialised signals to aid T and B lymphocyte activation and function, making them highly efficient antigen presenting cells (APCs) (Cabeza-Cabrerizo et al., 2021; Schnare et al., 2001). These functions are briefly outlined in the context of T cell activation below.

BCRs are membrane-bound immunoglobulins (Igs) but, following B cell activation, can also be secreted as antibodies. Both BCRs and secreted antibodies are comprised of variable and constant regions, responsible for antigen binding and effector functions, respectively. BCRs and antibodies recognise intact antigens and distinct Ig isotypes acquire functional properties through differences in their constant regions. Naïve B cells express IgM and IgD but upon activation can undergo class switching to express one of IgG, IgE or IgA. Class switching is mediated by signals derived from both innate and

adaptive immune cells (Cyster & Allen, 2019). Secretory IgA (sIgA – a dimeric form of IgA) is especially important in the mucosa where it is transported into lumen to aid the maintenance of symbiosis with microbes of the commensal flora (Lycke & Bemark, 2017). The generation of the variable region shares similarities with the assembly of TCR and is outlined later.

1.2 T LYMPHOCYTES

TCRs are structurally similar to BCRs but do not exist in a secreted form. In addition, TCRs are unable to recognise intact antigens. Instead, they are specific for antigenic peptide(p):major histocompatibility complex (MHC) complexes presented by APCs and other host cells (Doherty & Zinkernagel, 1975; Madrenas et al., 1997). T cells are subdivided into populations based on the type of TCR expressed. Cells carrying TCRα and β chains (αβ T cells) are the most common, however, T cells with TCRγ and δ chains (γδ T cells) also play important roles in the maintenance of homeostasis at barrier sites. Unlike most αβ T cells, γδ T cells do not recognise conventional p:MHC complexes. Similarly, unconventional αβ T cell TCRs bind alternative ligands (Godfrey et al., 2015). The processes described below are mostly specific to conventional αβ T cells.

1.2.1 Antigen receptor diversity

B and T cells must be able to recognise not only conserved but also novel antigens, a process that cannot be supported by germline encoded receptors. Instead, variable (V), joining (J) and in some cases diversity (D) regions within BCR and TCR genes undergo random deletions, insertions and binding during B and T lymphocyte development to generate unique antigen receptors. The result of V(D)J recombination is the creation of highly diverse sequences encoding receptors that show the highest variability within regions responsible for determining complementarity to antigens or p:MHC complexes. Both TCR and BCR gene recombination rely on the function of the recombination activating genes RAG1 and RAG2 (Briney et al., 2019; McBlane et al., 1995; Schatz et al., 1989). A crucial difference between T and B cells is that BCR sequences are further modulated during B cell activation.

This process, termed somatic hypermutation, serves to increase the quality of B cell responses through antibody affinity maturation (Dudley et al., 2005).

1.2.2 T cell activation

TCR-p:MHC binding relies on the co-receptors CD4 and CD8. These two TCR co-receptors also determine whether T cells are able to recognise peptide presented by class I or class II MHC (MHCI, MHCII). CD4 and CD8 are selected during T cell development and mature T cells do not co-express these two markers (Kruisbeek et al., 1985; Teh et al., 1988). In addition to determining MHC-specificity, TCR co-receptors further aid TCR ligation-induced signal transduction. This is essential as TCR chains do not possess large functional constant regions. In fact, TCR signalling relies on the formation of TCR complexes that further include CD3. Co-receptor intracellular domains serve as scaffolds and docking sites for cytosolic signal transducers, thus facilitating a signalling cascade that results in T cell activation or, in the case of previously activated T cells, effector functions (Hwang et al., 2020; Wucherpfennig et al., 2010). CD8 T cell activation results in the generation of cytotoxic T lymphocytes that perform important roles in the MHCI-mediated recognition and elimination of cells showing signs of infection or those that have undergone malignant transformations (Russell & Ley, 2002). Activated CD4 T cells, on the other hand, exert their effects primarily by tuning the responses of other immune and stromal cells, thus modulating their microenvironments. CD4 T cells exist in multiple subsets, each one adapted to the challenge leading to its activation (Raphael et al., 2015). Importantly, TCR ligation alone is not sufficient for the formation of effector T cell responses.

1.2.3 Costimulatory signals

In addition to TCR ligation, T cell activation requires two further types of APC-derived signals – costimulation and cytokine secretion. Costimulatory signals are required to stabilise the interaction between APCs and adaptive immune cells. Furthermore, costimulation plays important roles in modulating T cell function (Jenkins & Schwartz, 1987). The key groups of costimulatory receptors and ligands are the B7-CD28 superfamily and the tumour necrosis factor receptor superfamily (TNFRSF).

CD28 binds to CD80 and CD86. CD28 signalling is required early in the response and is crucial to T cell survival, proliferation and differentiation (Gmunder & Lesslauer, 1984; Harding et al., 1992; Srinivasan et al., 2001). Conversely, the activity of a further B7-CD28 superfamily member cytotoxic lymphocyte-associated antigen-4 (CTLA-4) inhibits T cell proliferation and activation. CTLA-4 carries out this function via two mechanisms. First, competition for ligand binding with CD28 in a process that is crucial to preventing inappropriate proinflammatory T cell responses (Karandikar et al., 1996). Second, CTLA-4-bearing cells were shown to capture, remove and degrade CD80 and CD86 in a CTLA-4 binding-mediated process, thus altering the ability of APCs to provide key costimulatory signals (Qureshi et al., 2011).

The TNFRSF contribute to a broad array of immunological processes including the regulation of CD4 T cell function. OX40 is a key TNFRSF member that, unlike CD28, is expressed on activated T cells only several days after TCR ligation and has important roles in supporting clonal expansion and survival (Gramaglia et al., 1998; Paterson et al., 1987). Previous work has shown that interaction of OX40 with its ligand (OX40L) is strongly linked to proinflammatory effector responses (Gajdasik et al., 2020; Gaspal et al., 2011; Withers et al., 2011). Importantly, others have shown that the OX40:OX40L pathway can also modulate suppressive regulatory T (Treg) cell function but this was found to be context-specific. While OX40 activated intestinal Treg cells, it blocked intratumoural suppressive function (Griseri et al., 2010; Piconese et al., 2008).

In summary, integration of opposing and diverse costimulatory signals is a central aspect of immune regulation. Importantly, this function is not restricted to CD4 T cell priming but can also regulate effector and memory responses upon TCR reactivation (Withers et al., 2011).

1.2.4 T cell memory

Following the initial T cell response and pathogen clearance the T cell pool contracts through apoptosis of unneeded effector cells. However, a small population of long-lived cells remains and forms the memory T cell pool. The exact mechanisms driving memory cell formation and maintenance are not

known but TCR repertoire, binding avidity to cognate p:MHC complexes and the availability of costimulation play important roles (Kim et al., 2013; Moon et al., 2007; Withers et al., 2011).

Memory T cells are not a homogeneous population but form phenotypically and functionally distinct subsets. Broadly, they can be categorised as central memory T (Tcm) cells, effector memory T (Tem) cells and tissue resident memory T (Trm) cells (Kumar et al., 2018). Landmark studies by Pepper and colleagues showed that Tcm and Tem cells develop independently following invasion by an intracellular pathogen (Pepper et al., 2010; Pepper et al., 2011). Tcm cells recirculate through 2LT and express markers including the chemokine receptors CCR7, CXCR5 and CD62L that enable this migration pattern. Upon reactivation Tcm proliferate and give rise to the other populations, including effector cells, T follicular helper (Tfh) cells and more Tcm cells (Pepper et al., 2011). Tem cells are thought to arise from committed effector cells and recirculate through nonlymphoid tissues(Pepper & Jenkins, 2011; Pepper et al., 2011). Conversely, Trm cells, the most recently described memory T cell population, are retained in nonlymphoid tissues and play important roles in barrier immunity. Trm cells arise from the local persistence of effector cells and their retention is mediated by the expression of adhesion molecules such as CD69 and CD103 (Amezcua Vesely et al., 2019; Mueller & Mackay, 2016). Both Tem and Trm cells are capable of generating rapid effector responses following antigen reencounter and were therefore thought of as sentinels that rapidly coordinate responses aimed at pathogen expulsion. Indeed, Tem cells generated following *Listeria monocytogenes* infection were reported to give rise to large numbers of effector cells but showed only a very limited ability to produce Tcm and Tfh (Pepper et al., 2011). However, Trm cell functions were recently linked to the Tcm cell arm of the response suggesting that Trm cells are not limited to the generation of effector responses (Fonseca et al., 2020). Interest in CD4 T cell memory, especially tissue resident memory, has been increasing, however, the majority of our understanding of Trm cells comes from studies of CD8 T cell biology (Schenkel & Masopust, 2014).

1.2.5 CD4 T cells responses

Antigen presentation and the provision of costimulatory signals are indispensable for CD4 T cell activation. However, a third signal arising from cytokine receptors is required for the differentiation of distinct CD4 T cell subsets. Cytokine receptor activation in naïve CD4 T cells triggers a signalling

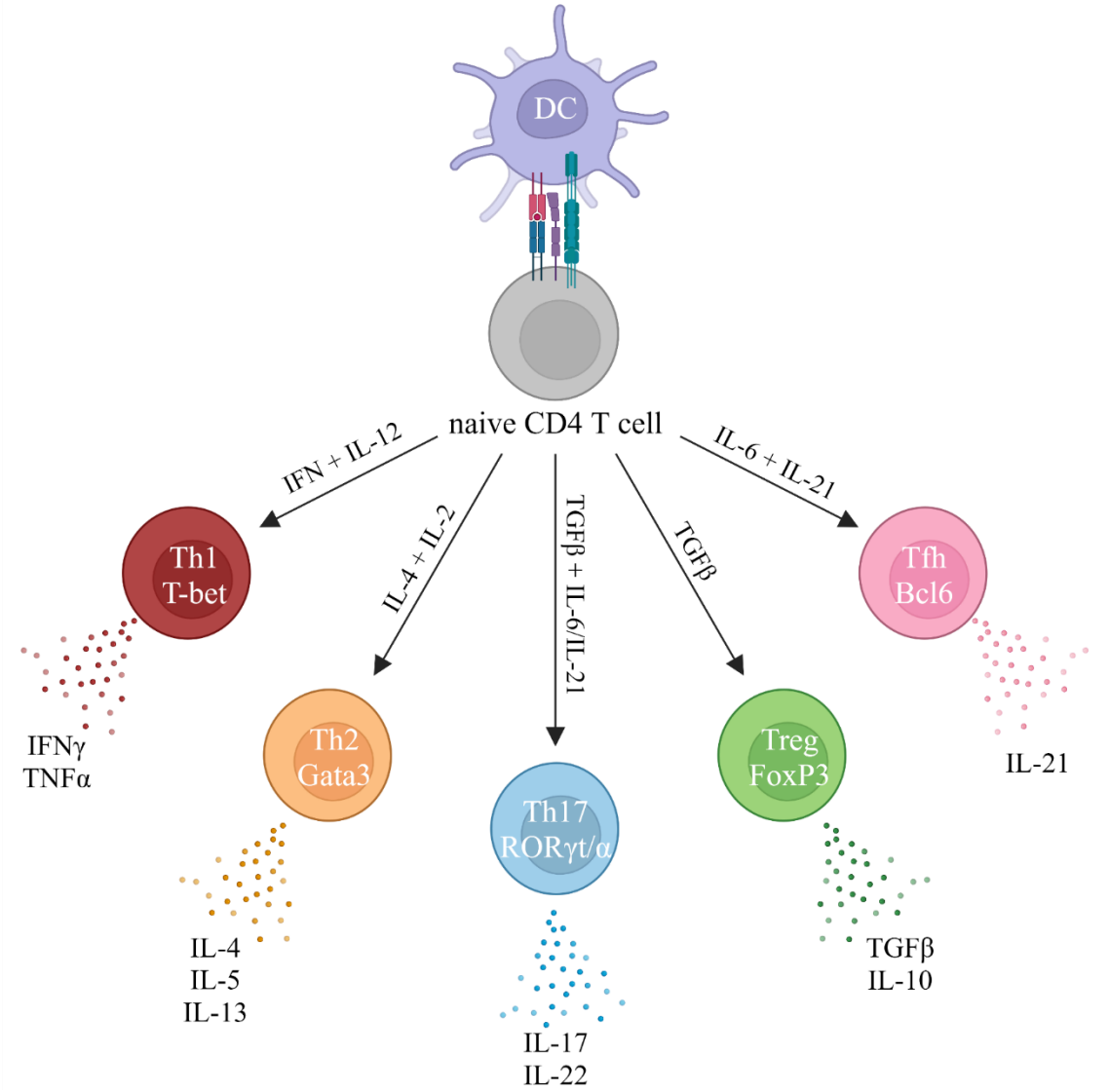

Figure 1.1. CD4 T cells differentiate into distinct subsets following activation through modular acquisition of effector functions. Images generated with BioRender.com.

cascade that results in the expression of lineage-defining 'master' transcription factors (TFs). Activated CD4 T cells are grouped based on their functional properties. The 5 best-defined and broadly accepted subsets (Fig1.1) are briefly described below.

1.2.4.1 T helper cells

CD4 T cells possessing distinct effector profiles are adapted to the orchestration of immune responses to distinct classes of pathogens. Interferon γ (IFNγ) and IL-12 induce expression of the TF T-box expressed in T cells (T-bet) and drive T helper 1 (Th1) cell differentiation (Szabo et al., 2000). Th1 cells are induced in response to intracellular bacterial infections and produce high levels of the cytokines IFNγ and tumour necrosis factor-α (TNFα). These molecules activate phagocytes enabling macrophage-mediated killing of the pathogen (Bogdan et al., 1990; Mosmann et al., 1986). In contrast, T helper 2 (Th2) cells are crucial to immune responses targeting multicellular parasites such as helminths. Th2 cells differentiate in the presence of IL-4 and IL-2 and express the TF GATA3 (Zheng & Flavell, 1997). Th2 cells secrete high levels of the cytokines IL-4, IL-5 and IL-13 and promote eosinophil activation as well as the production of IgA and IgE to aid parasite neutralisation and expulsion (Coffman & Carty, 1986; Mosmann et al., 1986).

Finally, T helper 17 (Th17) cells produce IL-17 family cytokines and IL-22 (Harrington et al., 2005; Liang et al., 2006) and are crucial in the response to extracellular bacteria and fungi (Ivanov et al., 2009; Okada et al., 2015). Th17 cells are enriched in mucosal surfaces and play a central role in the maintenance of mucosal barriers. Th17 cell induction and transcriptional regulation is discussed in detail later.

1.2.4.2 Tfh cells

Tfh cells are dependent on the TF B cell lymphoma 6 (Bcl6) and differentiate in the presence of APC-derived IL-6 and IL-21 (Nurieva et al., 2009). Tfh cells, required for the generation of humoral immune responses, act on antigen-specific B cells where they induce context-appropriate class switching and support high-affinity antibody generation. Distinct antibody isotypes interact with varied effector molecules. Therefore, Tfh cells are important in ensuring that the antibody response is not only highly specific but also triggers effector functions best adapted to the elimination of pathogens and other sources of antigens (Reinhardt et al., 2009).

1.2.4.3 Treg cells

Recognition of self-antigen or inappropriate inflammation following environmental signals has the potential to cause profound tissue damage. Treg cells are critical regulators of the immune system. Two Treg cell populations are defined based on their developmental origin. Natural thymic Treg are generated in the thymus while induced peripheral (p)Treg cells differentiate from naïve T cells in the periphery (Chen et al., 2003; Fu et al., 2004). Both cell groups produce transforming growth factor β (TGFβ), IL-10 and further effector molecules. Peripherally generated pTreg cells rely on TGFβ signalling that drives expression of the Forkhead box protein P3 (FoxP3). FoxP3 underpins Treg cell suppressive function (Fu et al., 2004). Suppression of effector T cells occurs through T cell cytokine receptor signalling-mediated effects and modulation of APC function.

1.3 THE MUCOSAL BARRIERS

The mucosal barriers that line the inner surfaces of the body face unique challenges. As the main interfaces with the environment, they face constant exposure to a barrage of both innocuous and potentially harmful antigens. Even though commensal bacteria, dietary and other environmental antigens are foreign to the body they must be tolerated in order to avoid inappropriate inflammation. On the other hand, mucosal surfaces are the main points of pathogen entry necessitating robust but well-controlled inflammatory responses. This dual requirement makes mucosal surfaces key sites of immune regulation. The mucosa contains a vast and specialised compartment of the immune system termed the mucosal immune system. Several interconnected layers protection mediate resistance to and expulsion of pathogens. Physical barriers are aimed at preventing pathogen entry. However, given that permeability must be maintained to enable nutrient, gas and water uptake, further defence mechanisms are required. Chemical barriers, along with the immune system, work to control both commensal and pathogenic microorganisms. Of all mucosal surfaces the intestine harbours the largest number of immune cells and is the most well-understood compartment.

The intestinal mucosa is comprised of a single layer of epithelium, underlying loose connective tissue termed lamina propria and a thin layer of smooth muscle. The epithelium and lamina propria are separated by a thin basement membrane and both contain large numbers of innate and adaptive immune cells. Despite their intimate interactions, the intraepithelial and lamina propria layers form two distinct immunological compartments (Mowat & Agace, 2014).

1.3.1 Physical and chemical barriers

The intestinal epithelium contains enterocytes, goblet cells, Paneth cells, tuft cells, microfold cells (M cells), enteroendocrine cells and intestinal epithelial stem cells (IESCs) joined by tight junctions. Intestinal epithelial cells (IECs) exhibit both diverse and overlapping functions and have important roles in interfacing with mucosal immune cells (Peterson & Artis, 2014).

1.3.1.1 Enterocytes

Enterocytes are polarised cells with an apical surface exposed to the intestinal lumen and basal surface attached to the basement membrane. This cell type makes up the majority of IECs and is found throughout the intestine. It has long been established that the primary function of enterocytes is nutrient and water uptake from the intestinal lumen along with the production of enzymes to aid nutrient breakdown (Henning, 1985). Importantly, however, it is now clear that enterocytes also help maintain mucosal homeostasis through the secretion of antimicrobial peptides (AMPs) and interactions with mucosal immune cells. AMPs serve as a chemical barrier to microbes, including commensal and pathogenic bacteria. Paneth cells, discussed later, are highly efficient producers of a wide range of secreted AMPs but enterocytes can also produce a limited number in a TLR-dependent manner (Cash et al., 2006; Vaishnava et al., 2008). In addition to secretion of AMPs into the lumen, TLR activation also drives the production of cytokines and chemokines that modulate immune cell function in the surrounding area (Abreu, 2010).

The intestinal epithelium resides in an abrasive environment resulting in the rapid loss of enterocytes. In addition, enterocyte invasion, a common form of pathogen entry, results in expulsion of the infected cell. This process, called enterocyte sloughing, is a key defence mechanism that not only maintains epithelial integrity but also signals the presence of pathogens to nearby IECs and immune cells (Knodler et al., 2014; Rauch et al., 2017; Sellin et al., 2014). Rapid loss of IECs necessitates their constant replacement, making the intestinal epithelium the tissue with the highest rate of cell turnover.

1.3.1.2 Intestinal epithelial stem cells

The intestinal epithelium is renewed by pluripotent IESCs found at the base of intestinal crypts, invaginations present throughout the intestine. IESC proliferation and IEC maturation are dependent on the Wingless-Int (Wnt)/β-catenin pathway with the Wnt target leucine-rich repeat-containing G-protein coupled receptor 5 (Lgr5) marking a population of IESCs tasked with homeostatic proliferation. Interestingly, a distinct IESC population expressing the Wnt-independent Bmi1 but not Lgr5 appears more important in tissue regeneration following injury (Barker et al., 2007; Yan et al., 2012).

Given the profound effect pathogens and a proinflammatory environment have on the intestinal epithelium it is crucial that mucosal cytokine signalling is integrated into IESC function. The cytokines IL-6 and IL-22 have been shown promote IESC survival and proliferation, driving epithelial regeneration following tissue injury (Aparicio-Domingo et al., 2015; Grivennikov et al., 2009; Hanash et al., 2012; Lindemans et al., 2015). IL-6/IL-22-mediated epithelial repair relies on the activation of the TF signal transducer of activation 3 (STAT3) and can also contribute to carcinogenesis when not regulated (Grivennikov & Karin, 2010), necessitating negative control mechanisms. The Th1 cell-associated cytokines IFNγ and TNFα synergise to drive increased expression of the Wnt and β-catenin inhibitors Dickkopf WNT signalling pathway inhibitor 1 and guanylate-binding protein 1, respectively, thus reducing the rate of IEC renewal (Capaldo et al., 2012; Nava et al., 2010).

1.3.1.3 Goblet cells

The intestinal epithelium contains a range of specialised secretory cells that are dedicated to producing mucus, AMPs and hormones. Goblet cells are the main sources of mucus and are present throughout the intestine, albeit not with an even distribution. Cell numbers show a gradual increase throughout the intestine with the highest frequency found in the distal colon. As a result, mucus composition also varies. The small intestine is lined by one loose layer while in the large intestine mucus forms a viscosity gradient resulting in two layers. These are a tightly packed inner layer closer to the epithelium and filling intestinal crypts, and a looser outer layer similar to that of the small intestine (Johansson et al., 2008). Bacteria are normally excluded from the inner mucus layer making it an effective barrier between the epithelium and most microbes (Johansson et al., 2008; van der Waaij et al., 2005).

The main building blocks of mucus are heavily glycosylated mucins with mucin 2 playing a crucial role in the separation of large intestinal epithelium and luminal microbes (Johansson et al., 2008). Mucin secretion by goblet cells is constitutive but can be tuned in response to the presence of both commensals and pathogens. In fact, lack of colonisation by commensal microbes in germ-free mice was shown to impair resistance to colitis in animal models partly through reduction of goblet cell numbers and abnormal mucus thickness and porosity (Johansson et al., 2015; Kitajima et al., 2001). Triggers of alterations in goblet cell function include cytokines and direct PRR-mediated recognition of PAMPs. Immune cell-derived cytokines, such as IL-13, augment mucin production and secretion to aid pathogen and parasite clearance (Campbell et al., 2019). In addition, mucin secretion is responsive to the ligation of multiple TLRs present within goblet cells. Compound exocytosis, the rapid release of large amounts of mucin 2 containing granules, is thought to be a key intestinal crypt defence mechanism coordinated by specialised ‘sentinel’ goblet cells in response to pathogen invasion (Birchenough et al., 2016). Cytokines, including IFNγ and IL-22, are potential additional triggers of this process (Songhet et al., 2011; Turner et al., 2013).

In addition to their well-known roles in mucus production, goblet cells have further functions that overlap with those of other IECs. Resistin-like molecule-β (RELM-β) is a further protein that promotes barrier functions. RELM-β, secreted by goblet and Paneth cells, increases mucin 2 production and regulates immune cell function while also exhibiting some anti-parasitic and anti-microbial properties (Artis et al., 2004; Propheter et al., 2017). On top of protein secretion, goblet cells have also been shown to facilitate antigen uptake by mucosal APCs, a characteristic shared with M cells. Specifically, it was demonstrated that small molecular weight soluble luminal antigen is delivered to lamina propria DCs through goblet cells in a process that is thought to aid mucosal homeostasis and immune tolerance (McDole et al., 2012).

1.3.1.4 Paneth cells

The physical barrier created by mucus is enhanced by AMPs secreted into and trapped in this layer. Paneth cells, found near IESCs in small intestinal crypts, are a further subset of specialised secretory IECs responsible for the majority of epithelial AMP synthesis and secretion. The main groups of AMPs produced by Paneth cells are defensins, cryptdin-related sequence (CRS) peptides, lysozymes, phospholipases, C-tyle lectins and ribonucleases. Some are secreted constitutively while the production of others is induced in response to environmental signals.

The first AMP to be identified in Paneth cells was lysozyme (Erlandsen et al., 1974). Through clearance of bacterial cell wall peptidoglycan, a key trigger of proinflammatory responses, lysozymes have important roles in dampening mucosal inflammation in addition to their antibacterial properties (Ganz et al., 2003). Defensins can be grouped into two categories based on their structure. In humans, α-defensins are dominant over β-defensins and are expressed constitutively (Ganz, 2003). Both groups exhibit broad antimicrobial activities and can interfere with both bacterial membranes and cell walls (de Leeuw et al., 2010; Sass et al., 2010). In addition, defensins can interface with the immune system by recruiting innate and adaptive immune cells expressing the chemokine receptor CCR6 (Yang et al., 1999). CRS peptides are closely related to α-defensins and perform very similar functions (Hornef et

al., 2004). Phospholipases are effective against a slightly smaller array of microbes as they target cell wall components primarily of Gram-positive bacteria (Nevalainen et al., 2008). Similarly, the C-type lectins regenerating islet-derived protein (REG) IIIα in humans and REGIIIγ in mice target Gram-positive bacteria. However, unlike in the case of defensins, the expression of these AMPs is inducible. Sensing of microbial presence, either directly through Paneth cell PRRs or indirectly through the effects of IL-17/IL-22 signalling, is a potent trigger of REGIIIα/γ and other AMP expression (Archer et al., 2016; Brandl et al., 2007; Cash et al., 2006; Liang et al., 2006; Vaishnava et al., 2008). Finally, angiogenin 4, a ribonuclease secreted by multiple IECs in response to commensal bacteria, has antibacterial, antifungal and antiviral effects (Hooper et al., 2003).

A further function of Paneth cells not discussed here is the generation and maintenance of the crypt base stem cell niche for $Lgr5^+$ IESCs (Sato et al., 2011).

1.3.1.5 Enteroendocrine cells

Enteroendocrine cells produce hormones in response to stimulation linking the intestine and the central neuroendocrine system. Microbial flora and nutrient-derived signals are integrated and collectively, hormones released by enteroendocrine cells have key roles in regulating appetite, digestion and nutrient uptake (Gribble & Reimann, 2019).

1.3.1.6 Tuft cells

Tuft cells are present throughout the intestine and were shown to have an important role orchestrating anti-helminth immune responses. IL-25, constitutively secreted by tuft cells but increased following parasite sensing, maintains and activates mucosal ILC2 populations. ILC2-deried cytokines, on the other hand, drive increased tuft cell differentiation, thus creating a positive feedback loop (Gerbe et al., 2016; von Moltke et al., 2016). More recently, an additional function was also described. Tuft cells were shown to express receptors to the constant region of IgG. Inhibition of IgG

binding was found to drive intestinal inflammation but the exact mechanisms and broader functional relevance of Tuft cell IgG sensing are currently unknown (Elmentaite et al., 2021).

1.3.1.7 Microfold cells

M cells are closely related to enterocytes but both their basal and apical surfaces are highly adapted to the delivery of luminal antigen lamina propria APCs. Folds forming a pocket in the basal surface enable close interactions with mucosal DCs, macrophages, T cells and B cells. This is further facilitated by secreted chemokine-mediated recruitment of immune cells and membrane-bound chemokine mediated M cell-lymphocyte interactions (Hase et al., 2006; Zhao et al., 2003). Several additional adaptations increase the ability of M cells to engulf antigens in the lumen. The mucus layer covering areas with a high frequency of M cells is thinner and more permeable than that of neighbouring areas. Thus, antigens and pathogen are not prevented from coming into contact with these IECs (Ermund, Gustafsson, et al., 2013; Ermund, Schutte, et al., 2013). In addition, IL-22-dependent AMP secretion is blocked, possibly through DC-derived inhibitors, to ensure that bacteria are not excluded from the vicinity of M cells (Jinnohara et al., 2017). Antigen and microbe uptake and transcytosis are thought to occur through a combination of passive non-specific and receptor-mediated processes. Glycoprotein 2, expressed on the luminal surface of M cells, was shown to be important in the recognition and transcytosis of certain types of bacteria (Hase et al., 2009). Antigen bound to sIgA present within the lumen is similarly delivered to mucosal lamina propria immune cells by M cells (Rey et al., 2004). Dectin-1, also present on M cells, was proposed as a receptor mediating this process (Rochereau et al., 2013). Subepithelial DC populations are the primary targets of antigen delivered by M cells.

1.3.2 Mucosal immune system

M cell-mediated delivery of antigen to DC aims to prime adaptive immune responses. Naïve mucosal adaptive immune cells do not populate the intestine at random, rather, they are found in MALTs. Therefore, M cell presence is largely associated with areas containing MALTs. Within the intestinal

wall MALTs include Peyer's patches, restricted to the small intestine, the caecal patch within the caecum and isolated lymphoid follicles (ILFs) distributed throughout the intestine. Peyer's patches form a subepithelial dome visible to the naked eye (Cornes, 1965) and contain multiple B cell follicles with germinal centres, indicating the constant priming and activation of B cell responses. Smaller T cell zones are present between these follicles, while in contrast, ILFs contain no or minimal T cell areas (Herbrand et al., 2008). MALTs are key sites of T cell priming and B cell activation and are highly responsive to microbial flora-derived signals. Within MALTs, B cell class switching and maturation into IgA-secreting plasma cells in response to commensal bacteria is crucial to the maintenance of mucosal homeostasis (Lee et al., 2008; Masahata et al., 2014). Microbial signals influence not only lymphocyte activation but also MALT development of and the recruitment of immune cells into these structures. B cells are recruited through a combination of PRR-mediated secretion of CCL20 from stromal cells, acting on B cell CCR6, and DC-derived CXCL13 binding B cell CXCR5 (Bouskra et al., 2008; Velaga et al., 2009).

Mesenteric lymph nodes (mLN) are the last member of gut associated lymphoid tissues but, as intestine-draining LNs, these do not include M cells or any other epithelial cells. MLNs are the largest LNs of the body and drain distinct, well-defined segments of the intestine (Carter & Collins, 1974).

Under homeostatic conditions it is crucial that no inappropriate inflammatory responses are primed within MALTs. The intestine is populated by unique APC populations adapted to inducing both suppressive and proinflammatory CD4 T cell development. These can be broadly split based on expression of three key markers – CD11b, CD11c and CD103. Cells lacking CD11b express CD11c and CD103 and, in mice, are found primarily in the colon. On the other hand, $CD11b^+$ APCs were shown to be $CD11c^+CD103^+$ DCs or $CD103^-$ macrophages expressing low levels of CD11c (Denning et al., 2011). $CD11b^+$ intestinal DCs were found to be dependent on the transcription factor interferon regulatory factor 4 and highly efficient at inducing proinflammatory mucosal Th17 cells (Persson et al., 2013;

Welty et al., 2013). Interestingly, distribution of these APCs also matched that of Th17 cells with the highest density in the proximal small intestine and lowest in the distal colon (Denning et al., 2011).

DCs lacking CD11b appear to have a crucial role in retinoic acid (RA)-mediated induction of gut-tropism through CCR9 and CD103 expression on activated T cells (Iwata et al., 2004; Johansson-Lindbom et al., 2005; Luda et al., 2016). IEC-derived signals such as TGFβ, RA and thymic stromal lymphopoietin imprint mucosal DCs with tolerigenic properties (Rimoldi et al., 2005; Taylor et al., 2009; Zeuthen et al., 2008). DCs exposed to these products upregulate expression of TGFβ and RA which, in turn, induce FoxP3 expression in naïve T cells. In addition, as described above, these cytokines drive expression of chemokine receptors that guide entry into the intestinal mucosa. Thus, mucosal $CD103^+$ DC are potent inducers of gut-homing pTreg cells (Coombes et al., 2007). In addition, the same IEC secretory products drive IL-10 expression in non-migratory mucosal macrophages, further reinforcing Treg cell activity and dampening pro-inflammatory immune responses (Kayama et al., 2012).

The lamina propria and intestinal epithelium contain large numbers of activated effector cells. ILCs, mimicking the functional division of CD4 T cells but lacking antigen receptors, are crucial to mucosal homeostasis. These cells are key sources of cytokines that influence IEC function and orchestrate adaptive immune responses (Peterson & Artis, 2014; Satoh-Takayama et al., 2008). Moreover, ILCs have been shown to express MHCII and thus possess the ability to directly interact with CD4 T cell regulating their effector functions and possibly participating in their priming and activation (Hepworth et al., 2015; Hepworth et al., 2013; Oliphant et al., 2014).

Treg and Th17 cells are key mucosal CD4 T cell populations and the balance of their activity is essential to mucosal homeostasis. Treg cell function to suppress potentially harmful inflammation and mediate tolerance to environmental antigens such as those derived from the diet (Kim et al., 2016). Orally administered antigen was shown to rapidly induce pTreg development in mLNs and Peyer's patches. This process relies on migratory mucosal DC populations and is TGFβ and RA-dependent. Differentiation of oral antigen-specific pTreg confers systemic tolerance (Hauet-Broere et al., 2003;

Pabst & Mowat, 2012; Sun et al., 2007; Worbs et al., 2006). Moreover, through controlling Th17 cell effector functions, intestinal Treg cells support the generation of niches permissive to commensal presence. Therefore, Treg cells are crucial to preventing mucosal dysbiosis (Campbell et al., 2018; Neumann et al., 2019; Xu et al., 2018). The Th17 cell-associated cytokines IL-17 and IL-22 strengthen the physical and chemical barriers, as outlined above. In addition, Th17 cells mediate recruitment of further adaptive and innate immune cells to assist clearance of microbes (Liang et al., 2007). Together, Th17 and Treg cell effector functions enable commensalism while also providing protection from extracellular infections. However, Th17 cells are also known drivers of several diseases characterised by inappropriate inflammation. While Th17 cell involvement is common in conditions affecting barrier sites, such as the intestine, eyes or skin (Annunziato et al., 2007; Ha et al., 2014; Yoshimura et al., 2009), it is not limited to these (Hirota et al., 2007). The study of mucosal Th17 cell responses is hindered by the great degree of plasticity exhibited by these cells. Both suppressive Treg and proinflammatory Th1-like cells can arise from Th17 cells (Gagliani et al., 2015; Hirota et al., 2011). While these processes are known contributors to disease (Downs-Canner et al., 2017; Hirota et al., 2011) they are also a feature of normal, protective responses (Gagliani et al., 2015; Hirota et al., 2013; Omenetti et al., 2019). Th17 cells' importance in both health and disease make them and their effector molecules key targets of a wide range of therapeutics.

1.4 TH17 CELL RESPONSES

CD4 T cells producing interleukin-17A (IL-17A) and other IL-17 family cytokines have long been described (Fossiez et al., 1996; Yao et al., 1995) but were accepted as a distinct effector lineage only upon identification of key cytokine combinations (Bettelli et al., 2006; Cua et al., 2003; Langrish et al., 2005; Mangan et al., 2006; Veldhoen et al., 2006) and a transcriptional programme (Ivanov et al., 2006; X. O. Yang, B. P. Pappu, et al., 2008) unique to their development. These cells are now known to be indispensable for appropriate protective responses against classes of pathogens not efficiently cleared by type 1 (Th1 cell) or type 2 (Th2 cell) immunity (Milner et al., 2008). In addition to directly

aiding pathogen clearance, Th17 cell effector functions also promote barrier repair and thus support the maintenance of mucosal function.

1.4.1 Th17 induction

Innate immune system activation in the presence of extracellular bacteria and fungi precipitates the conditions required for the differentiation of naïve CD4 T cells into IL-17-producing Th17 cells. Distinct classes of microbes were shown to induce phenotypically different Th17 cell populations (Omenetti et al., 2019). Segmented filamentous bacteria (SFB), a poorly defined genus of pathobionts, induce a homeostatic, highly stable population of Th17 cells not thought to be pro-inflammatory in the healthy intestine (Gaboriau-Routhiau et al., 2009; Ivanov et al., 2009; Lecuyer et al., 2014). It is now known that the adaptive immune system is engaged following mucosal invasion and attachment to the intestinal epithelium (Atarashi et al., 2015). Similarly, pathogenic bacteria that adhere to the epithelium, such as the *Escherichia coli* model organism *Citrobacter rodentium*, also drive Th17 cell induction (Mangan et al., 2006; Omenetti et al., 2019). Unlike Th17 cells generated in response to SFB, pathogen-induced Th17 are highly proinflammatory (Omenetti et al., 2019). Neutrophil apoptosis in the presence of pathogen invasion has also been shown to have the capacity to induce Th17 cell responses through providing the trigger for APC activation along with the production of Th17-polarising cytokines (Torchinsky et al., 2009).

The formation of proinflammatory Th17 cells was initially linked to IL-23 signalling (Langrish et al., 2005). However, given that naïve CD4 T cells are not able to respond to this cytokine (Oppmann et al., 2000) due to minimal expression of its receptor (Parham et al., 2002) further efforts focused on pinpointing other factors driving Th17 cell differentiation. Early studies seeking to identify ways to generate Th17 cells *in vitro* identified the combination of IL-6 and TGFβ as the cytokines required to induce IL-17 expression in CD4 T cells (Bettelli et al., 2006; Mangan et al., 2006; Veldhoen et al., 2006). Interestingly, expression of the Treg cell lineage-defining TF FoxP3 is also TGFβ-dependent in the periphery (Bettelli et al., 2006; Fu et al., 2004). The seemingly contradictory roles of TGFβ in supporting

both proinflammatory Th17 and suppressive Treg cells illustrate the important role IL-6 plays in integrating environmental signals. Indeed, FoxP3^{+} Treg cells appeared to be overrepresented in mice unable to produce IL-6 (Korn et al., 2007). However, later reports questioned the ability of IL-6 to drive the formation of stable human Th17 cell populations from naïve CD4 T cells and raised questions about whether other cytokines may be involved (L. Yang et al., 2008). The ability to generate Th17 cells in the absence of IL-6 signalling was partially restored by Treg cell depletion, further supporting the hypothesis that alternative, IL-6 independent pathways may also drive Th17 cell differentiation (Korn et al., 2007). These and other studies identified IL-21 as a factor that, combined with TGFβ, could drive robust IL-17A expression in CD4 T cells. Given that IL-21 is secreted by Th17 cells it is thought that IL-6 signalling in the presence of TGFβ promotes the induction of the Th17 cell transcriptional programme. The resulting IL-21 signalling would then act in a para- or autocrine manner to reinforce the differentiation process (Nurieva et al., 2007).

As outlined above, despite its link to pathogenic Th17 cell populations, IL-23 cannot drive Th17 cell differentiation alone due to the lack of IL-23R on naïve CD4 T cells (Parham et al., 2002). However, TGFβ and IL-6 signalling result in upregulation of IL-23R on recently activated CD4 T cells thus sensitising them to IL-23 signalling (Morishima et al., 2009; Zhou et al., 2007). The precise function of IL-23 in Th17 development is unclear but the pattern of early IL-23R expression is consistent with a role for IL-23 in supporting survival or expansion. In addition, IL-23 may act to reinforce differentiation away from a Treg cell fate and towards a proinflammatory phenotype by suppressing the expression of anti-inflammatory cytokines. This may explain why IL-23 and IL-23R are linked to Th17 cell-associated inflammatory conditions (Krausgruber et al., 2016; McGeachy et al., 2007).

1.4.2 Transcriptional regulation of Th17 cell differentiation

1.4.2.1 STAT proteins

Parallel to studies identifying cytokine triggers, others sought to pinpoint the lineage-defining TF driving Th17 cell differentiation. TCR and cytokine receptor signalling integrate within newly primed

CD4 T cells to activate linage-specific transcriptional programs and thus drive the acquisition of characteristic effector programmes. Cytokine receptors closely associate with Janus tyrosine kinase/signal transducers and activators of transcription (JAK/STAT) pathways to enable rapid integration of polarising signals. Selective expression of STAT transcriptional regulators has crucial roles in orchestrating effector T cell development, with STAT1 and STAT4 driving Th1 (Afkarian et al., 2002; Thierfelder et al., 1996) and STAT6 Th2 cell development (Kaplan et al., 1996; Shimoda et al., 1996; Takeda et al., 1996). Treg cell formation is partially reliant on STAT5 activation although this STAT family member may play important roles in the development of further CD4 T cell subsets, including Th17 cells (Amadi-Obi et al., 2007; Burchill et al., 2007). Th17 cells rely on STAT3 activation (Harris et al., 2007; Mathur et al., 2007; Yang et al., 2007). STAT3 integrates signalling from multiple Th17 cell-polarising cytokine receptors (Parham et al., 2002; Zhou et al., 2007) driving downstream activation of the Th17 cell master TF RAR-related orphan receptor γ two (RORγt), thus supporting commitment to the Th17 cell fate (Yang et al., 2007). Furthermore, STAT3 was shown to directly promote the expression of the Th17 cell cytokines IL-17 and IL-21 (Chen et al., 2006; Wei et al., 2007). Expression of IL-21, in turn, reinforces STAT3 activation in an autocrine manner creating a positive feedback loop aiding Th17 cell differentiation (Wei et al., 2007). Unsurprisingly, genetic defects in *STAT3* impair normal Th17 cell responses resulting in the overabundance of alternative CD4 T cell phenotypes and an inability to mount appropriate immune responses to extracellular bacterial and fungal infections (Milner et al., 2008).

1.4.2.2. ROR family transcription factors

STAT3 activation and TGFβ, at the right concentrations, can both trigger RORγt expression in activated CD4 T cells with the most potent induction observed when the two were combined (Yang et al., 2007; Zhou et al., 2007). RORγt expression was found to differentiate CD4 T cells from Th1 and Th2 cells, thus confirming that Th17 cells form a distinct effector lineage (Ivanov et al., 2006; Wilson et al., 2007). Deletion or inhibition of this TF was found to impair Th17 cell formation and IL-17 production,

however, complete loss of this function was only reported upon co-deletion of the related ROR family TF RORα (Lamb et al., 2021; X. O. Yang, B. P. Pappu, et al., 2008). The extent of redundancy in the two TF's function is unclear. Genes encoding core Th17 cell effector molecules were reported to be targets of both RORγt and RORα, however, the latter was found to exert a weaker influence (Castro et al., 2017). RORγt may also function by inhibiting transcriptional programmes linked to alternative effector cell fates both in T cells and other immune cell populations (Bhaumik et al., 2021; Fiancette et al., 2021).

1.4.2.3 Additional transcription factors

The control of Th17 cells, and indeed all CD4 T cell responses, is highly complex with a wide range of further transcriptional regulators involved. These act together with STAT proteins and ROR family TFs to enhance Th17 cell differentiation and function or integrate with alternative transcriptional programmes to either support or antagonise Th17 cell formation. Together, the networks formed by these transcription factors are important in fine-tuning CD4 T cell responses.

Runt-related transcription factors (Runx) can interact with and activate a range of CD4 T cell master TFs. Runx1, specifically, was reported to drive RORγt production and synergize with this TF to enhance Th17 cell effector functions (Lazarevic et al., 2011; Sekimata et al., 2019; Zhang et al., 2008). Interestingly, Runx1 was similarly found to support FoxP3 and Treg cell activity (Kitoh et al., 2009; Rudra et al., 2009). Adding further complexity to the transcriptional networks regulating CD4 T cell differentiation, the Th1 cell master TF T-bet may inhibit Th17 cell differentiation through disrupting Runx1-mediated RORγt activation (Lazarevic et al., 2011).

Mucosal interfaces, the main sites of Th17 responses, are constantly exposed to a barrage of environmental antigens. Thus, mechanisms that enable the integration of environmental signals are indispensable for appropriate Th17 cell responses. The small molecule-activated TF aryl hydrocarbon receptor (AhR) is expressed in a wide range of immune cells and provides a crucial molecular mechanism that enables responses to host metabolites, pollutants and microbial and dietary ligands

(Quintana et al., 2008; Rutz et al., 2011; Veldhoen et al., 2009; Veldhoen et al., 2008). AhR is expressed in multiple CD4 T cell lineages but its effects depend on the environment cells are in – combined signals from cytokines present in the microenvironment along with other TFs acting within the cell determine the outcome of AhR signalling. AhR is found in Th17 cells at high levels and plays important roles early in Th17 cell development (Veldhoen et al., 2009). Observations in RORγt^{+} innate immune cells suggest that AhR carries out this function partly through promoting cell survival (Qiu et al., 2012). Furthermore, AhR activation and translocation into the nucleus can prevent STAT family protein activation-mediated inhibition of Th17 cell development (Kimura et al., 2008).

1.4.3 Th17 cell effector functions

Th17 cells are induced in response to extracellular commensals and pathogens. Thus, their effector functions are aimed at establishing control of commensal microbes as well as supporting resistance to and clearance of pathogens. Through combined effects on innate immune cell populations, such as neutrophils, adaptive immune cells and the intestinal and mucosal epithelium, Th17 cells orchestrate responses to promote barrier integrity and defence. Key to these roles are the Th17 cell cytokines that act on target cells, and chemokine receptors that facilitate Th17 cell homing to effector sites.

1.4.3.1 IL-17 family cytokines

IL-17A, the first member of the IL-17 family to be isolated (Rouvier et al., 1993; Yao et al., 1995), is the canonical Th17 cell cytokine (Infante-Duarte et al., 2000) and gives this CD4 T cell subset its name. The IL-17 family of cytokines contains five additional members, IL-17B, IL-17C, IL-17D, IL-25 and IL-17F (McGeachy et al., 2019). IL-17A and IL-17F show high sequence homology, are regulated similarly and are often co-expressed by activated Th17 cells, forming IL-17A/IL-17F heterodimers (Akimzhanov et al., 2007; Liang et al., 2006). Furthermore, IL-17A and IL-17F homo- and heterodimers bind the same IL-17 receptor (IL-17RA/IL-17RC heterodimers), albeit with differing binding and signalling strength. As a result, IL-17A and IL-17F functions largely overlap (Chang & Dong, 2007; Wright et al., 2007).

IL-17A and IL-17F orchestrate a range of innate responses, all aimed at the protection of the mucosal barriers from invasion by extracellular bacterial and fungal pathogens. IL-17R ligation on target cells induces production of the chemokines CXCL1, CXCL2 and IL-8 which drive neutrophil recruitment. IL-6 and granulocyte colony stimulating factor (G-CSF) expression, also induced by IL-17R signalling, further support and regulate myeloid cells, including neutrophils (Fossiez et al., 1996). Therefore, a key outcome of IL-17A and IL-17F secretion by Th17 cells is to drive barrier site neutrophilia (Jones & Chan, 2002; McAllister et al., 2005; Ye et al., 2001). In addition to facilitating neutrophil recruitment, IL-17 secreted by activated Th17 cells was found to act on epithelial cells, both in the mucosa and in the skin, to promote AMP production and drive tight junction formation thus assisting control of commensal microbes and resistance to pathogens (Archer et al., 2016; Lee et al., 2015). An absence of IL17A, IL-17F or their receptor impairs appropriate anti-fungal responses in both mice and humans and enables opportunistic fungal infection-driven candidiasis (Conti et al., 2016; Levy et al., 2016). Finally, IL-17 further supports barrier integrity and repair by driving epithelial cell proliferation (Chen et al., 2019; Ha et al., 2014). IL-17B, IL-17C, IL-17D and IL-25 (formerly IL-17E) also play key roles in mucosal barrier maintenance as well as other immune responses (Owyang et al., 2006; Ramirez-Carrozzi et al., 2011; Reynolds et al., 2015; Saddawi-Konefka et al., 2016; Starnes et al., 2002). However, only IL-17A and IL-17F are secreted at high levels by CD4 T cells (Akimzhanov et al., 2007; Infante-Duarte et al., 2000).

It is important to note that the roles described above for IL-17A and IL-17F are not solely the results of Th17 cell activation as a multitude of further immune cells can also produce these cytokines (Cua & Tato, 2010).

1.4.3.2 IL-22

IL-22, an IL-10 family cytokine, is a further key Th17 cell effector molecule indispensable for mucosal barrier homeostasis. As described above in the case of IL-17, IL-22 is also expressed by a range of immune cells in addition to Th17 with Ahr activation significantly enhancing its expression (Veldhoen

et al., 2008). ILC3 are the primary source of this cytokine at steady state but infection triggers potent induction of IL-22 in Th17 (Satoh-Takayama et al., 2008). IL-22 is crucial to efficient protection against extracellular bacteria with IL-22-deficiency driving mild dysbiosis and severely impaired responses to enteric pathogens (Zheng et al., 2008).

In contrast to IL-17R, the expression of IL-22R is limited to epithelial cells (Aggarwal et al., 2001; Dudakov et al., 2012; Lindemans et al., 2015). Therefore, IL-22 exerts its protective functions through enabling communication between lymphocytes, including Th17, and epithelial surfaces. The exact epithelial cell populations targeted by IL-22 are still debated but multiple effects have been described, as briefly mentioned earlier. IL-22 promotes epithelial regeneration through stem cell proliferation and differentiation. Specifically, IL-22R signalling promotes intestinal stem cell survival in a STAT3-dependent manner (Aparicio-Domingo et al., 2015; Hanash et al., 2012; Lindemans et al., 2015). IL-22 further enhances resistance to microbial invasion by synergising with IL-17 to stimulate AMP secretion from epithelial cells (Liang et al., 2006). Moreover, IL-22 signalling not only increases mucin production by goblet cells (Sugimoto et al., 2008) but also goblet cell numbers (Turner et al., 2013) to enhance mucus production. Interestingly, some of these functions also appear to be STAT3-dependent (Sugimoto et al., 2008). Together, these effects serve to increase resistance to microbial invasion. However, IL-22 can also promote proinflammatory responses following disruption of barrier sites. IL-22 driven secretion of IL-18 is an effective means of innate immune cell recruitment to the site of damage (Munoz et al., 2015). In addition, IL-22 is also involved in activating further defence mechanisms aimed at pathogen expulsion. Signalling through the IL-22R activates the complement pathway (Trevejo-Nunez et al., 2016) and can contribute to triggering diarrhoea (Tsai et al., 2017). However, the latter also impairs tight junction function (Wang et al., 2017).

1.4.3.3 TNFα

Initial descriptions of pathogenic Th17 cells highlighted TNFα as a key cytokine mediating Th17 cell effector functions (Langrish et al., 2005). However, it has since been established that not all

populations of Th17 cells express this effector molecule. Soon after Th17 cells were established as a separate T helper cell lineage, a considerable degree of plasticity was noted within this population. Th17 cells were shown to possess the capacity to differentiate into Th1-like effector cells (Bending et al., 2009) and thus acquire the Th1 cell-associated cytokines IFNγ and TNFα (Hirota et al., 2011; Lee et al., 2009). TNFα is now a target of a multitude of therapeutics due to its involvement in diseases ranging from cancer to intestinal inflammation (Singh et al., 2018). However, TNFα also possesses a range of biological functions crucial to the maintenance of mucosal homeostasis. TNF receptor 1 (TNFR1), the receptor binding secreted TNFα, is widely expressed and can induce apoptosis of target cells. Through ligation of TNFR1, TNFα is thought to promote inflammation, tissue degeneration and, if uncontrolled, pathological tissue damage (Kalliolias & Ivashkiv, 2016).

1.4.3.4 CCR6

CCR6 is expressed on many mucosal immune cell populations including intestinal IL-17-producing T cells (Singh et al., 2008). CCR6 binds only one known ligand, CCL20 (Baba et al., 1997; Liao et al., 1999). This interaction enables Th17 cell homing to the intestine following a CCL20 gradient. Inflammatory cytokines drive increased expression of CCL20, thus driving increased immune cell trafficking to the site of inflammation (Hirota et al., 2007). Conversely, the anti-inflammatory cytokine IL-10 downregulates CCL20 expression in macrophages (Rossi et al., 1997). Thus, Th17 cell effector functions can be regulated through control of their recruitment into specific microenvironments.

1.4.4 Th17 cell plasticity

Commensal microbes and extracellular pathogens both induce Th17 cell responses. However, while the former are beneficial to their host and are ideally maintained at the mucosa the latter must be controlled and expelled rapidly to prevent excessive pathology. Thus, the nature of responses induced shows fundamental differences. Homeostatic and stable populations of Th17 cells are known to be induced by certain classes of commensal bacteria. These are crucial to the control of opportunistic pathogens and thus the establishment of commensalism (Ivanov et al., 2009; Omenetti et al., 2019).

These Th17 cells are characterised by RORγt and IL-17A expression (Harrington et al., 2005; Ivanov et al., 2006; Veldhoen et al., 2006; X. O. Yang, B. P. Pappu, et al., 2008). However, RORγt and IL-17A expression can give way to alternative CD4 T cell subset master TFs and effector cytokines in Th17 cells generated in response to pathogen invasion. Rather than being terminally differentiated, activated Th17 cells exhibit considerable functional plasticity (Fig1.2) with the capacity to produce Th1 cell-like responses, acquire a Treg cell phenotype and potentially contribute to the Tfh and Th2 cell pools (Gagliani et al., 2015; Hirota et al., 2011; Hirota et al., 2013; Lee et al., 2009; Panzer et al., 2012). Further complicating our understanding of the mucosal CD4 T cell compartment, Treg cells exhibiting Th17 cell-like characteristics, such as TF and cytokine expression, have also been described (Hovhannisyan et al., 2011; Sefik et al., 2015).

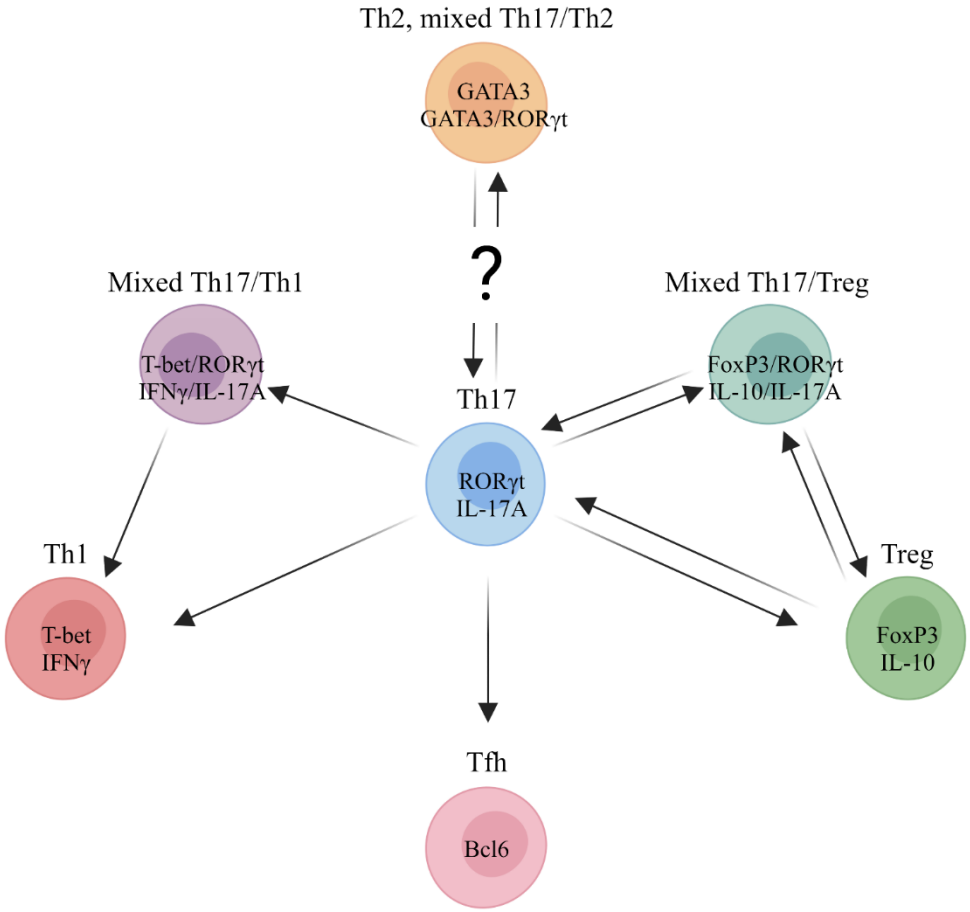

Figure 1.2. Th17 cells exhibit considerable post-developmental plasticity. Images generated with BioRender.com

1.4.4.1 Th17-Treg cell differentiation

Th17 and Treg cells, the two main mucosal CD4 T cell populations are intricately linked not only in their interactions but also in their fates. As described above, both are induced in the presence of TGFβ but Th17 cells require additional cytokines signalling the presence of pathogens (Bettelli et al., 2006; Veldhoen et al., 2006). In addition, mucosal lamina propria Treg cells have long been known to acquire Th17 cell-like characteristics, such as RORγt expression. It was initially thought that the expression of master TFs linked to effector T helper subsets served purely to drive appropriate homing to the same anatomical spaces occupied by the CD4 T cells that required Treg cell-mediated suppression. However, further functions have since been identified. RORγt^{+} mucosal Treg cells are indispensable for the control of commensal microbes (Ohnmacht et al., 2015; Sefik et al., 2015) and this TF may act to support suppressive function in part by blocking alternative effector programmes (Bhaumik et al., 2021). Furthermore, even though FoxP3 was reported to antagonise RORγt-driven gene expression (Zhou et al., 2008), Treg cells producing IL-17A have been observed in the intestine (Hovhannisyan et al., 2011). Whether this represents a physiological response to environmental cues or dysregulation is unresolved (Remedios et al., 2018). Reports that describe the formation of 'exTreg' Th17 cells and their entry into the intraepithelial layer of the mucosa are consistent with an important physiological role in responses to microbial signals (Sujino et al., 2016).

Th17-to-Treg cell differentiation is more commonly observed. Acquisition of FoxP3 expression under inflammatory conditions is not reported to be associated with suppressive functions (Tran et al., 2007) but the formation of 'exTh17' Treg cells, along with secretion of Treg cell-associated cytokines, is thought to be important during the resolution of acute inflammation (Gagliani et al., 2015). However, in different settings the same process has been shown to aid pathogenesis. Acquisition of FoxP3 and loss of IL-17A expression was found to aid murine tumour growth (Downs-Canner et al., 2017) pointing to Th17-Treg cell conversion being a potential target of cancer immunotherapy.

1.4.4.2 Th1-like exTh17 cells

Activated CD4 T cells with mixed Th17 and Th1 cell characteristics have long been linked to mucosal autoimmune and inflammatory disorders. Antigen-experienced cells producing a mix of IL-17 and the Th1 cell-associated cytokines IFNγ and TNFα are disease-causing agents in inflammatory bowel disease (Annunziato et al., 2007; Bishu, El Zaatari, et al., 2019). Studies making use of elegant lineage-tracing models have shown that Th17 cell-derived Th17/Th1 cells play a crucial role in this process (Hirota et al., 2011; Lee et al., 2009). Therefore, several therapies targeting Th17-to-Th1 cell conversion or both Th17 and Th1 cell-associated cytokines have been developed (Bilal et al., 2018; Targan et al., 2016). However, results of such treatments have been mixed, with success reported in some studies but worsening of inflammation in others (Hueber et al., 2012; Singh et al., 2018). Underlying this is the crucial function Th17 cells, including Th1-like exTh17 cells, play in maintaining mucosal homeostasis. Th17 cells are required for efficient control of certain classes of microbes (Ivanov et al., 2009; Milner et al., 2008). Therefore, blocking IL-17A function was highly detrimental to patients suffering from inflammatory bowel disease (Hueber et al., 2012; Targan et al., 2016) but successful in dampening skin inflammation (Bilal et al., 2018). Other approaches involve targeting Th1-like exTh17 cell cytokines such as TNFα. However, these are not consistently beneficial to patients (Singh et al., 2018). Crucially, pathogenic extracellular bacteria induce a robust Th1-like exTh17 cell response (Omenetti et al., 2019). Therefore, non-specific inhibition of Th17 cell function can have wide-ranging effects on mucosal homeostasis and susceptibility to opportunistic pathogen invasion. As outlined above, Th17 cell cytokines have important roles in regulating IEC function and mucosal barrier integrity, likely underlying the lack of success in targeting these cells in inflammatory bowel disease.

Th17 cells acquiring Th1 cell-associated cytokine expression were shown to upregulate T-bet expression, possibly in an IL-23-dependent manner (Lee et al., 2009). Interestingly, Th17 cell-driven mucosal and systemic pathologies are often linked to IL-23 (Ahern et al., 2010; McGeachy et al., 2009). However, different diseases are reported to show differential reliance on T-bet-associated Th17 cell

differentiation. Central nervous system inflammation and murine models of multiple sclerosis have identified a role for IFNγ^{+}IL-17A^{+} Th17 cells and fully differentiated Th1-like exTh17 cells in pathogenesis. However, there are conflicting reports on whether T-bet expression is required for disease onset (Bettelli et al., 2004; Duhen et al., 2013). Studies focused on the pancreas linked Th17 cell function to inflammation but showed this alone did not cause diabetes as disease onset was found to require differentiation into Th1-like cells (Martin-Orozco et al., 2009). However, it is unclear whether acquisition of Th1 cell-associated effector functions in mature Th17 cells actually relies on the Th1 cell master TF (Duhen et al., 2013). Finally, even though CD4 T cells showing a memory T cell phenotype and secreting both IL-17A and the Th1-associated cytokine TNFα are associated with Crohn's diseases pathology (Bishu, El Zaatari, et al., 2019) our understanding of how Th17 cell plasticity influences memory formation is limited.

1.4.4.3 Alternative fates

Th17 cells have also been described to give rise to Tfh and potentially Th2-like cells, however, these conversions are less well-studied. Differentiation into Tfh cells is reported to be beneficial and was shown to aid humoral immunity in the intestine (Hirota et al., 2013). Similarly, the rapid acquisition of Th2 cell-associated cytokine production following helminth infection likely aids parasite expulsion (Panzer et al., 2012). Conversely, respiratory mucosa cells with mixed Th17 and Th2 cell characteristics are described in patients suffering from severe chronic asthma (Irvin et al., 2014; Wang et al., 2010). However, whether these cells form from Th17 cells is unknown.

1.5 AIMS OF THIS INVESTIGATION

Since the initial description of exTh17 cell development only a limited number of studies explored Th17 cell fate. Here, I sought to probe this process *in vivo* to establish the most common differentiation routes.

A key challenge in the field is high degree of Th17 cell plasticity. It is established that Th17 cells give rise to a range of alternative CD4 T cell subsets *in vivo* but how this is regulated and how it impacts long-lived Th17 or exTh17 cells is poorly understood. One challenge in past studies has been the reliance on total TF knockout mouse models. While these were immensely useful tools in establishing the roles of certain pathways in immune regulation, in this context they cannot separate the effects of constitutive TF loss and deletion following induction. Furthermore, TFs driving CD4 T cell subset differentiation have important roles in other immune and non-immune populations. Therefore, these studies are unable to distinguish between Th17 cell-intrinsic and extrinsic TF effects. Moreover, rapid loss of Th17 cell identity confounds long-term tracking of these responses *in vivo*. Thus, novel tractable models of mucosal Th17 cell responses are needed and have the potential to significantly advance our understanding of the regulation of this vital CD4 T cell subset. In this investigation I aimed to exploit multiple lineage tracing tools to better establish the differentiation pathways of common 'exTh17' cell populations and test the roles key TFs play in supporting Th17 cell plasticity and function. Moreover, using a tractable infection model I further aimed to not only characterise mucosal Th17 cell-skewed CD4 T cell responses but also probe the mechanisms involved in their regulation. Through combining these approaches, I sought to address three main aims (Fig1.3):

1. Characterising the mucosal CD4 T cell compartment with a specific focus on the relationship between Th17 cells and alternative mucosal CD4 T cell populations, and assessing the signals governing cell fate decisions.
2. Developing tools to better understand the transcriptional regulation of Th1-like exTh17 cell differentiation and the requirement for Th17 and Th1 cell master TFs in supporting effector functions.

3. Establishing experimental systems that enable the study of mucosal infection-induced memory responses to assess the impact of Th17 cell plasticity on Th17 cell-derived CD4 T cell memory formation.

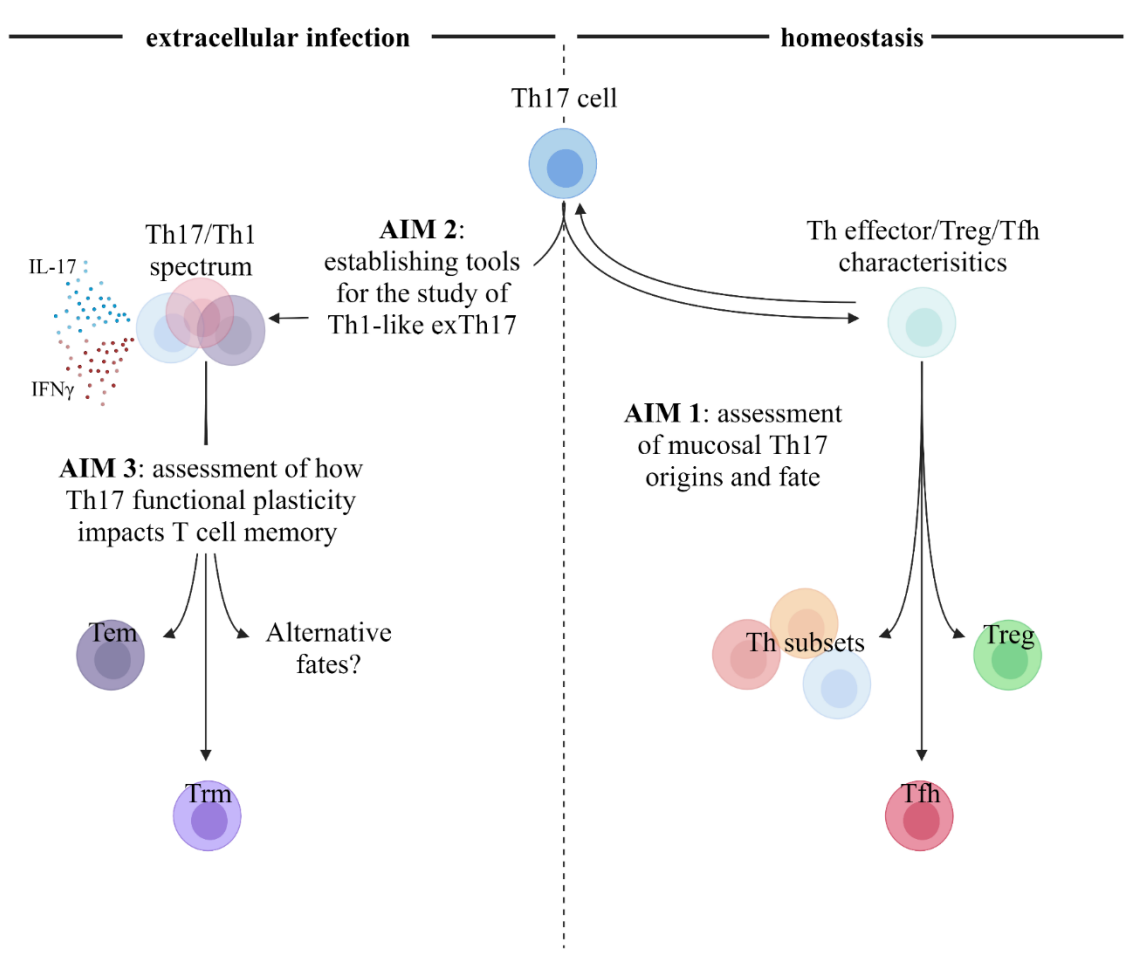

Figure 1.3. Aims of this investigation. Images generated with BioRender.com.

CHAPTER 2: MATERIALS AND METHODS

2.1 MICE

The mouse strains used in this investigation (Table 2.1) were all housed at 21 °C ± 2 °C, 55 % ± 10 % humidity with 12 hr light/dark cycle in 7-7 IVC caging with environmental enrichment of plastic housing and paper bedding at the University of Birmingham Biomedical Services Unit (BMSU) and used according to Home Office guidelines (Project licence P33E83BE5 granted to Professor David Withers). All mice were culled by cervical dislocation. Conditional knockout mice were compared with littermate or other appropriate controls to assess Th17 and Treg cells in unperturbed or genetically modified animals. Furthermore, fate mapping of key cytokine or TF expression were used to track CD4 T cell fate and assess the effects of genetic modifications. Where reporter mice were used, this was done to enable the assessment of cytokine production without the need for *ex vivo* manipulation of cells. For steady state experiments mice at least 6 weeks of age were used while infection models utilised mice at least 8 weeks old with a minimum weight of 20 g. All mice used were bread on the C57BL/6 background with haematopoietic cells expressing the CD45 isoform CD45.2.

Table 2.1. List of mouse models used in this investigation

Mouse strain	Formal name	Genetic modification	Source
Ai14	B6:129S6-*Gt(ROSA)26Sor*$^{tm14(CAG-tdTomato)Hze}$/J	Constitutive tdTomato expression following Cre-mediated recombination (Madisen et al., 2010)	Maintained in BMSU (kindly provided by Dr Wei-Yu Lu)
Cd4^{cre}	B6.Cg-Tg(CD4-cre)1Cwi/BfluJ	Cre expression under the control of the *Cd4* promoter (Lee et al., 2001)	Maintained in Withers colony in BMSU (originally purchased from JAX)
CD30$^{-/-}$	B6.129P2-*Tnfrsf8*^{tm1Mak}/J	Global CD30 deficiency (Amakawa et al., 1996)	Maintained in Withers colony in BMSU (originally provided by Prof Peter Lane)
FoxP3$^{eGFP-Cre-ERT2}$	*Foxp3*$^{tm9(EGFP/cre/ERT2)Ayr}$/J	Inducible Cre expression under the control of the *Foxp3* promoter (Rubtsov et al., 2010)	Maintained in BMSU (kindly provided by Dr Wei-Yu Lu)
Great	B6.129S4-*Ifng*$^{tm3.1Lky}$/J	Co-expression of IFNγ and eYFP (Reinhardt et al., 2009)	Maintained in Withers colony in BMSU (originally provided by Prof Richard Locksley)

Mouse strain	Formal name	Genetic modification	Source
Il17a^{cre}	*Il17a*$^{tm1.1(icre)Stck}$/J	Cre expression under the control of the *Il17a* promoter (Hirota et al., 2011)	Maintained in Withers colony in BMSU (originally provided by Prof Marc Veldhoen)
Itgax^{cre}	B6.cg-Tg(Itgax-cre)1-1Reiz/J	Cre expression under the control of the *Itgax* (encoding CD11c) promoter (Caton et al., 2007)	Maintained in Withers colony in BMSU (originally purchased from JAX)
OX40$^{-/-}$	B6.129S4-*Tnfrsf4*^{tm1Nik}/J	Global OX40 deficiency (Pippig et al., 1999)	Maintained in Withers colony in BMSU (originally provided by Prof Peter Lane)
Ox40l$^{fl/fl}$	*Tnfsf4*$^{tm1.1Tjv}$	Floxed *Ox40l* enabling Cre-mediated deletion (Cortini et al., 2017)	Maintained in Withers colony in BMSU (originally provided by Prof Marina Botto)
Pgk^{cre}	B6.C-Tg(Pgk1-cre)1Lni/CrsJ	Ubiquitous Cre expression under the control of the *Pgk1* (encoding phosphoglycerate kinase 1) promoter (Lallemand et al., 1998)	Maintained in Withers colony in BMSU (originally provided by Dr Caroline Chadwick)
Rora$^{fl/fl}$	Not applicable	Floxed *Rora* (encoding RORα) enabling Cre-mediated deletion (Oliphant et al., 2014)	Maintained in Withers colony in BMSU (originally provided by Dr Andrew McKenzie)
Rorc^{cre}	B6.FVB-Tg(Rorc-cre)1Litt/J	Cre expression under the control of the *Rorc* (encoding RORγt) promoter (Eberl & Littman, 2004)	Maintained in Withers colony in BMSU (originally provided by Prof Dan Littman)
Rorc$^{fl/fl}$	B6(Cg)-*Rorc*^{tm3Litt}/J	Floxed *Rorc* (encoding RORγt) enabling Cre-mediated deletion (Choi et al., 2016)	Maintained in Withers colony in BMSU (originally purchased from JAX)
Rosa26^{tdRFP}	B6.Cg-*Gt(ROSA)26Sor*^{tm1Hjf}	Constitutive tdRFP expression following Cre-mediated recombination (Luche et al., 2007)	Maintained in Withers colony in BMSU (originally provided by Prof Marc Veldhoen)
Smart-17a	B6.129S4-*Il17a*$^{tm1.1Lky}$/J	Co-expression of IL-17A and hNGFR (Price et al., 2012)	Maintained in Withers colony in BMSU (originally provided by Prof Richard Locksley)
Tbx21$^{fl/fl}$	B6.129-*Tbx21*^{tm2Srnr}/J	Floxed *Tbx21* (encoding T-bet) enabling Cre-mediated deletion (Intlekofer et al., 2008)	Maintained in Withers colony in BMSU (originally provided by Prof Marc Veldhoen)
WT	C57BL/6J	none – wild type	Maintained in BMSU

2.2 MEDIA AND REAGENTS

A list of reagents used in this work is provided in Table 2.2 below.

Table 2.2. List of media used on this investigation

Medium	Reagents and concentrations
Culture Medium	Roswell Park Memorial Institute 1640 medium (RPMI) with L- Glutamine (Gibco) with 1 % Penicillin and Streptomycin (Sigma-Aldrich), 1 % L-Glutamine (Sigma-Aldrich) and 10 % ($^{v}/_{v}$) Heat-inactivated foetal bovine serum (FBS) (Sigma-Aldrich).
Staining buffer (SB)	Dulbecco's Phosphate Buffered Saline (DPBS) +$CaCl_2$ +$MgCl_2$ (Sigma-Aldrich) with 2 % Heat-inactivated foetal bovine serum (FBS) (Sigma-Aldrich) and 2.5 M Ethylenediaminetetraacetic acid (EDTA) (Sigma-Aldrich)
Solution A for Haemolytic Gey's Solution	Distilled H_2O with 3.5 % ($^{w}/_{v}$) NH_4Cl, 0.185 % ($^{w}/_{v}$) KCl, 0.15 % ($^{w}/_{v}$) $Na_2HPO_4.12H_2O$, 0.0119 % ($^{w}/_{v}$) KH_2PO_4, 0.5 % ($^{w}/_{v}$) Glucose, 2.5 % ($^{w}/_{v}$) Gelatin and 0.15 % ($^{v}/_{v}$) 1% Phenol red Autoclaved and stored at room temperature (RT)
Solution B for Haemolytic Gey's Solution	Distilled H_2O with 0.42 % ($^{w}/_{v}$) $MgCl_2.6H_2O$, 0.14 % ($^{w}/_{v}$) $MgSO_4.7H_2O$, 0.34 % ($^{w}/_{v}$) $CaCl_2$ Autoclaved and stored at RT
Solution C for Haemolytic Gey's Solution	Distilled H_2O with 2.25 % ($^{w}/_{v}$) $NaHCO_5$ Autoclaved and stored at RT
Haemolytic Gey's Solution	70 % ($^{v}/_{v}$) distilled H_2O, 20 % ($^{v}/_{v}$) Solution A, 5 % ($^{v}/_{v}$) Solution B and 5 % ($^{v}/_{v}$) Solution C Passed through a 0.22 µm Minisart singe use filter unit (Sartorius Stedim) and stored at 4^{o}C
Hank's Balanced Salt Solution (HBSS) with EDTA	Calcium and Magnesium free HBSS (Sigma-Aldrich), 2.5M EDTA (Sigma-Aldrich)
HBSS with FBS	Calcium and Magnesium free HBSS (Sigma-Aldrich), 2% ($^{v}/_{v}$) FBS (Sigma-Aldrich)
Lysogeny broth (LB) for *C.rodentium* liquid cultures	Deionised water with 1% ($^{w}/_{v}$) sodium chloride (ThermoFrisher), 1% ($^{w}/_{v}$) tryptone (Sigma-Aldrich), 0.5% ($^{w}/_{v}$) yeast extract and 50 µg/ml nalidixic acid (Sigma-Aldrich)
LB Agar plates for *C.rodentium*	LB broth with 1% ($^{w}/_{v}$) Agar (Sigma-Aldrich)

2.3 PREPARATION OF CELL SUSPENSIONS FROM MURINE TISSUES

2.3.1 Centrifugation of single cell suspensions

Single cell suspensions were pelleted by centrifugation at 4^{o}C, 453 rcf for 6 minutes, unless otherwise stated.

2.3.2 Lymphocyte isolation from large intestinal lamina propria

Large intestine preparation was carried out using two methods over the course of this investigation. These were found to be equivalent, therefore, the individual method used is not highlighted for each experiment.

Colon and caecum were dissected and the surrounding fat removed using curved forceps. Following fat removal, colon and caecum were opened longitudinally and washed with HBSS with FBS. Tissue was then cut into 0.5 cm sections and incubated twice with HBSS with EDTA in a shaking incubator at 37 ^{o}C for 15 min, each time washing with HBSS, and then digested in culture medium with digestion enzyme mix at 37 ^{o}C with agitation until the connective tissue was fully digested (approximately 45 min). Cells were passed through 100 and 70 µm strainers (Greiner Bio-One), each time washed with 5 ml SB or RPMI (Gibco).

Method 1 digestion enzyme mix: culture medium with 0.85 mg/ml Collagenase V (Sigma), 1.25 mg/ml Collagenesae D (Roche), 1 mg/ml Dispase (Gibco) and 30 µg/ml DNAse I (Roche).

Method 2 digestion enzyme mix: culture medium with 1 mg/ml Collagenase VIII (Sigma) and 30 µg/ml DNAse I (Roche).

2.3.3 Lymphocyte isolation from small intestinal lamina propria

Small intestine was dissected and the surrounding fat removed using curved forceps. Following fat removal, Peyer's patches were excised and the small intestine opened longitudinally and washed with HBSS with FBS. Tissue was then cut into 0.5 cm sections and incubated twice with HBSS with EDTA with agitation at 37 oC for 20 min, each time washing with HBSS, and then digested in culture medium with 1 mg/ml Collagenase VIII (Sigma) and 30 µg/ml DNAse I (Roche) in a shaking incubator at 37 ^{o}C for 15 min. Cells were passed through a 100 µm and two 70 µm strainers (Greiner Bio-One), each time washed with 5 ml SB or RPMI (Gibco).

2.3.4 Lymphocyte isolation from spleen

Spleens were dissected and, following fat removal, crushed through 70 µm strainers (Greiner Bio-One) and washed thoroughly with RPMI (Gibco). Cells were harvested via centrifugation and the pellet resuspended in 5 ml Gey's solution. Following incubation at 4 °C for 5 min cells were passed through a 70 µm strainer (Greiner Bio-One), centrifuged and resuspended in RPMI (Gibco) or SB.

2.3.5 Lymphocyte isolation from lymph nodes

Dissected lymph nodes were placed in small petri dishes (Nunclon, ThermoScientific) with 3 ml RPMI (Gibco). Fat depositions around the lymph nodes were removed under a dissecting microscope using forceps. Lymph nodes were then teased apart by being placed in 1.5 ml microtubes (Eppendorf) and cut into small pieces with scissors. Teased tissue was crushed through 70 µm strainers (Greiner Bio-One) and washed with RPMI (Gibco).

2.3.6 Lymphocyte isolation from caecal and Peyer's patches

1 caecal and 5-7 Peyer's patches were excised from caecum and small intestine, respectively, taking care to minimise inclusion of intestinal wall tissue, and placed in RPMI (Gibco). Any remnants of luminal contents were removed and the tissues placed in 1.5 ml microtubes (Eppendorf) to be teased apart. Peyer's patches isolated from individual animals were processed together but separately from patches from other animals while caecal patches from 3-4 mice were pooled per experiment. Teased tissues were incubated in 1 ml RPMI (Gibco) with 250 µg/ml Collagenase/Dispase (Roche) and 25 µg/ml DNAse I (Roche) at 37 °C for 20 min. Digestion was stopped with 20 µl 0.5 M EDTA (Sigma-Aldrich), tissues crushed through 70 µm strainers (Greiner Bio-One) and washed thoroughly with RPMI or SB.

2.3.7 Lymphocyte isolation from lung

Prior to lung isolation but immediately after cervical dislocation, mice were perfused with ice-cold DPBS (Life Technologies). To perfuse the mouse the right atrium was pierced with scissors and a needle

inserted into the left ventricle. 10 ml DPBS (Life technologies) was injected flushing the lungs of blood. Lungs were then dissected and placed in a 1.5 ml microtube (Eppendorf) with culture media. The tissue was teased apart, as described before, and transferred into a 50 ml conical tube (Corning). The tissue was incubated with agitation in 5 ml culture medium with 42.4 µg Liberase TM (Roche) and 0.02 mg/ml DNAseI (Roche) at 37 °C for 45 min and crushed through 70 µm strainers (Greiner Bio-One). Samples were washed in RPMI, centrifuged and incubated in Gey's solution at 4 °C for 5 min. Following incubation cells were passed through a 70 µm strainer (Greiner Bio-One), centrifuged and resuspended in RPMI (Gibco) or SB.

2.4 *EX VIVO* RESTIMULATION OF ISOLATED LYMPHOCYTES

Single cell suspensions were incubated in culture media with 50 ng/ml phorbol-12-myristate 13-acetate (PMA, Sigma-Aldrich), 1.5 µM ionomycin (Sigma-Aldrich) and 10 µg/ml brefeldin A (Sigma-Aldrich) at 37 °C for 3 hrs. Restimulation was carried out in 0.3-1 ml final volume depending on the number of cells in culture, with each sample including no more than a 1/4 single cell suspension from an individual small intestine, 1/5 single cell suspension from an individual spleen, 1/2 single cell suspension from the mesenteric lymph node or the whole single cell suspension from the colon and other lymph nodes. Lymphocytes isolated from caecal and Peyer's patches or the lung did not undergo *ex vivo* restimulation.

2.5 FLOW CYTOMETRY

If not already in SB, single cell suspensions were centrifuged and each sample was resuspended in the appropriate volume of staining buffer. The proportion of single cell suspension stained varied for each tissue and experiment but generally included the whole colon and small peripheral lymph nodes but no more than 1/4 from the small intestine, 1/5 from the spleen and 1/2 from the mesenteric lymph node and lung. Antibody staining was performed in 100 µl final volume in 96-well plates (ThermoScientific), unless otherwise stated. Stains were removed by centrifugation at 4 °C, 453 rcf for

3 min. Cells were washed between steps by resuspension in DPBS (live cells) or permeabilisation buffer (fixed cells) followed by centrifugation. Table 2.3 lists the antibodies used in flow cytometric analyses.

Table 2.3. List of antibodies used in this investigation

Antibody specificity	Conjugate (dilution)	Clone	Manufacturer
B220 (CD45R)	FITC (1:200)	RA3-6B2	eBioscience
	PE/Cy7 (1:200)	RA3-6B2	eBioscience
	eFluor450 (1:200)	RA3-6B2	BioLegend
CD3ε	FITC (1:100)	145-2C11	eBioscience
	PE/Cy7 (1:200)	145-2C11	eBioscience
	APC (1:200)	145-2C11	eBioscience
	BV650 (1:200)	145-2C11	BD Horizon
	BV605 (1:200)	17A2	BioLegend
	BUV395	145-2C11	BD Horizon
CD4	BV785 (1:300)	RM4-5	BioLegend
	BV711 (1:300)	RM4-5	BioLegend
	BV510 (1:300)	RM4-5	BioLegend
	APC (1:200)	RM4-5	BioLegend
	BUV395	RM4-5	BD Horizon
CD8a	BV711 (1:300)	53-6.7	BioLegend
	APC (1:200)	53-6.7	BioLegend
	BV510 (1:300)	53-6.7	BD Horizon
CD11b	FITC (1:300)	M1/70	eBioscience
	PE/Cy7 (1:200)	M1/70	eBioscience
	eFluor450	M1/70	eBioScience
CD11c	FITC (1:300)	N418	eBioscience
	eFLuor450 (1:200)	N418	BioLegend
	PE/Cy7 (1:200)	N418	eBioscience
CD45	BV785 (1:100)	30-F11	BioLegend
	FITC (1:200)	30-F11	BD Horizon
	BUV395 (1:200)	30-F11	BD Horizon
CD45.2	eFluor450 (1:200)	104	eBioscience
	BV785 (1:100)	104	BioLegend
	FITC (1:200)	104	BD Horizon
	BUV395 (1:200)	104	BD Horizon
CD62L	BV711 (1:100)	MEL/14	BioLegend
	PE/Cy7 (1:500)	MEL/14	eBioscience
	APC (1:1500)	MEL/14	eBioscience
CD69	BV711 (1:100)	H1.2F3	eBioscience
CD103	PE/Cy7 (1:200)	2.00E+07	BioLegend
CD44	BV785 (1:200)	IM7	eBioscience
	APC (1:100)	IM7	BioLegend
OX40	BV711 (1:50)	OX86	BioLegend
hNGFR (CD271)	Pe/Cy7 (1:50)	ME20.4	BioLegend
RORγt	PE (1:100)	AFKJS-9	eBioscience
	APC (1:100)	AFKJS-9	eBioscience
	eFluor660 (1:100)	AFKJS-9	eBioscience
T-bet	eF660 (1:50)	eBio4B10	eBioscience
	PE-Cy7 (1:50)	eBio4B10	eBioscience
FoxP3	eFluor450 (1:100)	FJK-16s	eBioscience

Antibody specificity	Conjugate (dilution)	Clone	Manufacturer
	FITC (1:100)	FJK-16s	eBioscience
	APC (1:100)	FJK-16s	eBioscience
IL-17A	BV605 (1:100)	TC11-18H10	BioLegend
IL-17F	AF488 (1:100)	9D3.1C8	eBioscience
IL-22	PerCP/eFluor710 (1:100)	1H8PWSR	BioLegend
IFNγ	BUV737 (1:400)	XMG1.2	BD Horizon
TNFα	PE (1:200)	MP6-XT22	BioLegend
IL-10	PE/Cy7 (1:100)	JES5-16E3	eBioscience

2.5.1 2W1S:I-A^b and CLIP:I-A^b tetramer and antibody staining to detect surface marker expression

Where peptide:I-A^b tetramer staining was performed, this was carried out in SB at room temperature (RT) for 60min prior to any further antibody staining. Tetramers were diluted 1:200-1:400. Antibody staining for the detection of surface marker expression was carried out in SB at 37 °C for 40 min.

2.5.2 Dead cell identification

Immediately prior to fixation, or data acquisition if live cells were used, cell suspensions were incubated in LIVE/DEAD™ Fixable Near-IR Dead Cell Stain (Invitrogen, diluted 1:1000) viability dye. Dead cell staining was carried out in DPBS at 4 °C for 15 min.

2.5.3 Staining to detect intracellular protein expression

Following dead cell staining cells were washed in DPBS twice and fixed and permeabilised. Three fixation and permeabilisation methods were used depending on the aims of the experiment and mouse strains used. All methods used a combination of the fixatives and permeabilisation buffers from the BD Cytofix/Cytoperm™ Fixation/Permeabilisation Solution Kit (BD Bioscience) and the eBioscience™ FoxP3/Transcription Factor Staining Buffer Set (Invitrogen). Regardless of the kit used, fixation was carried out at 4 °C for 1 hour.

Method 1 – detection of cytoplasmic proteins: To enable detection of proteins present in the cytoplasm, such as cytokines following *ex vivo* restimulation, cells were fixed and permeabilised using the BD Cytofix/Cytoperm™ Fixation/Permeabilisation Solution Kit (BD Bioscience). Antibody staining

was carried out in the BD Cytofix/Cytoperm™ permeabilisation buffer (BD Biosciences) at RT for 1 hr or overnight.

Method 2 – detection of nuclear proteins in mice with no fluorescent reporter expression: To enable detection of nuclear proteins, such as TFs, cells were fixed and permeabilised using the eBioscience™ FoxP3/Transcription Factor Staining Buffer Set (Invitrogen). Antibody staining was carried out in the eBioscience™ FoxP3/Transcription Factor Staining Buffer Set permeabilisation buffer (Invitrogen) at RT for 1 hr or overnight. This method is also suitable for the detection of cytoplasmic proteins in mice without any fluorescent reporter expression.

Method 3 – detection of nuclear proteins in mice with fluorescent reporter expression: Cells fixed with the eBioscience™ FoxP3/Transcription Factor Staining Buffer Set fixative (Invitrogen) lose reliable expression of fluorescent reporters. Therefore, TF staining methods were modified to combine the BD Cytofix/Cytoperm™ fixative (BD bioscience) and eBioscience™ FoxP3/Transcription Factor Staining Buffer Set permeabilisation buffer (Invitrogen). Antibody staining in the permeabilisation buffer following this method must be carried out overnight with a minimum of 12 hrs required for optimal staining. This method is also suitable for the detection of cytoplasmic proteins in mice with fluorescent reporter expression.

2.5.4 Tetramer-based magnetic bead enrichment

2W1S:I-A^b tetramer-based magnetic bead enrichment was carried out on lymphocytes isolated from small intestinal lamina propria, spleen, mesenteric lymph nodes, pooled peripheral lymph nodes and lungs to enable identification and analyses of rare antigen-specific populations in these tissues. APC-conjugated 2W1S:I-A^b tetramer staining was carried out as before but in a modified staining volume (up to 300-500 µl depending on tissue) to account for the increased number of cells in each sample. Due to the increased volumes, staining was carried out in 5 ml round bottom tubes (BD Falcon) and wash steps in 1-2 ml DPBS with centrifugation for 5 min. Following, tetramer staining, the samples were washed twice and incubated with 60 µl Anti-APC MicroBeads (Miltenyi) with 240 µl SB at 4 °C

for 15 min. During incubation, LS MACS columns (Miltenyi) were placed in MACS Separator magnets (Miltenyi) and prepared by rinsing with 3 ml SB. following incubation, 2 ml DPBS was added to each sample, the cells were pelleted via centrifugation and the supernatant aspirated. Each sample was resuspended in 500 µl SB, passed through a 30 µm Pre-Seapartion filter (Miltenyi) and applied onto the prepared column. The column was washed 3 times with 3 ml SB, taking care to ensure that the column reservoir emptied completely between each step, and the flow-through containing unlabelled cells collected. To elute labelled cells, the column was removed from the magnetic MACS separator (Milteny) and placed in a collection tube. Cells retained in the column were flushed with 5 ml SB using the plunger. Flow-through and enriched fractions were pelleted and resuspended in the appropriate volume of SB, ready for antibody and tetramer staining. Flow-through was stained to enable assessment of enrichment efficiency and quantification of total numbers of 2W1S-specific CD4 T cells within each tissue.

2.5.5 Flow cytometric analyses

Samples were washed in DPBS following antibody staining and resuspended in up to 400 µl SB, depending on the total number of cells within each sample. 10 000 SPHERO™ AccuCount Particles (Spherotech) were added to each sample to enable quantification of the total number of cells within each sample and tissue. Samples were run on the BD LSRFortessa™ X-20 (BD Biosciences) and data acquired using the BD FACSDiva software (BD Biosciences, version 9.0). Acquired data were analysed using the FlowJo software (Treestar, version 10.8). Following data acquisition, the following equations were used to quantify the total number of cells per tissue:

Quantification of cells per tissue in the absence of tetramer-based enrichment

This method is used to quantify the total number of cells in any population of interest within a sample from any tissue that had not undergone tetramer-based enrichment.

$$x = \frac{10000 * cell\ count\ in\ sample\ acquired}{bead\ count\ in\ sample\ acquired} * \frac{1}{P}$$

where x is the total number of cells of interest within the whole tissue and P is the proportion of tissue stained.

Quantification of cells per tissue following tetramer-based enrichment

This method is used to quantify the number of 2W1S-specific CD4 T cells and subpopulations of 2W1S-specific CD4 T cells following 2W1S:I-A^b tetramer-based enrichment.

$$y = \frac{10000 * cell\ count\ in\ sample\ acquired}{bead\ count\ in\ sample\ acquired} * MF$$

where y is the total number of cells of interest within the whole tissue and MF is the multiplication factor that adjust for the lack of 100% efficiency in enrichment. MF is calculated as follows:

$$MF = \frac{\frac{10000 * 2W1S(enriched)}{beads(enriched)}}{\frac{10000 * 2W1S(enriched)}{beads(enriched)} + \frac{10000 * 2W1S(ft)}{beads(ft)} * \frac{1}{P(ft)}}$$

where 2W1S(enriched) and beads(enriched) are the numbers of 2W1S-specific CD4 T cells and beads in the acquired enriched sample, respectively, 2W1S(ft) and beads(ft) are the numbers of 2W1S-specific CD4 T cells and the number of beads acquired in the flow-through sample, respectively while P(ft) is the proportion of the flow-through stained. The proportion of the enriched sample stained does not appear in any equations as it was always equal to 1.

2.6 *CITROBACTER RODENTIUM* INFECTION

Mice were inoculated via oral gavage with 2-3*10^9 colony forming units (CFU) of *C.rodentium* (strain ICC169) resuspended in sterile DPBS. Wild type *C.rodentium* and *C.rodentium-2W1S* were prepared in the same way.

2.6.1 Preparation of *C.rodentium* inoculum

15 ml LB for *C.rodentium* (Table 2.2) was seeded with an aliquot of nalidixic acid-resistant *C.rodentium* from a frozen stock. Cultures were grown overnight at 37 ^oC with agitation. Following incubation, pre-

cultures were centrifuged (4 °C, 3220 rcf, 10 min) and bacterial pellets resuspended in 1.5 ml sterile DPBS. Each mouse received 200 µl inoculum via oral gavage, resulting in delivery of 2-3*10^9 CFU. Each 15 ml culture generates inoculum sufficient for the infection of only 5 mice due to loss of some volume in syringes and gavage needles used for infection. Where larger groups of mice were infected multiple 15 ml cultures were created and the inoculum pooled following resuspension in DPBS.

The precise number of viable CFU delivered in 200 µl of the inoculum was assessed by 8 serial 10-fold dilutions. 20 µl dots of the lowest three dilutions (10^{-8}, 10^{-7} and 10^{-6}) were placed on LB Agar plates (Table 2.2) and the plates incubated overnight at 37 °C. The number of colonies per 20 µl dot was counted and the total number viable *C.rodentium* CFUs delivered to each mouse calculated as follows:

$$CFU\ per\ 200\mu l\ inoculum = average\ number\ of\ CFU\ per\ 20\mu l\ dot * 10 * DF$$

where DF is the dilution factor (e.g. following 8 serial 10-fold dilutions DF is 10^8).

2.6.2 Frozen stock preparation

To prepare frozen *C.rodentium* stocks a 50-100 ml culture was grown overnight as described above. The bacteria were centrifuged (4 °C, 3220 rcf, 10 min) and resuspended in 5 ml LB for *C.rodentium* with 15 % ($^v/_v$) glycerol and stored at -80 °C in 1 ml aliquots. Viability of newly generated stocks was tested using following 3-7 days of storage following the method described in section 2.6.1. Stocks yielding at least 2*10^9 CFU in 200 µl inoculum were considered of acceptable for use in infections.

2.6.3 Colonisation assessment

Colonisation efficiency and duration were assessed by quantification of faecal bacterial load. Faecal samples were collected from individual mice placed in clean containers and allowed to produce stool pellets. Pellets were weighed, placed in 1.5 ml microtubes (Eppendorf) and homogenised in 1 µl DPBS for each 100 µg of faeces. Homogenates were pulsed in a microcentrifuge for 3 s to move large particles to the bottom of the tube and leave a liquid supernatant containing bacteria on top. 6 serial

10-fold dilutions were carried out and 20 µl dots of all dilutions plated and incubated as described in section 2.6.1. The bacterial burden was calculated as follows:

$$CFU\ per\ gram\ of\ faeces = \frac{average\ number\ of\ CFU\ per\ 20\mu l\ dot * 10000 * DF}{20}$$

Successfully colonised mice returned a faecal bacterial load of >10^7 CFU/g faeces on day 6-8 following inoculation. Tracking bacterial burden at later timepoints aided the assessment of the duration of antigen persistence and the ability of the animals to control the infection.

2.7 MICROBIOMICS

Microbiomic analyses required the collection of stool samples. Mice were placed in sterile containers and allowed to produce two pellets. Pellets were collected with sterile forceps, placed in barcoded collection tubes containing nucleic acid stabilisation buffer (Transnetyx) and transferred to Transnetyx. DNA extraction was performed by Transnetyx using the DNEasy 96 PowerSoil Pro QIAcube extraction kit (Qiagen) following manufacturer's instructions. Following DNA extraction and quality control, sequencing libraries were prepared using the KAPA HyperPlus library preparation protocol (Roche) using unique dual indexed adapters to ensure correct read and organism assignment. Libraries were sequenced on NovaSeq (Illumina) following the shotgun sequencing method. Sequencing data were analysed against the OneCodex database, consisting of over 100 000 microbial genomes and including the mouse genome to enable removal of host reads. Each sequence was compared against the OneCodex database by exact alignment using k-mers (k=31) (Wood & Salzberg, 2014). Following k-mer based classification sequencing artifacts were removed based on relative unique k-mer frequency. Finally, species-level relative abundance was estimated based on sequencing depth and coverage across the entirety of the OneCodex reference database.

2.7 STATISTICAL ANALYSES

Data were analysed using Graphpad Prism version 9.0. Datasets containing fewer than 3 datapoints were not included in statistical analyses. Where groups of data were shared between different figures,

the statistical analyses shown in each graph compared only the groups of data shown, not the entire dataset. Shapiro-Wilk tests were used to assess normality of data. Table 2.4 lists statistical tests used to compare datasets. Statistically significant differences are illustrated by p values.

Table 2.4. Statistical tests performed in this investigation

	Unpaired data		Paired data	
	Data normally distributed (mean±SD or mean+SD shown)	Data not normally distributed (median shown)	Data normally distributed (mean±SD or mean+SD shown)	Data not normally distributed (median shown)
2 groups	Unpaired t test	Mann-Whitney U test	Paired t test	Wilcoxon matched pairs test
3 or more groups	One-Way ANOVA	Kruskal-Wallis test	Repeated Measures One-Way ANOVA	X – not performed

CHAPTER 3: CHARACTERISING THE INTESTINAL CD4 T CELL COMPARTMENT

3.1 INTRODUCTION

When first identified, CD4 T cells producing IL-17 were not classified as a distinct T helper lineage (Fossiez et al., 1996; Yao et al., 1995). Later, Th17 characterised by IL-17A expression were thought to be IL-23-dependent CD4 T cells associated with pathology (Langrish et al., 2005). However, it has since been established that this CD4 T cell subset is highly heterogeneous with both protective and harmful effects. Th17 cells enriched in mucosal surfaces act in concert with other immune populations to maintain mucosal homeostasis by controlling commensal microbe expansion, promoting barrier repair and mediating pathogen clearance. An absence of Th17 cells impairs protection against certain bacterial and fungal species and drives mucosal dysbiosis (Atarashi et al., 2015; Okada et al., 2015). Conversely, Th17 cells can also drive disease pathogenesis both systemically and at barrier sites. Pro-inflammatory Th17 cells are associated with Crohn's disease, cancer, uveitis and multiple sclerosis in humans and confirmed as causative agents of disease progression using mouse models (Annunziato et al., 2007; Hirota et al., 2011; Langowski et al., 2006; Yoshimura et al., 2009). These observations have made Th17 cells and their effector cytokines important therapeutic targets.

Further increasing Th17 cells' appeal as targets of interventions, Th17 cell plasticity has been specifically linked to diseases characterised by inappropriate mucosal and systemic inflammation. CD4 T cells producing both IL-17A and the Th1 cell-associated cytokine IFNγ were described in inflammatory bowel disease patients (Annunziato et al., 2007). In addition, the generation of Th17 cell lineage tracing mouse models identified fully differentiated Th1-like IL-17A^{-}IFNγ^{+} cells of a Th17 cell origin. These cells are drivers of autoimmune and autoinflammatory diseases previously thought to arise simply from Th1 cell dysregulation (Hirota et al., 2011). Moreover, lineage tracing has also shown that Th17 cells have the capacity to transdifferentiate into Treg cells (Gagliani et al., 2015), a process

that may be subverted in the tumour microenvironment to dampen protective immune responses (Downs-Canner et al., 2017). Importantly, Th17 cell plasticity is not strictly detrimental to health. Th17 cells play important roles in pathogen clearance (Mangan et al., 2006) with potent induction of fully differentiated Th1-like IL-17A^{-}IFNγ^{+} 'exTh17' cells (Omenetti et al., 2019). Moreover, Th17 cell conversion to Tfh cells, another CD4 T cell subset, is thought to aid the generation of appropriate mucosal antibody responses (Hirota et al., 2013).

This extensive heterogeneity of cell function and phenotypes poses significant challenges to targeting these cells. Non-specific inhibition of Th17 cells may affect homeostatic populations crucial to the control of opportunistic mucosal pathogens (Ivanov et al., 2009). Consequently, interventions that successfully limit Th17 cell-mediated inflammation in one condition can be neutral or even detrimental in others (Bilal et al., 2018; Hueber et al., 2012; Singh et al., 2018; Targan et al., 2016). A great deal of work has therefore focused on assessing the signals controlling Th17 cell fate and stability, pinpointing both environmental and cell-intrinsic factors. Environmental signals, integrated through the actions of APC-derived cytokine combinations and AhR activation, drive potent induction of Th17 cell differentiation (Korn et al., 2007; Veldhoen et al., 2008; Veldhoen et al., 2006). Further signals, such as IL-23 have the potential to drive post-developmental functional plasticity associated with acquisition of alternative phenotypes (Lee et al., 2009), a process also linked to lower intrinsic lineage stability (Mukasa et al., 2010). However, gaps in our understanding remain with studies employing different approaches returning seemingly contradictory results. The work presented in this chapter therefore aimed to characterise intestinal CD4 T cell populations by employing a number of complementary experimental models and approaches that have become key tools in overcoming the difficulties associated with studying the mucosal immune compartment. I sought to better understand the relationship between intestinal CD4 T cell populations with a focus on the extent to which Th17 cells give rise to or differentiate from other major mucosal CD4 T cell subsets.

3.2 T HELPER 17 CELLS ARE ENRICHED AT MUCOSAL SURFACES

To assess Th17 cell prevalence at distinct anatomical locations I tested the expression of the Th17 master TF RORγt (Ivanov et al., 2006; X. O. Yang, B. P. Pappu, et al., 2008) and canonical cytokine IL-17A (Harrington et al., 2005; Veldhoen et al., 2006) in $CD44^{hi}$ CD4 T cells in the spleen, two intestinal mucosal sites (small intestine lamina propria – SILP and colon lamina propria – CLP) and their draining mLN. In 2LT this formed only part of the total CD4 T cell population due to the presence of numerous naïve $CD44^{lo}$ CD4 T cells. CD44 staining failed to resolve $CD44^{hi}$ and $CD44^{lo}$ CD4 T cell populations in the intestinal mucosal compartment but resulted in a decrease in overall signal intensity (Fig3.1a). This was not interpreted as the SILP and CLP containing only $CD44^{lo}$ naïve CD4 T cells. Instead, as both these effector sites are expected to harbour only activated CD4 T cells, the lower CD44 signal intensity is likely a result of limiting anti-CD44 antibody amounts.

The proportion of CD4 T cells expressing RORγt was found to be higher in the intestinal mucosa than in 2LT but not different between the two mucosal sites, SILP and CLP. In addition, $ROR\gamma t^{+}$ activated CD4 T cells were enriched in the mLN compared to splenic $CD44^{hi}$ CD4 T cells, reflecting the systemic compartment (Fig3.1b-d). Strikingly, IL-17A expression was not concordant with RORγt expression with a high frequency only evident in the SILP (Fig3.1e-g). In addition, the SILP contains the largest numbers of RORγt and IL-17A expressing cells pointing to an enrichment of Th17 cells at this site (Fig3.1d,g). However, while total cellularity provides key information on Th17 cell distribution, the site-specific differences in $CD44^{hi}$ CD4 T cell population size must be kept in mind when assessing these results – the CLP contains far fewer cells than SILP and 2LT. Nonetheless, the high frequency of CD4 T cells expressing the Th17 cell master TF RORγt but not the Th17 cell cytokine IL-17A highlight the fact that $ROR\gamma t^{+}$ T cell populations not dedicated to IL-17A production persist in some microenvironments. Possible explanations are that these are not Th17 cells or that they have lost part of their Th17 cell effector function. Th17 cells show a high degree of plasticity with a range of alternative fates described (Hirota et al., 2011; Hirota et al., 2013).

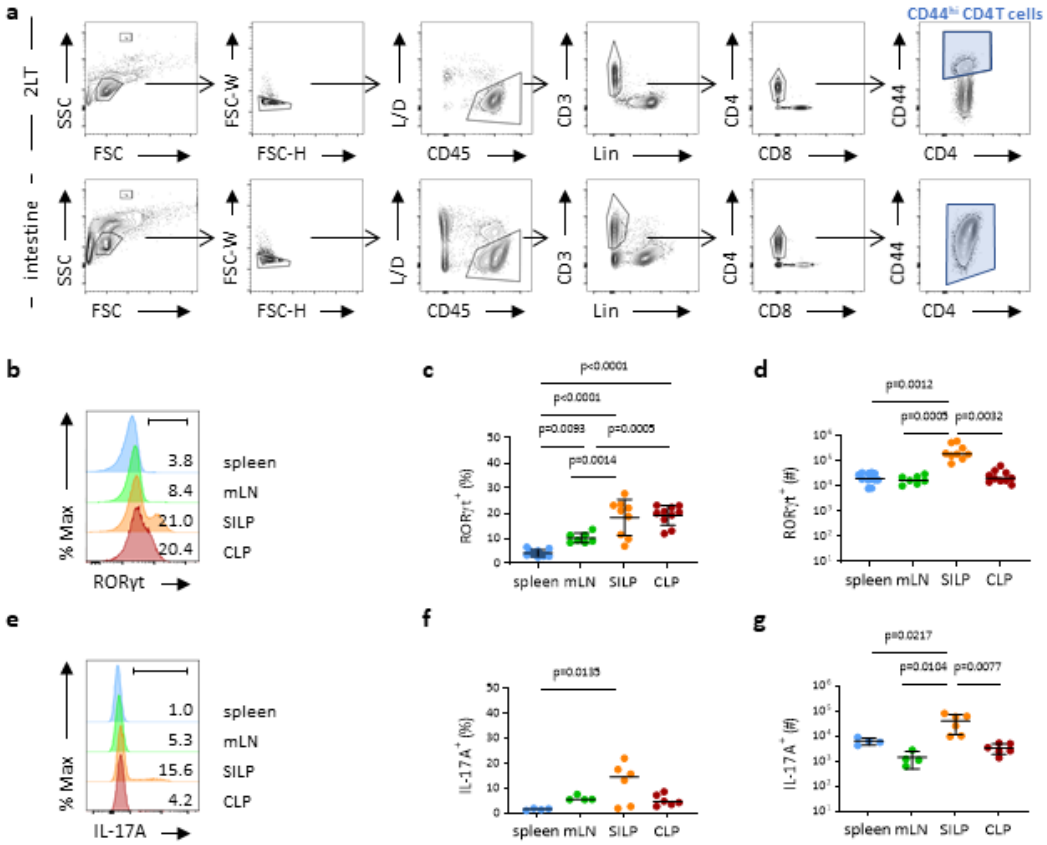
a
CD44hi CD4 T cells
2LT
intestine
SSC
FSC
FSC-W
FSC-H
L/D
CD45
CD3
Lin
CD4
CD8
CD44
b
% Max
RORγt
3.8
8.4
21.0
20.4
spleen
mLN
SILP
CLP
c
RORγt+ (%)
p<0.0001
p<0.0001
p=0.0093
p=0.0005
p=0.0014
spleen mLN SILP CLP
d
RORγt+ (#)
p=0.0012
p=0.0005
p=0.0032
spleen mLN SILP CLP
e
% Max
IL-17A
1.0
5.3
15.6
4.2
spleen
mLN
SILP
CLP
f
IL-17A+ (%)
p=0.0135
spleen mLN SILP CLP
g
IL-17A+ (#)
p=0.0217
p=0.0104
p=0.0077
spleen mLN SILP CLP

Figure 3.1. Th17 cells are enriched in intestinal mucosal surfaces at steady state

The prevalence of Th17 cells at steady state was assessed by Th17 cell master transcription factor RORγt and Th17 cell canonical cytokine IL-17A expression in $CD44^{hi}$ CD4 T cells.

a) Representative flow cytometry plots illustrating gating strategy to identify $CD44^{hi}$ CD4 T cells in 2LT, (top) and intestinal mucosa (bottom).

b) Representative histograms showing RORγt expression in parent populations identified in (a) in spleen, mLN, SILP and CLP.

c-d) Quantification of the proportion (c) and total number (d) of $ROR\gamma t^{+}$ cells within the parent population in spleen, mLN, SILP and CLP. Spleen n=12, data pooled from 5 independent experiments, mLN n=7, data pooled from 3 independent experiments, SILP n=9, data pooled from 4 independent experiments, CLP n=10, data pooled from 5 independent experiments.

e) Representative histograms showing IL-17A expression in parent populations identified in (a) in spleen, mLN, SILP and CLP following *ex vivo* restimulation with PMA and Ionomycin.

f-g) Quantification of the proportion (f) and total number (g) of $IL\text{-}17A^{+}$ cells within the parent population in spleen, mLN, SILP and CLP. Spleen and mLN n=4, data from 1 experiment, SILP and CLP n=6, data pooled from 2 independent experiments.

Values on histograms represent percentages. Normality was tested using Shapiro-Wilk test. Lines on graphs show mean±SD (c, g) or median (d, f). Significance was tested using One-Way ANOVA (c, g) or Kruskal-Wallis test (d, f).

3.3 IL-17A 'FATE MAPPING' REVEALS MICROENVIRONMENT-SPECIFIC CD4 T CELL FATES

The *Il17a*^{cre}*Rosa26*^{tdRFP} IL-17A 'fate-mapper' mouse was used to account for Th17 cell plasticity. *Il17a*^{cre} mice generated to enable Cre recombinase expression under the control of the *Il17a* promoter (Hirota et al., 2011) were crossed with 'fate mapping' mice that constitutively express tandem-dimer red fluorescent protein (tdRFP) following Cre-mediated recombination (Luche et al., 2007). The sequence encoding *Cre* is inserted into the *Il17a* locus, disrupting normal expression of IL-17A. Therefore, mice must be bred to be heterozygous for the wild type (WT) and *Cre* alleles to enable both IL-17A and Cre to be produced. TdRFP is inserted into the constitutively expressed *Rosa26* locus but is preceded by a transcriptional stopper sequence flanked by locus of crossover [x] in P1 (LoxP) sites (floxed) preventing protein expression. Cre recombinase recognises the LoxP sites and excises the stopper sequence enabling gene transcription and tdRFP expression (Fig3.2a). Therefore, in *Il17a*^{cre}*Rosa26*^{tdRFP} mice heterozygous for the WT and *Cre* alleles, Th17 cell priming results in IL-17A and Cre expression that, in turn, leads to tdRFP production in the cells. TdRFP expression is maintained on cessation of IL-17A production and even after cell division, permanently marking IL-17A-producing cells and their progeny.

A high frequency of IL-17A fate reporting tdRFP^{+} CD44^{hi} CD4 T cells was observed only in the SILP (Fig3.2b-c) suggesting that the relative scarcity of IL-17A^{+} cells in the CLP (Fig3.1) reflected not a loss of characteristic cytokine production by Th17 cells but a lack of IL-17A induction. Data therefore indicated that even though RORγt^{+} CD4 T cells were abundant in the colon they had not, at any point, made IL-17A. In line with cytokine expression data, CD44^{hi} CD4 T cells fate reporting IL-17A production were most abundant in the SILP (Fig3.2d).

Assessing *ex vivo* restimulation-induced IL-17A production and tdRFP expression in conjunction (Fig3.2b), it was evident that the 'fate mapping' system did not function with 100% efficiency. At steady state all tissues harboured IL-17A^{+}tdRFP^{-}, IL-17A^{+}tdRFP^{+} double positive and IL-17A^{-}tdRFP^{+} activated CD4 T cells (Fig3.2e-g). The presence of IL-17A^{+}tdRFP^{-} cells pointed to incomplete

recombination resulting in only partial fate reporting. Approximately half of all IL-17A$^+$ cells expressed tdRFP at steady state regardless of anatomical location (Fig3.2h-i) suggesting that Cre-mediated recombination can underreport IL-17A production history but shows no tissue-specific differences. Cells that fate report IL-17A production (tdRFP$^+$) but do not produce this cytokine could result from erroneous tdRFP expression or the loss of IL-17A following induction. The *Rosa26^{tdRFP}* transgene construct minimises the potential of read-through reporter expression in the absence of recombination (Luche et al., 2007), pointing to the latter being the main mechanism of action in IL-17A$^-$tdRFP$^+$ cell generation. The highest proportion of tdRFP$^+$ cells still expressing IL-17A was found in the mLN (Fig3.2j-k). Underlying this observation, Th17 cells are primed here and are expected to largely egress to effector sites prior to differentiation into alternative CD4 T cell subsets.

IL-17A expression was maintained in over half of intestinal CD4 T cells fate reporting cytokine production but lost in others (Fig3.2k). Th17 cell activation in different contexts has been shown to drive either stable IL-17A expression or eventual loss of IL-17A with or without acquisition of the Th1 cell-associated proinflammatory cytokine IFNγ (Hirota et al., 2011; Omenetti et al., 2019). Furthermore, Th17 cell differentiation into cells with a regulatory phenotype and Treg cell acquisition of Th17 cell-like functions such as IL-17A production have also been described (Downs-Canner et al., 2017; Gagliani et al., 2015; Hovhannisyan et al., 2011). Analyses were therefore expanded to assess Th1 cell-like properties in tdRFP$^+$ cells as well as the relationship between IL-17A production and Treg cell function.

IL-17A and IFNγ production in tdRFP$^+$ cells at steady state identified a spectrum of Th17 and so-called exTh17 cells with Th1 cell-like characteristics (Fig3.3a). Interestingly, while IFNγ$^-$IL-17A$^+$ Th17 cells were present in all assessed anatomical locations (Fig3.3b-c), IFNγ$^+$ Th17 cells appeared largely limited to the intestinal mucosa and its draining mLN (Fig3.3d-e). Fully mature IFNγ$^+$ exTh17 cells were found at the highest frequency in the SILP and CLP but were low both in frequency and numbers in the mLN (Fig3.3f-g), in line with the highest IL-17A/tdRFP concordance observed in the mLN (Fig3.2).

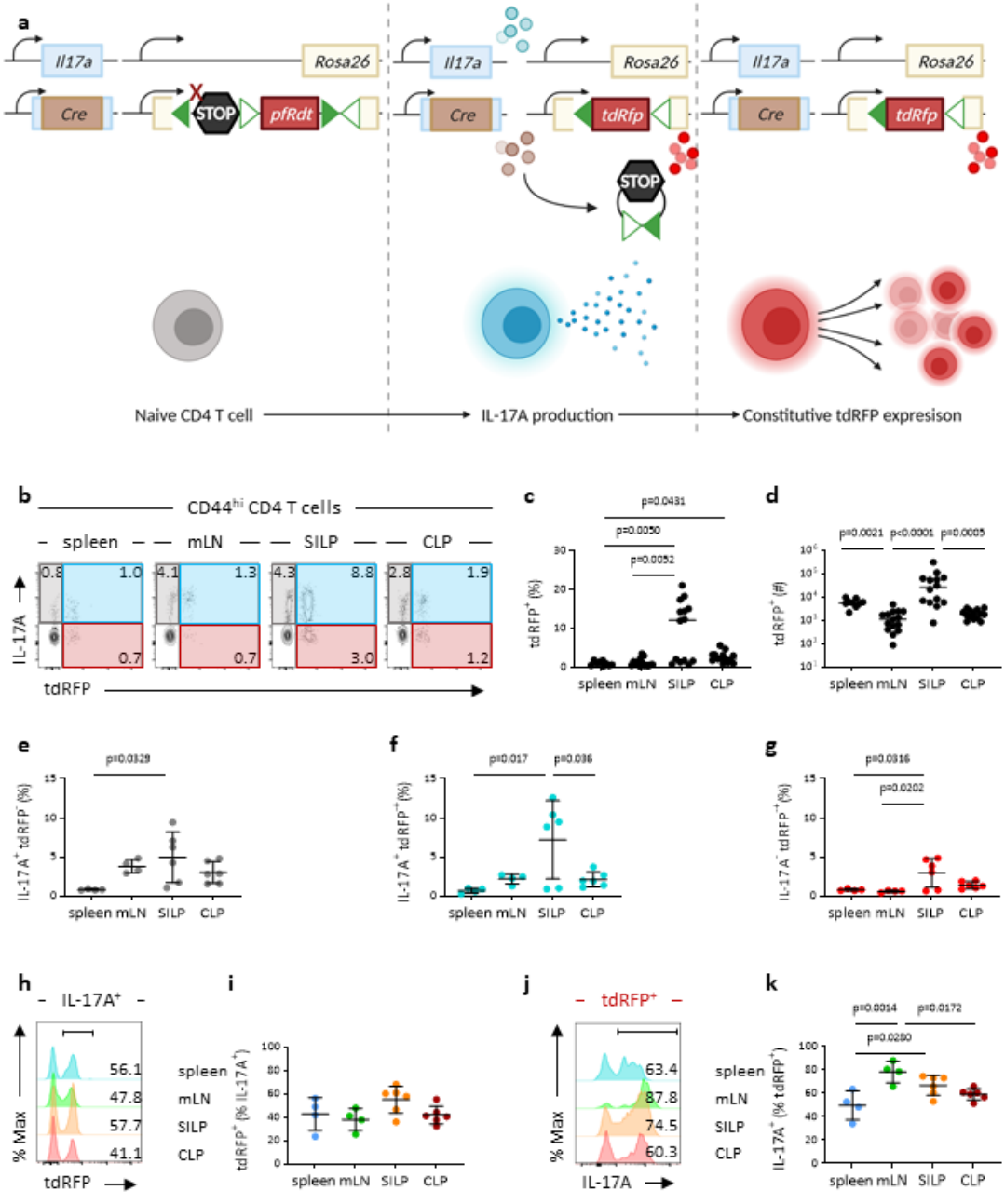
a
Il17a
Rosa26
Cre
STOP
pfRdt
tdRfp
Naive CD4 T cell
IL-17A production
Constitutive tdRFP expresison
b
CD44hi CD4 T cells
spleen
mLN
SILP
CLP
IL-17A
tdRFP
0.8
1.0
0.7
4.1
1.3
0.7
4.3
8.8
3.0
2.8
1.9
1.2
c
p=0.0431
p=0.0050
p=0.0052
tdRFP+ (%)
spleen mLN SILP CLP
d
p=0.0021
p<0.0001
p=0.0005
tdRFP+ (#)
spleen mLN SILP CLP
e
p=0.0329
IL-17A+ tdRFP- (%)
spleen mLN SILP CLP
f
p=0.017
p=0.036
IL-17A+ tdRFP+ (%)
spleen mLN SILP CLP
g
p=0.0316
p=0.0202
IL-17A- tdRFP+ (%)
spleen mLN SILP CLP
h
IL-17A+
% Max
56.1
47.8
57.7
41.1
tdRFP
i
spleen
mLN
SILP
CLP
tdRFP+ (% IL-17A+)
spleen mLN SILP CLP
j
tdRFP+
% Max
63.4
87.8
74.5
60.3
IL-17A
k
p=0.0014
p=0.0172
p=0.0280
spleen
mLN
SILP
CLP
IL-17A+ (% tdRFP+)
spleen mLN SILP CLP

Figure 3.2. The importance of tracking *Il17a* expression history in accurately assessing Th17 cell plasticity

Il17a^{cre}*Rosa26*^{tdRFP} (IL-17A 'fate mapper') mice used to track cells with a history of IL-17A production enable assessment of Th17 cell fate.

a) Schematic representation of IL-17A fate mapping. The sequence encoding Cre recombinase was inserted into the *Il17a* locus and the sequence encoding Cre-inducible tdRFP into the ubiquitously expressed *Rosa26* locus. Cells heterogeneous for the WT and transgenic *Il17a* alleles co-express IL-17A and Cre resulting in permanent tdRFP expression. Images generated with BioRender.com.

b) Representative flow cytometry plots showing IL-17A and tdRFP expression in CD44^{hi} CD4 T cells in spleen, mLN, SILP and CLP following *ex vivo* restimulation with PMA and Ionomycin.

c-d) Quantification of the proportion (c) and total number (d) of tdRFP^{+} cells within the parent populations in spleen, mLN, SILP and CLP. Spleen n=9, data pooled from 7 independent experiments, mLN n=15, data pooled from 5 independent experiments, SILP and CLP n=14, data pooled from 5 independent experiments.

e-g) Quantification of the proportion of IL-17A^{+} cells expressing no tdRFP (e), cells expressing both IL-17A and tdRFP (f) and cells expressing tdRFP but no IL-17A (g) within the parent populations in spleen, mLN, SILP and CLP. Spleen and mLN n=4, data from 1 experiment, SILP and CLP n=6, data pooled from 2 independent experiments.

h) Representative histograms showing tdRFP expression in IL-17A^{+}CD44^{hi} CD4 T cells in spleen, mLN, SILP and CLP following *ex vivo* restimulation with PMA and Ionomycin.

i) Quantification of the proportion of IL-17A^{+} cells expressing tdRFP in the spleen, mLN, SILP and CLP. Spleen and mLN n=4, data from 1 experiment, SILP and CLP n=6, data pooled from 2 independent experiments.

j) Representative histograms showing IL-17A expression in tdRFP^{+}CD44^{hi} CD4 T cells in spleen and mLN, SILP and CLP following *ex vivo* restimulation with PMA and Ionomycin.

g) Quantification of the proportion of tdRFP^{+} cells producing IL-17A in spleen, mLN, SILP and CLP. spleen and mLN n=4, data from 1 experiment, SILP and CLP n=6, data pooled from 2 independent experiments.

Values on flow cytometry plots and histograms represent percentages. Normality was tested using Shapiro-Wilk test. Lines on graphs show mean±SD (e, f, g, I, k) or median (c, d). Significance was tested using One-Way ANOVA (e, f, g, I, k) or Kruskal-Wallis test (c, d).

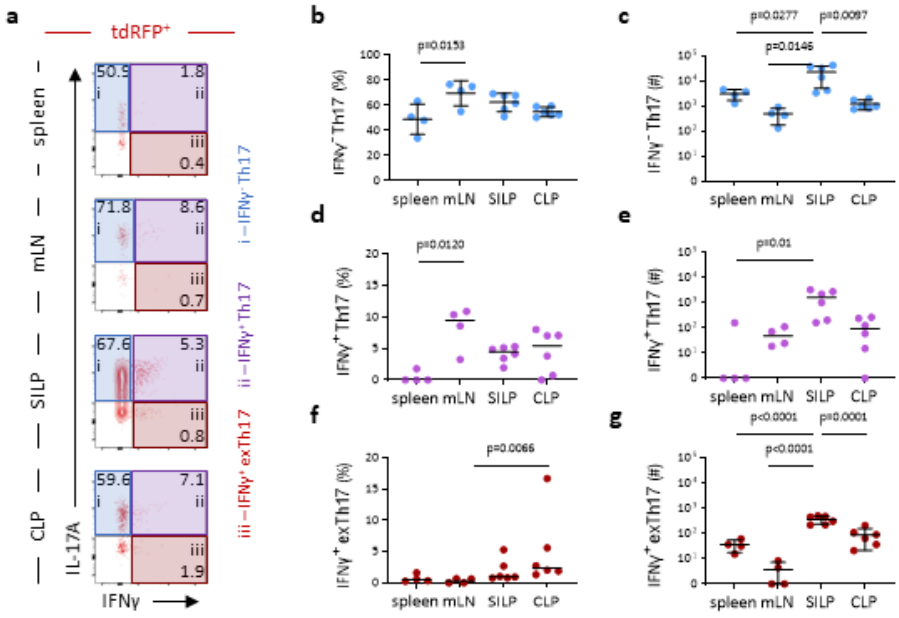
a
tdRFP+
spleen
mLN
SILP
CLP
IL-17A
IFNγ
50.9
1.8
71.8
8.6
67.6
5.3
59.6
7.1
0.4
0.7
0.8
1.9
i – IFNγ- Th17
ii – IFNγ+ Th17
iii – IFNγ+ exTh17
b
p=0.0153
IFNγ- Th17 (%)
c
p=0.0277
p=0.0097
p=0.0146
IFNγ- Th17 (#)
d
p=0.0120
IFNγ+ Th17 (%)
e
p=0.01
IFNγ+ Th17 (#)
f
p=0.0066
IFNγ+ exTh17 (%)
g
p<0.0001
p=0.0001
p<0.0001
IFNγ+ exTh17 (#)
spleen mLN SILP CLP

Figure 3.3. Th17 cells give rise to a spectrum of pro-inflammatory exTh17 cells by acquiring Th1 cell-like cytokine expression

Il17a^{cre}*Rosa26*^{tdRFP} mice enable the identification of Th17 cells that acquire alternative cytokine profiles at steady state.

a) Representative flow cytometry plots gated on tdRFP^{+} CD44^{hi} CD4 T cells showing IL-17A and IFNγ expression following *ex vivo* restimulation with PMA and Ionomycin, and identification of IFNγ^{-} Th17, IFNγ^{+} Th17 and IFNγ^{+} exTh17 cell populations.

b-g) Quantification of the proportion of total number of IFNγ^{-} Th17 (b, c), IFNγ^{+} Th17 (d, e) and IFNγ^{+} exTh17 (f, g) cells within the tdRFP^{+} population in spleen, mLN, SILP and CLP. Spleen and mLN n=4, data from 1 experiment, SILP and CLP n=6, data pooled from 2 independent experiments.

Values on flow cytometry plots represent percentages. Normality was tested using Shapiro-Wilk test. Lines on graphs show mean±SD (b, c, g) or median (d, e, f). Significance was tested using One-Way ANOVA (b, c, g) or Kruskal-Wallis test (d, e, f).

3.4 IL-17A PRODUCING TREG CELLS ARE PRESENT IN THE INTESTINAL LAMINA PROPRIA AT STEADY STATE BUT DO NOT GIVE RISE TO TH17 CELLS

Treg cells, CD4 T cells identified by the expression of their master TF FoxP3, are a prominent mucosal CD4 T cell subset with key roles in maintaining immune homeostasis through suppression of inflammatory pathways. Thymically derived central Treg cells are thought to be a highly stable CD4 T cell subset but FoxP3^{+} suppressive cells can also be generated in the periphery in a TGF-β-dependent process. Peripherally induced pTreg cells share this characteristic with Th17 cells (Bettelli et al., 2006; Mangan et al., 2006; Veldhoen et al., 2006). In addition, mucosal Treg cells are known to acquire other Th17 cell-like characteristics such as RORγt and STAT3 expression in a process that was thought to aid suppressive function by allowing entry into the anatomical locations that Th17 cells occupy and enabling Treg cells to dampen potentially harmful inflammation preventing tissue damage. However, Th17 cell-associated TFs are now known to also help maintain FoxP3 expression by suppressing alternative CD4 T cell programmes and fates (Bhaumik et al., 2021). In addition, Treg and Th17 cell function are intricately linked with both subsets able to promote or suppress the other's function in a context-specific manner (Pandiyan et al., 2011). Th17-to-Treg cell conversion and acquisition of Th17 cell function by Treg cells has been described in disease settings and can be both beneficial and detrimental to health (Downs-Canner et al., 2017; Hovhannisyan et al., 2011).

To better understand the contributions of Th17 and Treg cell differentiation to regulatory and effector pools I sought to fate map both differentiation pathways using mouse colonies housed within the same facility. This approach aimed to minimise microbiota-induced differences. Firstly, *Il17a* expression was mapped in *Il17a*^{cre}*Rosa26*^{tdRFP} mice (Fig3.4a). Enumeration of the proportion of FoxP3^{+} cells within the tdRFP^{+} CD44^{hi} CD4 T cell pool confirmed that the colon harboured significantly more Treg cells than the systemic or small intestinal compartments (Fig3.4b). In line with previous observations, cells with a history of IL-17A production but no expression of FoxP3 were most abundant in the small intestine (Fig3.4c). Despite the indications that cells expressing both FoxP3 and tdRFP

made up a large proportion of the total colonic activated CD4 T cell pool with a history of IL-17A production (Fig3.4b), the overall frequency of this population was small (less than 3%, Fig3.4d). The highest frequency of tdRFP$^-$ Treg cells was found in the mLN and CLP (Fig3.4e). Assessing the total number of the CD4 T cell populations defined by tdRFP and IL-17A expression (Fig3.4a) confirmed that the SILP harboured most non-Treg tdRFP$^+$ cells (Fig3.4f) with further differences identified on frequency assessment likely hidden by tissue-specific differences in the size of the parent population (Fig3.4g-h). The comparatively high proportion of both tdRFP$^+$ and tdRFP$^-$ Treg cells in mLN and CLP but not SILP pointed to microenvironment-specific differences in the regulation of CD4 T cell fate that exist even between two intestinal mucosal sites and their draining LNs.

The steady state data generated provided a snapshot in time and did not reveal whether tdRFP$^+$ Treg cells were exTh17 cells that have acquired FoxP3 or dedicated suppressive cells that also produced IL-17A. Therefore, functional properties of the three populations identified by tdRFP and FoxP3 expression were assessed. Namely, their ability to produce the anti-inflammatory cytokine IL-10 (Fig3.4i-m) and the Th17 cell-associated cytokine IL-17A (Fig3.4n-r) upon *ex vivo* restimulation with PMA and ionomycin. Production of IL-10 was limited to FoxP3$^+$ activated CD4 T cells but no differences in the proportion of cells expressing this cytokine, regardless of IL-17A expression history, were evident (Fig3.4j-m). Moreover, levels of IL-10 produced by the two Treg cell populations in the CLP were comparable with only a modest decrease associated with tdRFP expression in SILP Treg cells (Fig3.4s-t). Conversely, tdRFP$^+$ Treg cells expressed intermediate levels of IL-17A, both in terms of proportions of cells producing the cytokine (Fig3.4o-r) and the amounts produced (Fig3.4u-v). It has been reported that a reduction in IL-17A production is a result of antagonistic effects between the RORγt and FoxP3 (Zhou et al., 2008), but whether these data truly represent a transient state of Th17 cells becoming Treg cells and losing IL-17A production or Treg cells acquiring Th17 cell function is unclear and the experimental model using the *Il17a^{cre}Rosa26^{tdRFP}* fate mapper mouse does not enable resolution of this.

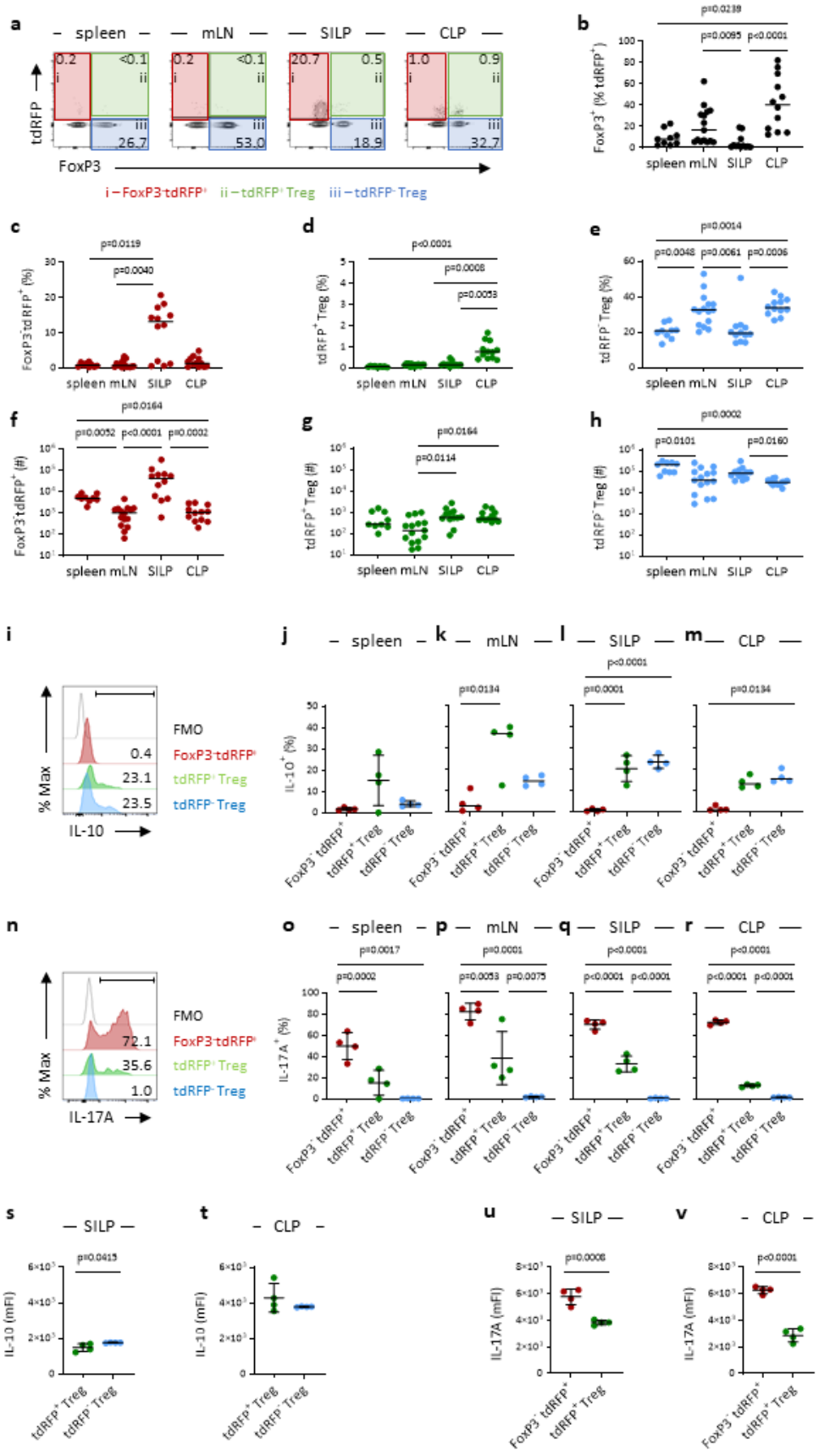
a
spleen
mLN
SILP
CLP
tdRFP
FoxP3
i – FoxP3⁻tdRFP⁺ ii – tdRFP⁺ Treg iii – tdRFP⁻ Treg
b
FoxP3⁺ (% tdRFP⁺)
c
FoxP3⁻tdRFP⁺ (%)
d
tdRFP⁺ Treg (%)
e
tdRFP⁻ Treg (%)
f
FoxP3⁻tdRFP⁺ (#)
g
tdRFP⁺ Treg (#)
h
tdRFP⁻ Treg (#)
i
FMO
FoxP3⁻tdRFP⁺
tdRFP⁺ Treg
tdRFP⁻ Treg
% Max
IL-10
j
k
l
m
IL-10⁺ (%)
n
IL-17A
o
p
q
r
IL-17A⁺ (%)
s
t
u
v
IL-10 (mFI)
IL-17A (mFI)

Figure 3.4. The distribution of Treg cells with a history of IL-17A expression points to microenvironment-specific Th17-Treg cell links

To assess the ability of Th17 cells to differentiate into Treg cells, expression of tdRFP and FoxP3, the master Treg cell TF, was assessed in *Il17a*^{cre}*Rosa26*^{tdRFP} mice at steady state.

a) Representative flow cytometry plots gated on CD44^{hi} CD4 T cells showing tdRFP and FoxP3 expression in spleen, mLN, SILP and CLP, and identification of FoxP3^{-}tdRFP^{+}, tdRFP^{+} Treg and tdRFP^{-} Treg cell populations.

b) Quantification of the proportion of tdRFP^{+} cells expression FoxP3. Spleen n=9, data pooled from 3 independent experiments, mLN n=15, data pooled from 5 independent experiment, SILP and CLP n=12, data pooled from 4 independent experiments.

c-h) Quantification of the proportion and total number of FoxP3^{-}tdRFP^{+} (c, f), tdRFP^{+} Treg (d, g) and tdRFP^{-} Treg (e, h) cells in spleen, mLN, SILP and CLP. Spleen n=9, data pooled from 3 independent experiments, mLN n=15, data pooled from 5 independent experiment, SILP and CLP n=12, data pooled from 4 independent experiments.

i) Representative histograms showing IL-10 expression in the populations identified in (a) following *ex vivo* restimulation with PMA and Ionomycin.

j-m) Quantification of the proportion of cells expressing IL-10 in the populations identified in (a). Spleen (j), mLN (k), SILP (l) and CLP (m) n=4, data from 1 experiment.

n) Representative histograms showing IL-17A expression in the populations identified in (a) following *ex vivo* restimulation with PMA and Ionomycin.

o-r) Quantification of the proportion of cells expressing IL-17A in the populations identified in (a). Spleen (o), mLN (p), SILP (q) and CLP (r) n=4, data from 1 experiment.

s-t) IL-10 median fluorescence intensity (mFI) in tdRFP^{+} and tdRFP^{-} Treg cells in SILP (s) and CLP (t). n=4, data from 1 experiment

u-v) IL-17A median fluorescence intensity (mFI) in tdRFP^{+} and tdRFP^{-} Treg cells in SILP (u) and CLP (v). n=4, data from 1 experiment

Values on flow cytometry plots and histograms represent percentages. Normality was tested using Shapiro-Wilk test. Lines on graphs show mean±SD (j, l, o, p, q, r, s, t, u, v) or median (b, c, d, e, f, g, h, k). Significance was tested using unaired t test (s, t, u, v), One-Way ANOVA (j, l, m, o, p, q, r) or Kruskal-Wallis test (b, c, d, e, f, g, h, k).

To investigate further, I turned to the *Foxp3*$^{eGFP\text{-}Cre\text{-}ERT2}$*Ai14* tamoxifen-inducible FoxP3 fate reporter mouse model (Madisen et al., 2010; Rubtsov et al., 2010). Much like IL-17A fate reporting, this system relies on Cre recombinase, but under the control of the FoxP3 promoter. However, a key difference is that FoxP3 activation alone is not sufficient to drive Cre translocation to the nucleus but also requires tamoxifen-treatment. Dosing mice with tamoxifen enables Cre-mediated recombination following which tdTomato identifies cells that expressed FoxP3 during tamoxifen treatment (Fig3.5a). However, cells that activate FoxP3 after cessation of treatment express no fluorescent protein. Therefore, incorporating a resting period (no tamoxifen) prior to tissue harvest and assessment of tdTomato expression enables the evaluation of the stability of the Treg cell compartment. A high proportion of CD4 T cells expressing both FoxP3 and tdTomato points to early accumulation of a Treg cell population that is then either unchanged or self-renewing. On the other hand, incomplete FoxP3-tdTomato signal concurrence can result from three things. First, erroneous readthrough expression of the tdTomato transgene in the absence of recombination. The lack of a tdTomato signal in control mice not dosed with tamoxifen (Fig3.5b) suggested that this event did not occur at a high frequency in this experimental model. Second, higher Treg cell turnover with post-tamoxifen generation of FoxP3-expressing cells that would result in the detection of tdTomato^{-} Treg cells. Lastly, Treg cell conversion to alternative CD4 T cell subsets would result in the presence of tdTomato^{+} FoxP3^{-} cells.

A dosing regimen consisting of oral tamoxifen administration followed by one month rest prior to FoxP3 fate reporting assessment in mucosal and lymphoid tissue was devised (Fig3.5a). The proportion and number of CD4 T cells fate reporting FoxP3 expression in 2LT was lower than that in the intestinal lamina propria with the highest proportion of tdTomato^{+} cells found in the CLP (Fig3.5b-d). These data were at odds with the high proportion of Treg cells observed in the mLN earlier (Fig3.4). However, this was likely the effect of inclusion of all CD4 T cells, rather than only activated CD44^{hi} CD4 T cells, in the parent gate in *Foxp3*$^{eGFP=Cre\text{-}ERT2}$*Ai14* mLN. This is a technical limitation that was not corrected due limited availability of these mice. Nonetheless, the high proportion of CD4 T cells fate reporting FoxP3 in the SILP and CLP one month after cessation of tamoxifen treatment suggested that intestinal Treg

cells were a fairly stable population at steady state. To test the extent of Treg-to-Th17 cell conversion three populations were identified based on IL-17A and FoxP3 expression – IL-17a^{+}FoxP3^{-} cells (Th17), IL-17A^{+} Treg and IL-17A^{-} Treg cells – and tdTomato expression in these was assessed (Fig3.5e-f). The very limited tdTomato signal in Th17 cells suggested that CD4 T lymphocytes with a Th17 cell identity but of a Treg cell origin did not accumulate within the tissues analysed (Fig3.5g-j). Large proportions of both the IL-17A^{-} and IL-17A^{+} Treg cell populations expressed tdTomato confirming high stability of the Treg cell lineage. However, FoxP3 fate reporting within intestinal Treg cell populations revealed that a higher proportion of the IL-17A^{+} population, especially in the CLP, acquired FoxP3 in the month between tamoxifen treatment and the experimental endpoint than that of the IL-17A^{-} Treg cell population (Fig3.5i-j).

Taken together, the observations in IL-17A and FoxP3 fate mapper mice suggested that mLN and intestinal lamina propria Treg cells were able to acquire not only Th17 cell master TF but also characteristic cytokine expression at steady state. These data leave open the possibility of Th17-to-Treg cell conversion but show no clear evidence that FoxP3^{+} CD4 T cells give rise to intestinal lamina propria Th17 cells in the absence of infection.

3.5 THE OX40:OX40L PATHWAY PROVIDES SUPPORT TO SOME BUT NOT ALL MUCOSAL CD4 T CELL POPULATIONS

Site-specific differences in the proportion of Treg cell fate reporting IL-17A expression highlight the role specific microenvironments play in the regulation of mucosal CD4 T cell fate and identity. The context within which CD4 T cells are activated plays a key role in the nature of the eventual immune response. Signalling through costimulatory molecules, along with the presence of certain combinations of cytokines, during and after initial priming is central to determining the functional outcome of CD4 T cell activation, leading to the hypothesis that tissue-specific costimulatory signal provision contributes to Th17-to-Treg cell differentiation in different anatomical locations.

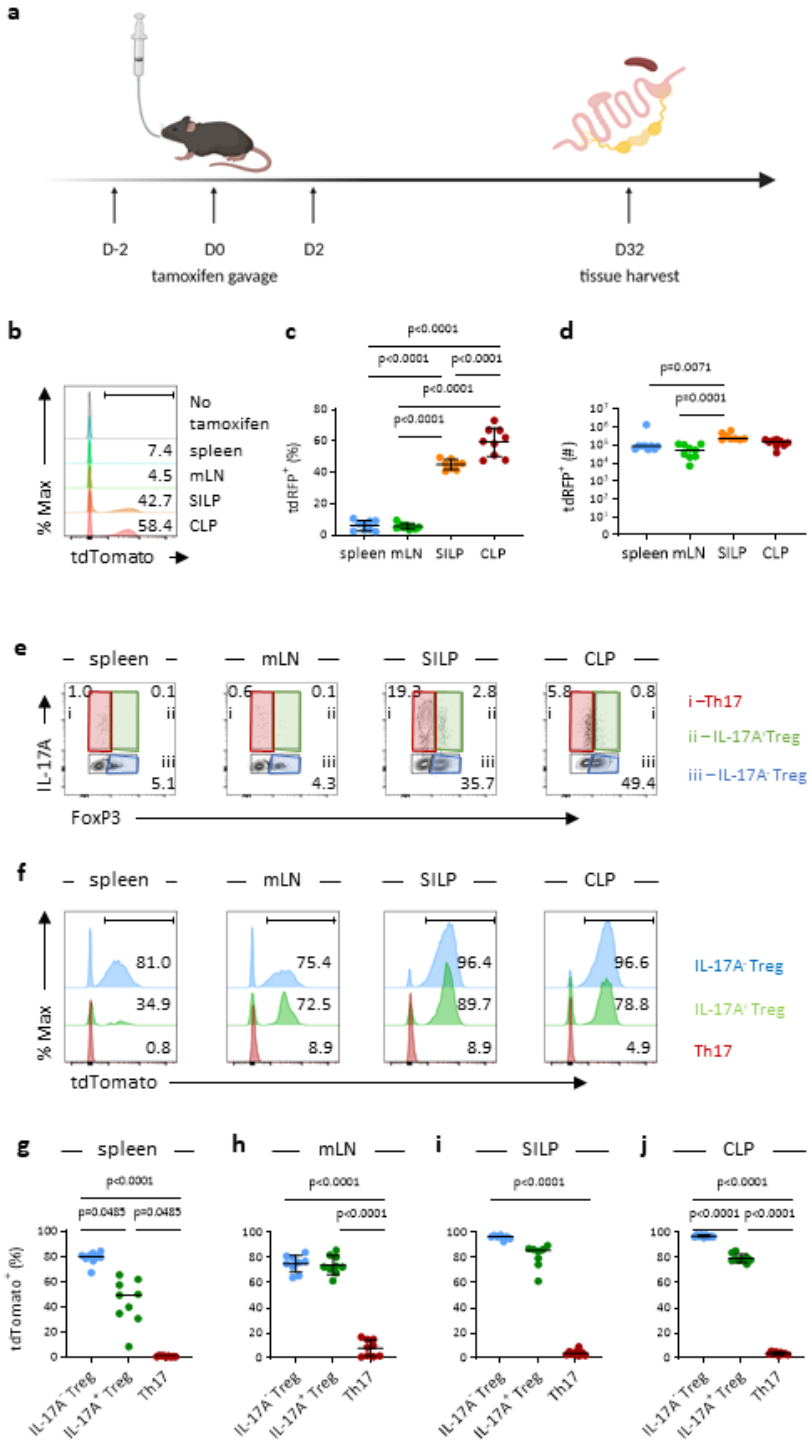
a
D-2
D0
tamoxifen gavage
D2
D32
tissue harvest
b
No tamoxifen
7.4 spleen
4.5 mLN
42.7 SILP
58.4 CLP
% Max
tdTomato
c
p<0.0001
p<0.0001
p<0.0001
p<0.0001
p<0.0001
tdRFP+ (%)
spleen mLN SILP CLP
d
p=0.0071
p=0.0001
tdRFP+ (#)
spleen mLN SILP CLP
e
spleen
mLN
SILP
CLP
1.0 0.1 5.1
0.6 0.1 4.3
19.3 2.8 35.7
5.8 0.8 49.4
IL-17A
FoxP3
i –Th17
ii – IL-17A+Treg
iii – IL-17A- Treg
f
spleen
mLN
SILP
CLP
81.0 34.9 0.8
75.4 72.5 8.9
96.4 89.7 8.9
96.6 78.8 4.9
% Max
tdTomato
IL-17A- Treg
IL-17A+ Treg
Th17
g
spleen
p<0.0001
p=0.0485
p=0.0485
tdTomato+ (%)
IL-17A- Treg
IL-17A+ Treg
Th17
h
mLN
p<0.0001
p<0.0001
IL-17A- Treg
IL-17A+ Treg
Th17
i
SILP
p<0.0001
IL-17A- Treg
IL-17A+ Treg
Th17
j
CLP
p<0.0001
p<0.0001
p<0.0001
IL-17A- Treg
IL-17A+ Treg
Th17

Figure 3.5. Tracking FoxP3 expression history reveals no Th17 cell-like exTreg cells

Tamoxifen-inducible FoxP3 fate reporter *Foxp3*$^{eGFP\text{-}Cre\text{-}ERT2}$*Ai14* mice used to track FoxP3 expression history enable the assessment of Treg-to-Th17 cell conversion at steady state. Images generated with BioRender.com.

a) Schematic representation of experimental design.

b) Representative histograms gated on CD4 T cells showing tdTomato expression in spleen, mLN, SILP and colon.

c-d) Quantification of the proportion (c) and total number (d) of tdTomato$^+$ cells within the parent populations in spleen, mLN, SILP and CLP. Spleen and mLN n=9, data pooled from 2 independent experiments, SILP and CLP n=8, data pooled from 2 independent experiments.

e) Representative flow cytometry plots gated on CD4 T cells showing IL-17A and FoxP3 expression following *ex vivo* restimulation with PMA and ionomycin and identification of Th17, IL-17A$^+$ Treg and IL-17A$^-$ Treg cell populations in spleen, mLN, SILP and CLP.

f) Representative histograms showing tdTomato expression in the populations identified in (e) in spleen, mLN, SILP and CLP.

g-j) Quantification of the proportion of tdTomato$^+$ cells within the populations identified in (e) in spleen (g), mLN (h), SILP (i) and CLP (j).

Values on flow cytometry plots and histograms represent percentages. Normality was tested using Shapiro-Wilk test. Lines on graphs show mean±SD (c, h, j) or median (d, g, i). Significance was tested using One-Way ANOVA (c, h, j) or Kruskal-Wallis test (d, g, i).

OX40, a TNFRSF member, was first identified as a T cell activation marker (Paterson et al., 1987) and later shown to support effector T cell clonal expansion and survival upon ligation of its ligand, OX40L (Gramaglia et al., 1998). More recently, the OX40:OX40L pathway was linked to the control of both Th17 and Treg cell function, albeit with mixed, often contradictory results. While OX40 was found to promote Treg cell proliferation, survival and accumulation at both steady state and in colitis (Griseri et al., 2010; Piconese et al., 2010) it has also been shown to inhibit suppressive effects in tumours (Piconese et al., 2008). The role of OX40 in regulating Th17 cell function is similarly obscure with an inhibitory effect described in animal models of multiple sclerosis but activation in models of Th17 cell-driven ocular inflammation (Xiao et al., 2016; Zhang et al., 2010). Moreover, OX40 signalling has even been linked to the control of the Th17 cell programme in Treg cells, suppressing the acquisition of IL-17A production during skin inflammation (Remedios et al., 2018). Together, these reports suggest that the effects OX40 ligation has on CD4 T cells are highly context-specific and may contribute to the regulation of mucosal Th17 and Treg cell identity and fate. Furthermore, recent observations highlighted key differences in the activation of the OX40:OX40L pathway between the systemic and mucosal immune compartments (Gajdasik et al., 2020). I therefore sought to assess mucosal Treg and Th17 cell costimulatory requirements with a focus on the OX40:OX40L pathway.

3.5.1 Intestinal Treg cells are partially reliant on ILC3 OX40L

To test OX40-reliance at steady state I compared FoxP3 and RORγt expression in $CD44^{hi}$ CD4 T cells from WT control and OX40 knockout ($OX40^{-/-}$) mice (Fig3.6a-b). Normal accumulation of cells expressing the Th17 cell master TF RORγt but not the Treg cell master TF FoxP3 appeared reliant on OX40 signalling only in the 2LT. Conversely, a modest but consistent reduction of approximately 50% in Treg cells (activated CD4 T cells expressing FoxP3 wither with or without RORγt) was only evident in the SILP and CLP indicating that normal numbers of intestinal Treg cells were OX40-reliant (Fig3.6c-z).

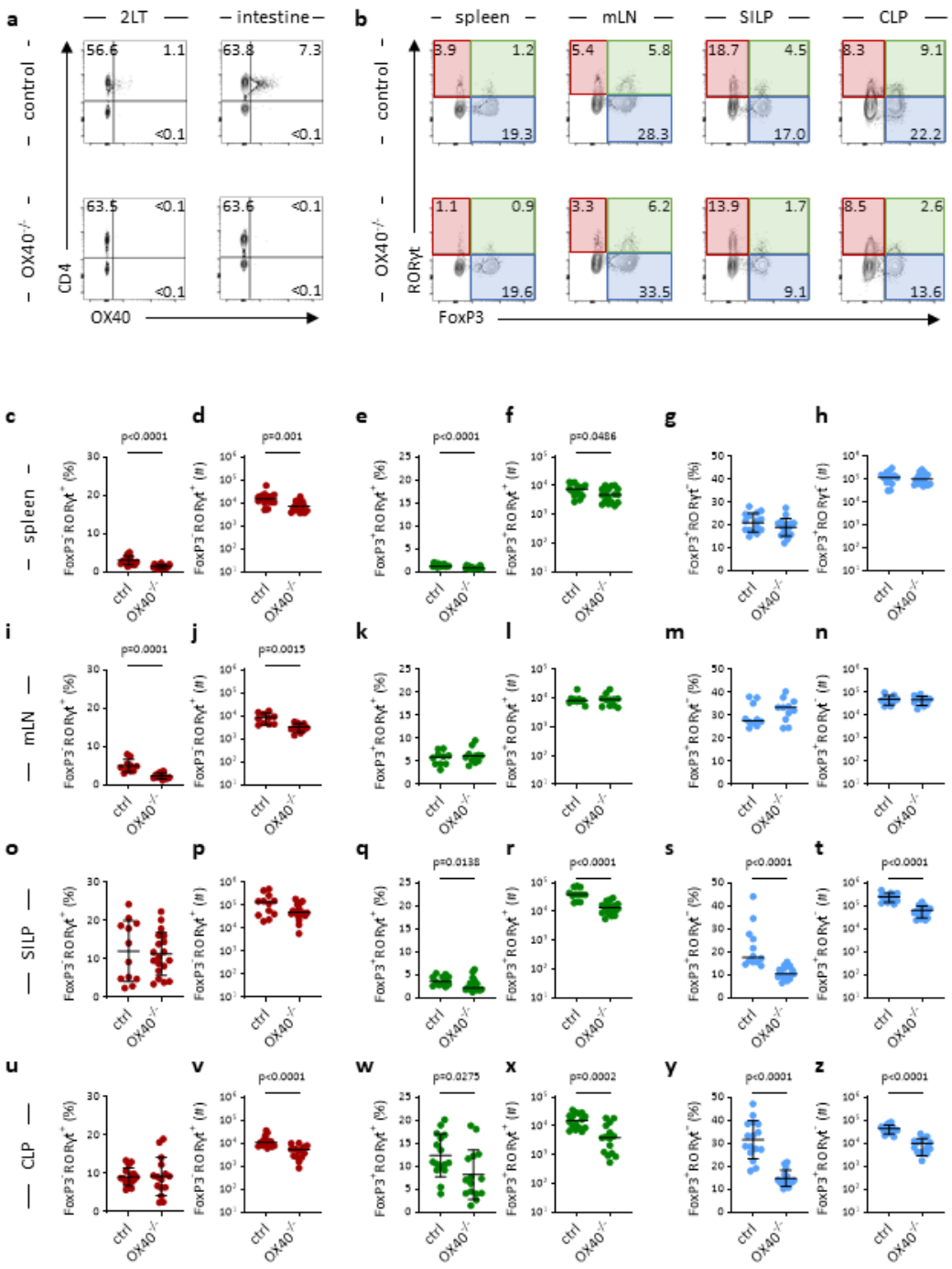
a
2LT
intestine
control
OX40-/-
CD4
OX40
56.6
1.1
<0.1
63.8
7.3
63.5
63.6
b
spleen
mLN
SILP
CLP
RORγt
FoxP3
3.9
1.2
19.3
5.4
5.8
28.3
18.7
4.5
17.0
8.3
9.1
22.2
1.1
0.9
19.6
3.3
6.2
33.5
13.9
1.7
9.1
8.5
2.6
13.6
c
d
e
f
g
h
i
j
k
l
m
n
o
p
q
r
s
t
u
v
w
x
y
z
p<0.0001
p=0.001
p=0.0486
p=0.0015
p=0.0138
p=0.0275
p=0.0002
FoxP3+RORγt+ (%)
FoxP3+RORγt+ (#)
FoxP3-RORγt+ (%)
FoxP3-RORγt+ (#)
ctrl
OX40-/-

Figure 3.6. OX40-deficient mice lack normal intestinal mucosal FoxP3 and RORγt expression

OX40 sufficient (Cre^{-} $OX40L^{fl/fl}$, control) and OX40 deficient ($OX40^{-/-}$) mice were assessed to determine the requirement for OX40 on $FoxP3^{+}$ and $ROR\gamma t^{+}$ $CD44^{hi}$ CD4 T cells at steady state.

a) Representative flow cytometry plots gated on $CD44^{hi}$ CD4 T cells showing OX40 expression in control and OX40 deletion in $OX40^{-/-}$ mice in 2LT and intestinal mucosa.

b) Representative flow cytometry plots gated on $CD44^{hi}$ CD4 T cells showing RORγt and FoxP3 expression in spleen, mLN, SILP and CLP.

c-h) Quantification of the proportion and total number of $FoxP3^{-}ROR\gamma t^{+}$ (c, d), $Fox\ P3^{+}ROR\gamma t^{+}$ (e, f) and $FoxP3^{+}ROR\gamma t^{-}$ (g, h) $CD44^{hi}$ CD4 T cells in control and $OX40^{-/-}$ spleen. Control n=15, data pooled from 6 independent experiments, $OX40^{-/-}$ n=17, data pooled from 6 independent experiments.

i-n) Quantification of the proportion and total number of $FoxP3^{-}ROR\gamma t^{+}$ (i, j), $FoxP3^{+}ROR\gamma t^{+}$ (k, l) and $FoxP3^{+}ROR\gamma t^{-}$ (m, n) $CD44^{hi}$ CD4 T cells in control and $OX40^{-/-}$ mLN. Control n=10, data pooled from 4 independent experiments, $OX40^{-/-}$ n=11, data pooled from 4 independent experiments.

o-t) Quantification of the proportion and total number of $FoxP3^{-}ROR\gamma t^{+}$ (o, p), $FoxP3^{+}ROR\gamma t^{+}$ (q, r) and $FoxP3^{+}ROR\gamma t^{-}$ (s, t) $CD44^{hi}$ CD4 T cells in control and $OX40^{-/-}$ SILP. Control n=12, data pooled from 5 independent experiments, $OX40^{-/-}$ n=19, data pooled from 7 independent experiments.

u-z) Quantification of the proportion and total number of $FoxP3^{-}ROR\gamma t^{+}$ (u, v), $FoxP3^{+}ROR\gamma t^{+}$ (w, x) and $FoxP3^{+}ROR\gamma t^{-}$ (y, z) $CD44^{hi}$ CD4 T cells in control and $OX40^{-/-}$ spleen. Control n=16, data pooled from 6 independent experiments, $OX40^{-/-}$ n=15, data pooled from 6 independent experiments.

Values on flow cytometry plots represent percentages. Normality was tested using Shapiro-Wilk test. Lines on graphs show mean±SD (c, g, i, j, n, o, t, u, w, y, z) or median (d, e, f, h, k, l, m, p, q, r, s, v, x). Significance was tested unpaired t test (c, g, i, j, n, o, t, u, w, y, z) or Mann-Whitney U test (d, e, f, h, k, l, m, p, q, r, s, v, x).

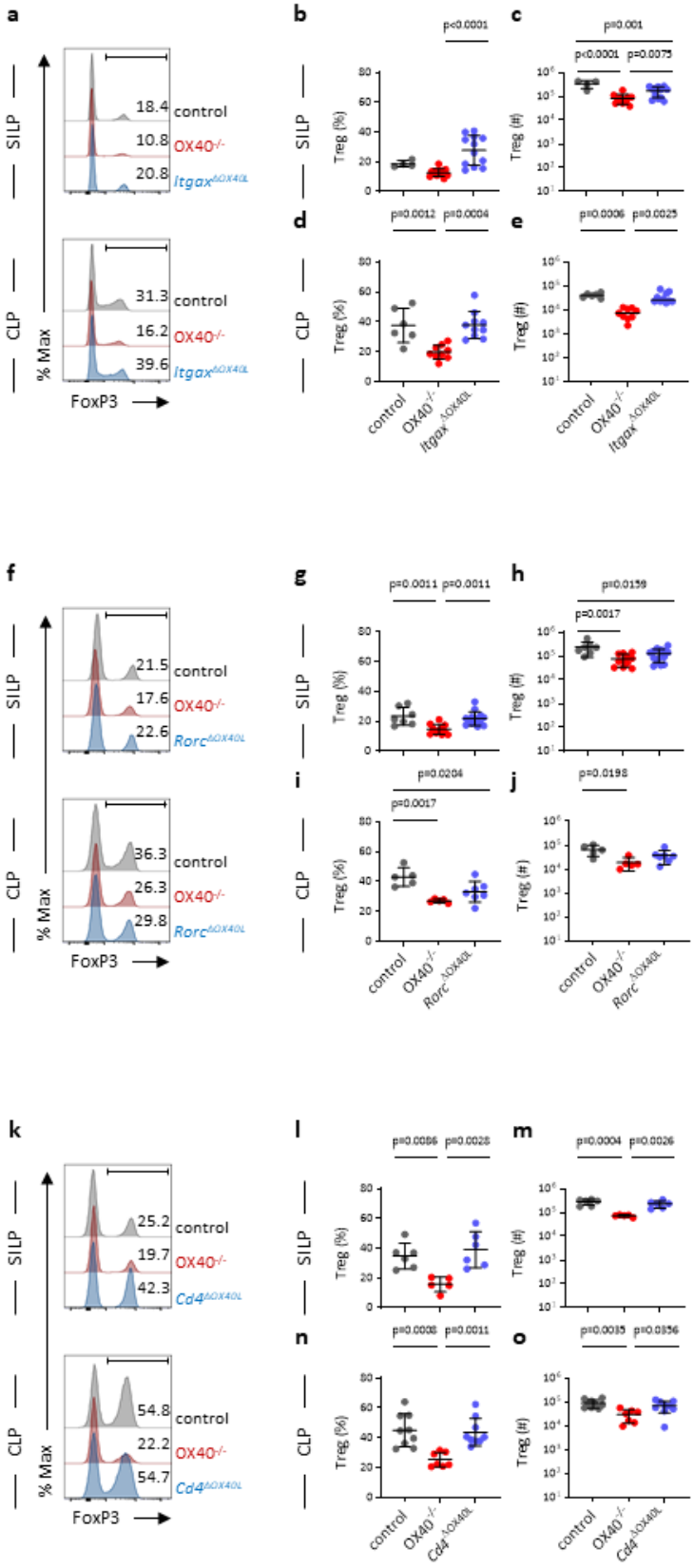
a
SILP
CLP
18.4
control
10.8
OX40-/-
20.8
Itgax ΔOX40L
31.3
control
16.2
OX40-/-
39.6
Itgax ΔOX40L
% Max
FoxP3
b
p<0.0001
Treg (%)
c
p=0.001
p<0.0001
p=0.0075
Treg (#)
d
p=0.0012
p=0.0004
Treg (%)
control
OX40-/-
Itgax ΔOX40L
e
p=0.0006
p=0.0025
Treg (#)
f
21.5
control
17.6
OX40-/-
22.6
Rorc ΔOX40L
36.3
control
26.3
OX40-/-
29.8
Rorc ΔOX40L
% Max
FoxP3
g
p=0.0011
p=0.0011
Treg (%)
h
p=0.0159
p=0.0017
Treg (#)
i
p=0.0204
p=0.0017
Treg (%)
control
OX40-/-
Rorc ΔOX40L
j
p=0.0198
Treg (#)
k
25.2
control
19.7
OX40-/-
42.3
Cd4 ΔOX40L
54.8
control
22.2
OX40-/-
54.7
Cd4 ΔOX40L
% Max
FoxP3
l
p=0.0066
p=0.0028
Treg (%)
m
p=0.0004
p=0.0026
Treg (#)
n
p=0.0008
p=0.0011
Treg (%)
control
OX40-/-
Cd4 ΔOX40L
o
p=0.0035
p=0.0356
Treg (#)

Figure 3.7. ILC3-derived OX40L may support some intestinal Treg cells

The contributions of DC and ILC3 OX40L provision to intestinal Treg cells were assessed at steady state. *Itgax*^{cre}*Ox40l*$^{fl/fl}$ (*Itgax*$^{\Delta X040L}$) mice delete DC OX40L upon CD11c expression, *Rorc*^{cre}*Ox40l*$^{fl/fl}$ (*Rorc* $^{\Delta OX40L}$) mice delete ILC3 and T cell OX40L on RORγt^{+} expression and *Cd4*^{cre}*Ox40l*$^{fl/fl}$ (*Cd4* $^{\Delta OX40L}$) mice delete only T cell OX40L upon CD4 expression.

a) Representative histograms gated on CD44^{hi} CD4 T cells showing FoxP3 expression in control, OX40$^{-/-}$ and *Itgax*$^{\Delta OX40L}$ SILP and CLP. Controls are Cre$^{-/-}$ littermates of *Itgax*$^{\Delta OX40L}$.

b-e) Quantification of the proportion (b, d) and total number (c, e) of FoxP3^{+} CD44^{hi} CD4 T cells in control, OX40$^{-/-}$ and *Itgax*$^{\Delta OX40L}$ SILP and CLP. SILP control n=4, data pooled from 2 independent experiments, SILP OX40$^{-/-}$ and *Itgax*$^{\Delta OX40L}$ n=12, data pooled from 4 independent experiments, CLP control n=6, data pooled from 3 independent experiments, CLP OX40$^{-/-}$ n=9, data pooled from independent experiments, CLP *Itgax*$^{\Delta OX40L}$ n=10, data pooled from 3 independent experiments.

f) Representative histograms gated on CD44^{hi} CD4 T cells showing FoxP3 expression in control, OX40$^{-/-}$ and *Rorc* $^{\Delta OX40L}$ SILP and CLP. Controls are Cre$^{-/-}$ littermates of *Itgax* $^{\Delta OX40L}$ and *Cd4* $^{\Delta OX40L}$.

g-j) Quantification of the proportion (g, i) and total number (h, j) of FoxP3^{+} CD44^{hi} CD4 T cells in control, OX40$^{-/-}$ and *Rorc*$^{\Delta OX40L}$ SILP and CLP. SILP control n=7, data pooled from 3 independent experiments, SILP OX40$^{-/-}$ n=11, data pooled from 4 independent experiments, SILP *Rorc*$^{\Delta OX40L}$ n=14, data pooled from 4 independent experiments, CLP control and OX40$^{-/-}$ n=5, data pooled from 2 independent experiments, CLP *Rorc*$^{\Delta OX40L}$ n=7, data pooled from 2 independent experiments.

k) Representative histograms gated on CD44^{hi} CD4 T cells showing FoxP3 expression in control, OX40$^{-/-}$ and *Cd4*$^{\Delta OX40L}$ SILP and CLP. Controls are Cre$^{-/-}$ littermates of *Cd4*$^{\Delta OX40L}$.

l-o) Quantification of the proportion (l, n) and total number (m, o) of FoxP3^{+} CD44^{hi} CD4 T cells in control, OX40$^{-/-}$ and *Cd4*$^{\Delta OX40L}$ SILP and CLP. SILP control and *Cd4*$^{\Delta OX40L}$ n=6, data pooled from 2 independent experiments, SILP OX40$^{-/-}$ n=5, data pooled from 2 independent experiments, CLP controls n=9, data pooled from 3 independent experiments, CLP OX40$^{-/-}$ n=7, data pooled from 3 independent experiments, CLP *Cd4*$^{\Delta OX40L}$ n=7, data pooled from 2 independent expeirments.

Values on histograms represent percentages. Normality was tested using Shapiro-Wilk test. Lines on graphs show mean±SD (b, c, d, g, h, i, j, l, m, n, o) or median (e). Significance was tested using One-Way ANOVA (b, c, d, g, h, i, j, l, m, n, o) or Kruskal-Wallis test (e).

Signalling through OX40 relies on the availability of OX40L and recently published data have shown that OX40L provision is compartment-specific (Gajdasik et al., 2020). A wide range of immune and non-immune cells are able to present this molecule, likely reflecting the functional diversity of OX40:OX40L signalling (Imura et al., 1996; Ohshima et al., 1997; Stuber et al., 1995). Nonetheless, OX40L expression on APCs, ILC3s and activated T cells has a key role in shaping CD4 T cell responses (Castellanos et al., 2018; Takasawa et al., 2001). To test the key cellular source of OX40L in the steady state intestine the Treg cell compartment was assessed in *Itgax*^{cre}*Ox40l*$^{f/f}$, *Rorc*^{cre}*Ox40l*$^{f/f}$ and *Cd4*^{cre}*Ox40l*$^{f/f}$ mice with DC (*Itgax*$^{\Delta OX40L}$), ILC3/T cell- (*Rorc*$^{\Delta OX40L}$) and T cell-specific OX40L ablation (*Cd4*$^{\Delta OX40L}$), respectively. Components of the microbiota shape the intestinal CD4 T cell compartment with substantial effects on Treg cell heterogeneity (Al Nabhani et al., 2019; Miragaia et al., 2019). Therefore, Cre^{-} littermates were used as controls where possible (*Itgax*^{cre}*Ox40l*$^{f/f}$ and *Cd4*^{cre}*Ox40l*$^{f/f}$ mice) with the aim of limiting microbiota-induced differences. Looking simply at FoxP3 expression in mucosal CD4 T cells, there appeared to be no clear defect upon DC-specific OX40L deletion, only a modest drop in SILP Treg cell numbers compared to littermate controls (Fig3.7a-e). These data pointed to DC OX40L being mostly redundant for intestinal Treg cells. However, reduction in CLP Treg cell frequency upon *Rorc* promoter-driven OX40L deletion (Fig3.7f-j) coupled with no such effect on T cell-specific OX40L ablation (Fig3.7k-o) indicated at least partial reliance on ILC3 OX40L. This result is in line with the recent report that systemic Th1 cell responses require DC provision of OX40L but mucosal Th1 cells rely on ILC3 (Gajdasik et al., 2020).

Interestingly, cells expressing RORγt were enriched in the SILP and CLP Treg cell compartments of mice lacking OX40L on ILC3 compared to controls but did not change in absolute numbers (Fig3.8), indicating that RORγt^{+} Treg cells did not require OX40L from ILC3. However, drawing conclusions from these data is complicated due to the absence of littermate controls of *Rorc*^{cre}*Ox40l*$^{f/f}$ mice in these studies. Therefore, breeding strategies were adapted to yield both Cre^{+} and Cre^{-} mice in this strain. In addition, OX40L$^{-/-}$ animals were generated to test whether the effects observed on OX40 deletion

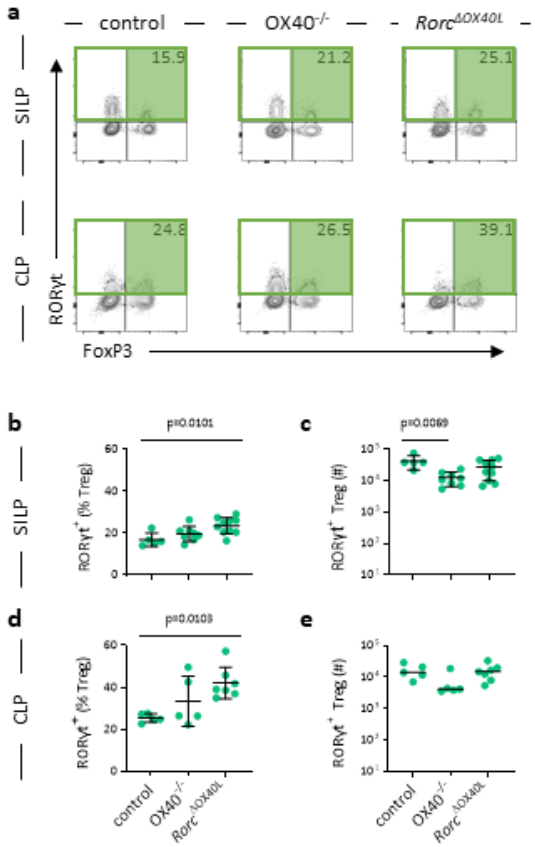
a
control
OX40-/-
RorcΔOX40L
SILP
CLP
RORγt
FoxP3
15.9
21.2
25.1
24.8
26.5
39.1
b
c
d
e
p=0.0101
p=0.0069
p=0.0103
RORγt+ (% Treg)
RORγt+ Treg (#)
control
OX40-/-
RorcΔOX40L

Figure 3.8. RORγt^{+} Treg cells are not reliant on ILC3 OX40L provision

The role of ILC3 OX40L provision in normal RORγt^{+} Treg cell frequency and number was assessed in *Rorc^{cre}Ox40l$^{fl/fl}$* (*Rorc$^{\Delta OX40L}$*) SILP and CLP at steady state.

a) Representative flow cytometry plots gated on CD44^{hi} CD4 T cells showing RORγt and FoxP3 expression in control, OX40$^{-/-}$ and *Rorc$^{\Delta OX40L}$* SILP and CLP. Controls are Cre$^{-/-}$ non-littermates.

b-e) Quantification of the proportion (b, d) and total number (c, e) of Treg cells expressing RORγt. SILP control n=5, data pooled from 2 independent experiments, SILP OX40$^{-/-}$ n=8, data pooled from 2 independent experiments, SILP *Rorc$^{\Delta OX40L}$* n=10, data pooled from 3 independent experiments, CLP control and OX40$^{-/-}$ n=5, data pooled from 2 independent experiments, CLP *Rorc$^{\Delta OX40L}$* n=7, data pooled from 2 independent experiments.

Values on flow cytometry plots represent percentage of population in shaded areas of population in total green areas. Normality was tested using Shapiro-Wilk test. Lines on graphs show mean±SD (b, c, d) or median (e). Significance was tested using One-Way ANOVA (b, c, d) or Kruskal-Wallis test (e).

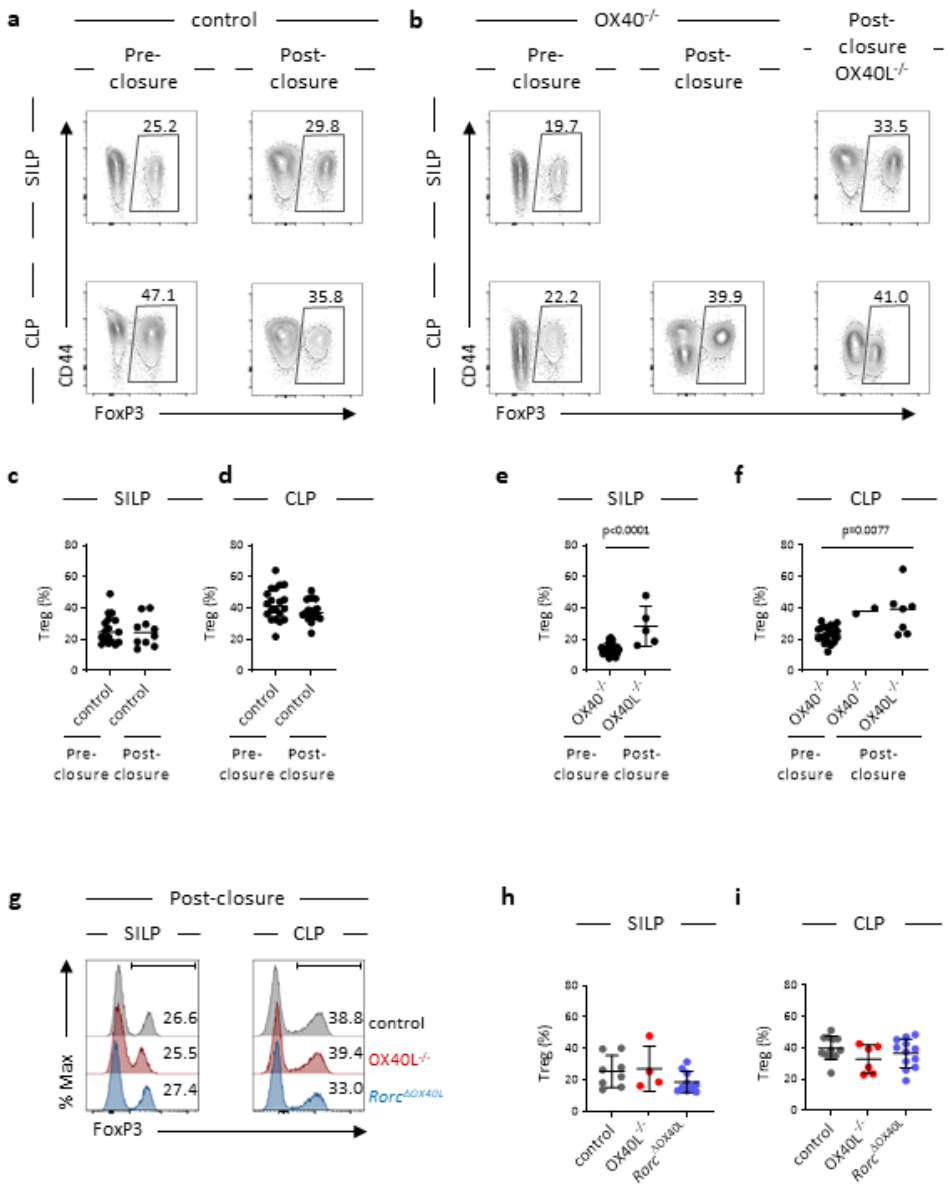
a
control
Pre-closure
Post-closure
SILP
CLP
CD44
FoxP3
25.2
29.8
47.1
35.8
b
OX40-/-
Pre-closure
Post-closure
Post-closure OX40L-/-
19.7
33.5
22.2
39.9
41.0
c
SILP
d
CLP
Treg (%)
control
control
Pre-closure
Post-closure
e
SILP
p<0.0001
OX40-/-
OX40L-/-
f
CLP
p=0.0077
g
Post-closure
SILP
CLP
% Max
26.6
25.5
27.4
38.8
39.4
33.0
control
OX40L-/-
RorcΔOX40L
h
SILP
i
CLP
control
OX40L-/-
RorcΔOX40L

Figure 3.9. Modest changes in intestinal Treg cell frequency were absent following prolonged animal facility closure

Intestinal Treg cells were assessed in control OX40 and OX40L-sufficient, OX40-deficient ($OX40^{-/-}$) and OX40L-deficient ($OX40L^{-/-}$) mice before and after extended animal facility closure.

a) Representative flow cytometry plots gated on CD4 T cells showing CD44 and FoxP3 expression in control SILP and CLP prior to and following animal facility closure. Controls are $Cre^{-/-}$ littermates of $Itgax^{\Delta OX40L}$, $Rorc^{\Delta OX40L}$ and $Cd4^{\Delta OX40L}$.

b) Representative flow cytometry plots gated on CD4 T cells showing CD44 and FoxP3 expression in $OX40^{-/-}$ SILP and CLP prior to and following animal facility closure, and $OX40L^{-/-}$ SILP and CLP following animal facility closure.

c-d) Quantification of the proportion of $FoxP3^{+}$ CD4 T cells prior to and following animal facility closure in control SILP (c) and CLP (d). SILP pre-closure and CLP post-closure n=17, data pooled from 7 independent experiments, SILP post-closure n=10, data pooled from 5 independent experiments and CLP pre-closure n=20, data pooled from 8 independent experiments.

e-f) Quantification of the proportion of $FoxP3^{+}$ CD4 T cells prior to animal facility closure in $OX40^{-/-}$ SILP and CLP, and following animal facility closure in $OX40^{-/-}$ CLP and $OX40L^{-/-}$ SILP and CLP. SILP $OX40^{-/-}$ pre-closure n=28, data pooled from 10 independent experiments, SILP $OX40L^{-/-}$ post-closure n=5, data pooled from 4 independent experiments, CLP $OX40^{-/-}$ pre-closure n=21, data pooled from 8 independent experiments, CLP $OX40^{-/-}$ post-closure n=2, data from 1 experiment and CLP $OX40L^{-/-}$ n=7, data pooled from 5 independent experiments.

g) Representative histograms showing FoxP3 expression in $CD44^{hi}$ CD4 T cells in control, $OX40L^{-/-}$ and $Rorc^{\Delta OX40L}$ SILP and CLP following animal facility closure. Controls are $Cre^{-/-}$ littermates of $Rorc^{\Delta OX40L}$.

h-i) Quantification of the proportion of $FoxP3^{+}$ CD4 T cells in control, $OX40L^{-/-}$ and $Rorc^{\Delta OX40L}$ SILP (h) and CLP (i) following animal facility closure. SILP control n=8, data pooled from 4 independent experiments, SILP $OX40L^{-/-}$ n=4, data pooled from 3 independent experiments, SILP $Rorc^{\Delta OX40L}$ n=10, data pooled from 4 independent experiments, CLP control n=12, data pooled from 5 independent experiments, CLP $OX40L^{-/-}$ n=6, data pooled from 4 independent experiments and CLP $Rorc^{\Delta OX40L}$ n=12, data pooled from 5 independent experiments.

Values on flow cytometry plots and histograms represent percentages. Normality was tested using Shapiro-Wilk test. Lines on graphs show mean±SD (e, h, i) or median (c, d, f). Significance was tested using unpaired t test (e), Mann-Whitney U test (c, d, f) or One-Way ANOVA (h, i).

were specifically due to a lack of OX40:OX40L interaction, not an as yet unidentified mechanism. As new mouse strains were established the facility housing these animal colonies shut and would not reopen for several months due to the COVID-19 pandemic. Surprisingly, comparison of intestinal Treg cell populations in control and $OX40^{-/-}$ or $OX40L^{-/-}$ mice prior to and following this closure (Fig3.9a-b) revealed a shift in the mucosal Treg cell compartment as Treg cell proportion increased specifically in OX40- and OX40L-deficient mice (Fig3.9c-f). The modest but significant reduction in intestinal Treg cells of *Rorc*^{cre}*Ox40l*$^{f/f}$ mice observed prior to closure was also no longer evident (Fig3.9g-i) providing further evidence of a change in mucosal Treg cell OX40 reliance. In the absence of sufficiently sophisticated models that could aid the study of intestinal Treg cell OX40L reliance these investigations were stopped, and further studies focused on mucosal CD4 T cell responses to pathogens.

3.5.2 Colonic pathogen clearance is impaired in the absence of OX40

Unlike Treg cells, murine effector T cells express OX40 only transiently following activation (Vu et al., 2007). The unperturbed intestinal RORγt^{+}FoxP3^{-} CD4 T cell compartment of $OX40^{-/-}$ mice (Fig3.6) may not reflect a lack of reliance on OX40 signalling and could instead have resulted from these analyses not capturing an active type 3 CD4 T cell response. Therefore, a model that induces a large intestinal Th17 cell-dominated response was included in further studies (Fig3.10a).

C.rodentium is a widely used experimental tool as it is a natural mouse pathogen with characteristics similar to those of enteropathogenic and enterohaemorrhagic *E.coli* (Petty et al., 2010). Oral *C.rodentium* administration results in colonisation of the large intestinal mucosa (Wiles et al., 2005) and has several features that make it a useful mucosal Th17 cell model. First, evident from assessment of IL-17A expression in CLP CD4 T cells from control and infected mice (Fig3.10b), the infection precipitates a Th17 cell-dominated response. In addition to the large increase in both the proportion and total number of CD4 T cells producing this cytokine (Fig3.10c-d), Th17 cell induction was further supported by the expansion of CD4 T cells showing a history of IL-17A expression in *Il17a*^{cre}*Rosa26*^{tdRFP}

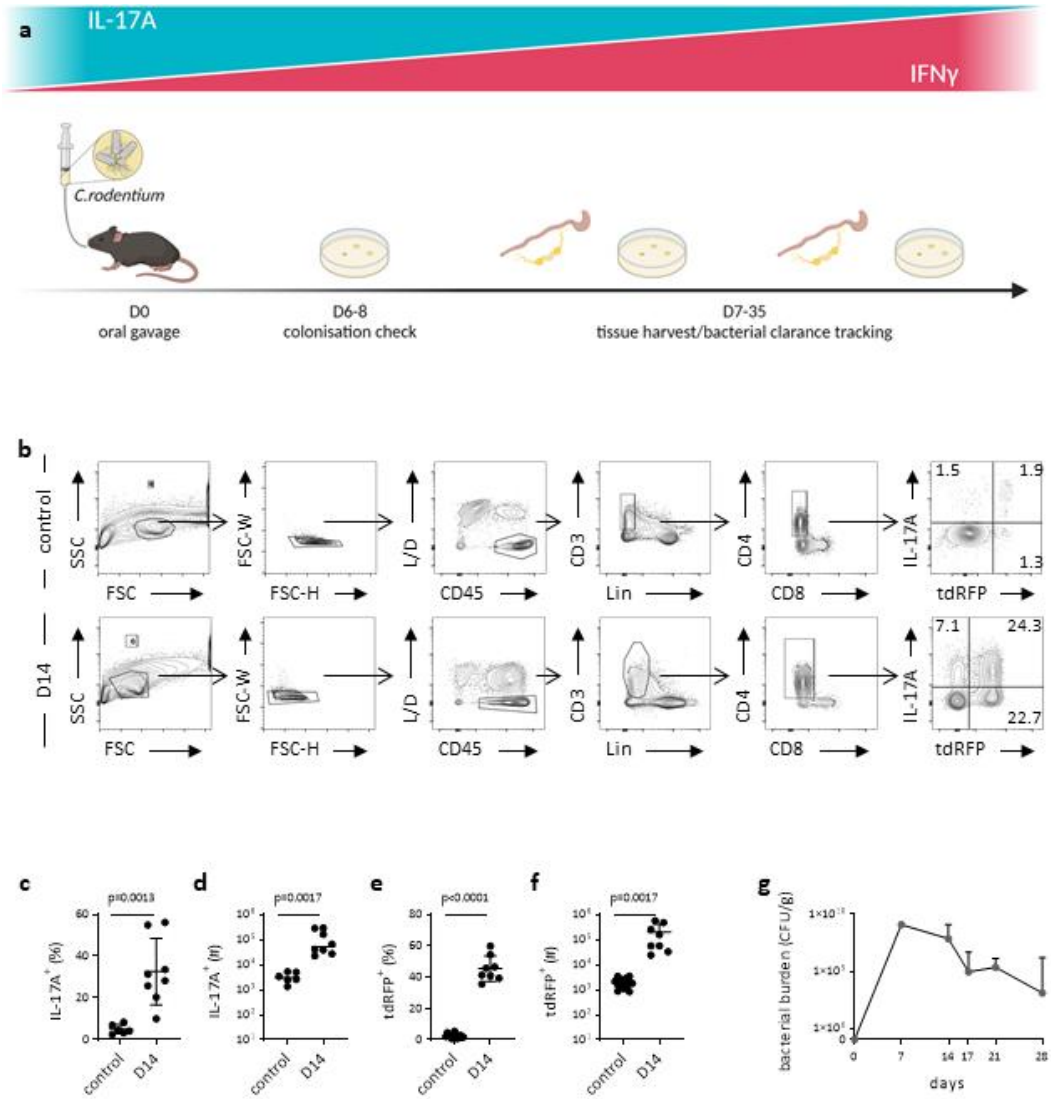
a
IL-17A
IFNγ
C.rodentium
D0
oral gavage
D6-8
colonisation check
D7-35
tissue harvest/bacterial clarance tracking
b
control
D14
SSC
FSC
FSC-W
FSC-H
L/D
CD45
CD3
Lin
CD4
CD8
IL-17A
tdRFP
1.5
1.9
1.3
7.1
24.3
22.7
c
p=0.0013
IL-17A+ (%)
d
p=0.0017
IL-17A+ (#)
e
p<0.0001
tdRFP+ (%)
f
p=0.0017
tdRFP+ (#)
control
D14
g
bacterial burden (CFU/g)
days

Figure 3.10. *C.rodentium* infection elicits a Th17 cell-dominated colonic immune response

The *C.rodentium* infection model enables the assessment of a *de novo* generated colonic Th17 cell response.

a) Schematic representation of the experimental model. *C.rodentium* gavage results in colonisation of the large intestinal mucosa, identifiable by day 6-8 (D6-8) from faecal bacterial burden, and enables the assessment of a Th17 cell immune response showing the characteristic Th17-IFNγ^{+} exTh17 cell switch, and the tracking of bacterial clearance from faecal bacterial burden.

b) Representative flow cytometry plots illustrating the gating strategy to identify CD4 T cells, and showing IL-17A and tdRFP expression in *Il17a^{cre}Rosa26^{tdRFP}* CLP with no infection (control) or on D14 of *C.rodentium* infection.

c-d) Quantification of the proportion (c) and total number (d) of CD4 T cells producing IL-17A in *Il17a^{cre}Rosa26^{tdRFP}* CLP with no infection (control) or on D14 of *C.rodentium* infection. Control n=6, data pooled from 2 independent experiments, D14 n=8, data pooled from 3 independent experiments.

e-f) Quantification of the proportion (e) and total number (f) of CD4 T cells expressing tdRFP in *Il17a^{cre}Rosa26^{tdRFP}* CLP with no infection (control) or on D14 of *C.rodentium* infection. Control n=14, data pooled from 5 independent experiments, D14 n=8, data pooled from 3 independent experiments.

g) Bacterial burden shown as colony forming units per gram of faeces (CFU/g) of successfully colonised *Il17a^{cre}Rosa26^{tdRFP}* mice up to D28 of the infection. D7, D14, D28 n=6, data from 1 experiment, D17, D21 n=5, data from 1 experiment.

Values on flow cytometry plots represent percentages. Normality was tested using Shapiro-Wilk test. Lines on graphs show mean±SD (c, e, f) or median (d). Significance was tested using unpaired t test (c, e, f) or Mann-Whitney U test (d). Datapoints show median+95%CI (g).

CLP (Fig3.10e-f). Further increasing this system's appeal as a mucosal Th17 cell model, *C.rodentium*-induced Th17 cells show a high degree plasticity towards a Th1-like exTh17 cell state, unlike those induced by commensal microbes (Omenetti et al., 2019). The observation that CD4 T cells with a history of IL-17A expression but no active cytokine production (IL-17A^{-}tdRFP^{+}) were present at a high frequency (nearly a quarter of all CD4 T cells) in CLP harvested from infected mice (Fig3.10b) was consistent with this differentiation process occurring in mouse colonies used in these investigations following *C.rodentium* colonisation. Finally, quantification of faecal bacterial burden, a measure of the amounts of bacteria shed into the intestinal lumen, allowed tracking of colonisation and bacterial clearance (Fig3.10g). These, in turn, served as key functional readouts of the immune response.

As reported earlier, there was no evidence of any OX40 ablation-related defect in the accumulation of Th17 cells present in the intestine at steady state (Fig3.6). However, to account for transient OX40 expression on newly induced Th17 cells, I sought to further assess OX40:OX40L reliance in the *C.rodnetium* infection model. Preliminary studies suggested that there may have been a delay in *C.rodentium* clearance. Interestingly, neither DC- nor ILC3/T cell-specific deletion phenocopied this observation (Fig3.11a-b). However, further repeats with larger sample sizes would be desirable to confirm these results. In addition, tracking faecal bacterial burden did not reveal whether potential defects in CD4 T cell cytokine production or other immune functions were behind the impairment in *C.rodentium* clearance. *Great/Smart-17a* mice that report IFNγ and IL-17A production by co-expression of enhanced yellow fluorescent protein (eYFP) and human nerve growth factor receptor (hNGFR), respectively (Price et al., 2012; Reinhardt et al., 2009), enabled assessment of cytokine production in the absence of *ex vivo* manipulation (Fig3.11c). These dual reporter mice were therefore crossed with control, *Itgax^{cre}Ox40l$^{f/f}$* and CD30/OX40 double knockout (DKO) mice and infected with *C.rodentium*. Expression of eYFP and hNGFR induced by *C.rodentium* colonisation was assessed to test infection-induced cytokine expression (Fig3.11d). Roughly 2 weeks following infection IL-17A and IFNγ production in control animals was found to be largely limited to the effector site (Fig3.11e-p). In addition, the CLP of these animals showed very limited CD4 T cell populations reporting IL-17A

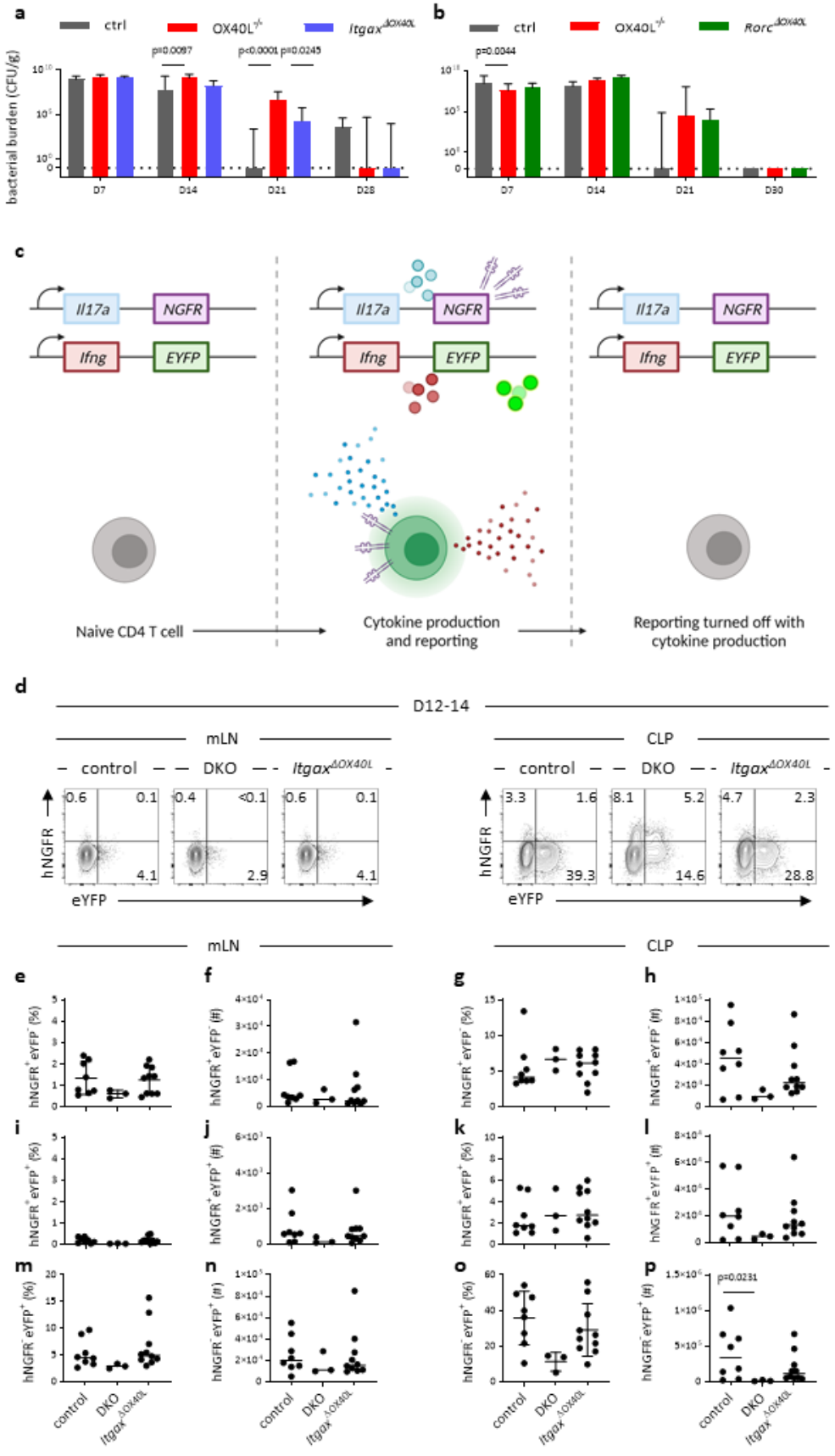
a
ctrl
OX40L-/-
Itgax ΔOX40L
bacterial burden (CFU/g)
p=0.0097
p<0.0001
p=0.0245
D7
D14
D21
D28
b
ctrl
OX40L-/-
Rorc ΔOX40L
p=0.0044
D7
D14
D21
D30
c
Il17a
NGFR
Ifng
EYFP
Naive CD4 T cell
Cytokine production and reporting
Reporting turned off with cytokine production
d
D12-14
mLN
CLP
control
DKO
Itgax ΔOX40L
hNGFR
eYFP
0.6
0.1
4.1
0.4
<0.1
2.9
0.6
0.1
4.1
3.3
1.6
39.3
8.1
5.2
14.6
4.7
2.3
28.8
mLN
CLP
e
f
g
h
i
j
k
l
m
n
o
p
hNGFR+eYFP- (%)
hNGFR+eYFP- (#)
hNGFR+eYFP+ (%)
hNGFR+eYFP+ (#)
hNGFR-eYFP+ (%)
hNGFR-eYFP+ (#)
p=0.0231
control
DKO
Itgax ΔOX40L

Figure 3.11. OX40:OX40L interactions support bacterial clearance through an unknown mechanism

Mice lacking OX40L (OX40L$^{-/-}$) or CD30 and OX40 (CD30/OX40 double knockout, DKO), and mice deleting OX40L on DC (*Itgax*$^{\Delta OX40L}$) or T cells and ILC3 (*Rorc*$^{\Delta OX40L}$) were assessed to test the requirement for OX40:OX40L interactions in mounting appropriate responses to *C.rodentium* infection. *Great/Smart-17a* mice used enabled detection of IL-17A and IFNγ production without the need for *ex vivo* restimulation with OMA and ionomycin.

a) Bacterial burden shown as colony forming units per gram of faeces (CFU/g) of successfully colonised control, OX40L$^{-/-}$ and *Itgax*$^{\Delta OX40L}$ mice up to D28 of the infection. Controls are Cre$^{-/-}$ littermates of *Itgax*$^{\Delta OX40L}$. D7 control and D7 *Itgax*$^{\Delta OX40L}$ n=9, D14 control n=8, D21 and D28 control n=10, D7, D21, D28 OX40L$^{-/-}$, and D14 *Itgax*$^{\Delta OX40L}$ n=6, D14 OX40L$^{-/-}$ n=4, D21 and D28 *Itgax*$^{\Delta OX40L}$ n=11. All data from 1 experiment.

b) Bacterial burden shown as colony forming units per gram of faeces (CFU/g) of successfully colonised control, OX40L$^{-/-}$ and *Rorc*$^{\Delta OX40L}$ mice up to D30 of the infection. Controls are Cre$^{-/-}$ littermates of *Rorc*$^{\Delta OX40L}$. D7, D21, D30 control and D21 OX40L$^{-/-}$ n=7, D14 control n=6, D7 and D30 OX40L$^{-/-}$ n=8, D14 OX40L$^{-/-}$ n=5, D7, D14, D21 and D30 *Rorc*$^{\Delta OX40L}$ n=4. All data from 1 experiment.

c) Schematic representation of IFNγ and IL-17A detection in *Great/Smart-17a* mice. Cells co-express IL-17A with the cell surface protein human nerve growth factor receptor (hNGFR) and IFNγ with enhanced yellow fluorescent protein (eYFP).

d) Representative flow cytometry plots showing hNGFR and eYFP expression in CD44^{hi} CD4 T cells in *Great/Smart*-17a x control, DKO and *Itgax*$^{\Delta OX40L}$ mLN and CLP on D12-14 of *C.rodentium* infection.

e-h) Quantification of the proportion and total number of CD44^{hi} CD4 T cells expressing hNGFR but no eYFP in control, DKO and *Itgax*$^{\Delta OX40L}$ mLN (e, f) and CLP (g, h) on D12-14 of *C.rodentium* infection. Control n=8, data pooled from 3 independent experiments, DKO n=3, data pooled from 2 independent experiments and *Itgax*$^{\Delta OX40L}$ n=10, data pooled from 3 independent experiments.

i-l) Quantification of the proportion and total number of CD44^{hi} CD4 T cells expressing both hNGFR and eYFP in control, DKO and *Itgax*$^{\Delta OX40L}$ mLN (i, j) and CLP (k, l) on D12-14 of *C.rodentium* infection. Control n=8, data pooled from 3 independent experiments, DKO n=3, data pooled from 2 independent experiments and *Itgax*$^{\Delta OX40L}$ n=10, data pooled from 3 independent experiments.

m-p) Quantification of the proportion and total number of CD44^{hi} CD4 T cells expressing eYFP but no hNGFR in control, DKO and *Itgax*$^{\Delta OX40L}$ mLN (m, n) and CLP (o, p) on D12-14 of *C.rodentium* infection. Control n=8, data pooled from 3 independent experiments, DKO n=3, data pooled from 2 independent experiments and *Itgax*$^{\Delta OX40L}$ n=10, data pooled from 3 independent experiments.

Values on flow cytometry plots represent percentages. Normality was tested using Shapiro-Wilk test. Bars show median+95%CI (a, b). Lines on graphs show mean±SD (e, o) or median (f, g, h, i, j, k, l, m, n, p). Significance was tested using One-Way ANOVA (e, o) or Kruskal-Wallis test (a, b, f, g, h, i, j, k, l, m, n, p).

expression (Fig3.11g,k) and an accumulation of cells reporting IFNγ (Fig3.11o). This could point to the presence of a large IFNγ^{+} exTh17 cell population, however, in the absence of IL-17A fate mapping the induction of Th1 cells cannot be excluded. The lack of significant defects in cytokine production in total OX40 and conditional OX40L knockout mice suggested that either a larger sample size is required to resolve differences or that impairment of *C.rodentium* control was caused by mechanisms unrelated to IL-17A and IFNγ production. Furthermore, it is clear that *C.rodentium* infection-induced IL-17A reporting by hNGFR expression (Fig3.11) was 5-7-fold lower than IL-17A expression following *ex vivo* restimulation (Fig3.10). While it is possible that hNGFR staining efficiency is low it must also be noted that *ex vivo* manipulation could force cells that would not produce IL-17A under physiological conditions to express the cytokine, therefore overestimating population size.

In summary, preliminary experiments investigating the contribution of OX40 signals to Th17/Treg cell persistence and function indicated limited but clear effects on Treg cell and a potential impact on IFNγ^{+} exTh17 cell differentiation.

3.6 PATHOGEN INVASION DOES NOT TRIGGER INTESTINAL LAMINA PROPRIA TREG-TO-TH17 CELL CONVERSION

As previously reported, the steady state intestinal lamina propria was found to harbour only a minimal population of Th17 cells with a history of Treg cell master TF FoxP3 expression. However, Treg cell acquisition of Th17 cell characteristics and full conversion into 'exTreg' Th17 cells has been reported mainly in inflammatory microenvironments associated with the development of pathology (Hovhannisyan et al., 2011; Komatsu et al., 2014; Massoud et al., 2016). Therefore, I sought to test the hypothesis that Treg-to-Th17 cell conversion occurs more readily following *C.rodentium* infection than at steady state. Using the *FoxP3$^{eGFP\text{-}Cre\text{-}ERT2}$Ai14* mice the tamoxifen-dosing schedule was modified to include *C.rodentium* infection without affecting the resting period between tamoxifen treatment and assessment of cytokine production (Fig3.12a). This system was used to test whether an inflammatory

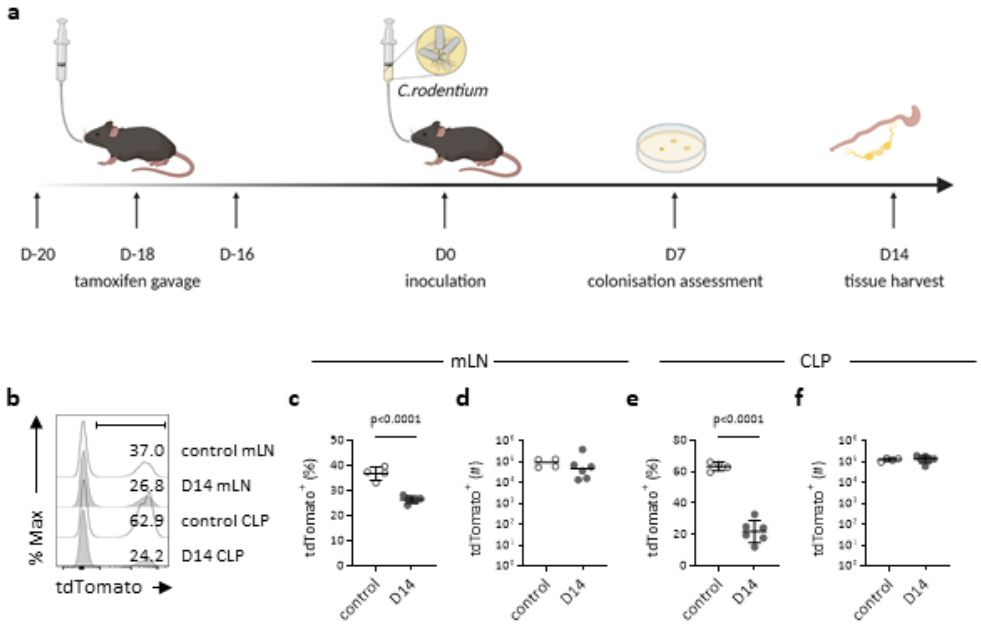
a
C.rodentium
D-20
D-18
D-16
D0
D7
D14
tamoxifen gavage
inoculation
colonisation assessment
tissue harvest
mLN
CLP
b
37.0
control mLN
26.8
D14 mLN
62.9
control CLP
24.2
D14 CLP
% Max
tdTomato
c
d
e
f
p<0.0001
p<0.0001
tdTomato+ (%)
tdTomato+ (#)
control
D14

Figure 3.12. *C.rodentium* infection increases mLN and CLP cell turnover

Foxp3$^{eGFP\text{-}Cre\text{-}ERT2}$*Ai14* mice inoculated with *C.rodentium* enabled assessment of pathogen-induced changes in FoxP3 expression history in mLN and CLP.

a) Schematic representation of experimental design.

b) Representative histograms gated on CD44^{hi} CD4 T cells showing tdRFP expression in mLN and CLP on D14 following gavage with PBS (control) or *C.rodentium* (D14).

c-f) Quantification of the proportion and total number of tdRFP^{+} CD44^{hi} CD4 T cells in mLN (c, d) and CLP (e, f) on D14 following gavage with PBS or *C.rodentium*. Control mLN and CLP n=4, D14 mLN and CLP n=6. All data from 1 experiment.

Values on histograms represent percentages. Normality was tested using Shapiro-Wilk test. Lines on graphs show mean±SD (c, e, f) or median (d). Significance was tested using unpaired t test (c, e, f) or Mann-Whitney U test (d).

stimulus could push lamina propria Treg cells to differentiate into Th17 cells, losing FoxP3 expression in the process. Infection appeared to induce increased $CD44^{hi}$ CD4 T cell turnover in both the CLP and mLN, as evidenced by the reduction in the proportion but not total number of cells fate reporting FoxP3 expression (Fig3.12b-f). Importantly, these data were not directly comparable to those reported at steady state. The parent populations differed in the mLN due to the inclusion of CD44 staining in the *C.rodentium* infection studies. Further assessing populations defined by IL-17A and FoxP3 expression (Fig3.13a) identified clear differences only in the CLP and not in the CLP-draining mLN (Fig3.13b-m). The reduction of proportion but not number of IL-$17A^-$ Treg cells (Fig3.13d-e) and concurrent increase of both the proportion and number of Th17 cells (Fig3.13l-m) suggested that CLP Treg cells were fairly stable with an influx of Th17 cells responsible for their decreased frequency. However, changes in the Treg cell compartment became evident on assessment of tdTomato expression (Fig3.13n-z). The 2-4-fold decrease in the frequency of FoxP3 fate reporting in Treg cell populations compared to uninfected controls pointed to an increase in CLP Treg cell turnover following infection (Fig3.13q,u). The decrease in the number of $tdTomato^+$IL-$17A^-$ Treg cells in the CLP (Fig3.13r) raised the possibility that these cells acquired IL-17A following infection, although this was not supported by the lack of change in the number of $tdTomato^+$IL-$17A^+$ Treg cells (Fig3.13v). *C.rodentium* triggered a drop in the frequency but not number of CLP Th17 cells fate reporting FoxP3 expression (Fig3.13y-z) suggesting that newly generated pathogen-responsive Th17 cells did not go through a $FoxP3^+$ stage during their differentiation. Given the context of an inflammatory response this was unsurprising. Changes in the mLN Treg and Th17 cell compartment were modest but largely followed the patterns observed in the CLP (Fig3.13o-p,s-t,w-x). In summary, these data revealed no evidence to support the hypothesis that Treg cell conversion to Th17 cells forms part of the response to *C.rodentium* infection.

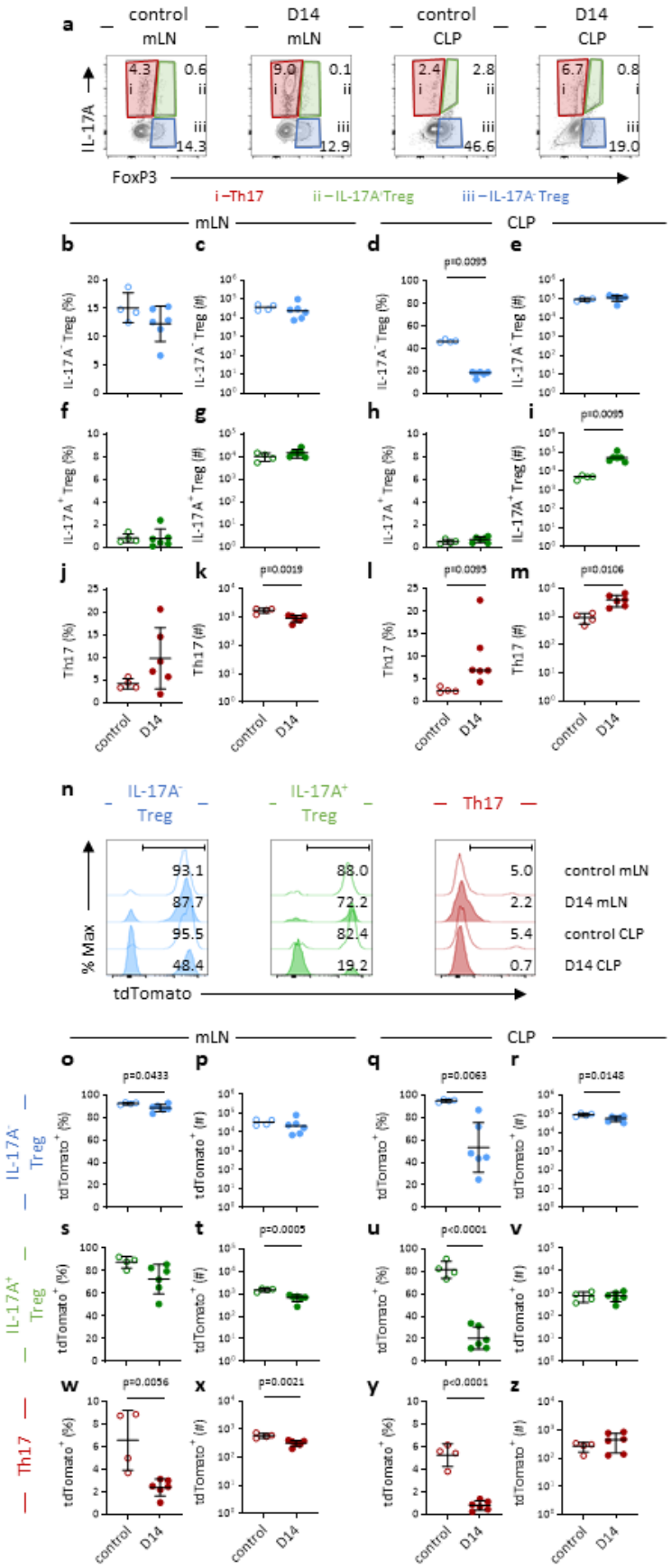
a
control mLN
D14 mLN
control CLP
D14 CLP
IL-17A
FoxP3
i –Th17
ii – IL-17A+Treg
iii – IL-17A- Treg
mLN
CLP
b
c
d
e
f
g
h
i
j
k
l
m
p=0.0095
p=0.0019
p=0.0106
control
D14
n
IL-17A- Treg
IL-17A+ Treg
Th17
% Max
tdTomato
control mLN
D14 mLN
control CLP
D14 CLP
o
p
q
r
s
t
u
v
w
x
y
z
p=0.0433
p=0.0063
p=0.0148
p=0.0005
p<0.0001
p=0.0056
p=0.0021
p<0.0001

Figure 3.13. *C.rodentium* infection increases Treg cell turnover but not Treg-toTh17 cell conversion

Foxp3$^{eGFP\text{-}Cre\text{-}ERT2}$*Ai14* mice inoculated with *C.rodentium* enabled assessment of pathogen-induced Treg-to-Th17 cell conversion.

a) Representative flow cytometry plots gated on CD44^{hi} CD4 T cells showing IL-17A and FoxP3 expression following *ex vivo* restimulation with PMA and ionomycin and identification of Th17, IL-17A^{+} Treg and IL-17A^{-} Treg cell populations in mLN and CLP on D14 following gavage with PBS (control) or *C.rodentium* (D14).

b-m) Quantification of the proportion and total number of the populations identified in (a) within the parent population in mLN (b, c, f, g, j, k) and CLP (d, e, h, i, l, m) on D14 following gavage with PBS or *C.rodentium*. Control mLN and CLP n=4, D14 mLN and CLP n=6. All data from 1 experiment.

n) Representative histograms showing tdRFP expression in the populations identified in (a) in mLN and CLP on D14 following gavage with PBS or *C.rodentium*.

o-z) Quantification of the proportion of tdRFP^{+} cells within the populations identified in (a) in mLN (o, p, s, t, w, x) and CLP (q, r, u, v, y, z) on D14 following gavage with PBS or *C.rodentium*. Control mLN and CLP n=4, D14 mLN and CLP n=6. All data from 1 experiment.

Values on flow cytometry plots and histograms represent percentages. Normality was tested using Shapiro-Wilk test. Lines on graphs show mean±SD (c, e, f, g, h, j, k, m, o, q, r, s, t, u, v, w, x, y, z) or median (b, d, i, l, p). Significance was tested using unpaired t test (c, e, f, g, h, j, k, m, o, q, r, s, t, u, v, w, x, y, z) or Mann-Whitney U test (b, d, i, l, p).

3.7 SUMMARY

The characterisation of mucosal and systemic CD4 T cell populations presented here has shown that, in line with published data, RORγt$^+$ cells accumulate in mucosal and mucosal-draining sites with limited systemic presence. This could point to Th17 cell enrichment at these sites. As expected based on published literature, IL-17A-producing cells were found at a higher frequency in the small intestine than in the colon. Interestingly, this observation was made despite both these mucosal barrier sites having the same frequency of RORγt$^+$ CD4 T cells. Potentially underlying these observations, microbes known to be potent inducers of homeostatic Th17 cells, such as SFB, reside in the distal small intestine but are not found in the colon (Ivanov et al., 2009). The limited colonic CD4 T cell IL-17A production but abundant RORγt expression observed could be explained by several reported observations. RORγt expression in activated CD4 T cells does not solely mark Th17 cells but has also been described in mucosal pTreg cells (Ohnmacht et al., 2015; Sefik et al., 2015) with important roles in aiding suppressive capacity (Bhaumik et al., 2021). Therefore, it is likely that not all RORγt$^+$ CD44^{hi} CD4 T cells identified in the intestinal mucosa, and especially in the CLP were Th17 cells. In addition, colonic Th17 cells may not produce large amounts of IL-17A at steady state and, given their comparatively low stability (Mukasa et al., 2010), could give rise to alternative CD4 T cell subsets. Relying on IL-17A fate mapping to specifically address the issue of Th17 cell stability and plasticity, IFNγ$^+$ Th1-like cells with a history of IL-17A expression were identified not only in the colon but also in the small intestine. The presence of Th1-like exTh17 cells in the small intestine contradicts published literature as homeostatic Th17 cells in this location, especially populations induced by SFB, are thought to show a lower predisposition towards acquisition of alternative effector programmes (Omenetti et al., 2019). The SFB colonisation state of animals used in these investigations is unknown, but should SFB be absent in the animal facility or in specific mouse colonies results presented here may not fully recapitulate other reported observations (Ivanov et al., 2009). Future assessment of SFB colonisation, and the composition of the animals' intestinal flora generally, would be of great interest and benefit the interpretation of these results. Nonetheless, the data presented in this chapter demonstrate that

IFNγ^{+} exTh17 cells may play important roles in the maintenance of mucosal homeostasis. The precise role these cells play at steady state must be explored, especially given that IFNγ producing cells of a Th17 cell origin are currently predominantly associated with diseases making them targets of therapeutic interventions (Annunziato et al., 2007; Bilal et al., 2018; Langowski et al., 2006).

Further to identifying Th1 cell-like exTh17 cells, a microenvironment-specific link between mucosal Th17 and Treg cell populations and functions was also observed. Even though cytokine expression was found to be minimal in the colon at steady state the data presented here identified Treg cells fate reporting IL-17A production at a higher frequency in the colon than in the small intestine. As previously mentioned, RORγt and other Th17 cell-associated TFs are often co-expressed with FoxP3 in mucosal Treg cells, but this is only reported to be associated with IL-17A production during pathogen invasion. There, it is unclear whether this has a protective role or merely represents a dysregulation of the Th17 cell programme (Remedios et al., 2018). Interestingly, the Treg cells identified in this work with a history of IL-17A production appeared to possess intermediate Th17 cell-like characteristics, including IL-17A production, raising the possibility that I was observing Th17/Treg cell conversion at steady state. However, the models used were not able to resolve the direction of this conversion. Turning to FoxP3 fate reporter mice to further probe the link between intestinal Th17 and Treg cells provided no evidence, at steady state or during infection, that Treg cells give rise to large populations of Th17 cells. Interestingly, these data did somewhat unexpectedly suggest that the inflammation triggered by pathogen invasion resulted in not just Th17 but also Treg cell population expansion. A potential explanation is that *C.rodentium*-driven Treg cell induction serves to generate a pool of cells poised to control Th17 cell-mediated inflammation and limit tissue damage. Importantly, such activity must be inhibited until the infection is contained and mechanisms that limit FoxP3-mediated suppression in inflammatory microenvironments have been proposed (van Loosdregt et al., 2013). On the other hand, an apparent increase in Treg cell induction could also be the result of FoxP3 expression by effector T cells, a phenomenon observed under inflammatory conditions but not associated with suppressive function (Tran et al., 2007). A possible interpretation of these data is Th17 cells could give

rise to Treg cells, but intestinal Treg cells are a stable population that do not lose FoxP3 expression even during pathogen invasion or when Th17 cell-associated effector functions are activated. In fact, Treg-to-Th17 cell conversion is mostly linked with pathology (Komatsu et al., 2014; Massoud et al., 2016) but Treg cell acquisition of Th17 cell functions and Th17-to-Treg cell differentiation can have both beneficial and detrimental effects. Th17 cell transdifferentiation into Treg cells is key to resolution of acute inflammation and return to homeostasis (Gagliani et al., 2015). However, the same process also contributes to disease progression in models of ovarian cancer (Downs-Canner et al., 2017). Moreover, an increase in IL-17A-producing Treg cell numbers is associated with a multitude of autoimmune and inflammatory conditions affecting a range of barrier sites (Hovhannisyan et al., 2011; Remedios et al., 2018). Importantly, the work presented in this chapter focused on the mucosal lamina propria. However, a microbiota-dependent physiological conversion of Treg cells into effector subsets was described in healthy mice but only in cell populations that entered the intestinal epithelium (Sujino et al., 2016). Therefore, all conclusions drawn are limited to lamina propria CD4 T cells and it is conceivable that my analyses simply missed 'exTreg' Th17 cells. Inclusion of the intraepithelial lymphocyte (IEL) compartment would be beneficial in future studies. Nonetheless, these data show that Treg cells producing IL-17A are present in the intestinal mucosa in the absence of pathology, suggesting that, much like the IFNγ^{+} exTh17 cell population, IL-17A^{+} Treg cells may have unappreciated roles in barrier maintenance at steady state.

The clear differences observed between colonic and small intestinal Th17 and Treg cell populations prompted assessment of potential mechanisms controlling CD4 T cell fate. Following previous work from showing that OX40L provision is highly compartment-specific (Gajdasik et al., 2020), and given the importance of but lack of clarity on the role of the OX40:OX40L pathway in Treg and Th17 cell regulation I hypothesised that microenvironment-specific OX40 activation partially accounts for the observed differences. Interestingly, even though the absence of OX40L was found to impair the control of mucosal *C.rodentium* infection studies presented here did not link the defect to a specific

cellular source of OX40L or to aberrant Th17 or exTh17/Th1 cell function. However, this work suffered from a small sample size and the inclusion of further repeats and datapoints would be beneficial.

An OX40-dependent mucosal Treg cell subpopulation that likely relied on ILC3 for OX40L provision was identified in the absence of infection, in line with reported data on the costimulatory requirements of mucosal CD4 T cell responses (Gajdasik et al., 2020). However, prolonged closure of the facility housing these animal colonies resulted in a loss of this phenotype. These changes could potentially have been caused by modifications in the composition of the Treg cell compartment with subpopulations reliant on OX40 for normal frequency and numbers absent or diminished. The microbiota has profound effects on shaping the mucosal and systemic immune compartments. Therefore, it is possible that that during facility closure changes in animal husbandry, such as feed composition or staff shift patterns, impacted the mucosal CD4 T cell compartment through modulation of the microbiota or environmental signals (Franklin & Ericsson, 2017).

Given that the reduction in FoxP3^{+} activated CD4 T cells in the absence of OX40 was small even when observed, teasing apart the exact mechanisms involved in the small proportion of intestinal Treg cells that did rely on OX40 likely requires more detailed analyses than our models allowed. *Helicobacter hepaticus* is a pathobiont that can induce both pathogenic Th17 and pTreg cells. Murine T cells responding to *H.hepaticus* can be identified with the aid of a peptide:MHCII complex (Xu et al., 2018) providing a tractable model of commensal-induced Th17 and pTreg cell responses. Future work could focus specifically on Th17/pTreg cell homeostasis and the role OX40 signalling plays in this process by employing this colonisation model.

In summary, the data presented in this chapter confirm that I was able to identify mucosal Th17 cell populations and, as established by others, found them predominantly in the small intestine at steady state. Moreover, I have shown how the IL-17A 'fate mapper' mouse enables assessment for Th17 cell plasticity and differentiation into alternative CD4 T cell subsets. Using this model, Th17 cell conversion into both pro-inflammatory and regulatory populations was observed. However, results presented

here indicated that Treg cell differentiation into ‘exTreg’ Th17 cells is far less prevalent. Furthermore, my assessment of cell fate decision regulation did not reveal a specific role for the OX40:OX40L pathway and if this mechanism is involved, it would appear to play a subtle role.

CHAPTER 4: TRANSCRIPTIONAL REGULATION OF TH17 CELL FATE AND IDENTITY

4.1 INTRODUCTION

Naïve CD4 T cells primed by cognate antigen presentation differentiate into distinct lineages dictated by defined polarising cytokine cocktails derived from APCs (Harrington et al., 2005; Mosmann et al., 1986). Primed CD4 T cells activate genetic programmes driven by lineage-defining 'master' TFs, resulting in modular acquisition of functional properties, such as cytokine, chemokine and chemokine receptor expression (Fu et al., 2004; Ivanov et al., 2006; Nurieva et al., 2009; Szabo et al., 2000; X. O. Yang, B. P. Pappu, et al., 2008; Zhang et al., 1997; Zheng & Flavell, 1997; J. Zhu et al., 2010). Importantly, unlike initially thought, activated CD4 T cells are not terminally differentiated but instead exhibit considerable functional plasticity in response to environmental changes (Gagliani et al., 2015; Hirota et al., 2011; Hirota et al., 2013; Voo et al., 2009).

The presence of certain microbial species, along with sensing of cells undergoing apoptosis in the context of an infection, triggers DC expression of IL-6 and TGF-β (Ivanov et al., 2009; Torchinsky et al., 2009). When activated in the presence of these cytokines, CD4 T cells turn on the expression of the Th17 lineage-defining 'master' TF RORγt in a STAT3 and IL-21-dependent manner (Ivanov et al., 2006; Lee et al., 2009; Mangan et al., 2006; Veldhoen et al., 2006). A further ROR family TF, RORα, was reported to have a minor role in Th17 development (X. O. Yang, B. P. Pappu, et al., 2008). RORγt^{+} Th17 cells produce IL-17 family cytokines and, to a lesser extent at steady state, IL-22 (Liang et al., 2006). Homeostatic Th17 cell-derived effector molecules act on epithelial cells promoting barrier integrity directly by enhancing tight junction formation and indirectly by driving antimicrobial peptide production (Lee et al., 2015; Liang et al., 2006). Thus, these cells orchestrate control of microbial proliferation and are crucial to supporting commensalism. An absence of Th17 cells or their effector molecules leads to dysbiosis and increased susceptibility to pathogen invasion (Milner et al., 2008;

Okada et al., 2015). However, antigen-experienced Th17 cells resident in the mucosa do not necessarily maintain their characteristic cytokine profile. Instead, these cells show a high degree of plasticity and are poised to acquire alternative effector programmes following environmental cues. Triggers exist in multiple forms and can result in both transient phenotypic changes and permanent differentiation. CD4 T cells can co-express IL-17 and the suppressive cytokine IL-10, and, following inflammatory responses, Th17 cells can transdifferentiate into suppressive pTreg cells, a process thought to limit tissue damage (Gagliani et al., 2015; McGeachy et al., 2007). Differentiation into Tfh is possibly required to aid mucosal antibody responses (Hirota et al., 2013). Moreover, Th17 cells can also acquire Th2- and Th1 cell-like properties. CD4 T cell populations with mixed Th17 and Th2 characteristics in the lung are linked to allergic asthma although whether they are derived from Th17 or Th2 cells is unclear (Irvin et al., 2014; Wang et al., 2010). The fact that Th17 cells generated *in vitro* rapidly switch IL-17 production for the type 2 cytokine IL-4 in response to parasitic infections suggests that Th17-to-Th2 cell differentiation is possible (Panzer et al., 2012). Further supporting this hypothesis, skin-resident IL-17-producing CD8 T cells respond to epithelial damage by transient acquisition of a type 2 effector programme (Harrison et al., 2019). Th17 cell polarisation towards a Th1-like phenotype, driven by IL-23 signalling (Lee et al., 2009; McGeachy et al., 2009), on the other hand, is better-defined and known to occur in response to extracellular pathogen invasion (Omenetti et al., 2019). This extensive plasticity enables rapid functional adaptation to changing microenvironments and is therefore crucial to protection against infection and resolution of inflammation-induced tissue damage. However, the same process can become a key contributor to pathology if it escapes appropriate regulation and $FoxP3^+$ Treg cell-mediated suppression (Bishu, El Zaatari, et al., 2019; Downs-Canner et al., 2017; Dutzan et al., 2018; Wang et al., 2010). Cells on the Th17/Th1-like exTh17 spectrum, specifically, have long been linked to autoimmune and autoinflammatory pathology. At the mucosa, Th17 cells producing the type 1 cytokines IFNγ and TNFα are associated with inflammatory bowel disease and Crohn's disease pathogenesis (Bishu, El Zaatari, et al., 2019; Lee et al., 2009). Moreover, even though Th17 cells are mostly restricted to barrier sites

in health, they can also promote disease at distinct anatomical locations. Th17 cells drive central nervous system inflammation and promote pathogenesis in animal models of multiple sclerosis. Importantly, although IL-17A-producing Th17 cells are capable of driving disease (Ferber et al., 1996), IL-23 signalling and acquisition of Th1-like functions are heavily implicated (Bettelli et al., 2004; Duhen et al., 2013; Hirota et al., 2011). Similarly, full conversion of Th17 into Th1-like exTh17 cells is required for the development of diabetes in some mouse models of the disease (Martin-Orozco et al., 2009).

Type 1 functions, such as IFNγ expression are associated with the master TF T-bet (Szabo et al., 2000), driven by IL-12 and STAT4 signalling (Thierfelder et al., 1996). Even though Th17 cells develop as an independent CD4 T cell lineage, certain populations maintain their responsiveness to polarising signals, such as IL-23 and IL-12, and can be pushed to co-express STAT3 and STAT4, resulting in a RORγt/T-bet double positive state with mixed Th17/Th1 cell characteristics or even a complete loss of type 3 TFs and function (Annunziato et al., 2007; Harrington et al., 2005; Hirota et al., 2011; Lee et al., 2009). Interestingly, however, Th1-like exTh17 cell-associated pathology is not always IL-12-driven (Becher et al., 2002; Zhang et al., 2003) and shows varied dependence on T-bet (Bettelli et al., 2004; Duhen et al., 2013). Moreover, Th17 cells can acquire Th1-like cytokine expression even in the complete absence of this Th1 cell TF (Duhen et al., 2013). Overall, this indicates that the transcriptional networks governing Th1-like exTh17 cell differentiation remain incompletely understood and are likely tissue and context dependent.

The extensive links between Th17 cell plasticity and pathology make IFNγ/TNFα^{+} Th17 and Th1-like exTh17 cells highly desirable targets of therapeutic interventions. Specifically targeting Th17 cell TFs has been considered. Surprisingly, blocking RORγt function affected Th17 cells but failed to impair ILC3 function (Withers et al., 2016). Given that ILC3 are the innate counterpart to Th17 cells and are also reliant on RORγt, this observation highlighted the need to consider not only the effect master TFs have on lineage development but also the role their continued expression plays in supporting function. Further complicating the study of this field is the scale of Th17 cell functional and phenotypic

heterogeneity with all stages of the Th17/exTh17 spectrum observed in healthy animals, as shown in the previous chapter. I therefore set out to establish better tools that enable analysis of Th1-like exTh17 cell differentiation. The work presented in this chapter aimed to define the post-developmental requirement for Th17 and Th1 cell associated TF expression and characterise mouse models to be used as tools to better understand exTh17 cell differentiation.

4.2 PHENOTYPING OF *C.RODENTIUM*-INDUCED TH17 CELLS POINTS TO GRADUAL LOSS OF TH17 AND ACQUISITON OF TH1 CELL-ASSOCIATED FUNCTIONS

C.rodentium infection is a well-established and well-characterised animal model of mucosal infection. Much like enterohaemorrhagic and enteropathogenic *E.coli*, *C.rodentium* forms attaching/effacing lesions in the large intestinal mucosal (Petty et al., 2010). The resulting epithelial damage triggers Th17 cell responses that, importantly, show a predisposition towards acquisition of Th1 cell-like properties (Higgins et al., 1999; Omenetti et al., 2019). This acquisition of type 1 functions is crucial to the anti-*C.rodentium* response with bacterial control impaired in its absence (Mangan et al., 2006; Shiomi et al., 2010). Colonisation by the pathogen is detectable by day 4 of the infection, reaching its peak around one week after inoculation. Gradual clearance follows from the second week (Wiles et al., 2004; Wiles et al., 2006). Bacterial clearance and protection are eventually mediated by IgG responses together with microbes found in the normal flora (Kamada et al., 2012; Kamada et al., 2015).

To study pathogen-induced Th17 and Th1 cell-like responses I assessed IL-17A and IFNγ production following *ex vivo* restimulation in CLP CD4 T cells (Fgi4.1a-b). Assessing cytokine-producing cells 2 weeks after inoculation revealed a significant increase in the proportion of IL-17A^{+}IFNγ^{-} Th17 cells compared to steady state controls that translated into a near-30-fold increase in the number of these cells. Interestingly, IL-17A^{+}IFNγ^{+} double positive CD4 T cell populations also appeared and IL-17A^{-}IFNγ^{+} CD4 T cells expanded in numbers (Fig4.1c-h). These data raised the possibility that Th1 cells were also induced. Combining the infection model with fate mapping of *Il17a* expression enables assessment of the contribution of Th17 cells to the Th1-like CD4 T cell pool. As expected based on cytokine

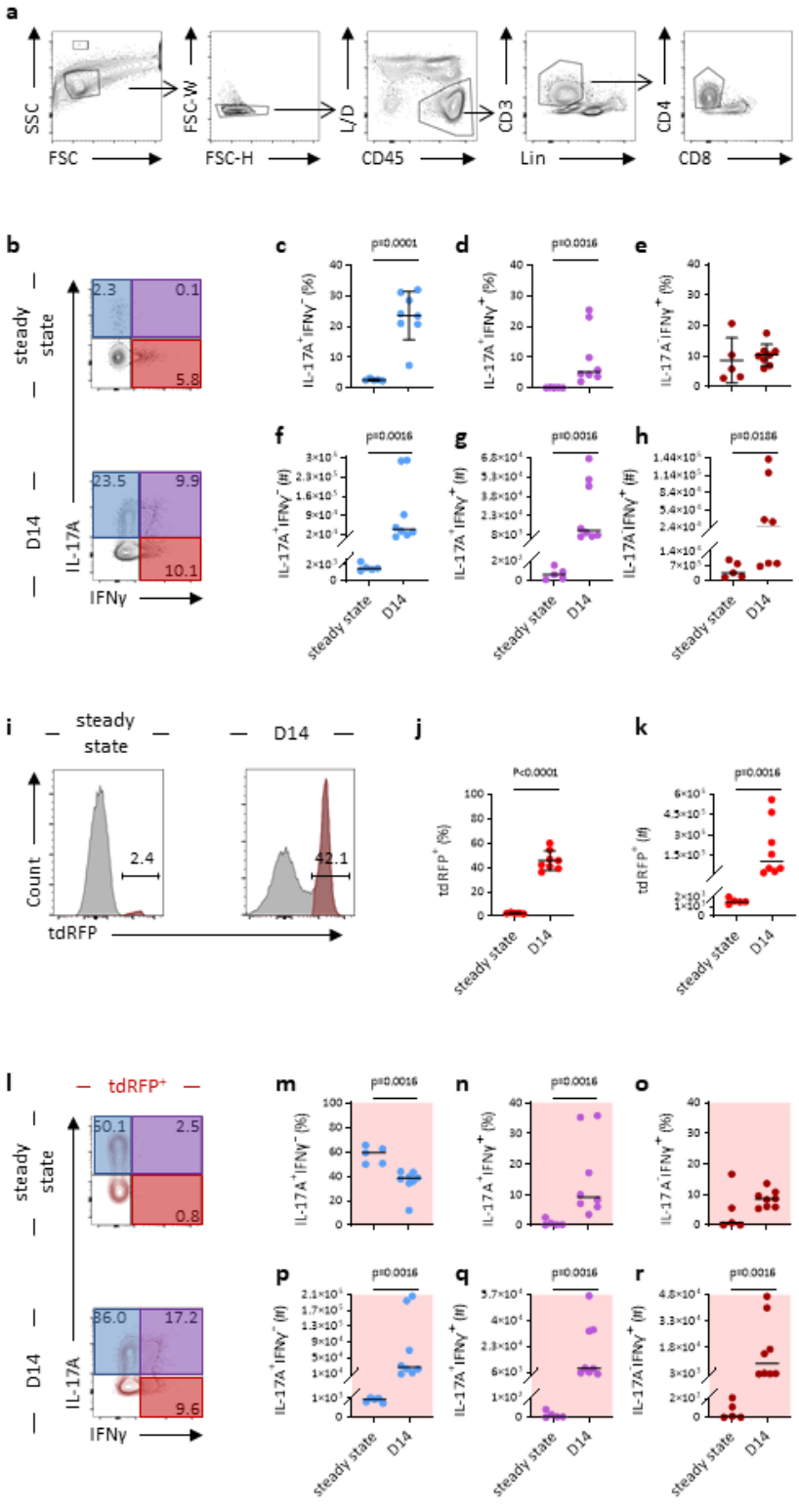
a
SSC
FSC
FSC-W
FSC-H
L/D
CD45
CD3
Lin
CD4
CD8
b
steady state
D14
IL-17A
IFNγ
2.3
0.1
5.8
23.5
9.9
10.1
c
d
e
f
g
h
p=0.0001
p=0.0016
p=0.0186
steady state
D14
i
steady state
D14
Count
tdRFP
2.4
42.1
j
k
P<0.0001
p=0.0016
l
tdRFP⁺
50.1
2.5
0.8
36.0
17.2
9.6
m
n
o
p
q
r

Figure 4.1. *C.rodentium* infection induces colonic Th17 cells that acquire Th1 cell-like effector functions

Cytokine production was assessed in the absence of infection and following *C.rodentium* colonisation in CLP CD4 T cells of *Il17a*^{Cre}*Rosa26*^{tdRFP} IL-17A fate mapper mice.

a) Representative flow cytometry plots illustrating gating strategy to identify CD4 T cells in CLP.

b) Representative flow cytometry plots showing IL-17A and IFNγ expression in CD4 T cells in CLP of mice with no infection (steady state) and on D14 of *C.rodentium* infection following *ex vivo* restimulation with PMA and Ionomycin.

c-h) Quantification of the proportion (c-e) and total number (f-h) of CD4 T cells expressing IL-17A only (IL-17A$^+$IFNγ$^-$), both IL-17A and IFNγ (IL-17A$^+$IFNγ$^+$) or IFNγ only (IL-17A$^-$IFNγ$^+$) in the CLP of mice at steady state and on D14 of *C.rodentium* infection. Steady state n=5, data pooled from 2 independent experiments, D14 n=8, data pooled from 3 independent experiments.

i) Representative histograms showing tdRFP expression in CD4 T cells in the CLP of mice with no infection or on D14 following *C.rodentium* inoculation.

j-k) Quantification of the proportion (j) and total number (k) of tdRFP$^+$ CD4 T cells in the CLP of mice at steady state or on D14 following *C.rodentium* inoculation. Steady state n=5, data pooled from 2 independent experiments, D14 n=8, data pooled from 3 independent experiments.

l) Representative flow cytometry plots gated on tdRFP$^+$ CD4 T cells showing IL-17A and IFNγ expression in CLP of mice at steady state and on D14 of *C.rodentium* infection following *ex vivo* restimulation with PMA and Ionomycin.

m-r) Quantification of the proportion (m-o) and total number (p-r) of tdRFP$^+$ CD4 T cells expressing IL-17A only (IL-17A$^+$IFNγ$^-$), both IL-17A and IFNγ (IL-17A$^+$IFNγ$^+$) or IFNγ only (IL-17A$^-$IFNγ$^+$) in the CLP of mice at steady state and on D14 of *C.rodentium* infection. Steady state n=5, data pooled from 2 independent experiments, D14 n=8, data pooled from 3 independent experiments.

Values on flow cytometry plots and histograms represent percentages. Normality was tested using Shapiro-Wilk test. Lines on graphs show mean±SD (c, e, j) or median (d, f, g, h, k, m, n, o, p, q, r). Significance was tested using unpaired t test (c, e, j) or Mann-Whitney U test (d, f, g, h, k, m, n, o, p, q, r).

production data, the frequency of CLP CD4 T cells with a history of *Il17a* expression (tdRFP$^+$) increased 20-fold with an even larger expansion in their numbers following *C.rodentium* infection (Fig4.1i-k). Interestingly, assessment of IL-17A and IFNγ production within the fate mapped population (Fig4.1l) revealed an infection-induced drop in the proportion of tdRFP$^+$ CD4 T cells producing IL-17A (Fig4.1m) and an increase in cells making both IL-17A and IFNγ, and possibly cells producing IFNγ only (Fig4.1n-o). However, further repeats would be needed to account for the large degree of variability. The total number of all three tdRFP$^+$ CD4 T cell populations defined by IL-17A and IFNγ expression increased (Fig4.1p-r), consistent with overall expansion of the colonic CD4 and tdRFP$^+$ CD4 T cell pools.

Murine and human Th17 cells produce further type 3 (Th17 cell-associated) and type 1 (Th1 cell-associated) cytokines. IL-17F is another well-characterised IL-17 family cytokine closely related to IL-17A. The two effector molecules have both overlapping and individual roles in mucosal barrier protection and the orchestration of inflammation (X. O. Yang, S. H. Chang, et al., 2008). Early reports have shown that both IL-17A and IL-17F rely on the expression of the Th17 cell master TF RORγt (Ivanov et al., 2006; X. O. Yang, B. P. Pappu, et al., 2008). However, there are suggestions that RORα may have differential roles in the regulation of their secretion with IL-17F less reliant on this TF than IL-17A (X. O. Yang, B. P. Pappu, et al., 2008). A further type 3 cytokine that can be expressed by Th17 cell is IL-22. This cytokine synergizes with IL-17A and IL-17F to promote antimicrobial peptide production (Liang et al., 2006). IL-22 further supports barrier repair by acting on epithelial cells to stimulate proliferation (Lindemans et al., 2015). Tumour necrosis factor-α (TNFα) is a type 1 cytokine that can be expressed by Th17 cells together with IL-17A and IL-17F in health, but its upregulation coupled with the loss of IL-17A is associated with Th17-driven autoimmune diseases (Bishu, El Zaatari, et al., 2019; Hirota et al., 2011). Mucosal Th17 cell analyses were therefore expanded to include these three cytokines in addition to IL-17A and IFNγ. Assessing IL-22 expression in tdRFP$^+$ CD4 T cells (Fig4.2a) revealed very limited IL-22 expression at steady state but an increase following *C.rodentium* infection (Fig4.2b-c). Conversely, IL-17F was largely found to be co-expressed with IL-17A both in the absence and presence of *C.rodentium*. An infection-induced increase was evident only in total numbers

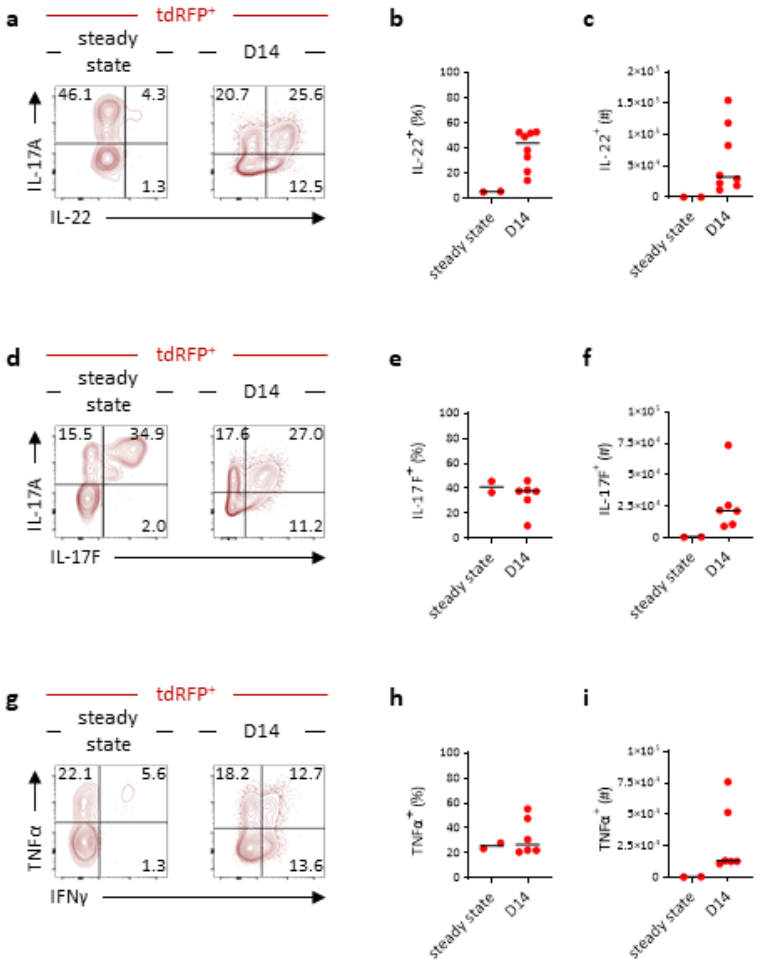
a
tdRFP+
steady state
D14
46.1
4.3
1.3
20.7
25.6
12.5
IL-17A
IL-22
b
IL-22+ (%)
steady state
D14
c
IL-22+ (#)
steady state
D14
d
tdRFP+
steady state
D14
15.5
34.9
2.0
17.6
27.0
11.2
IL-17A
IL-17F
e
IL-17F+ (%)
steady state
D14
f
IL-17F+ (#)
steady state
D14
g
tdRFP+
steady state
D14
22.1
5.6
1.3
18.2
12.7
13.6
TNFα
IFNγ
h
TNFα+ (%)
steady state
D14
i
TNFα+ (#)
steady state
D14

Figure 4.2. Additional type 3 and type 1 cytokine production is induced by *C.rodentium* infection

Additional type 3 and type 1 cytokine production was assessed in the absence of infection and following *C.rodentium* colonisation in CLP CD4 T cells of *Il17a*^{Cre}*Rosa26*^{tdRFP} IL-17A fate mapper mice.

a, d, g) Representative flow cytometry plots gated on tdRFP^{+} CD4 T cells showing IL-22 (a) and IL-17F (d) expression against IL-17A TNFα (g) expression with IFNγ in CLP of mice at steady state and on D14 of *C.rodentium* infection following *ex vivo* restimulation with PMA and Ionomycin.

b-c) Quantification of the proportion (b) and total number (c) of tdRFP^{+} CD4 T cells producing IL-22 in the CLP of mice at steady state and on D14 of *C.rodentium* infection. Steady state n=2, data from 1 experiment, D14 n=8, data pooled from 3 independent experiments.

e-f) Quantification of the proportion (e) and total number (f) of tdRFP^{+} CD4 T cells producing IL-17F in the CLP of mice at steady state and on D14 of *C.rodentium* infection. Steady state n=2, data from 1 experiment, D14 n=6, data pooled from 2 independent experiments.

h-i) Quantification of the proportion (h) and total number (i) of tdRFP^{+} CD4 T cells producing TNFα in the CLP of mice at steady state and on D14 of *C.rodentium* infection. Steady state n=2, data from 1 experiment, D14 n=6, data pooled from 2 independent experiments.

Values on flow cytometry plots represent percentages. Lines on graphs show median (b, c, e, f, h, i). No statistical analyses were performed.

(Fig4.2d-f). Similarly, there was no evidence of an infection-induced change in the proportion of tdRFP$^+$ CD4 T cells producing TNFα despite the increase in the total number of such cells (Fig4.2g-i).

In summary, analysis of IL-17A and IFNγ expression within cells with a history of IL-17A production revealed the existence of a spectrum of Th17 and Th1-like exTh17 cells. Given that Th17 cells rely on RORγt (Ivanov et al., 2006; X. O. Yang, B. P. Pappu, et al., 2008) and Th1-like cells require T-bet (Szabo et al., 2000) for their appropriate development I further investigated the expression of these two lineage-defining TFs in CLP tdRFP$^+$ CD4 T cells 14 days after infection with *C.rodentium*. Assessment of both cytokine (IL-17A and IFNγ) and TF (RORγt and T-bet) expression yielded three populations (Fig4.3a). Th17 cells were defined as cells that produced IL-17A but not IFNγ based on cytokine expression or as cells that were RORγt$^+$ but T-bet$^-$ based on TF expression. On the other end of the spectrum, fully mature exTh17 cells were identified as those tdRFP$^+$ CD4 T cells that only produced IFNγ and expressed T-bet. Finally, an intermediate stage characterised by co-expression of both cytokines or both TFs was defined. The composition of the tdRFP$^+$ CD4 T cell pool was similar regardless of the set of definitions used – Th17 cells were most abundant while exTh17 cells no longer producing IL-17A or expressing RORγt were present as the smallest population (Fig4.3b-c). Taken together, and consistent with work reported by others (Hirota et al., 2011; Omenetti et al., 2019), these data showed that following *C.rodentium* infection RORγt$^+$ Th17 cells producing IL-17 family cytokines and IL-22 are induced but can progressively lose this characteristic phenotype giving way to T-bet and Th1 cell-associated cytokine expression instead (Fig4.3d). RORγt and T-bet play clear roles in Th17 and Th1 cell differentiation (Ivanov et al., 2006; Szabo et al., 2000; X. O. Yang, B. P. Pappu, et al., 2008), but how their continued expression supports Th17 and exTh17 cell function is unclear. RORγt deficiency was reported to result in a decrease of Th17 cell function, but published literature suggests that T-bet absence may not necessarily preclude the acquisition of Th1 cell-like effector functions such as IFNγ production (Duhen et al., 2013; X. O. Yang, B. P. Pappu, et al., 2008). I therefore sought to test Th17 post-developmental requirements for RORγt and T-bet.

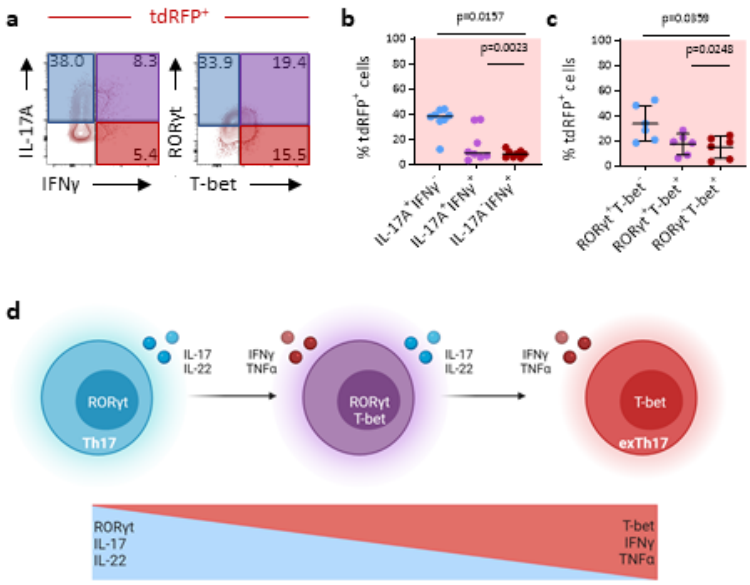
a
tdRFP+
38.0
8.3
5.4
IL-17A
IFNγ
33.9
19.4
15.5
RORγt
T-bet
b
p=0.0157
p=0.0023
% tdRFP+ cells
IL-17A+IFNγ-
IL-17A+IFNγ+
IL-17A-IFNγ+
c
p=0.0859
p=0.0248
% tdRFP+ cells
RORγt+T-bet-
RORγt+T-bet+
RORγt-T-bet+
d
RORγt
Th17
IL-17
IL-22
IFNγ
TNFα
RORγt
T-bet
IL-17
IL-22
IFNγ
TNFα
T-bet
exTh17
RORγt
IL-17
IL-22
T-bet
IFNγ
TNFα

Figure 4.3. *C.rodentium* infection-induced Th17 cells acquire a spectrum of Th1 cell-like characteristics

Assessment of cytokine production in *Il17a*^{cre}*Rosa26*^{tdRFP} mice enables identification of Th17 cell conversion into Th1-like exTh17 cells following *C.rodentium* infection.

a) Representative flow cytometry plots gated on tdRFP$^+$ CD4 T cells showing IL-17A and IFNγ (left), and RORγt and T-bet (right) expression in CLP following *ex vivo* restimulation with PMA and Ionomycin on D14 following *C.rodentium* inoculation.

b) Quantification of the proportion of IL-17A$^+$IFNγ$^-$, IL-17A$^+$IFNγ$^+$ and IL-17A$^-$IFNγ$^+$ cells within the tdRFP$^+$ CD4 T cell population in CLP on D14 following *C.rodentium* inoculation. n=8, data pooled from 3 independent experiments.

c) Quantification of the proportion of RORγt$^+$T-bet$^-$, RORγt$^+$T-bet$^+$ and RORγt$^-$T-bet$^+$ cells within the tdRFP$^+$ CD4 T cell population in CLP on D14 following *C.rodentium* inoculation. n=6, data pooled from 2 independent experiments.

d) Schematic representation of the Th17-to-exTh17 cell differentiation process with cytokine production and TF expression. Images generated with BioRender.com.

Values on flow cytometry plots represent percentages. Normality was tested using Shapiro-Wilk test. Lines on graphs show mean±SD (c) or median (b). Significance was tested using One-Way ANOVA (c) or Kruskal-Wallis test (b).

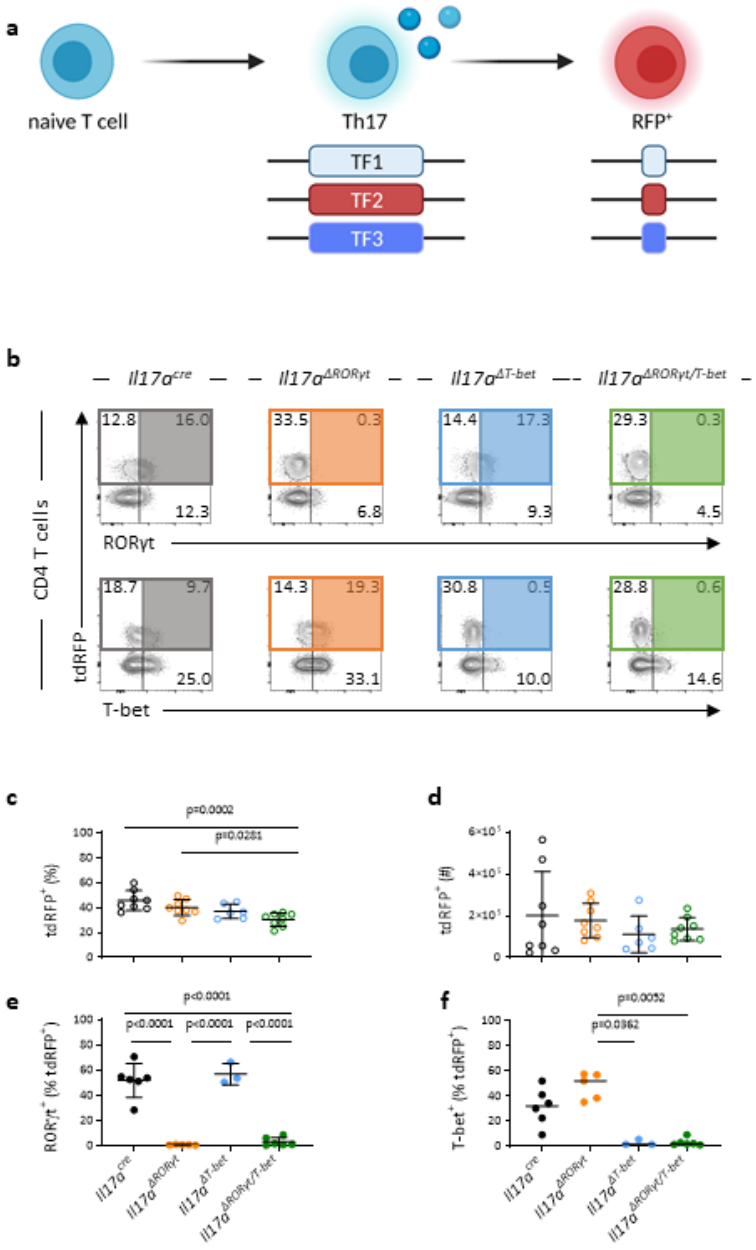
a
naive T cell
Th17
RFP+
TF1
TF2
TF3
b
Il17a^cre
Il17a^ΔRORγt
Il17a^ΔT-bet
Il17a^ΔRORγt/T-bet
CD4 T cells
tdRFP
RORγt
T-bet
12.8
16.0
12.3
33.5
0.3
6.8
14.4
17.3
9.3
29.3
0.3
4.5
18.7
9.7
25.0
14.3
19.3
33.1
30.8
0.5
10.0
28.8
0.6
14.6
c
tdRFP+ (%)
p=0.0002
p=0.0281
d
tdRFP+ (#)
e
RORγt+ (% tdRFP+)
p<0.0001
p<0.0001
p<0.0001
p<0.0001
f
T-bet+ (% tdRFP+)
p=0.0052
p=0.0362

Figure 4.4. Conditional RORγt$^{-/-}$ and T-bet$^{-/-}$ mice delete key TFs in established Th17 cells

Il17a^{Cre}*Rosa26*^{tdRFP} (*Il17a*^{cre}) mice crossed with *Rorc*$^{fl/fl}$ (*Il17a*$^{\Delta RORγt}$), *Tbx21*$^{fl/fl}$ (*Il17a*$^{\Delta T\text{-}bet}$) and *Rorc*$^{fl/fl}$*Tbx21*$^{fl/fl}$ (*Il17a*$^{\Delta RORγt/T\text{-}bet}$) enable assessment of the continued requirement for RORγt and T-bet expression in the maintenance of Th17 cell effector functions. Images generated with BioRender.com.

a) Schematic representation of TF deletion and IL-17A fate mapping in Th17 cells. Cells heterogeneous for the *Il17a* WT and *Cre* alleles co-express IL-17A and Cre resulting in permanent tdRFP expression and excision of TF exons. Images generated with BioRender.com.

b) Representative flow cytometry plots gated on CD4 T cells showing tdRFP and RORγt (top) or T-bet (bottom) expression in CLP on D14 following *C.rodentium* inoculation.

c-d) Quantification of the proportion (c) and total number (d) of tdRFP$^+$ cells within the CLP CD4 T cell population on D14 following *C.rodentium* inoculation. *Il17a*^{cre} and *Il17a*$^{\Delta RORγt/T\text{-}bet}$ n=8, data pooled from 3 independent experiments, *Il17a*$^{\Delta RORγt}$ n=8, data pooled from 2 independent experiments, *Il17a*$^{\Delta T\text{-}bet}$ n=6, data pooled from 2 independent experiments.

e-f) Quantification of the proportion of RORγt$^+$ (e) and T-bet$^+$ (f) cells within the tdRFP$^+$ CD4 T cell population in CLP on D14 following *C.rodentium* inoculation. *Il17a*^{cre} and *Il17a*$^{\Delta RORγt/T\text{-}bet}$ n=6, data pooled from 2 independent experiments, *Il17a*$^{\Delta RORγt}$ n=5, data from 1 experiment, *Il17a*$^{\Delta T\text{-}bet}$ n=3, data from 1 experiment.

Values on flow cytometry plots represent percentages. Normality was tested using Shapiro-Wilk test. Lines on graphs show mean±SD (c, d, e) or median (f). Significance was tested using One-Way ANOVA (c, d, e) or Kruskal-Wallis test (f).

4.3 ROR FAMILY TRANSCRIPTION FACTORS SUPPORT TH17 CELL FUNCTION BY A COMBINATION OF ACTIVATION AND SILENCING OF ALTERNATIVE GENETIC PROGRAMMES

Modified *Il17a*^{cre}*Rosa26*^{tdRF} IL-17A fate mapper mice were generated to test the roles of RORγt and T-bet in the regulation of Th17 cell fate and function. Fate mappers were crossed with *Rorc*$^{fl/fl}$ (Choi et al., 2016) and *Tbx21*$^{fl/fl}$ (Intlekofer et al., 2008) strains to generate RORγt single knockout (*Il17a*$^{\Delta RORγt}$) or RORγt/T-bet double knockout (*Il17a*$^{\Delta RORγt/T\text{-}bet}$) mice with IL-17A fate mappers (*Il17a*^{cre}) used as controls. In these mice *Il17a* promoter-driven Cre recombinase production results not only in tdRFP expression but also disruption of the genes encoding the Th17 and Th1 cell-associated TFs. Thus, these models allow normal development of Th17 cells but drive deletion of key TFs upon IL-17A production. TdRFP expression served as a marker not only of IL-17A production history but also of cells that had undergone recombination (Fig4.4a). Assessment of RORγt and T-bet expression in tdRFP$^+$ CLP CD4 T cells following *C.rodentium* infection (Fig4.4b) revealed efficient TF deletion in all mouse strains but also a slight decrease in the frequency of CD4 T cells with a history of IL-17A production in mice lacking both RORγt and T-bet (Fig4.4c-f). This may in part be caused by reduced recombination efficiency, due to the increased number of Cre targets, but the possibility that RORγt/T-bet co-deletion resulted in impaired Th17 cell development or survival could not be excluded. However, maintenance of normal tdRFP$^+$ CD4 T cell numbers in the conditional knockout strains (Fig4.4d) was suggestive of no or very limited effects on survival.

Combining the *C.rodentium* infection and conditional TF knockout mouse models, I next assessed cytokine production in colonic tdRFP$^+$ Th17 and exTh17 cells 14 days after infection (Fig4.5a). A small reduction in the proportion of tdRFP$^+$ CD4 T cells producing IL-17A in the absence of RORγt was observed. However, this was not found to be statistically significant and the change in the total number of these cells was not suggestive of a RORγt-deletion induced defect (Fig4.5b-d). Similarly, the level of IL-17A produced in RORγt-deficient tdRFP$^+$ cells was reduced compared to controls (Fig4.5e) but this was, again, not statistically significant. Given the variability in the data it is possible that these

experiments were underpowered for confident detection of small changes in cytokine production. Interestingly, there was some evidence of a return towards normal IL-17A$^+$ population size but no change in the level of this cytokine produced upon co-deletion of T-bet and RORγt (Fig4.5b-e). Conversely, the proportion of tdRFP$^+$ CD4 T cells producing the exTh17 cell cytokine IFNγ appeared to increase in the absence of RORγt but return to lower levels upon T-bet co-deletion (Fig4.5f-g). Even though these observations were mirrored by changes in the number of IFNγ$^+$ cells (Fig4.5h), a larger sample size is required to confirm whether a true biological difference exists. This is especially important given that changes in the size of the IFNγ-producing population were not followed by the amount of cytokine produced (Fig4.5i). Crucially, no complete loss of IL-17A production was observed raising the possibility that further TFs are involved in supporting Th17 cell function.

RORα is a ROR family TF related to RORγt and linked to Th17 cell function (X. O. Yang, B. P. Pappu, et al., 2008). and recent publications have shown that this TF can support type 3 lymphocytes when RORγt is absent (Fiancette et al., 2021; Stehle et al., 2021). Therefore, mouse models that enable assessment of the role RORα plays in supporting IL-17A expression in RORγt deficient Th17 cells were generated by crossing *Il17a*$^{\Delta RORγt}$ and *Il17a*$^{\Delta RORγt/T\text{-}bet}$ mice with *Rora*$^{fl/fl}$ animals (Oliphant et al., 2014). In response to *C.rodentium* infection mice lacking RORα in addition to RORγt generated a proportionally smaller colonic tdRFP$^+$ CD4 T cell population that was further diminished when T-bet was also absent (Fig4.6a-b). This, similarly to results reported above (Fig4.4) pointed to possible effects on fitness, proliferation or survival. TdRFP$^+$ cells lacking all three transcription factors were present in lowest numbers (Fig4.6c) indicating a potential differentiation or survival defect. RORγt deletion was found to be efficient in all strains (Fig4.6d). However, RORα expression was not tested as reliable anti-RORα antibodies suitable for flow cytometry were not available. Efficient TF deletion in a similar model driven by a different promoter was previously confirmed by via alternative methods (Fiancette et al., 2021) increasing the likelihood that *Il17a* promoter-driven models also worked as expected. Nonetheless, confirmation of RORα deletion driven by the *Il17a* promoter would be desirable. Strikingly, in addition to efficient T-bet deletion in *Il17a*$^{\Delta RORγt/RORα/T\text{-}bet}$ mice an increase in the

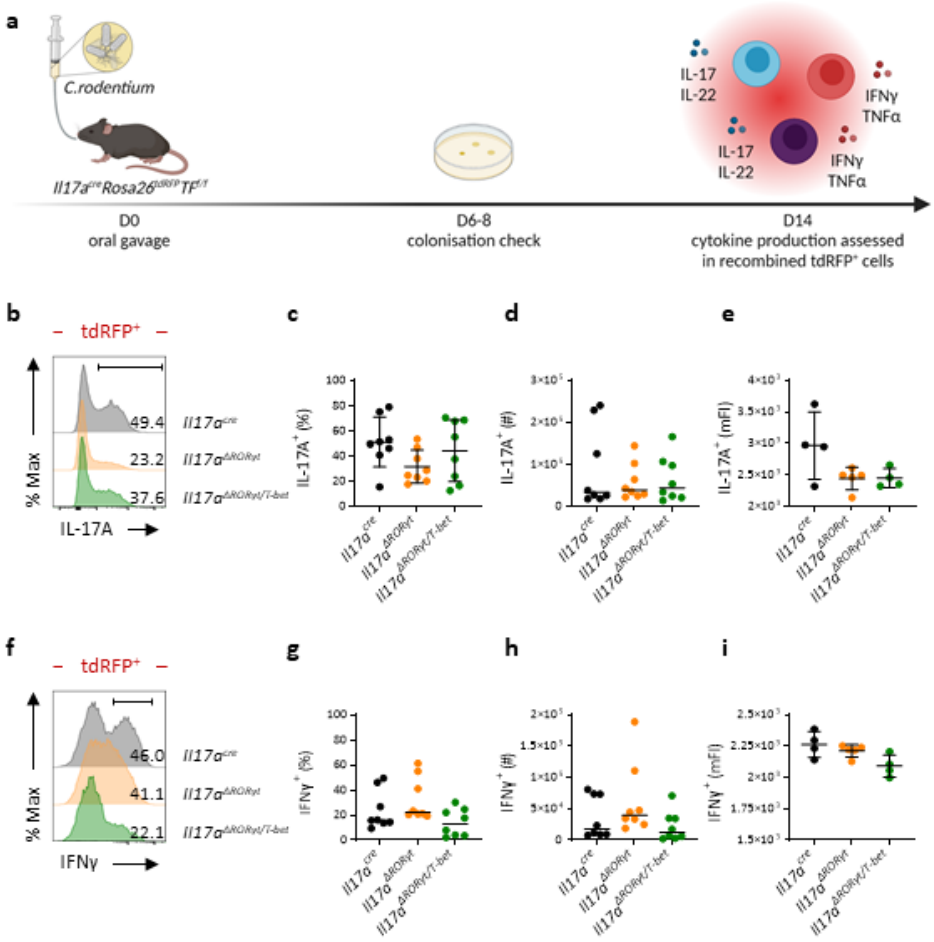
a
C.rodentium
Il17a^cre Rosa26^tdRFP Tf^f/f
D0
oral gavage
D6-8
colonisation check
D14
cytokine production assessed
in recombined tdRFP+ cells
IL-17
IL-22
IFNγ
TNFα
b
– tdRFP+ –
% Max
IL-17A
49.4
23.2
37.6
Il17a^cre
Il17a^ΔRORγt
Il17a^ΔRORγt/T-bet
c
IL-17A+ (%)
d
IL-17A+ (#)
e
IL-17A+ (mFI)
f
– tdRFP+ –
% Max
IFNγ
46.0
41.1
22.1
g
IFNγ+ (%)
h
IFNγ+ (#)
i
IFNγ+ (mFI)

Figure 4.5. RORγt and T-bet act together to determine Th17 cell fate and function

Cytokine production was assessed in *Il17a*^{cre}, *Il17a*$^{\Delta RORγt}$ and *Il17a*$^{\Delta RORγt/T\text{-}bet}$ mice to test Th17 cell function reliance on continued TF expression.

a) Schematic representation of experimental design. Images generated with BioRender.com.

b, f) Representative histograms gated on CLP tdRFP^{+} CD4 T cells showing IL-17A (b) and IFNγ (f) expression following *ex vivo* restimulation with PMA and ionomycin on D14 of *C.rodentium* infection in *Il17a*^{cre}, *Il17a*$^{\Delta RORγt}$ and *Il17a*$^{\Delta RORγt/T\text{-}bet}$ mice.

c-d) Quantification of the proportion (c) and total number (d) of IL-17A^{+} cells within the parent population in CLP of *Il17a*^{cre}, *Il17a*$^{\Delta RORγt}$ and *Il17a*$^{\Delta RORγt/T\text{-}bet}$ mice on D14 following *C.rodentium* inoculation. *Il17a*^{cre} and *Il17a*$^{\Delta RORγt/T\text{-}bet}$ n=8, data pooled from 3 independent experiments, *Il17a*$^{\Delta RORγt}$ n=8, data pooled from 2 independent experiments.

e) IL-17A median fluorescence intensity (mFI) in CLP of *Il17a*^{cre}, *Il17a*$^{\Delta RORγt}$ and *Il17a*$^{\Delta RORγt/T\text{-}bet}$ mice on D14 following *C.rodentium* inoculation. *Il17a*^{cre} and *Il17a*$^{\Delta RORγt/T\text{-}bet}$ n=4, *Il17a*$^{\Delta RORγt}$ n=5, all data from 1 experiment.

g-h) Quantification of the proportion (g) and total number (h) of IFNγ^{+} cells within the parent population in CLP of *Il17a*^{cre}, *Il17a*$^{\Delta RORγt}$ and *Il17a*$^{\Delta RORγt/T\text{-}bet}$ mice on D14 following *C.rodentium* inoculation. *Il17a*^{cre} and *Il17a*$^{\Delta RORγt/T\text{-}bet}$ n=8, data pooled from 3 independent experiments, *Il17a*$^{\Delta RORγt}$ n=8, data pooled from 2 independent experiments.

i) IFNγ median fluorescence intensity (mFI) in CLP of *Il17a*^{cre}, *Il17a*$^{\Delta RORγt}$ and *Il17a*$^{\Delta RORγt/T\text{-}bet}$ mice on D14 following *C.rodentium* inoculation. *Il17a*^{cre} and *Il17a*$^{\Delta RORγt/T\text{-}bet}$ n=4, *Il17a*$^{\Delta RORγt}$ n=5, all data from 1 experiment.

Values on histograms represent percentages. Normality was tested using Shapiro-Wilk test. Lines on graphs show mean±SD (c, e, i) or median (d, g, h). Significance was tested using One-Way ANOVA (c, e, i) or Kruskal-Wallis test (d, g, h).

proportion of tdRFP$^+$ CD4 T cells expressing T-bet in *Il17a*$^{\Delta RORγt}$ CLP was noted compared to controls with a further expansion of this population in *Il17a*$^{\Delta RORγt/RORα}$ mice following *C.rodentium* infection (Fig4.6e). These data are consistent with ROR family TFs acting in part to inhibit T-bet expression.

Adding to reported observations that both RORγt and RORα contribute to Th17 cell development (X. O. Yang, B. P. Pappu, et al., 2008), exacerbated loss of IL-17A$^+$ CD4 T cells upon inducible deletion of the two ROR family TFs indicated a key role for continued expression of both in supporting type 3 effector functions (Fig4.7a-c). In addition, a lower level of IL-17A production was observed in both strains when compared to controls (Fig4.7d). Unlike the results reported above (Fig4.5), T-bet co-deletion did not appear to rescue type 3 function (Fig4.7a-d). In summary, near-complete loss of IL-17A was only observed upon conditional deletion of both RORγt and RORα, consistent with ROR family TF functional redundancy.

Assessing exTh17 cell function revealed an increase in the frequency of tdRFP$^+$ CD4 T cells producing IFNγ in RORγt/RORα double knockouts compared to control mice (Fig4.7e-f). Likely underlying this observation is the increase in T-bet expression in this strain (Fig4.6). In addition, it is possible that on further repeats a robust increase in IFNγ produced by *Il17a*$^{\Delta RORγt}$ CLP Th17 and exTh17 cells would also become apparent. However, this dataset is currently underpowered to really assess differences in IFNγ$^+$ Th17 and exTh17 cell populations. Available results pointed to a possible reduction in the number of IFNγ$^+$ cells in mice lacking all three TFs (Fig4.7g) but the smaller tdRFP$^+$ CD4 T cell pool in these mice (Fig4.6) raised the possibility that this was not specifically due to a lack of IFNγ induction. The level of IFNγ produced by cells still able to make this cytokine in *Il17a*$^{\Delta RORγt/RORα/T\text{-}bet}$ CLP appeared comparable to controls but lower than that in mice deleting the two ROR family TFs only (Fig4.7h), further suggesting Th1 cell programme upregulation in the absence of RORγt and RORα. However, much like total numbers, cytokine production levels must be interpreted carefully as it is currently unclear whether T-bet-sufficient Th17 and exTh17 cells have a fitness advantage over cells lacking all three TFs. Interpretation of these data would benefit from assessment of these factors in the future.

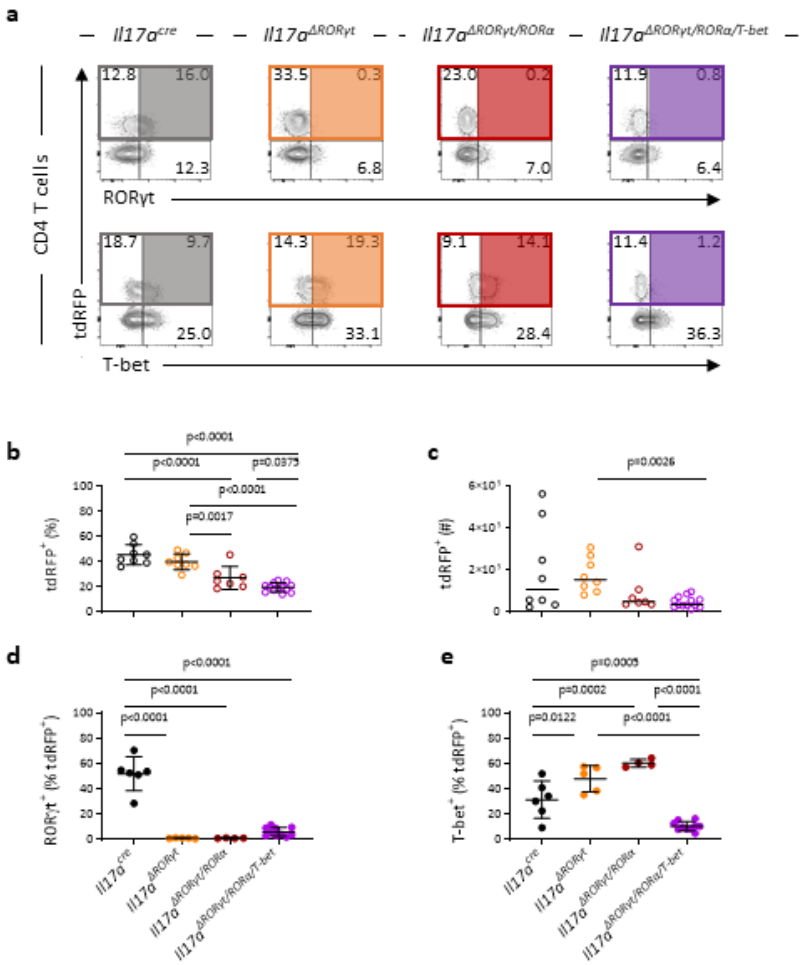
a
Il17a^cre
Il17a^ΔRORγt
Il17a^ΔRORγt/RORα
Il17a^ΔRORγt/RORα/T-bet
CD4 T cells
RORγt
tdRFP
T-bet
12.8
16.0
12.3
33.5
0.3
6.8
23.0
0.2
7.0
11.9
0.8
6.4
18.7
9.7
25.0
14.3
19.3
33.1
9.1
14.1
28.4
11.4
1.2
36.3
b
tdRFP+ (%)
p<0.0001
p<0.0001
p=0.0375
p<0.0001
p=0.0017
c
tdRFP+ (#)
p=0.0026
d
RORγt+ (% tdRFP+)
p<0.0001
p<0.0001
p<0.0001
e
T-bet+ (% tdRFP+)
p=0.0005
p=0.0002
p<0.0001
p=0.0122
p<0.0001
Il17a^cre
Il17a^ΔRORγt
Il17a^ΔRORγt/RORα
Il17a^ΔRORγt/RORα/T-bet

Figure 4.6. Conditional RORα$^{-/-}$ mice delete RORα in established Th17 cells

Il17a^{Cre}*Rosa26*^{tdRFP} (*Il17a*^{cre}) mice crossed with *Rorc*$^{fl/fl}$ (*Il17a*$^{\Delta RORγt}$), *Rorc*$^{fl/fl}$*Rora*$^{fl/fl}$ (*Il17a*$^{\Delta RORγt/RORα}$) and *Rorc*$^{fl/fl}$*Rora*$^{fl/fl}$*Tbx21*$^{fl/fl}$ (*Il17a*$^{\Delta RORγt/RORα/T\text{-}bet}$) enable assessment of the continued requirement for RORα expression in established Th17 cells when both RORγt and T-bet are absent.

a) Representative flow cytometry plots gated on CD4 T cells showing tdRFP and RORγt (top) or T-bet (bottom) expression in CLP of *Il17a*^{cre}, *Il17a*$^{\Delta RORγt}$, *Il17a*$^{\Delta RORγt/RORα}$ and *Il17a*$^{\Delta RORγt/RORα/T\text{-}bet}$ mice on D14 following *C.rodentium* inoculation.

b-c) Quantification of the proportion (b) and total number (c) of tdRFP$^+$ cells within the CLP CD4 T cell population of *Il17a*^{cre}, *Il17a*$^{\Delta RORγt}$, *Il17a*$^{\Delta RORγt/RORα}$ and *Il17a*$^{\Delta RORγt/RORα/T\text{-}bet}$ mice on D14 following *C.rodentium* inoculation. *Il17a*^{cre} n=8, data pooled from 3 independent experiments, *Il17a*$^{\Delta RORγt}$ n=8, data pooled from 2 independent experiments, *Il17a*$^{\Delta RORγt/RORα}$ n=7, data pooled from 2 independent experiments, *Il17a*$^{\Delta RORγt/RORα/T\text{-}bet}$ n=13, data pooled from 3 independent experiments. *Il17a*^{cre} and *Il17a*$^{\Delta RORγt}$ data also appear in fig4.4c.

d-e) Quantification of the proportion of RORγt$^+$ (d) and T-bet$^+$ (e) cells within the tdRFP$^+$ CD4 T cell population in CLP of *Il17a*^{cre}, *Il17a*$^{\Delta RORγt}$, *Il17a*$^{\Delta RORγt/RORα}$ and *Il17a*$^{\Delta RORγt/RORα/T\text{-}bet}$ mice on D14 following *C.rodentium* inoculation. *Il17a*^{cre} n=6, data pooled from 2 independent experiments, *Il17a*$^{\Delta RORγt}$ n=5, data from 1 experiment, *Il17a*$^{\Delta RORγt/RORα}$ n=4, data pooled from 1 experiment, *Il17a*$^{\Delta RORγt/RORα/T\text{-}bet}$ n=10, data pooled from 2 independent experiments. *Il17a*^{cre} and *Il17a*$^{\Delta RORγt}$ data also appear in fig4.4d-e.

Values on flow cytometry plots represent percentages. Normality was tested using Shapiro-Wilk test. Lines on graphs show mean±SD (b, d, e) or median (c). Significance was tested using One-Way ANOVA (b, d, e) or Kruskal-Wallis test (c).

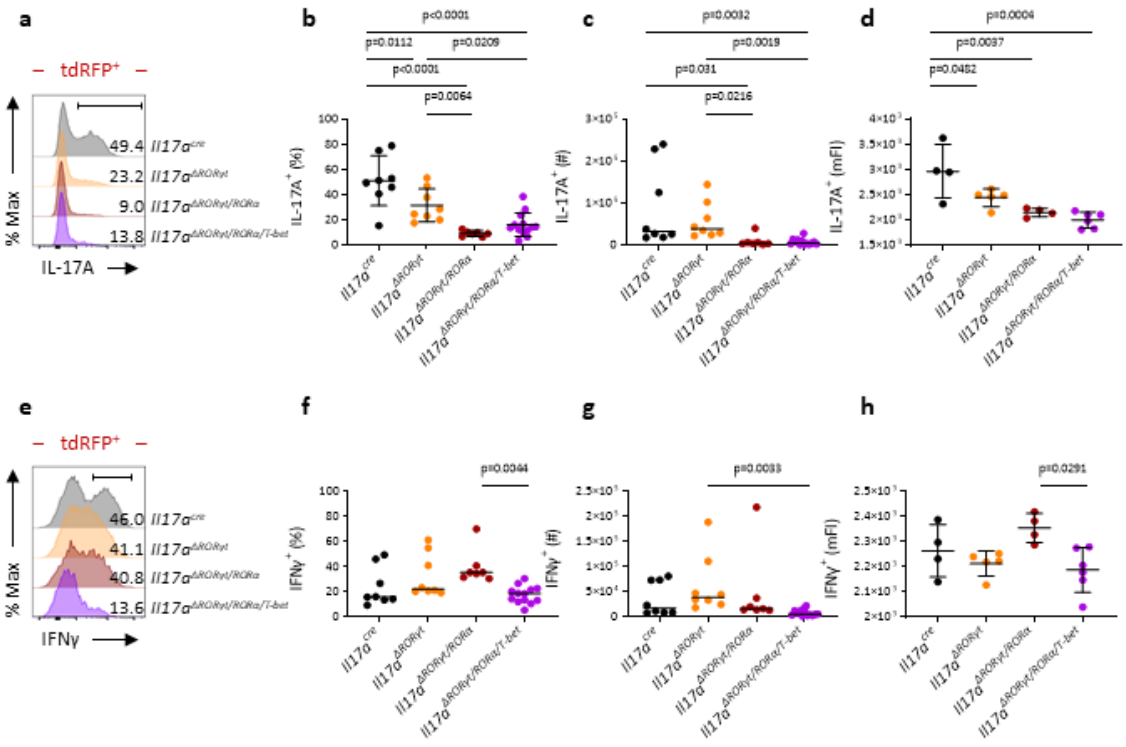
a
– tdRFP+ –
% Max
IL-17A
49.4 Il17a^cre
23.2 Il17a^ΔRORγt
9.0 Il17a^ΔRORγt/RORα
13.8 Il17a^ΔRORγt/RORα/T-bet
b
IL-17A+ (%)
p<0.0001
p=0.0112
p=0.0209
p<0.0001
p=0.0064
c
IL-17A+ (#)
p=0.0032
p=0.0019
p=0.031
p=0.0216
d
IL-17A+ (mFI)
p=0.0004
p=0.0037
p=0.0452
e
– tdRFP+ –
% Max
IFNγ
46.0 Il17a^cre
41.1 Il17a^ΔRORγt
40.8 Il17a^ΔRORγt/RORα
13.6 Il17a^ΔRORγt/RORα/T-bet
f
IFNγ+ (%)
p=0.0044
g
IFNγ+ (#)
p=0.0033
h
IFNγ+ (mFI)
p=0.0291
Il17a^cre
Il17a^ΔRORγt
Il17a^ΔRORγt/RORα
Il17a^ΔRORγt/RORα/T-bet

Figure 4.7. RORα is both sufficient and necessary for Th17 cell function if RORγt and T-bet are absent

Cytokine production was assessed in *Il17a*^{cre}, *Il17a*$^{\Delta RORγt}$, *Il17a*$^{\Delta RORγt/RORα}$ and *Il17a*$^{\Delta RORγt/RORα/T\text{-}bet}$ mice to test Th17 cell function reliance on continued TF expression.

a, e) Representative histograms gated on CLP tdRFP^{+} CD4 T cells showing IL-17A (a) and IFNγ (e) expression following *ex vivo* restimulation with PMA and ionomycin on D14 of *C.rodentium* infection in *Il17a*^{cre}, *Il17a*$^{\Delta RORγt}$, *Il17a*$^{\Delta RORγt/RORα}$ and *Il17a*$^{\Delta RORγt/RORα/T\text{-}bet}$ mice.

b-c) Quantification of the proportion (b) and total number (c) of IL-17A^{+} cells within the parent population in CLP of *Il17a*^{cre}, *Il17a*$^{\Delta RORγt}$, *Il17a*$^{\Delta RORγt/RORα}$ and *Il17a*$^{\Delta RORγt/RORα/T\text{-}bet}$ mice on D14 of *C.rodentium* infection. *Il17a*^{cre} n=8, data pooled from 3 independent experiments, *Il17a*$^{\Delta RORγt}$ n=8, data pooled from 2 independent experiments, *Il17a*$^{\Delta RORγt/RORα}$ n=7, data pooled from 2 independent experiments, *Il17a*$^{\Delta RORγt/RORα/T\text{-}bet}$ n=13, data pooled from 3 independent experiments. *Il17a*^{cre} and *Il17a*$^{\Delta RORγt}$ data also appear in fig4.5c-d.

d) IL-17A median fluorescence intensity (mFI) in CLP of *Il17a*^{cre}, *Il17a*$^{\Delta RORγt}$, *Il17a*$^{\Delta RORγt/RORα}$ and *Il17a*$^{\Delta RORγt/RORα/T\text{-}bet}$ mice on D14 following *C.rodentium* inoculation. *Il17a*^{cre} n=4, *Il17a*$^{\Delta RORγt}$ n=5, *Il17a*$^{\Delta RORγt/RORα}$ n=4, *Il17a*$^{\Delta RORγt/RORα/T\text{-}bet}$ n=6, all data from 1 experiment. *Il17a*^{cre} and *Il17a*$^{\Delta RORγt}$ data also appear in fig4.5e.

f-g) Quantification of the proportion (f) and total number (g) of IFNγ^{+} cells within the parent population in CLP of *Il17a*^{cre}, *Il17a*$^{\Delta RORγt}$, *Il17a*$^{\Delta RORγt/RORα}$ and *Il17a*$^{\Delta RORγt/RORα/T\text{-}bet}$ mice on D14 of *C.rodentium* infection. *Il17a*^{cre} n=8, data pooled from 3 independent experiments, *Il17a*$^{\Delta RORγt}$ n=8, data pooled from 2 independent experiments, *Il17a*$^{\Delta RORγt/RORα}$ n=7, data pooled from 2 independent experiments, *Il17a*$^{\Delta RORγt/RORα/T\text{-}bet}$ n=13, data pooled from 3 independent experiments. *Il17a*^{cre} and *Il17a*$^{\Delta RORγt}$ data also appear in fig4.5g-h.

h) IFNγ median fluorescence intensity (mFI) in CLP of *Il17a*^{cre}, *Il17a*$^{\Delta RORγt}$, *Il17a*$^{\Delta RORγt/RORα}$ and *Il17a*$^{\Delta RORγt/RORα/T\text{-}bet}$ mice on D14 following *C.rodentium* inoculation. *Il17a*^{cre} n=4, *Il17a*$^{\Delta RORγt}$ n=5, *Il17a*$^{\Delta RORγt/RORα}$ n=4, *Il17a*$^{\Delta RORγt/RORα/T\text{-}bet}$ n=6, all data from 1 experiment. *Il17a*^{cre} and *Il17a*$^{\Delta RORγt}$ data also appear in fig4.5i.

Values on histograms represent percentages. Normality was tested using Shapiro-Wilk test. Lines on graphs show mean±SD (b, d, h) or median (c, f, g). Significance was tested using One-Way ANOVA (b, d, h) or Kruskal-Wallis test (c, f, g).

4.4 T-BET IS REQUIRED FOR FULLY MATURE EXTH17 CELL DIFFERENTIATION

To establish the specific role T-bet plays in sustaining Th1-like exTh17 cell function, a further conditional knockout model was generated by crossing the *Il17a*^{cre}*Rosa26*^{tdRFP} and *Tbx21*$^{fl/fl}$ strains. The resulting *Il17a*$^{\Delta T\text{-}bet}$ mice delete T-bet in Th17 cells and other IL-17A-producing cells. Comparing control and *Il17a*$^{\Delta T\text{-}bet}$ mice revealed no statistically significant changes in IFNγ production by tdRFP^{+} CD4 T cells following *C.rodentium* infection. However, a small reduction in frequency, numbers and signal intensity, corresponding to the amount of cytokine produced in per cell, was clear (Fig4.8a-d). To test whether removal of T-bet had an effect on type 3 function in tdRFP^{+} CD4 T cells IL-17A production was also assessed (Fig4.8e). Surprisingly, despite the suppressive role of T-bet in regulating Th17 cell function (Lazarevic et al., 2011), no statistically significant increase in IL-17A^{+} tdRFP^{+} CD4 T cell frequency or numbers was observed (Fig4.8f-g). Furthermore, there was no increase in the amount of IL-17A produced by T-bet-deficient cells (Fig4.8h). While it is possible that further biological repeats would be required to account for variability in these data, the available results suggested that T-bet expression did not have a large impact on either type 1 or type 3 function within Th17 cells generated in response to infection.

IFNγ^{+} Th17 cells and IFNγ^{+} CD4 T cells of a Th17 cells origin that no longer produce IL-17 have been linked to a multitude of autoimmune and inflammatory diseases (Annunziato et al., 2007; Bending et al., 2009; Bishu, El Zaatari, et al., 2019; Hirota et al., 2011; Krausgruber et al., 2016). However, there are conflicting reports on whether pathogenesis is T-bet dependent (Bettelli et al., 2004; Duhen et al., 2013). A possible interpretation is that different Th17 and exTh17 cell populations, perhaps at different stages of the Th17/exTh17 spectrum (Fig4.3d), were the key drivers of disease progression. Therefore, analyses of *Il17a*$^{\Delta T\text{-}bet}$ mice were expanded to test the three tdRFP^{+} CD4 T cell populations identified by IL-17A and IFNγ expression (Fig4.8i). Indeed, while the frequency and numbers of cells producing IL-17A, regardless of their ability to express IFNγ, remained unchanged between controls

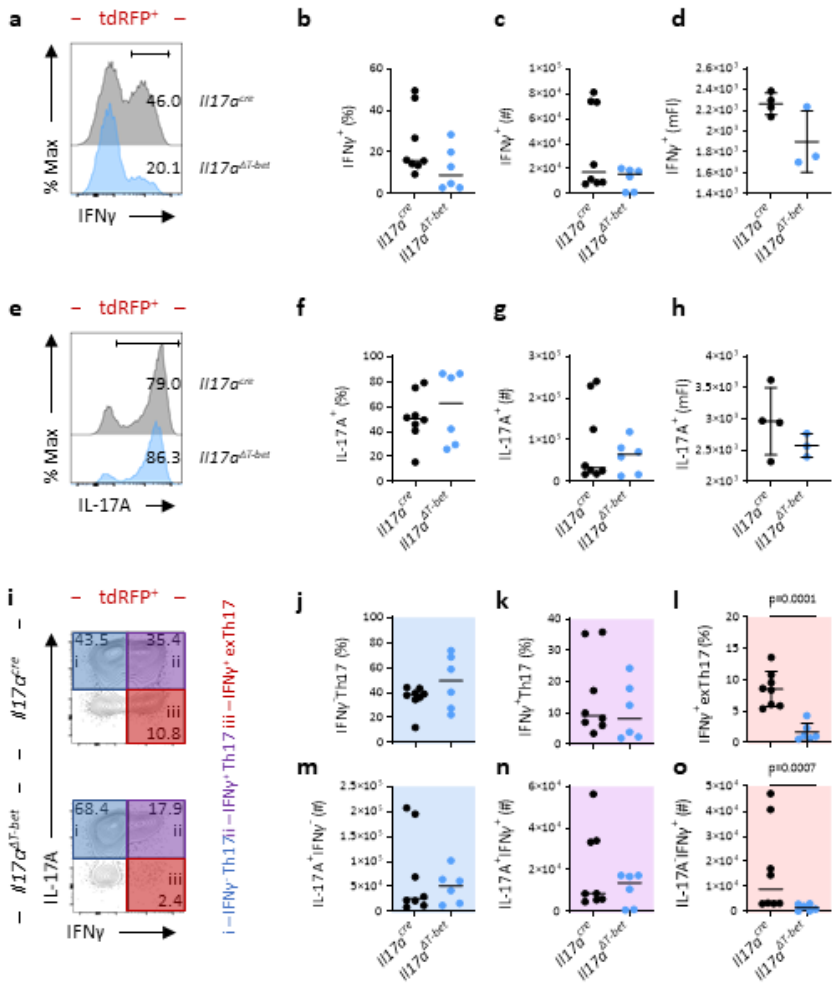
a
– tdRFP+ –
46.0
Il17a^cre
20.1
Il17a^ΔT-bet
% Max
IFNγ
b
IFNγ+ (%)
c
IFNγ+ (#)
d
IFNγ+ (mFI)
e
– tdRFP+ –
79.0
Il17a^cre
86.3
Il17a^ΔT-bet
% Max
IL-17A
f
IL-17A+ (%)
g
IL-17A+ (#)
h
IL-17A+ (mFI)
i
– tdRFP+ –
Il17a^cre
Il17a^ΔT-bet
43.5
35.4
10.8
68.4
17.9
2.4
IL-17A
IFNγ
i = IFNγ- Th17i ii = IFNγ+ Th17 iii = IFNγ+ exTh17
j
IFNγ-Th17 (%)
k
IFNγ+Th17 (%)
l
p=0.0001
IFNγ+exTh17 (%)
m
IL-17A+IFNγ- (#)
n
IL-17A+IFNγ+ (#)
o
p=0.0007
IL-17A IFNγ+ (#)

Figure 4.8. T-bet is required for fully mature IFNγ$^+$ exTh17 cell differentiation

Cytokine production was assessed in *Il17a^{cre}* and *Il17a$^{\Delta T\text{-}bet}$* mice to test Th17 function reliance on continued TF expression.

a, e) Representative histograms gated on CLP tdRFP$^+$ CD4 T cells showing IFNγ (a) and IL-17A (e) expression following *ex vivo* restimulation with PMA and ionomycin on D14 of *C.rodentium* infection in *Il17a^{cre}* and *Il17a$^{\Delta T\text{-}bet}$* mice.

b-c) Quantification of the proportion (b) and total number (c) of IFNγ$^+$ cells within the parent population in CLP of *Il17a^{cre}* and *Il17a$^{\Delta T\text{-}bet}$* mice on D14 of *C.rodentium* infection. *Il17a^{cre}* n=8, data pooled from 3 independent experiments, *Il17a$^{T\text{-}bet}$* n=6, data pooled from 2 independent experiments. *Il17a^{cre}* data also appear in fig4.5g-h and fig4.7f-g.

d) IFNγ median fluorescence intensity (mFI) in CLP of *Il17a^{cre}* and *Il17a$^{\Delta T\text{-}bet}$* mice on D14 of *C.rodentium* infection. *Il17a^{cre}* n=4, *Il17a$^{T\text{-}bet}$* n=3, all data from 1 experiment. *Il17a^{cre}* data also appear in fig4.5i and fig4.7h.

f-g) Quantification of the proportion (f) and total number (g) of IL-17A$^+$ cells within the parent population in CLP of *Il17a^{cre}* and *Il17a$^{\Delta T\text{-}bet}$* mice on D14 of *C.rodentium* infection. *Il17a^{cre}* n=8, data pooled from 3 independent experiments, *Il17a$^{T\text{-}bet}$* n=6, data pooled from 2 independent experiments. *Il17a^{cre}* data also appear in fig4.5c-d and fig4.7b-c.

h) IL-17A median fluorescence intensity (mFI) in CLP of *Il17a^{cre}* and *Il17a$^{\Delta T\text{-}bet}$* mice on D14 of *C.rodentium* infection. *Il17a^{cre}* n=4, *Il17a$^{T\text{-}bet}$* n=3, all data from 1 experiment. *Il17a^{cre}* data also appear in fig4.5e and fig4.7d.

i) Representative flow cytometry plots gated on tdRFP$^+$ CD4 T cells showing IL-17A and IFNγ with identification of IFNγ$^-$ Th17, IFNγ$^+$ Th17 and IFNγ$^+$ exTh17 populations in CLP of *Il17a^{cre}* (left) and *Il17a$^{\Delta T\text{-}bet}$* (right) following *ex vivo* restimulation with PMA and Ionomycin on D14 following *C.rodentium* inoculation.

j-o) Quantification of the proportion and total number of IFNγ$^-$ Th17 (j, m), IFNγ$^+$ Th17 (k, n) and IFNγ$^+$ exTh17 (l, o) cells within the parent population in CLP of *Il17a^{cre}* and *Il17a$^{\Delta T\text{-}bet}$* mice on D14 of *C.rodentium* infection. *Il17a^{cre}* n=8, data pooled from 3 independent experiments, *Il17a$^{T\text{-}bet}$* n=6, data pooled from 2 independent experiments.

Values on flow cytometry plots and histograms represent percentages. Normality was tested using Shapiro-Wilk test. Lines on graphs show mean±SD (d, h, l) or median (b, c, f, g, j, k, m, n, o). Significance was tested using unpaired t test (d, h, l) or Mann-Whitney U test (b, c, f, g, j, k, m, n, o).

and *Il17a*$^{\Delta T\text{-}bet}$ mice the absence of T-bet resulted in a 2-3-fold drop in fully mature IFNγ^{+} exTh17 cell frequency along with a decline in their numbers (Fig4.8i-o).

4.5 FURTHER TYPE 3 AND TYPE 1 CYTOKINES SHOW VARIED RELIANCE ON THE THREE KEY TFS

IL-17A and IFNγ are key cytokines produced by Th17 and Th-1ike exTh17 cells. However, alternative Th17 and Th1 cell-associated cytokines can enhance effector functions or even mediate processes unrelated to IL-17A and IFNγ (Bogdan et al., 1990; Darrah et al., 2007; Kannanganat et al., 2007; Liang et al., 2006; X. O. Yang, S. H. Chang, et al., 2008). Therefore, the requirement for continued expression of RORγt, RORα and T-bet in supporting expression of the Th17 cell cytokines IL-17F and IL22, and the Th1 cell cytokine TNFα was also tested.

To assess type 3 function IL-17F and IL-22 expression were tested in colonic tdRFP^{+} CD4 T cells following *C.rodentium* infection (Fig4.9a-b). Overall, both cytokines appeared to show similar alterations to IL-17A with a large reduction in both the proportion and number of cells producing them in the combined absence of RORγt and RORα. Moreover, as observed when assessing IL-17A only, co-deletion of T-bet failed to rescue IL-17F and IL-22 production. (Fig4.9c-f). Importantly, changes in cellularity must be interpreted in the context of a reduction in the total colonic tdRFP^{+} CD4 T cell pool and may not be caused by a specific loss of IL-17F^{+} or IL-22^{+} cells. Therefore, cytokine production levels were also assessed (Fig4.9g-h). IL-17F production was diminished in all mouse strains lacking either ROR family TF (Fig4.9g). Testing IL-22 expression levels revealed a shift between the assessed mouse models in signal intensity within both the IL-22^{-} and IL-22^{+} populations. This phenomenon is unexplained but was consistently reproducible. Therefore, I elected to quantify the fold change in signal intensity between the IL-22^{+} and IL-22^{-} populations rather than simply comparing IL-22 levels within the former. Surprisingly, IL-22 expression levels increased in the absence of RORγt but decreased in all other conditional knockouts, including mice lacking T-bet in Th17. Moreover, IL-22^{+} cells lacking both ROR family TFs appeared express higher levels of the cytokine than those with a T-bet-deficiency (Fig4.9h). However, such cells are very limited in numbers, as evidenced by population

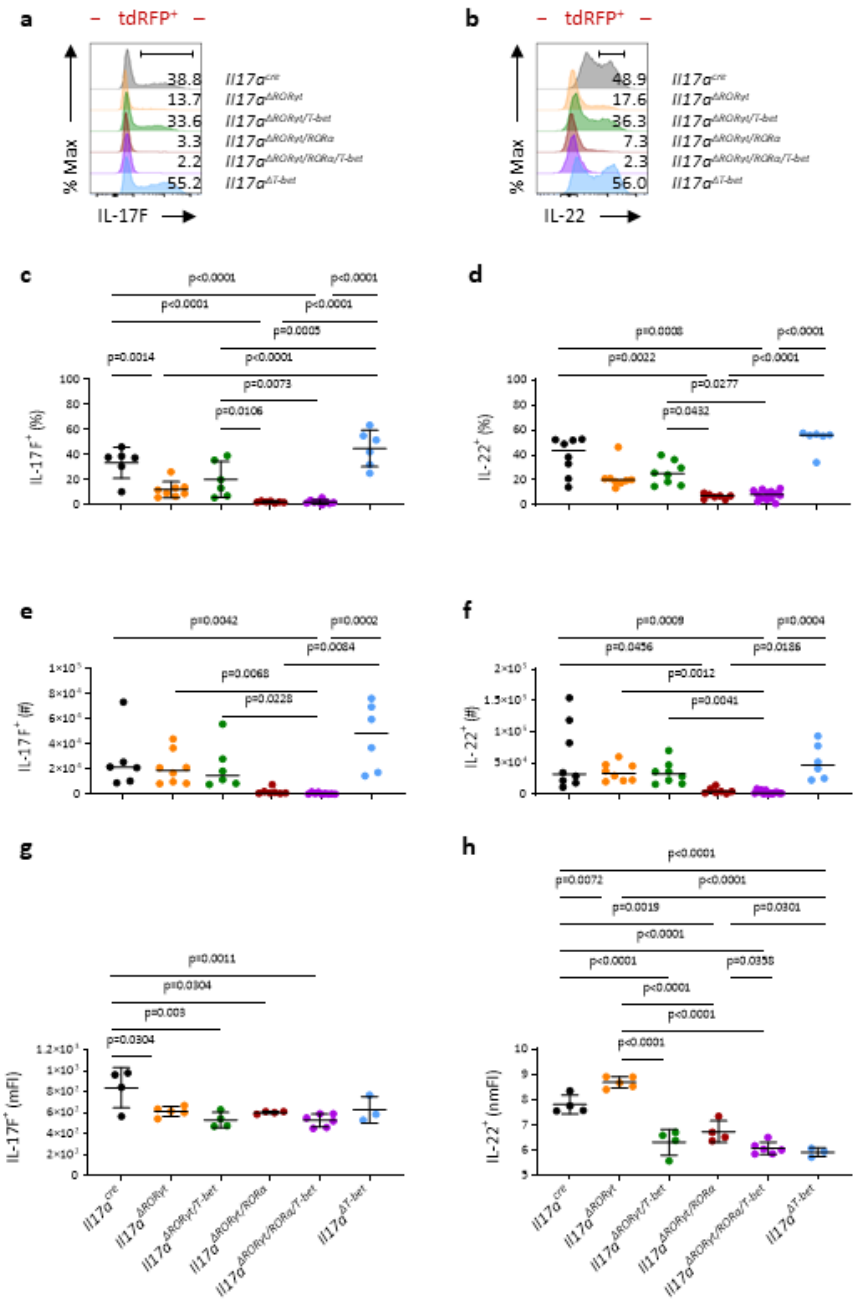
a
– tdRFP+ –
% Max
IL-17F
38.8
13.7
33.6
3.3
2.2
55.2
Il17a cre
Il17a ΔRORγt
Il17a ΔRORγt/T-bet
Il17a ΔRORγt/RORα
Il17a ΔRORγt/RORα/T-bet
Il17a ΔT-bet
b
– tdRFP+ –
% Max
IL-22
48.9
17.6
36.3
7.3
2.3
56.0
c
IL-17F+ (%)
d
IL-22+ (%)
e
IL-17F+ (#)
f
IL-22+ (#)
g
IL-17F+ (mFI)
h
IL-22+ (nmFI)

Figure 4.9. ROR family TF and T-bet deletion impacts further Th17 cell-associated cytokines

The effect of combinatorial RORγt, RORα and T-bet deletion on type 3 cytokine production was assessed in *Il17a*^{cre}, *Il17a*$^{\Delta RORγt}$, *Il17a*$^{\Delta RORγt/T\text{-}bet}$, *Il17a*$^{\Delta RORγt/RORα}$, *Il17a*$^{\Delta RORγt/RORα/T\text{-}bet}$ and *Il17a*$^{\Delta T\text{-}bet}$ mice.

a-b) Representative histograms gated on CLP tdRFP^{+} CD4 T cells showing IL-17F (a) and IL-22 (b) expression following *ex vivo* restimulation with PMA and ionomycin on D14 of *C.rodentium* infection in *Il17a*^{cre}, *Il17a*$^{\Delta RORγt}$, *Il17a*$^{\Delta RORγt/T\text{-}bet}$, *Il17a*$^{\Delta RORγt/RORα}$, *Il17a*$^{\Delta RORγt/RORα/T\text{-}bet}$ and *Il17a*$^{\Delta T\text{-}bet}$ mice.

c, e) Quantification of the proportion (c) and total number (e) of IL-17F^{+} cells within the parent population in CLP of *Il17a*^{cre}, *Il17a*$^{\Delta RORγt}$, *Il17a*$^{\Delta RORγt/T\text{-}bet}$, *Il17a*$^{\Delta RORγt/RORα}$, *Il17a*$^{\Delta RORγt/RORα/T\text{-}bet}$ and *Il17a*$^{\Delta T\text{-}bet}$ mice on D14 of *C.rodentium* infection. *Il17a*^{cre}, *Il17a*$^{\Delta RORγt/T\text{-}bet}$ and *Il17a*$^{\Delta T\text{-}bet}$ n=6, *Il17a*$^{\Delta RORγt}$ n=8, *Il17a*$^{\Delta RORγt/RORα}$ n=7 and *Il17a*$^{\Delta RORγt/RORα/T\text{-}bet}$ n=9, all data pooled from 2 independent experiments.

d, f) Quantification of the proportion (d) and total number (f) of IL-22^{+} cells within the parent population in CLP of *Il17a*^{cre}, *Il17a*$^{\Delta RORγt}$, *Il17a*$^{\Delta RORγt/T\text{-}bet}$, *Il17a*$^{\Delta RORγt/RORα}$, *Il17a*$^{\Delta RORγt/RORα/T\text{-}bet}$ and *Il17a*$^{\Delta T\text{-}bet}$ mice on D14 of *C.rodentium* infection. *Il17a*^{cre} and *Il17a*$^{\Delta RORγt/T\text{-}bet}$ n=8, data pooled from 3 independent experiments, *Il17a*$^{\Delta RORγt}$ n=8, data pooled from 2 independent experiments, *Il17a*$^{\Delta RORγt/RORα}$ n=7, data pooled from 2 independent experiments, *Il17a*$^{\Delta RORγt/RORα/T\text{-}bet}$ n=13, data pooled from 3 independent experiments and *Il17a*$^{\Delta T\text{-}bet}$ n=6, data pooled from 2 independent experiments.

g-h) IL-17F (g) median fluorescence intensity (mFI) and IL-22 (h) median fluorescence intensity normalised to IL-22^{-} population (nmFI) in CLP of *Il17a*^{cre}, *Il17a*$^{\Delta RORγt}$, *Il17a*$^{\Delta RORγt/T\text{-}bet}$, *Il17a*$^{\Delta RORγt/RORα}$, *Il17a*$^{\Delta RORγt/RORα/T\text{-}bet}$ and *Il17a*$^{\Delta T\text{-}bet}$ mice on D14 of *C.rodentium* infection. *Il17a*^{cre}, *Il17a*$^{\Delta RORγt/T\text{-}bet}$ and *Il17a*$^{\Delta RORγt/RORα}$ n=4, *Il17a*$^{\Delta RORγt}$ n=5, *Il17a*$^{\Delta RORγt/RORα/T\text{-}bet}$ n=6 and *Il17a*$^{\Delta T\text{-}be}$ n=3, all data from 1 experiment.

Values on histograms represent percentages. Normality was tested using Shapiro-Wilk test. Lines on graphs show mean±SD (c, g, h) or median (d, e, f). Significance was tested using One-Way ANOVA (c, g, h) or Kruskal-Wallis test (d, e, f).

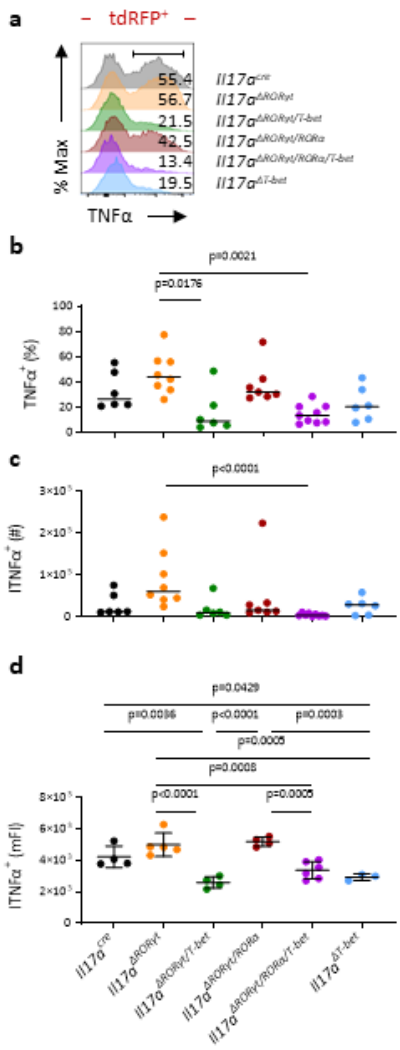
a
– tdRFP+ –
55.4
56.7
21.5
42.5
13.4
19.5
% Max
TNFα
b
p=0.0021
p=0.0176
TNFα+ (%)
c
p<0.0001
ITNFα+ (#)
d
p=0.0429
p=0.0036
p<0.0001
p=0.0003
p=0.0005
p=0.0008
p<0.0001
p=0.0005
ITNFα+ (mFI)

Figure 4.10. ROR family TF and T-bet deletion impacts further type 1 cytokines

The effect of combinatorial RORγt, RORα and T-bet deletion on production of the type 1 cytokine TNFα was assessed in *Il17a*^{cre}, *Il17a*$^{\Delta RORγt}$, *Il17a*$^{\Delta RORγt/T\text{-}bet}$, *Il17a*$^{\Delta RORγt/RORα}$, *Il17a*$^{\Delta RORγt/RORα/T\text{-}bet}$ and *Il17a*$^{\Delta T\text{-}bet}$ mice.

a) Representative histograms gated on CLP tdRFP^{+} CD4 T cells showing TNFα expression following *ex vivo* restimulation with PMA and ionomycin on D14 of *C.rodentium* infection in *Il17a*^{cre}, *Il17a*$^{\Delta RORγt}$, *Il17a*$^{\Delta RORγt/T\text{-}bet}$, *Il17a*$^{\Delta RORγt/RORα}$, *Il17a*$^{\Delta RORγt/RORα/T\text{-}bet}$ and *Il17a*$^{\Delta T\text{-}bet}$ mice.

b-c) Quantification of the proportion (b) and total number (c) of TNFα^{+} cells within the parent population in CLP of *Il17a*^{cre}, *Il17a*$^{\Delta RORγt}$, *Il17a*$^{\Delta RORγt/T\text{-}bet}$, *Il17a*$^{\Delta RORγt/RORα}$, *Il17a*$^{\Delta RORγt/RORα/T\text{-}bet}$ and *Il17a*$^{\Delta T\text{-}bet}$ mice on D14 of *C.rodentium* infection. *Il17a*^{cre}, *Il17a*$^{\Delta RORγt/T\text{-}bet}$ and *Il17a*$^{\Delta T\text{-}bet}$ n=6, *Il17a*$^{\Delta RORγt}$ n=8, *Il17a*$^{\Delta RORγt/RORα}$ n=7 and *Il17a*$^{\Delta RORγt/RORα/T\text{-}bet}$ n=9, all data pooled from 2 independent experiments.

d) TNFα median fluorescence intensity (mFI) in CLP of *Il17a*^{cre}, *Il17a*$^{\Delta RORγt}$, *Il17a*$^{\Delta RORγt/T\text{-}bet}$, *Il17a*$^{\Delta RORγt/RORα}$, *Il17a*$^{\Delta RORγt/RORα/T\text{-}bet}$ and *Il17a*$^{\Delta T\text{-}bet}$ mice on D14 of *C.rodentium* infection. *Il17a*^{cre}, *Il17a*$^{\Delta RORγt/T\text{-}bet}$ and *Il17a*$^{\Delta RORγt/RORα}$ n=4, *Il17a*$^{\Delta RORγt}$ n=5, *Il17a*$^{\Delta RORγt/RORα/T\text{-}bet}$ n=6 and *Il17a*$^{\Delta T\text{-}be}$ n=3, all data from 1 experiment.

Values on histograms represent percentages. Normality was tested using Shapiro-Wilk test. Lines on graphs show mean±SD (d) or median (b, c). Significance was tested using One-Way ANOVA (d) or Kruskal-Wallis test (b, c).

frequency and cellularity (Fig4.9d, f). It is possible that a proportion of tdRFP$^+$ cells underwent incomplete recombination, retaining expression of RORγt, RORα or both. This would result in unexpectedly high expression of type 3 cytokines. Therefore, exclusion of the small number of cells with detectable TF expression would benefit future experiments.

Turning to type 1 effector functions, TNFα production within Th17 and exTh17 cell populations generated in response to *C.rodentium* infection in our conditional knockout strains was also assessed (Fig4.10a). Spread within the data did not allow clear conclusions to be drawn, however, the largest TNFα$^+$ tdRFP$^+$ population was observed in *Il17a*$^{\Delta RORγt}$ and *Il17a*$^{\Delta RORγt/RORα}$ mice with an exTh17 cell-skewed response (Fig4.10b-c). The reduction in TNFα expression in T-bet-deficient mouse strains compared to those lacking ROR family TFs is consistent with at least a partial role for T-bet in driving the production of this cytokine. In addition, TNFα expression levels increased only if ROR family TFs were absent but not if T-bet was deleted, further supporting this hypothesis (Fig4.10d).

4.6 MANIPULATION OF THE TH17/EXTH17 AXIS PERTURBS THE MICROBIOTA AND IMPACTS PATHOGEN CONTROL

Having established the requirement for RORγt, RORα and T-bet in driving key effector functions I next sought to assess functional outcomes of Th17/exTh17 continuum perturbations. Beginning approximately 4-5 days following oral *C.rodentium* administration, the number of bacteria shed into the lumen is indicative of mucosal bacterial burden (Wiles et al., 2004; Wiles et al., 2005). Specifically, a value of over 10^7 colony forming units per gram of faeces (CFU/g) was established as a surrogate marker of mucosal invasion and colonisation. Early on in this body of work conditional knockout strain-specific differences in susceptibility to *C.rodentium* were noted. Specifically, mice with IL-17A-driven T-bet deletion appeared least resistant to infection, regardless of the presence or absence or ROR family TFs (Fig4.11a). Building on this observation, the colonisation and clearance kinetics of the infection were assessed in the different strains through tracking of bacterial burden over the course of the infection. To assess whether bacterial burden at the predicted peak of the infection was

comparable, faecal counts were made at D6-8. These investigations revealed no clear differences at this early stage of the infection (Fig4.11b). Next, control of the infection and the ability to clear bacteria was assessed through tracking of bacterial burden over time. Despite the increased susceptibility in all T-bet-deficient knockout models only mice lacking all three TFs showed impaired *C.rodentium* clearance by D28 of the infection (Fig4.11c). These data do not establish whether clearance was delayed or simply not achieved and longer follow-up of infections would likely be informative.

C.rodentium is a pathogen that is heavily reliant on microbial species within the normal flora for its ability to colonise. While certain classes of commensals, such as SFB, appear protective, the presence of others is required for mucosal infection (Curtis et al., 2014; Ghosh et al., 2011; Ivanov et al., 2009; Mullineaux-Sanders et al., 2017). Moreover, following immune system-driven clearance from the mucosa, expulsion of luminal *C.rodentium* was reported to be mediated by competition for nutrients with further commensal bacteria (Kamada et al., 2012). Th17 cells, as well as other IL-17A-producing innate and adaptive immune cell populations, and the microbiota reciprocally regulate one-another (Dutzan et al., 2018; Ivanov et al., 2009; Liang et al., 2006). I therefore hypothesised that the differences in susceptibility to and clearance of this pathogen were caused by strain-specific alterations in the microbiome of conditional knockout models. To begin to test this hypothesis I assessed the composition of the faecal microbiome of control, *Il17a*$^{\Delta ROR\gamma t/ROR\alpha}$, *Il17a*$^{\Delta ROR\gamma t/ROR\alpha/T\text{-}bet}$ and *Il17a*$^{\Delta T\text{-}bet}$ mice in the absence of infection. Quantifying the dissimilarity in microbiota composition at the genus level yielded two clear clusters defined by the presence or absence of T-bet in IL-17A-producing cells (Fig4.11d). Strikingly, investigation of specific differences showed that even though *Helicobacter* was the most abundant genus in T-bet-sufficient mice it was completely absent in ones lacking this TF (Fig4.11e). This was found to be caused by a single *Helicobacter* species, *H.ganmani* (Fig4.11f). Thus, initial microbiome analyses supported the theory that manipulation of ROR family TF/T-bet balance perturbs the microbiota with potentially detrimental effects on susceptibility to

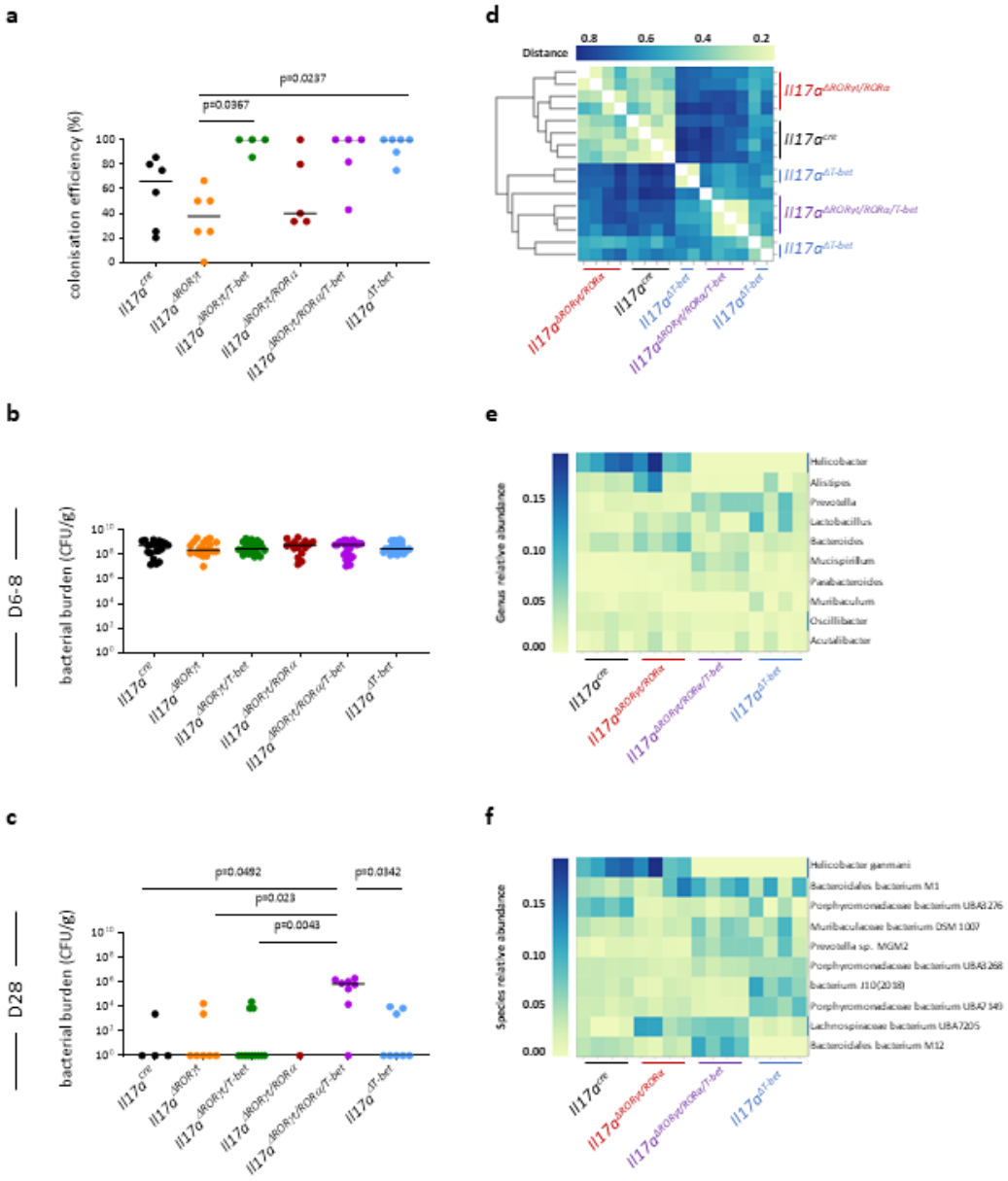
a
p=0.0237
p=0.0367
colonisation efficiency (%)
d
Distance
0.8
0.6
0.4
0.2
b
D6-8
bacterial burden (CFU/g)
e
Genus relative abundance
Helicobacter
Alistipes
Prevotella
Lactobacillus
Bacteroides
Mucispirillum
Parabacteroides
Muribaculum
Oscillibacter
Acutalibacter
c
D28
p=0.0492
p=0.0342
p=0.023
p=0.0043
f
Species relative abundance
Helicobacter ganmani
Bacteroidales bacterium M1
Porphyromonadaceae bacterium UBA8276
Muribaculaceae bacterium DSM 1007
Prevotella sp. MGM2
Porphyromonadaceae bacterium UBA8268
bacterium J10(2018)
Porphyromonadaceae bacterium UBA7140
Lachnospiraceae bacterium UBA7205
Bacteroidales bacterium M12

Figure 4.11. ROR family TF and T-bet deletion change pathogen responses and drive strain-specific microbiome alterations

Early and late *C.rodentium* bacterial burden was assessed to test susceptibility to and clearance of this pathogen in *Il17a*^{cre}, *Il17a*$^{\Delta ROR\gamma t}$, *Il17a*$^{\Delta ROR\gamma t/T\text{-}bet}$, *Il17a*$^{\Delta ROR\gamma t/ROR\alpha}$, *Il17a*$^{\Delta ROR\gamma t/ROR\alpha/T\text{-}bet}$ and *Il17a*$^{\Delta T\text{-}bet}$ mice along with the composition of *Il17a*^{cre}, *Il17a*$^{\Delta ROR\gamma t/ROR\alpha}$, *Il17a*$^{\Delta ROR\gamma t/ROR\alpha/T\text{-}bet}$ and *Il17a*$^{\Delta T\text{-}bet}$ microbiome in the absence of infection.

a) Quantification of the proportion of mice colonised out of all inoculated *Il17a*^{cre}, *Il17a*$^{\Delta ROR\gamma t}$, *Il17a*$^{\Delta ROR\gamma t/T\text{-}bet}$, *Il17a*$^{\Delta ROR\gamma t/ROR\alpha}$, *Il17a*$^{\Delta ROR\gamma t/ROR\alpha/T\text{-}bet}$ and *Il17a*$^{\Delta T\text{-}bet}$ animals per experiment. *Il17a*^{cre}, *Il17a*$^{\Delta ROR\gamma t}$ and *Il17a*$^{\Delta T\text{-}bet}$ n=6, *Il17a*$^{\Delta ROR\gamma t/T\text{-}bet}$ n=4, *Il17a*$^{\Delta ROR\gamma t/ROR\alpha}$ and *Il17a*$^{\Delta ROR\gamma t/ROR\alpha/T\text{-}bet}$ n=5, all datapoints represent 1 independent experiment.

b) Quantification of faecal bacterial burden in successfully colonised *Il17a*^{cre}, *Il17a*$^{\Delta ROR\gamma t}$, *Il17a*$^{\Delta ROR\gamma t/T\text{-}bet}$, *Il17a*$^{\Delta ROR\gamma t/ROR\alpha}$, *Il17a*$^{\Delta ROR\gamma t/ROR\alpha/T\text{-}bet}$ and *Il17a*$^{\Delta T\text{-}bet}$ mice on D6-8 following *C.rodentium* inoculation. *Il17a*^{cre} n=19, data pooled from 6 independent experiments, *Il17a*$^{\Delta ROR\gamma t}$ n=20, data pooled from 5 independent experiments, *Il17a*$^{\Delta ROR\gamma t/T\text{-}bet}$ n=24, data pooled from 4 independent experiments, *Il17a*$^{\Delta ROR\gamma t/ROR\alpha}$ n=16, data pooled from 5 independent experiments, *Il17a*$^{\Delta ROR\gamma t/ROR\alpha/T\text{-}bet}$ n=29, data pooled from 5 independent experiments and *Il17a*$^{\Delta T\text{-}bet}$ n=30, data pooled from 6 independent experiments.

c) Quantification of faecal bacterial burden in successfully colonised *Il17a*^{cre}, *Il17a*$^{\Delta ROR\gamma t}$, *Il17a*$^{\Delta ROR\gamma t/T\text{-}bet}$, *Il17a*$^{\Delta ROR\gamma t/ROR\alpha}$, *Il17a*$^{\Delta ROR\gamma t/ROR\alpha/T\text{-}bet}$ and *Il17a*$^{\Delta T\text{-}bet}$ mice on D28 following *C.rodentium* inoculation. *Il17a*^{cre} n=4, *Il17a*$^{\Delta ROR\gamma t}$ n=7, *Il17a*$^{\Delta ROR\gamma t/T\text{-}bet}$ and *Il17a*$^{\Delta T\text{-}bet}$ n=8, *Il17a*$^{\Delta ROR\gamma t/ROR\alpha}$ n=1 and *Il17a*$^{\Delta ROR\gamma t/ROR\alpha/T\text{-}bet}$ n=12, all data from 1 experiment. *Il17a*$^{\Delta ROR\gamma t/ROR\alpha}$ data not included in statistical analyses.

d) Dendrogram and heatmap representing Bray-Curtis dissimilarity matrix based on relative abundance of microbial genera in *Il17a*^{cre}, *Il17a*$^{\Delta ROR\gamma t/ROR\alpha}$, *Il17a*$^{\Delta ROR\gamma t/ROR\alpha/T\text{-}bet}$ and *Il17a*$^{\Delta T\text{-}bet}$ faecal matter. Darker squares represent more dissimilar samples. *Il17a*^{cre}, *Il17a*$^{\Delta ROR\gamma t/ROR\alpha}$, *Il17a*$^{\Delta ROR\gamma t/ROR\alpha/T\text{-}bet}$ and *Il17a*$^{\Delta T\text{-}bet}$ n=4, all data from 1 experiment.

e-f) Heatmaps representing relative abundance of top 10 microbial genera (e) and species (f) in *Il17a*^{cre}, *Il17a*$^{\Delta ROR\gamma t/ROR\alpha}$, *Il17a*$^{\Delta ROR\gamma t/ROR\alpha/T\text{-}bet}$ and *Il17a*$^{\Delta T\text{-}bet}$ faecal matter. *Il17a*^{cre}, *Il17a*$^{\Delta ROR\gamma t/ROR\alpha}$, *Il17a*$^{\Delta ROR\gamma t/ROR\alpha/T\text{-}bet}$ and *Il17a*$^{\Delta T\text{-}bet}$ n=4, all data from 1 experiment.

Normality was tested using Shapiro-Wilk test. Lines on graphs show median (a, b, c). Significance was tested using Kruskal-Wallis test (a, b, c).

pathogen invasion. However, further work is required to assess all mouse strains and elucidate precise mechanisms.

4.7 SUMMARY

Here I assessed how Th17 and exTh17 cell functions within the colon change following *C.rodentium* colonisation and investigated the role of continued lineage defining TF expression in this process. First, I explored the composition of the effector CD4 T cell compartment at steady state in the colon, building on previous studies that have described intestinal compartment-specific Th17 cell populations (Omenetti et al., 2019). I established that in the absence of infection the colon is home to both Th17 and Th1 cell populations with a limited IFNγ$^+$ exTh17 cell pool. These analyses suggested that, in line with published literature, *C.rodentium* infection triggered not only an expansion in Th17 cell numbers but also the acquisition of a type 1 programme in these cells, as shown by IFNγ production in CD4 T cells with a history of IL-17A production (Omenetti et al., 2019). Expanding experimental aims to test expression of the key Th17 cell cytokines IL-17F and IL-22, I found that IL-17F was largely co-expressed with IL-17A regardless of infection status. Conversely, the very limited IL-22 production by Th17 cells only increased following infection. This is in line with the reported observation that *C.rodentium* colonisation drives IL-22$^+$ CD4 T cell expansion that is maintained even into the memory phase, and suggests that as Th17 cells expand they also upregulate functions related to barrier repair (Bishu, Hou, et al., 2019; Liang et al., 2006; Wolk et al., 2006). Importantly, IL-22 is also required in the absence of infection for appropriate control of commensals. The limited size of the IL-22$^+$ Th17 cell population prior to infection suggested that other cells may be key sources of this cytokine at homeostasis. Indeed, mucosal ILC3-derived IL-22 has been shown to be central to maintenance of commensalism and resistance to pathogen invasion (Satoh-Takayama et al., 2008).

Surprisingly, the Th1 cell-associated cytokine TNFα was produced by approximately a quarter of all colonic Th17/exTh17 cells even at steady state and, much like IL-17F, did not show a clear increase following infection. This contrasted IFNγ expression patterns as production of this cytokine was limited

in CD4 T cells with a history of IL-17A production in the absence of infection. Taken together, these data point to differential regulation of these two type 1 cytokines. Moreover, expression of TNFα in such a substantial part of the Th17/exTh17 cell pool at steady state raises the possibility that this cytokine, produced by these cells, has central roles in the maintenance of mucosal homeostasis. Importantly, the lack of infection-induced change in the proportion of IL-17F$^+$ and TNFα$^+$ cells did not signal an absence of functional changes as the large increase in their numbers is expected to significantly alter the colonic environment. In addition, while no statistically significant changes in the proportion of tdRFP$^+$ CD4 T cells producing these cytokines were observed, the spread of the data indicated that the studies outlined in this chapter were underpowered. Further repeats are needed before conclusions can be drawn with confidence.

As widely reported by others, and shown here, *C.rodentium* infection is a potent trigger of Th1-like Th17 and exTh17 cell differentiation from Th17 cell precursors (Omenetti et al., 2019). However, exactly how this process is controlled is unclear. RORγt and RORα, two ROR family TFs have established roles in the development of Th17 cells but there is now evidence that different Th17 responses show differences in the requirement for these TFs (Brucklacher-Waldert et al., 2016; Ivanov et al., 2006; Withers et al., 2016; X. O. Yang, B. P. Pappu, et al., 2008). Parallel to these investigations, work with similar conditional knockout models to those described in this chapter was ongoing to assess the transcriptional control of post-developmental plasticity exhibited by ILC3, the innate counterparts to Th17 cells. Through this work, mouse strains enabling the conditional deletion of both ROR family TFs and T-bet were established in our lab (Fiancette et al., 2021). Taking advantage of these models, I undertook the first detailed assessment of the requirement for the continued expression of different combinations of TFs in intestinal Th17 cells.

RORγt has a well-established role in Th17 cell development (Ivanov et al., 2006; X. O. Yang, B. P. Pappu, et al., 2008). Additionally, the results presented here showed that loss of RORγt expression in newly formed Th17 cells resulted in diminished type 3 function, as assessed by cytokine secretion.

Interestingly, however, these data contradict reports of an impairment in IFNγ production in certain CD4 T cell populations with mixed Th17/Th1 cell characteristics in RORγt-deficient humans (Ivanov et al., 2006; Milner et al., 2008; Okada et al., 2015; X. O. Yang, B. P. Pappu, et al., 2008). Importantly, cases of perturbations in *RORC*, the gene encoding RORγt in humans, are different to our models in that the genetic defect has a global effect. Given the requirement for RORγt in lymphoid tissue formation and normal thymic T cell development (Eberl et al., 2004; Guo et al., 2016) it is possible that RORγt deficiency in humans drives impaired IFNγ induction through mechanisms not recapitulated in our models. The strength of the approach reported in this chapter is the use of mice that drive post-developmental TF deletion only. Nonetheless, no complete abrogation of Th17 cell function was associated with RORγt deletion. On assessing the reasons behind maintained type 3 function in the absence of RORγt a role for the related TF RORα was identified. The observation that RORγt/RORα co-deletion exacerbated Th17 cell functional impairment phenocopies recent results on the regulation of the IL-17A expression within ILC3 (Fiancette et al., 2021). These data are therefore consistent with RORγt and RORα having similar roles in supporting Th17 cell function. A possible mechanism underlying this functional redundancy is the two TFs' ability to recognise the same ROR response-element DNA binding motifs (Jetten, 2009). However, in the absence of RORα single knockouts the possibility that this TF also plays non-redundant roles in the post-developmental regulation of Th17 and exTh17 cell fate or function cannot be excluded.

Strikingly, observations reported in this chapter indicated that IL-17A production may be rescued in RORγt-deficient Th17 cells by co-deletion of T-bet. Variability within the data necessitates caution when drawing conclusions, however, should these results prove reproducible on further repeats, changes in IL-17A production upon RORγt and T-bet deletion raise the possibility that rather than the presence or absence of RORγt alone, it is the balance of ROR family TF and T-bet antagonism that determines Th17 cell fate and function. Importantly, these data leave open the possibility that RORγt deficiency, regardless of the presence or absence of T-bet, still results in an impairment in the amounts

of IL-17A and IFNγ Th17 and exTh17 cells are able to produce, as shown by reduced signal intensity in both RORγt single knockouts at RORγt/T-bet double knockouts.

Interestingly, even though IL-22 appeared to be regulated by the three TFs similarly to IL-17A, IL-17F production diminished to a greater extent in ROR family TF-deficient mice. This is in contrast to reports that IL-17F is less reliant on RORα expression than IL-17A is (X. O. Yang, B. P. Pappu, et al., 2008). The exact mechanism behind this observation is unclear but suggests that further TFs may have a role in supporting IL-17A and IL-22 expression. Furthermore, my results also pointed to an increase in the frequency of cells able to produce TNFα but a decrease in the amount of the cytokine produced in the absence of RORγt and RORα. These seemingly conflicting results raise the possibility that RORγt and RORα may contribute to the networks regulating TNFα through an unappreciated mechanism or that other TFs may also be involved.

RORγt and T-bet have been shown to be antagonistic in multiple settings. In certain mucosal Treg cells RORγt appears to be required for suppression of T-bet with loss of the Th17 cell master TF resulting in impaired Treg cell function (Bhaumik et al., 2021). Similarly, RORγt is required to restrain T-bet and type 1 function in certain mature ILC3 subsets (Fiancette et al., 2021). Moreover, a RORγt-T-bet antagonism was also observed in lymphoid tissue inducer (Lti) cells as RORγt deficiency-induced impairment in lymphoid tissue development was rescued on T-bet co-deletion (Stehle et al., 2021). The observed antagonism between the two TFs is clearly a fundamental aspect of the relationship between these two transcriptional programmes, regardless of the cell type. Nonetheless, given the differential effects TF deletion has on various ILC3 subsets, assessment of Th17 cell heterogeneity, with a focus on the outcomes of TF deletion in specific populations, would be of great interest. For example, it was reported that Lti-like ILC3 do not show a predisposition towards acquisition of an ILC1-like phenotype even upon RORγt deletion and can maintain normal IL-22, if not IL-17A, levels (Fiancette et al., 2021). Whether analogous Th17 cells exists is unclear but homeostatic small intestinal IL-17A^{+}IL-22^{+} Th17 cells induced by certain commensals have been shown to be stable over time with

no skewing towards a type 1 effector programme (Ivanov et al., 2009; Omenetti et al., 2019). Crucially, the studies reported here assessed only colonic cell populations the vast majority of which were generated in response to infection, possibly excluding key Th17 cell subsets. Assessment of whether such Th17 cells would maintain some type 3 function even in the absence of RORγt is of great interest. If observed, a similar phenomenon could also explain why type 3 and type 1 cytokines are lost in some but not all tdRFP$^+$ cells. Unbiased approaches, such as single cell RNA sequencing of Th17 cells generated in response to varied stimuli could greatly increase our understanding of Th17 cell transcriptional regulation. Importantly, Th17 cell function lost following deletion of both ROR family TFs was not recovered upon T-bet deletion suggesting that RORα is both sufficient and necessary for Th17 cell function when RORγt and T-bet are absent.

In summary, I have found that the balance of ROR family TFs and T-bet, rather than just their simple presence or absence, is the key determinant of Th17 and exTh17 cell function. In addition to directly supporting certain effector properties by activating gene transcription, these TFs also carry out their roles by limiting the functions of the other. This phenomenon has also been observed in other transcriptional networks and is likely true of most TFs as they function both by direct activation of gene transcription and antagonism of alternative genetic programmes (Shaw et al., 2016). The exact mechanisms mediating reciprocal antagonism between ROR family TFs and T-bet within Th17 cell populations are not known but T-bet is known to prevent Runx1-mediated *Rorc* transcription by directly binding this transcription factor (Lazarevic et al., 2011). It is possible that this interaction plays a role in the formation of fully mature IFNγ$^+$ exTh17 but unclear how it relates to intermediate stages of the Th17/exTh17 spectrum. Given the increase in T-bet expression in the absence of RORγt and RORα, these TFs may similarly mediate T-bet suppression.

On testing the need for T-bet in supporting Th1-like exTh17 cell function, I showed that while T-bet is not required for the generation of IFNγ$^+$ Th17 cells its deletion results in a block in IL-17A$^-$ exTh17 cell formation. Taken together, these data are consistent with reports that T-bet is dispensable for the

acquisition of a Th1 cell programme in Th17 cells (Duhen et al., 2013) but I further showed that it is needed for loss of IL-17A production and differentiation of fully mature exTh17 cell populations in response to *C.rodentium* infection. This observation, if widely applicable, may explain why other studies have still found a link between T-bet and Th17 cell-driven inflammatory diseases (Bending et al., 2009; Bettelli et al., 2004). A potential mechanism explaining these observations is that microenvironment-derived or cell-intrinsic signals induce IFNγ expression and T-bet upregulation. Above a threshold of T-bet expression it is possible that the antagonism between the two TFs would result in suppression of RORγt expression and a loss of type 3 function, allowing the formation of fully mature exTh17 cells. Importantly, recent work has shown that the requirement for T-bet in the formation of IFNγ^{+} Th17 cells is context specific (Brucklacher-Waldert et al., 2016) pointing to the involvement of further TFs not considered in this work.

In addition to impairing fully mature exTh17 cell differentiation, T-bet deficiency was also found to impact resistance to infection. Taken together, these data suggested that T-bet expression in Th17 cells (and other IL-17A producing cell populations) plays an important role in shaping the microbiota and thus influencing resistance to pathogen invasion. This observation prompted assessment of the functional consequences of Th17 and exTh17 cell perturbations. Strikingly, preliminary data assessing microbiome composition, along with the observed increased susceptibility to *C.rodentium*, suggested that T-bet-deficiency-driven dysbiosis may predispose mice to *C.rodentium* colonisation. SFB colonisation was previously reported to be protective against *C.rodentium* but it is not thought to drive expansion of Th17 cells that acquire Th1 cell-like properties (Ivanov et al., 2009; Omenetti et al., 2019). Data presented here are consistent with a role for alternative microbial species that require T-bet-driven functional adaptations in Th17 cells. However, given that I have observed no complete loss of type 1 function in Th17 and exTh17 cells on T-bet deletion it remains to be seen exactly what role T-bet plays in this process. The specific differences in microbiota composition in terms of functional outcomes, and how Th17 cell-expressed T-bet contributes to the maintenance of *H.ganmani* in the murine microbiota remains to be addressed. Moreover, I did not test whether the species present

across multiple mouse strains were phenotypically identical. It is possible that the microbes present in different intestinal microenvironments adapted differently resulting in fundamental phenotypic differences. Changes, such as carbohydrate use and vitamin synthesis may in turn have an impact on predisposition not only to infection but also intestinal inflammation and abnormal enterocyte proliferation (O'Keefe et al., 2009; Vernia et al., 1988). Crucially, my dataset contains the information necessary for testing potential differences but the sample size is currently limited. Expanding analyses to enable better assessment of all strains as well as sex- and cage-related effects would benefit future studies. Finally, despite the increased susceptibility to infection in all T-bet-deleting strains, impaired bacterial control was only evident in mice lacking all three TFs. This could either be explained by combined TF-deletion related defects in effector function or possibly general changes in cell fitness and population size. Studies that separate cytokine production from other TF-deletion effects are needed but likely require more sophisticated models.

Through assessment of post-developmental TF requirements, I have shown that manipulation of the antagonism between ROR family TFs and T-bet can enrich for specific stages of the Th17/exTh17 spectrum. Control mice are able to produce cells of all stages but cells were pushed towards an intermediate or even fully mature exTh17 cell phenotype by ROR family TF deletion. Conversely, exTh17 cell differentiation could be blocked by T-bet deletion. Finally, co-deletion of all three TFs may result in cells of a dysregulated phenotype, unable to produce either Th17- or Th1-like responses (Fig4.12). Crucially, it is yet to be established whether the observed differences are solely due to defects in cytokine production or overall effects on Th17 fitness. Although changes in the size of the tdRFP^{+} CD4 T cell population suggested that a disadvantage exists only in cells lacking all three TFs, future studies would benefit from detailed characterisation of this effect. Furthermore, no comprehensive analysis of Th17 cell populations present in the intestinal mucosa at steady state have been carried out. Nonetheless, these models have the potential to become greatly informative tools in identifying the molecular pathways regulating Th17 differentiation.

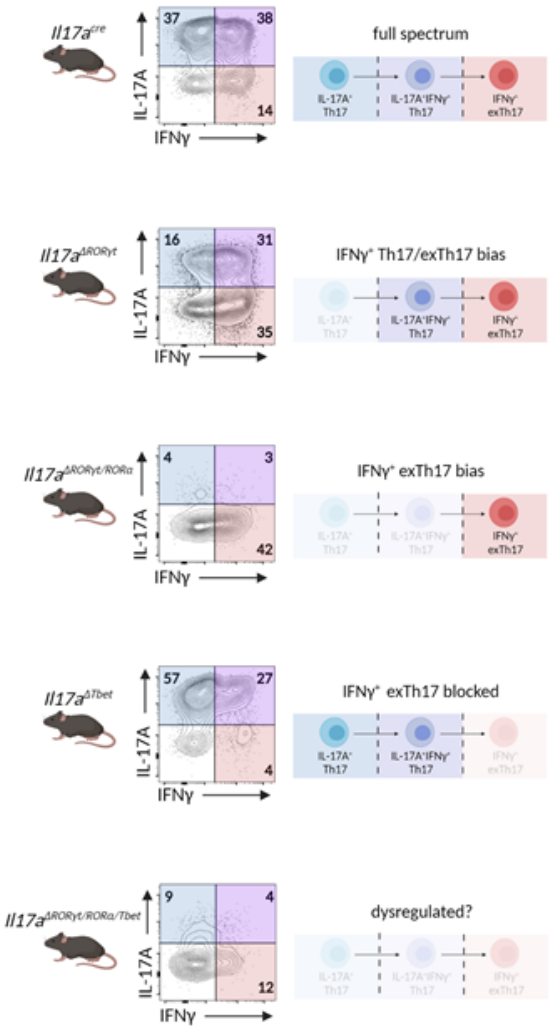
Il17a^cre
37
38
14
IL-17A
IFNγ
full spectrum
IL-17A+ Th17
IL-17A+IFNγ+ Th17
IFNγ+ exTh17
Il17a^ΔRORγt
16
31
35
IFNγ+ Th17/exTh17 bias
Il17a^ΔRORγt/RORα
4
3
42
IFNγ+ exTh17 bias
Il17a^ΔTbet
57
27
4
IFNγ+ exTh17 blocked
Il17a^ΔRORγt/RORα/Tbet
9
4
12
dysregulated?

Figure 4.12. Manipulating the antagonism between ROR family TFs and T-bet enriches for specific stages of the Th17/exTh17 spectrum

Schematic representation of how the mouse models generated to assess post-developmental RORγt/RORα/T-bet requirements enable assessment of stages of the exTh17 cell differentiation process.

In conclusion, I have established key experimental models that enable better assessment of Th1-like exTh17 cell differentiation. These mice will enable assessment of not only the cell-intrinsic changes in response to pathogen invasion but also alterations in the intestinal microenvironment and the effects these may have on intestinal inflammation.

CHAPTER 5: GENERATION OF CD4 T CELL MEMORY FOLLOWING *C.RODENTIUM* INFECTION

5.1 INTRODUCTION

The formation of immunological memory is a key output of adaptive immune responses. Memory T and B cells generated following primary infection or immunisation provide rapid responses and mediate long-term protection from secondary infection. CD4 T cells and their offspring, including memory cells, are crucial to appropriate adaptive immunity. Studies of CD4 T cell memory largely focused on systemic responses (Ciucci et al., 2019; Dileepan et al., 2011; Harrington et al., 2008; Pepper et al., 2011). Yet, natural infections arise predominantly through mucosal sites and become systemic only when mucosal control mechanisms fail. While it is well-established that the context within which CD4 T cells are activated shapes the resulting effector response (Mosmann et al., 1986), how diverse microenvironments feed into the formation of tissue- or response-specific CD4 T cell memory populations *in vivo* is poorly understood.

Memory T cells have been shown to emerge from effector (Teff) cells equipped to aid pathogen clearance and precursors that never go through a Teff cell phase (Amezcua Vesely et al., 2019; Bishu, Hou, et al., 2019; Pepper et al., 2010; Pepper et al., 2011). The memory T cell pool is divided into populations with distinct functions carried out at different anatomical locations. Central memory T (Tcm) cells are self-renewing cells that recirculate through 2LT (Pepper & Jenkins, 2011). Upon challenge they are thought to generate effector cells, Tfh cells and Tcm cells. Studies of the antigen-specific CD4 T cell response to *L.monocytogenes* demonstrated early bifurcation in the development of cells with a circulating phenotype from those that acquire the Th1 cell effector programme (Pepper et al., 2011). Whether this early divergence of Tcm and Teff cell fates is a universal feature of all CD4 T cell responses or applies only to systemic infection is unknown.

Unlike Tcm cells, effector memory T (Tem) cells arising from Teff cells are sequestered to non-lymphoid tissues where they produce effector cytokines in response to TCR ligation (Harrington et al., 2008). Long after the identification of circulating Tcm and Tem cell populations a further memory compartment was described. Tissue-resident memory T (Trm) cells are retained in peripheral organs, often at the site of infection, and function as crucial sentinels, reacting rapidly to pathogen re-encounter (Bartolome-Casado et al., 2019; Masopust et al., 2010). Despite their importance in protective tissue-specific immunity, little is known about CD4 Trm responses. In fact, most studies investigating Trm cells have focused on CD8 T cell biology (Schenkel & Masopust, 2014). Interestingly, recent work has shown that CD8 Trm cells have previously unappreciated stem-like roles in addition to providing rapid effector functions (Fonseca et al., 2020). Whether mucosal CD4 Trm contribute to systemic responses remains untested.

The work presented in this chapter aimed to develop and characterise key tools that enable tracking of an antigen-specific Th17-skewed CD4 T cell response so that the systemic and mucosal CD4 T cell populations formed following extracellular mucosal infections could be assessed.

5.2 A TRACTABLE MUCOSAL INFECTION MODEL

Seminal works from the Jenkins group provide some of the best data assessing the kinetics of the effector CD4 T cell response to pathogen (Pepper et al., 2010; Pepper et al., 2011). These studies elegantly showed that following early expansion, effector cell numbers contract and eventually just a small number of Tem remain. However, these data focused on systemic infections which fail to recapitulate key host-pathogen interactions at mucosal surfaces, the main sites of pathogen entry. While attempts to assess mucosal Th17 cell responses were made (Dileepan et al., 2011), natural mucosal pathogen-induced immune memory has proven harder to study. Tracking of cytokine production history, as described in previous chapters using *Il17a*^{cre}*Rosa26*^{tdRFP} mice, is not suitable for the study of the memory phase at late timepoints due to the expected contraction of the population. Moreover, the studies highlighted above reported that Tfh cells present in lymphoid tissues and Tcm

cells recirculating between the blood and lymphoid tissues branched early from the effector response (Pepper et al., 2011) and so may never report a signature effector cytokine. Therefore, fate mapping *Il17a* expression may fail to capture these cells. The study of these cells, that may be present at very low numbers, relies on the identification of CD4 T cells responding to pathogen-derived antigens. Historically, a lot of work on antigen-specific T cell responses relied on methods such as the use of TCR transgenic mice or adoptive transfer of TCR transgenic T cells into WT mice. While these studies have been highly informative, they may fail to capture a normal T cell response due to the limited TCR repertoire the high number of cells recognising the same antigen (Hataye et al., 2006). Identification of pathogen-derived peptides presented to and recognised by T cells enables the generation of p:MHC complexes (McSorley et al., 2000; Moon et al., 2007) and these have proven invaluable in the tracking of endogenous polyclonal T cell responses (Dileepan et al., 2011; Pepper et al., 2010; Pepper et al., 2011). Therefore, I sought to apply them to the study of CD4 T cell responses to mucosal *C.rodentium* infection. However, immunodominant *C.rodentium* antigenic epitopes have not yet been characterised. Therefore, *C.rodentium* was engineered to express a known peptide through a collaboration with Professor Gad Frankel. The modified *C.rodentium* strain expresses the highly immunogenic 2W1S variant of the I-E$\alpha_{52\text{-}68}$ chain (Rees et al., 1999; Rudensky et al., 1991) fused to the EspA translocator. 2W1S-specific CD4 T cells have been shown to be easily identifiable using 2W1S:I-A^b tetramers (Moon et al., 2007).

Following oral administration of *C.rodentium-2W1S* I sought to identify 2W1S-specific CD4 T cells in successfully colonised mice by combining 2W1S:I-A^b tetramers and flow cytometric analyses (Fig5.1a). Tetramer staining identified a distinct population of 2W1S-specific CD4 T cells present in the colonic lamina propria of colonised but not control mice (Fig5.1b). To account for the possibility of non-specific interactions sham peptide:I-A^b tetramer binding to CD4 T cells and 2W1S:I-A^b tetramer binding to MHCI-restricted CD8 T cells in colonised mice were assessed. The absence of a signal in either case confirmed binding through the TCR and recognition of the 2W1S:MHCII complex, rather than just part of the MHCII molecule (Fig5.1b).

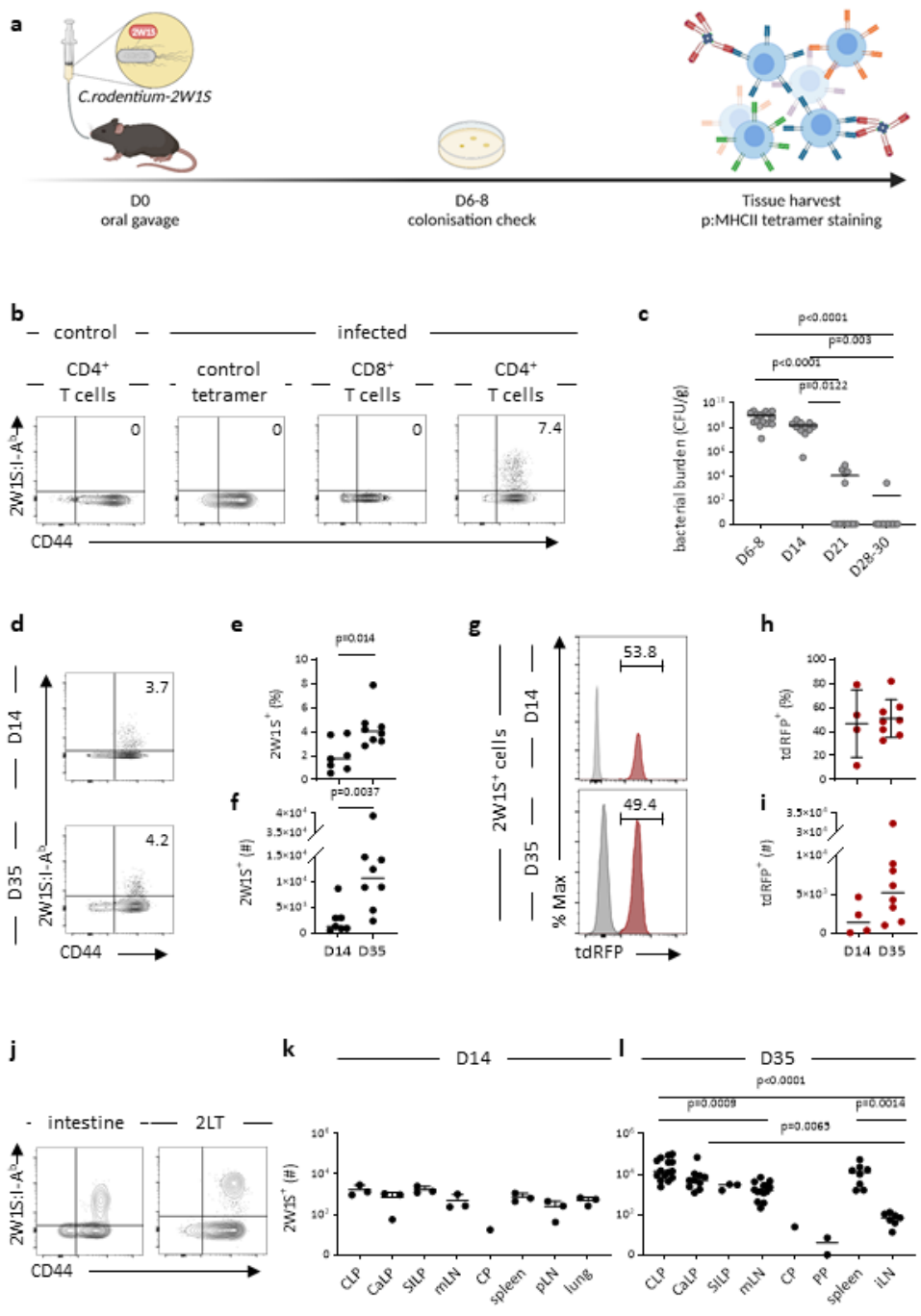
a
C.rodentium-2W1S
D0
oral gavage
D6-8
colonisation check
Tissue harvest
p:MHCII tetramer staining
b
control
infected
CD4+ T cells
control tetramer
CD8+ T cells
CD4+ T cells
2W1S:I-Ab
CD44
c
bacterial burden (CFU/g)
D6-8
D14
D21
D28-30
d
D14
D35
3.7
4.2
e
2W1S+ (%)
f
2W1S+ (#)
D14 D35
g
2W1S+ cells
53.8
49.4
% Max
tdRFP
h
tdRFP+ (%)
i
tdRFP+ (#)
j
intestine
2LT
k
D14
l
D35
CLP
CaLP
SILP
mLN
CP
spleen
pLN
lung
PP
iLN

Figure 5.1. *C.rodentium-2W1S* infection induces a tractable CD4 T cell response

C.rodentium-2W1S infection was used to enable assessment of an antigen-specific CD4 T cell population.

a) Schematic representation of experimental design. Mice were inoculated with *C.rodentium-2W1S* to enable p:MHCII tetramer-based identification of antigen-specific CD4 T cells in colonised mice.

b) Representative flow cytometry plots showing 2W1S:I-A^b tetramer staining on CLP CD4 T cells from control uncolonized mice and control or 2W1S:I-A^b tetramer staining on CLP CD4 and CD8 T cells from infected mice.

c) Quantification of faecal bacterial counts from mice colonised with WT *C.rodentium*. D6-8 n=17, data pooled from 3 independent experiments, D14 and D28-30 n=11, data pooled from 2 independent experiments and D21 n=14, data pooled from 2 independent experiments.

d) Representative flow cytometry plots gated on CLP CD4 T cells showing 2W1S:I-A^b tetramer and CD44 staining on D14 and D35 following *C.rodentium-2W1S* infection.

e-f) Quantification of the proportion (e) and total number (f) of antigen-specific (2W1S$^+$) CD4 T cells in the CLP of mice on D14 and D35 following *C.rodentium-2W1S* infection. D14 n=7, data pooled from 2 independent experiments and D35 n=8, data pooled from 3 independent experiments.

g) Representative histograms showing tdRFP expression in CLP 2W1S$^+$ CD4 T cells on D14 and D35 following *C.rodentium-2W1S* infection.

h-i) Quantification of the proportion (h) and total number (i) of tdRFP$^+$ 2W1S$^+$ CD4 T cells in the CLP of mice on D14 and D35 following *C.rodentium-2W1S* infection. D14 n=4, data from 1 experiment and D35 n=8, data pooled from 3 independent experiments.

j) Representative flow cytometry plots gated on intestinal and 2LT CD4 T cells showing 2W1S:I-A^b tetramer and CD44 staining following *C.rodentium-2W1S* infection

k) Quantification of the total number of 2W1S$^+$ CD4 T cells throughout the body on D14 following *C.rodentium-2W1S* infection. CLP, CaLP, SILP, mLN, spleen, pLN and lung n=3 and CP n=1 average of 3 pooled samples, all data from 1 experiment.

l) Quantification of the total number of 2W1S$^+$ CD4 T cells throughout the body on D35 following *C.rodentium-2W1S* infection. CLP n=15, data pooled from 6 independent experiments, CaLP n=10, data pooled from 5 independent experiments, SILP n=3, data from 1 experiment, mLN n=14, data pooled from 5 independent experiments, CP n=1 average of 3 pooled samples, data from 1 experiment, spleen n=8, data pooled from 4 independent experiments, PP n=2, data from 1 experiment and iLN n=7, data pooled from 3 independent experiments.

Values on flow cytometry plots and histograms represent percentages. Normality was tested using Shapiro-Wilk test. Lines on graphs show mean±SD (h), mean+SD (k) or median (c, e, f, i, l). Significance was tested using unpaired t test (h), Mann-Whitney U test (e, f, i), One-Way ANOVA (k) or Kruskal-Wallis test (c, l).

Having shown that I could reliably identify CD4 T cells responding to the infection I next sought to assess this population both during antigen presence and following its clearance. Tracking faecal bacterial load following infection of mice lacking any genetic defects revealed high bacterial burdens in the first 14 days of infection followed by gradual clearance between days 21 and 30 (Fig5.1c). This observation was consistent with published literature showing that bacteria are first expelled from the mucosa by the immune system and then slowly cleared from the colonic lumen by the interplay of the immune system and commensal microbes of the normal flora (Bishu, Hou, et al., 2019; Kamada et al., 2012; Kamada et al., 2015). Given that T cell responses to *C.rodentium* are reported to take up to 14 days to develop (Atarashi et al., 2015; Basu et al., 2012; Bishu, Hou, et al., 2019) I elected to study the antigen-specific CD4 T cell compartment on days 14, near the peak of faecal bacterial load but at the beginning of the adaptive response, and on day 35 when most mice are expected to have resolved the infection. Surprisingly, assessment of the colonic 2W1S-specific CD4 T cell population (Fig5.1d) revealed a small but statistically significant increase, rather than contraction, in both the proportion and number of these cells (Fig5.1e-f).

Having established that the modified infection model enabled specific tracking of CD4 T cells induced by *C.rodentium* infection, I turned to *Il17a*^{cre}*Rosa26*^{tdRFP} mice to enable *Il17a* expression history to be assessed. Surprisingly, at either timepoint only an average of half of the responding colonic cells had a history of IL-17A production (Fig5.1g-i). This observation clearly illustrates the need for expanding *Il17a* fate mapping-based approaches when assessing the total CD4 T cell response to this pathogen. The tdRFP^{-} CD4 T cells population likely included a mix of effector cells that did not make IL-17A (such as Th1 cells) and those where Cre-mediated recombination was defective. Furthermore, non-effector CD4 T cells may also be present in the colon.

Th17 effector cells are expected to home to and be retained in the intestine. However, the presence of mucosal 2W1S-specific CD4 T cells that lacked *Il17a* expression history suggested that the *C.rodentium-2W1S* model enabled tracking of multiple cell types. The emergence of non-effector CD4

T cells has not been well-described Th17-skewed responses, especially within the intestinal mucosa. Therefore, analyses were expanded to include further mucosal and lymphoid tissues. These studies aimed to begin to capture the distribution of different *C.rodentium*-induced CD4 T cell populations (Fig5.1j). Given the anticipated low frequency of antigen-specific cells I elected to perform 2W1S:I-A^b tetramer-based magnetic bead enrichment on SILP, mLN, spleen, pooled peripheral lymph nodes (pLN) and lungs. Furthermore, due to their minimal total cellularity caecal patches (CP) were pooled from multiple mice with the average number of 2W1S-specific CD4 T cells reported here. Quantification of 2W1S-specific cells revealed that *C.rodentium*-induced CD4 T cells were distributed throughout the body as early as day 14 and remained so at day 35 of the infection (Fig5.1k-l). Although the day 14 data are limited, these analyses suggested that *C.rodentium*-induced antigen-specific cells were most abundant in the intestinal mucosa followed by the intestinal draining mLN, and the spleen. 2W1S-specific CD4 T cells were detected in both the CP and small intestinal Peyer's patches (PP) albeit in numbers too low to enable further analyses. The inguinal lymph nodes (iLN) and pLN (comprising iLN, brachial (b)LN and axillary (a)LN) were also found to harbour smaller numbers of antigen-specific cells. Assessment of the total pLN was preferable due to larger numbers of cells enabling better analysis but technical limitations prevented bLN and aLN from being harvested along with iLN at the late day 35 timepoint. Assessing potential trafficking to distinct mucosal sites identified approximately 500 2W1S-specific CD4 T cells in the lungs of infected mice as early as day 14 of the infection. However, as *C.rodentium-2W1S* is excreted in faeces it is possible that it could enter the respiratory tract and thus explain the presence of these antigen-specific CD4 T cells. Given the absence of testing for a role this route of infection could play, his site was excluded from further analyses. Taken together, these data provide the first description of the breadth of the CD4 T cell response to a natural mouse pathogen that colonises the intestinal tract and capture the dissemination of antigen-specific cells while showing heterogeneity in their cytokine expression history.

5.2.1 Early divergence of effector Th17 and Tcm cell fates

Having established that the *C.rodentium-2W1S* model generates a tractable CD4 T cell response, I next sought to understand the nature of the different CD4 T cell populations induced by the infection. Studies focusing on Th1 cell responses identified at least two populations – Tcm and effector cells producing IFNγ – and showed that these were generated from different precursors following systemic infection (Pepper et al., 2011). Whether such a relationship between effector and recirculating cells is a hallmark of all CD4 T cell responses or is restricted to Th1-skewed infections has not been tested experimentally *in vivo*. Therefore, the *C.rodentium-2W1S* infection model and *Il17a*^{cre}*Rosa26*^{tdRFP} IL-17A fate mapper mice were combined again and *Il17a* expression history used as an indicator of commitment to a Th17 state. Tcm cell precursors were reported to express the TF Bcl6 and chemokine receptor CXCR5 (Pepper et al., 2011). Therefore, these markers were targeted in the *C.rodentium-2W1S* infection mode. However, commercially available antibodies did not provide appropriate staining in this experimental model. Therefore, an alternative way of identifying these cells was sought. The surface molecule CD62L is required for entry into lymphoid tissues (Cyster, 2005). In the absence of optimal CXCR5 and Bcl6 detection this marker was used as an indicator of a circulating phenotype. Testing for CD62L on 2W1S^{+}CD44^{hi} CD4 T cells combined with tdRFP enabled assessment of the relationship between the effector and Tcm cell arms of the response to *C.rodentium*. Analysis of these two markers early in the response (Fig5.2a) indicated that cells with a history of IL-17A expression were enriched in the intestine, although these data are not sufficiently powered to show statistical significance (Fig5.2b). Conversely, CD62L^{+} antigen-specific cells were only present in 2LT with pLN harbouring the highest proportion (Fig5.2c). Thus, early CD62L and tdRFP expression matched effector and migratory functions. Following bacterial clearance, the large proportion of tdRFP^{+} infection-induced CD4 T cells was maintained in the intestinal mucosa but also showed some evidence of increase in the lymphoid tissues assessed (Fig5.2d-e). As expected, CD62L expression remained restricted to 2W1S-specific CD4 T cells present in lymphoid tissues and was most enriched on iLN 2W1S-specific CD4 T cells (Fig5.2f). Taken together, the day 14 data raised the possibility that,

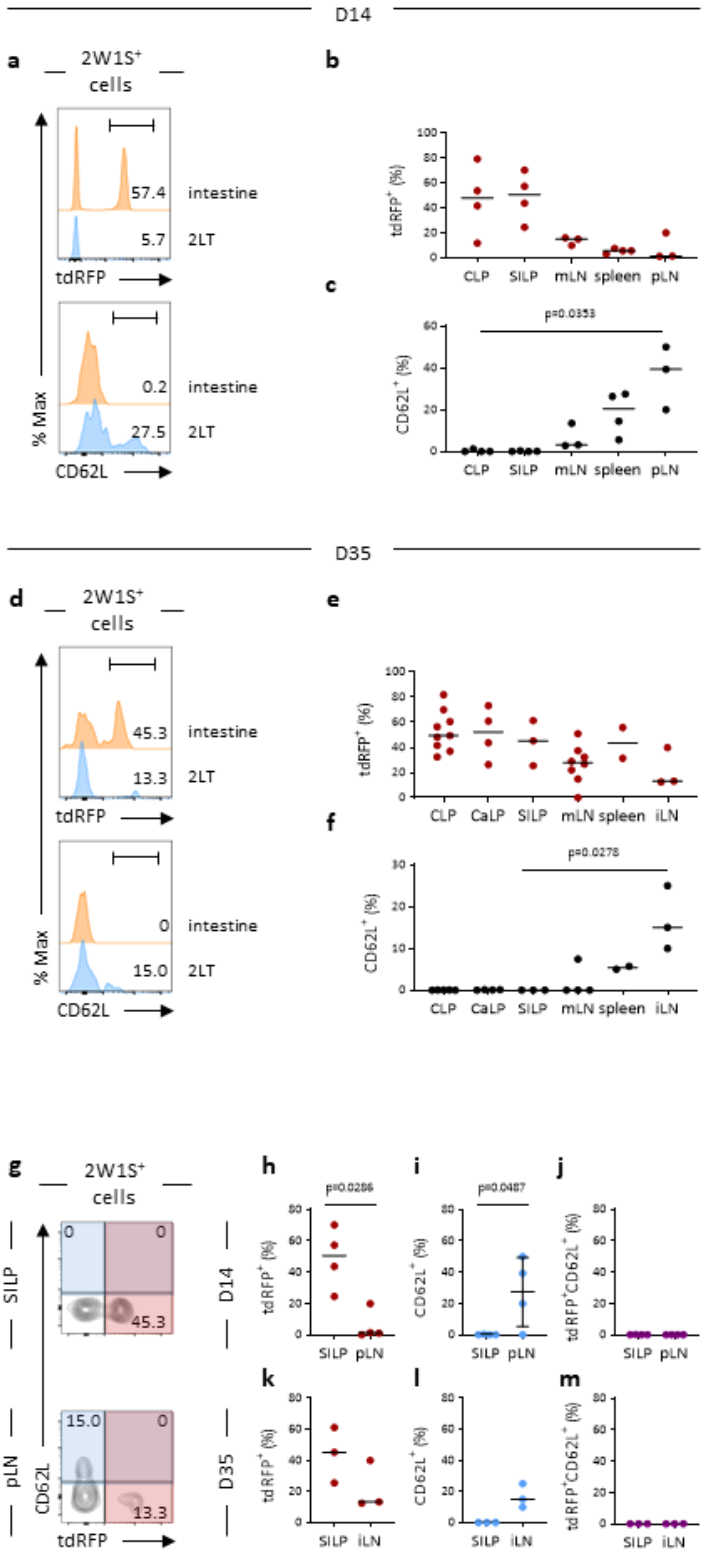
D14
a
2W1S+ cells
57.4
intestine
5.7
2LT
tdRFP
0.2
intestine
27.5
2LT
% Max
CD62L
b
tdRFP+ (%)
CLP SILP mLN spleen pLN
c
p=0.0353
CD62L+ (%)
CLP SILP mLN spleen pLN
D35
d
2W1S+ cells
45.3
intestine
13.3
2LT
tdRFP
0
intestine
15.0
2LT
% Max
CD62L
e
tdRFP+ (%)
CLP CaLP SILP mLN spleen iLN
f
p=0.0278
CD62L+ (%)
CLP CaLP SILP mLN spleen iLN
g
2W1S+ cells
SILP
pLN
D14
D35
0
0
45.3
15.0
0
13.3
CD62L
tdRFP
h
p=0.0286
tdRFP+ (%)
SILP pLN
i
p=0.0487
CD62L+ (%)
SILP pLN
j
tdRFP+CD62L+ (%)
SILP pLN
k
tdRFP+ (%)
SILP iLN
l
CD62L+ (%)
SILP iLN
m
tdRFP+CD62L+ (%)
SILP iLN

Figure 5.2. *C.rodentium* infection results in early divergence of effector and recirculating Tcm-like CD4 T cell fates

The relationship between cytokine production history and CD62L expression was assessed in the 2W1S$^+$ CD4 T cell pool.

a) Representative histograms gated on 2W1S$^+$ CD4 T cells showing tdRFP and CD62L expression in the intestine and 2LT of *Il17a^{cre}Rosa26^{tdRFP}* mice on D14 following *C.rodentium-2W1S* infection.

b-c) Quantification of the proportion of tdRFP$^+$ (b) and CD62L$^+$ (c) 2W1S$^+$ CD4 T cells throughout the body of *Il17a^{cre}Rosa26^{tdRFP}* mice on D14 following *C.rodentium-2W1S* infection. CLP, SILP and spleen n=4, mLN and pLN n=3, data from 1 experiment.

d) Representative histograms gated on 2W1S$^+$ CD4 T cells showing tdRFP and CD62L expression in the intestine and 2LT of *Il17a^{cre}Rosa26^{tdRFP}* mice on D35 following *C.rodentium-2W1S* infection.

e-f) Quantification of the proportion of tdRFP$^+$ (e) and CD62L$^+$ (f) 2W1S$^+$ CD4 T cells throughout the body of *Il17a^{cre}Rosa26^{tdRFP}* mice on D14 following *C.rodentium-2W1S* infection. CLP tdRFP n=9, data pooled from 4 independent experiments, CLP CD62L n=5, data pooled from 3 independent experiments, CaLP n=4, data pooled from 2 independent experiments, SILP and iLN n=3, data from 1 experiments, mLN tdRFP n=8, data pooled from 3 independent experiments, mLN CD62L n=4, data pooled from 2 independent experiment and spleen n=2, data pooled from 2 independent experiments.

g) Representative flow cytometry plots showing tdRFP and CD62L staining in SILP and pLN 2W1S$^+$ CD4 T cells of *Il17a^{cre}Rosa26^{tdRFP}* mice following *C.rodentium-2W1S* infection.

h-j) Quantification of the proportion of tdRFP$^+$ (h), CD62L$^+$ (i) or tdRFP$^+$CD62L$^+$ (j) 2W1S$^+$ CD4 T cells in the SILP and pLN of *Il17a^{cre}Rosa26^{tdRFP}* mice on D14 following *C.rodentium-2W1S* infection. n=4, all data from 1 experiment.

k-m) Quantification of the proportion of tdRFP$^+$ (k), CD62L$^+$ (l) or tdRFP$^+$CD62L$^+$ (m) 2W1S$^+$ CD4 T cells in the SILP and iLN of *Il17a^{cre}Rosa26^{tdRFP}* mice on D35 following *C.rodentium-2W1S* infection. n=5, all data from 1 experiment.

Values on histograms and flow cytometry plots represent percentages. Lines on graphs show mean±SD (i) or median (b, c, e, f, h, j, k, l, m). Significance was tested using unpaired t test (i), Mann-Whitney U test (h, j, k, l, m), or Kruskal-Wallis test (b, c, e, f).

much like in the case of systemic Th1 cell responses, at least two functionally distinct populations were generated early in the response to a mucosal pathogen. However, the potential increase of tdRFP$^+$ cells in 2LT observed at day 35 left open the possibility of cells with a history of IL-17A production entering the recirculating Tcm cell pool. Therefore, the relationship between the two markers was also tested (Fig5.2g). Regardless of the timepoint assessed, tdRFP$^+$ cells were most abundant in the intestine and CD62L$^+$ cells in the 2LT. However, at no time were there cells co-expressing the two markers (Fig5.2h-m).

5.2.2 *C.rodentium* infection induced Trm cell generation

Unlike Tcm cells, Trm cells are thought to arise from the local persistence of effector cells. This population is sequestered in organs where they form self-renewing memory T cell pool that is an important part of the immune system. Despite their relevance to long-term protection against pathogens and involvement in autoimmune disorders (Bishu, El Zaatari, et al., 2019; Christensen et al., 2017; Krebs et al., 2020), comparatively little is known about Trm cells induced by extracellular mucosal infections. In fact, the majority of our understanding of Trm cell biology relies on studies of CD8 T cells. The tissue resident phenotype of these cells is often, although not always, associated with expression of the markers CD69 and CD103 (Kok et al., 2021). The limited literature focusing on mucosal Th17 cell-derived Trm identified CD69 but not CD103 as a CD4 tissue retention marker (Amezcua Vesely et al., 2019; Bishu, Hou, et al., 2019), likely reflecting the different anatomical spaces occupied by CD8 and CD4 T cells – CD103 binds E-cadherin expressed on epithelial cells, directing entry into the intraepithelial layer from the lamina propria (Karecla et al., 1995; Kilshaw & Baker, 1988), where the majority of CD8 but not CD4 T cells reside in mice. Nonetheless, both CD4 and CD8 T cells expressing CD103 have been found in the lamina propria (Bartolome-Casado et al., 2019; Braun et al., 2015). Therefore, the expression of both CD69 and CD103 was tested in the antigen-specific CD4 T cell pool on day 35 of *C.rodentium* infection (Fig5.3a). The vast majority of intestinal but not 2LT 2W1S-specific CD4 T cells were found to express CD69 (Fig5.2b-c). Conversely, even though some expression

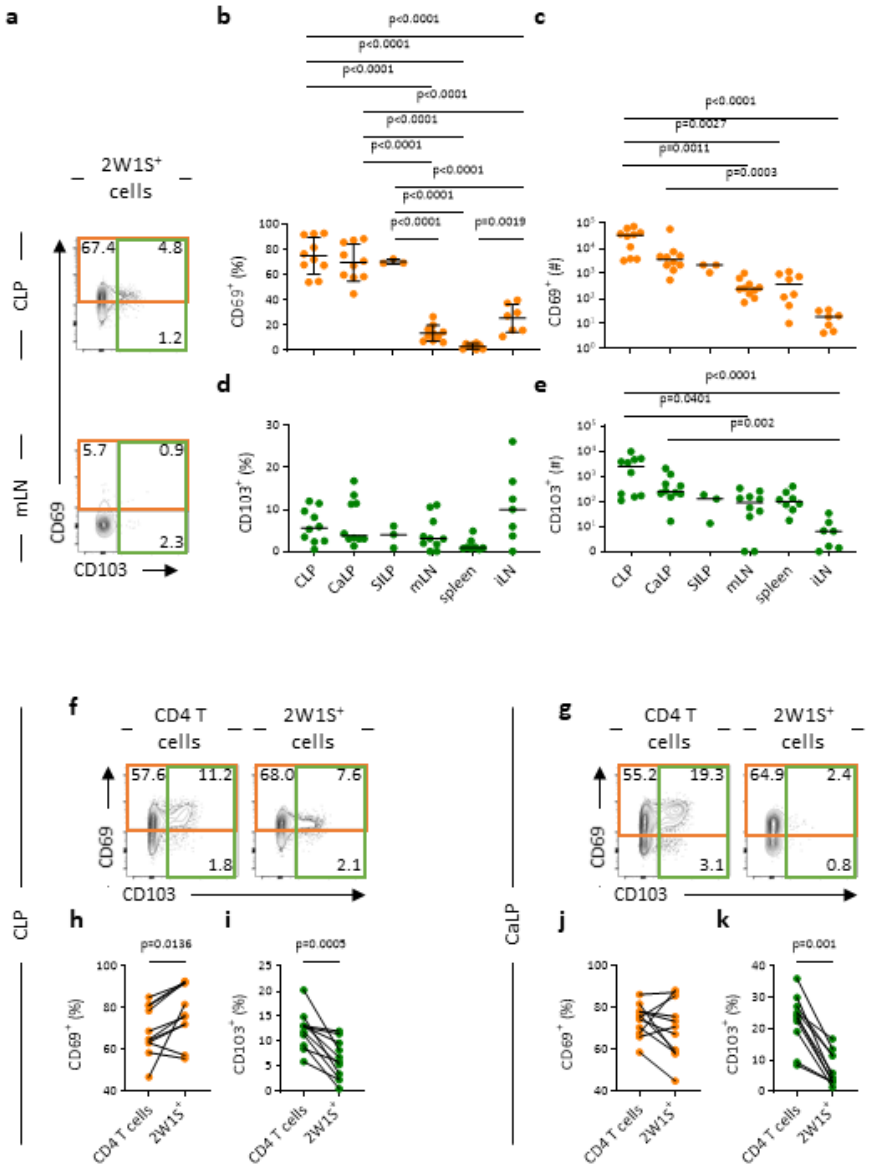
a
b
c
2W1S+ cells
CLP
mLN
67.4
4.8
1.2
5.7
0.9
2.3
CD69
CD103
p<0.0001
p<0.0001
p<0.0001
p<0.0001
p<0.0001
p<0.0001
p<0.0001
p<0.0001
p<0.0001
p=0.0019
CD69+ (%)
p<0.0001
p=0.0017
p=0.0011
p=0.0003
CD69+ (#)
d
e
CD103+ (%)
p<0.0001
p=0.0401
p=0.002
CD103+ (#)
CLP
CaLP
SILP
mLN
spleen
iLN
f
g
CD4 T cells
2W1S+ cells
57.6
11.2
1.8
68.0
7.6
2.1
55.2
19.3
3.1
64.9
2.4
0.8
h
i
j
k
p=0.0136
p=0.0005
p=0.001
CD4 T cells
2W1S+

Figure 5.3. Residency markers are enriched on intestinal 2W1S$^+$ CD4 T cells following *C.rodentium* infection

The expression of putative residency markers CD69 and CD103 was assessed on 2W1S$^+$ CD4 T cells on D35 following infection.

a) Representative flow cytometry plots gated on 2W1S$^+$ CD4 T cells showing CD69 and CD103 staining in CLP and mLN on D35 following *C.rodentium-2W1S* infection.

b-e) Quantification of the proportion and total number of CD69$^+$ (b-c) and CD103$^+$ (d-e) 2W1S$^+$ CD4 T cells throughout the body on D35 following *C.rodentium-2W1S* infection. CLP, CaLP and mLN n=10, data pooled from 5 independent experiments, SILP n=3, data from 1 experiment, spleen n=8, data pooled from 5 independent experiments and iLN n=7, data pooled from 3 independent experiments.

f-g) Representative flow cytometry plots showing CD69 and CD103 expression in the total CLP (f) and CaLP (g) CD4 T cell pool and 2W1S$^+$ CD4 T cells on D35 following *C.rodentium-2W1S* infection.

h-i) Comparison of the proportion of CD69$^+$ (h) and CD103$^+$ (i) cells within the total CLP CD4 T cell pool and 2W1S$^+$ CD4 T cells on D35 following *C.rodentium-2W1S* infection. n=11, data pooled from 3 independent experiments.

j-k) Comparison of the proportion of CD69$^+$ (j) and CD103$^+$ (k) cells within the total CaLP CD4 T cell pool and 2W1S$^+$ CD4 T cells on D35 following *C.rodentium-2W1S* infection. n=11, data pooled from 3 independent experiments.

Values on flow cytometry plots represent percentages. Normality was tested using Shapiro-Wilk test. Lines on graphs show mean±SD (b), median (c, d, e) or pairwise comparisons (h, i, j, k). Significance was tested using One-Way ANOVA (b), Kruskal-Wallis test (c, d, e), paired t test (h, i, j) or Wilcoxon matched pairs test (k).

of CD103 was evident, this was minimal and only differed between mucosal sites and 2LT due to the different sizes of the 2W1S-specific populations here (Fig5.3d-e). Lack of enrichment of CD103 on intestinal CD4 T cells following infection is in line with reports suggesting that this marker is not expressed on Trm cells induced by extracellular mucosal infections (Amezcua Vesely et al., 2019; Bishu, Hou, et al., 2019). Interestingly, however, 5-15% of mucosal antigen-specific CD4 T cells did express low levels of CD103 raising questions over the potential function of these cells. Due to the low frequency and number of $CD69^+$ 2W1S-specific cells in the 2LT further analyses of *C.rodentium*-induced Trm cells focused on the intestinal mucosa.

To test whether expression of residency markers was enriched on 2W1S-specific cells likely present in the mucosa for several weeks compared to the total CD4 T cell pool, the proportion of $CD69^+$ and $CD103^+$ cells was contrasted in the two populations (Fig5.3f-g). $CD69^+$ cells were found to be enriched in the 2W1S-specific CD4 T cell population compared to the total CD4 T cell pool in the colon (Fig5.3h). Conversely, $CD103^+$ cells were present at a lower frequency (Fig5.3i). Interestingly, the same pattern of CD103 but not CD69 expression was observed in the caecum (Fig5.3j-k). Such analyses were not possible in the small intestine due to the need for 2W1S-specific cell enrichment.

The high frequency of intestinal $CD69^+$ 2W1S-specific CD4 T cells is consistent with the generation of *C.rodentium*-induced Trm. Cells of a Th17 cell origin responding to extracellular pathogens have been shown to enter the memory pool and be retained at the mucosal surface (Amezcua Vesely et al., 2019; Bishu, Hou, et al., 2019). However, the contribution of other effector CD4 T cell populations is unclear. Therefore, the infection model was again combined with $Il17a^{cre}Rosa26^{tdRFP}$ mice, enabling assessment of whether Th17 and exTh17 cells gave rise to *C.rodentium*-induced Trm cells more efficiently. Surprisingly, testing tdRFP expression in the total 2W1S-specific CD4 T cell pool and comparing this to that in $CD69^+$ and $CD103^+$ 2W1S-specific cells (Fig5.4a) revealed no evidence of an enrichment of Th17-derived cells in the populations expressing putative residency markers (Fig5.4b-d). Similarly, when testing whether CD69 or CD103 expression was enriched in $tdRFP^+$ 2W1S-specific cells compared to

the total antigen-specific pool (Fig5.4e), I observed no such effects (Fig5.4f-k). A possible explanation of these data is that by day 35 of the infection all mucosal 2W1S-specific CD4 T cells were derived from effector but not necessarily from Th17 cells. To test this, the relationship between residency marker expression and Th1- and Th17 cell-associated cytokine production, following *ex vivo* restimulation, was studied. Cytokine expression in the total antigen-specific and $CD69^+$ or $CD103^+$ populations (Fig5.5a) pointed to no clear differences (Fig5.5b-g). Comparing cells producing IL-17A or IFNγ to the total 2W1S-specific CD4 T cell pool also failed to identify any differences in CD69 or CD103 expression (Fig5.5h-n). Taken together, these results suggested that expression of either IL-17A or IFNγ is not linked to residency marker expression on CD4 T cells induced by *C.rodentium* infection.

5.3 PERTURBATIONS OF THE TH17/EXTH17 CONTINUUM AND CD4 T CELL MEMORY

As previously described, intestinal pathogen induced Th17 cells show a high degree of plasticity and adopt a spectrum of Th1 cell-like characteristics (Hirota et al., 2011; Lee et al., 2009; Omenetti et al., 2019). Trm cells with mixed Th17/Th1 cell characteristics have been described and have roles in both health and disease. Stable IL-$17A^+IFN\gamma^+$ CD4 Trm cell populations are linked to autoimmune pathology (Bishu, El Zaatari, et al., 2019). Recent work focusing on a respiratory Th17-skewed infection identified mucosal CD4 Trm cells with the capacity to produce not only Th17- but also Th1 cell-associated cytokines, albeit at a lower frequency (Amezcua Vesely et al., 2019). Together, these observations raise the possibility that Trm cells may arise from different stages of the Th17/exTh17 spectrum. However, this has not been specifically assessed *in vivo*. Furthermore, whether Trm cells developing from distinct Th17 and exTh17 cell populations are phenotypically different is untested. Therefore, I combined the conditional TF knockout mice described in Chapter 4 with the *C.rodnetium-2W1S* infection model. This approach takes advantage of the ability to lock effector cells into better-defined stages of the Th17/exTh17 spectrum (Fig4.12) while enabling long-term tracking of responding CD4 T cells. Together, these models provide a powerful tool for dissecting extracellular mucosal infection-driven Trm cell differentiation, function and relationship to the Tcm cell response. The system is

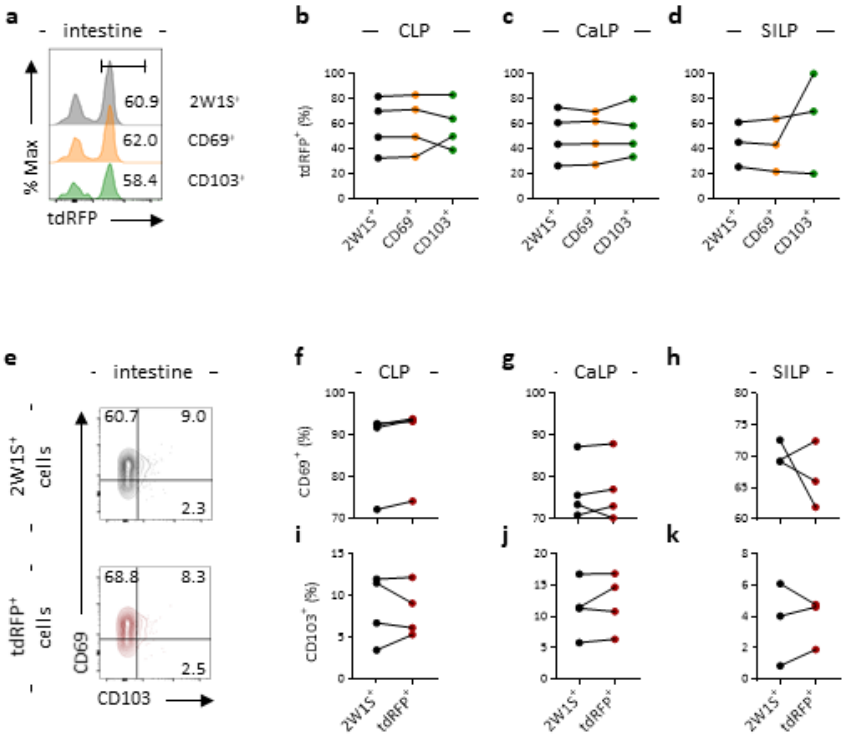
a
intestine
60.9
62.0
58.4
2W1S+
CD69+
CD103+
% Max
tdRFP
b
CLP
c
CaLP
d
SILP
tdRFP+ (%)
2W1S+
CD69+
CD103+
e
intestine
2W1S+ cells
tdRFP+ cells
60.7
9.0
2.3
68.8
8.3
2.5
CD69
CD103
f
CLP
g
CaLP
h
SILP
CD69+ (%)
i
j
k
CD103+ (%)
2W1S+
tdRFP+

Figure 5.4. Residency markers are not enriched on intestinal tdRFP$^+$ 2W1S$^+$ CD4 T cells following *C.rodentium* infection

The expression of putative residency markers CD69 and CD103 was assessed on tdRFP$^+$ 2W1S$^+$ CD4 T cells on D35 following infection.

a) Representative histograms showing tdRFP expression in intestinal 2W1S$^+$ CD4 T cells and CD69$^+$ or CD103$^+$ 2W1S$^+$ CD4 T cells on D35 following *C.rodentium-2W1S* infection.

b-d) Comparison of the proportion of tdRFP$^+$ cells within the total 2W1S$^+$ CD4 T cell population and CD69$^+$ or CD103$^+$ 2W1S$^+$ CD4 T cells in the CLP (b), CaLP (c) or SILP (d) on D35 following *C.rodentium-2W1S* infection. CLP and CaLP n=4, data pooled from 2 independent experiments and SILP n=3, data from 1 experiment.

e) Representative flow cytometry plots showing CD69 and CD103 expression in the total intestinal 2W1S$^+$ CD4 T cell pool and tdRFP$^+$ 2W1S$^+$ CD4 T cells on D35 following *C.rodentium-2W1S* infection.

f-h) Comparison of the proportion of CD69$^+$ cells within the total 2W1S$^+$ CD4 T cell pool and tdRFP$^+$ 2W1S$^+$ CD4 T cells in the CLP (f), CaLP (g) and SILP (h) on D35 following *C.rodentium-2W1S* infection. CLP and CaLP n=4, data pooled from 2 independent experiments and SILP n=3, data from 1 experiment.

i-k) Comparison of the proportion of CD103$^+$ cells within the total 2W1S$^+$ CD4 T cell pool and tdRFP$^+$ 2W1S$^+$ CD4 T cells in the CLP (i), CaLP (j) and SILP (k) on D35 following *C.rodentium-2W1S* infection. CLP and CaLP n=4, data pooled from 2 independent experiments and SILP n=3, data from 1 experiment.

Values on histograms and flow cytometry plots represent percentages. Normality was tested using Shapiro-Wilk test. Lines on graphs show pairwise comparisons. Significance was tested using Repeated Measures One-Way ANOVA (b, c, d), paired t test (g, h, i, j, k) or Wilcoxon matched pairs test (f).

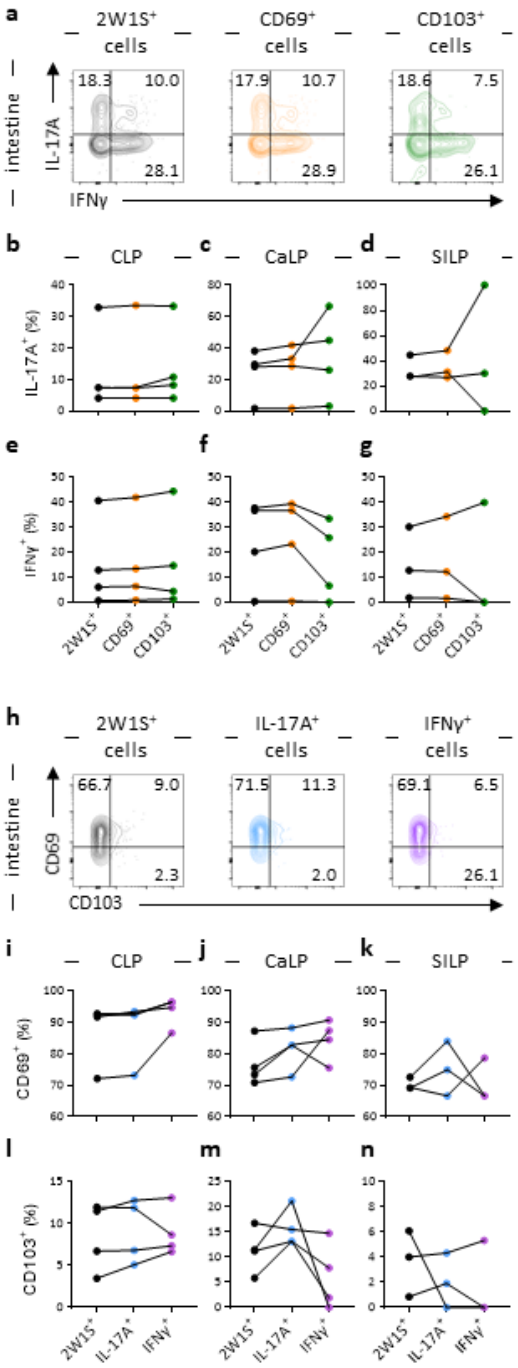
a
2W1S+ cells
CD69+ cells
CD103+ cells
intestine
IL-17A
IFNγ
18.3
10.0
28.1
17.9
10.7
28.9
18.6
7.5
26.1
b
CLP
c
CaLP
d
SILP
IL-17A+ (%)
e
f
g
IFNγ+ (%)
2W1S+
CD69+
CD103+
h
2W1S+ cells
IL-17A+ cells
IFNγ+ cells
intestine
CD69
CD103
66.7
9.0
2.3
71.5
11.3
2.0
69.1
6.5
26.1
i
CLP
j
CaLP
k
SILP
CD69+ (%)
l
m
n
CD103+ (%)
2W1S+
IL-17A+
IFNγ+

Figure 5.5. Residency markers are not enriched on intestinal cytokine producing 2W1S$^+$ CD4 T cells following *C.rodentium* infection

The expression of putative residency markers CD69 and CD103 was assessed on IL-17A$^+$ and IFNγ$^+$ 2W1S$^+$ CD4 T cells on D35 following infection.

a) Representative flow cytometry plots showing IL-17A and IFNγ expression following *ex vivo* restimulation with PMA and ionomycin in intestinal 2W1S$^+$ CD4 T cells and CD69$^+$ or CD103$^+$ 2W1S$^+$ CD4 T cells on D35 following *C.rodentium-2W1S* infection.

b-d) Comparison of the proportion of IL-17A$^+$ cells within the total 2W1S$^+$ CD4 T cell population and CD69$^+$ or CD103$^+$ 2W1S$^+$ CD4 T cells in the CLP (b), CaLP (c) or SILP (d) on D35 following *C.rodentium-2W1S* infection. CLP and CaLP n=4, data pooled from 2 independent experiments and SILP n=3, data from 1 experiment.

e-g) Comparison of the proportion of IFNγ$^+$ cells within the total 2W1S$^+$ CD4 T cell population and CD69$^+$ or CD103$^+$ 2W1S$^+$ CD4 T cells in the CLP (e), CaLP (f) or SILP (g) on D35 following *C.rodentium-2W1S* infection. CLP and CaLP n=4, data pooled from 2 independent experiments and SILP n=3, data from 1 experiment.

h) Representative flow cytometry plots showing CD69 and CD103 expression in the total intestinal 2W1S$^+$ CD4 T cell pool and IL-17A$^+$ or IFNγ$^+$ 2W1S$^+$ CD4 T cells on D35 following *C.rodentium-2W1S* infection.

i-k) Comparison of the proportion of CD69$^+$ cells within the total 2W1S$^+$ CD4 T cell pool and IL-17A$^+$ or IFNγ$^+$ 2W1S$^+$ CD4 T cells in the CLP (i), CaLP (j) and SILP (k) on D35 following *C.rodentium-2W1S* infection. CLP and CaLP n=4, data pooled from 2 independent experiments and SILP n=3, data from 1 experiment.

l-n) Comparison of the proportion of CD103$^+$ cells within the total 2W1S$^+$ CD4 T cell pool and IL-17A$^+$ or IFNγ$^+$ 2W1S$^+$ CD4 T cells in the CLP (l), CaLP (m) and SILP (n) on D35 following *C.rodentium-2W1S* infection. CLP and CaLP n=4, data pooled from 2 independent experiments and SILP n=3, data from 1 experiment.

Values on flow cytometry plots represent percentages. Normality was tested using Shapiro-Wilk test. Lines on graphs show pairwise comparisons. Significance was tested using Repeated Measures One-Way ANOVA (c, d, e, f, j, l, m) or Friedman test (b, g, i, k, n).

currently incompletely characterised, however, preliminary observations and potential interpretations are reported below.

Assessment initially focused on strain-specific differences on the late day 35 timepoint in control IL-17A fate mapper mice, *Il17a*$^{\Delta ROR\gamma t/ROR\alpha}$ mice within which Th17 cells are pushed towards a 'fully mature' IFNγ^{+} exTh17 cell state, *Il17a*$^{\Delta T\text{-}bet}$ mice that block Th17 cells at the 'intermediate' IL-17A^{+}IFNγ^{+} Th17 cell state, and *Il17a*$^{\Delta ROR\gamma t/ROR\alpha/T\text{-}bet}$ animals that contain none of the identified Th17-exTh17 cell stages, respectively (Fig5.6a). Testing the size of the antigen-specific population within intestinal and lymphoid tissues pointed to a potential defect in the colonic population in *Il17a*$^{\Delta T\text{-}bet}$ animals (Fig5.6b-g). These data raised the possibility that differences in the responses to the pathogen reflected different survival or retention of Teff cells within the colon. However, the proportion of antigen-specific CD4 T cells showing a history of IL-17A production showed no clear strain-specific differences in any of the tissues analysed (Fig5.6h-n), consistent with normal *C.rodentium*-induced Th17 cell survival up to day 35 of the infection even in the absence of key TFs.

Having established that early Tcm cells arising from *C.rodentium* infection developed independently of Th17 cells, no gross changes in the recirculating CD62L^{+} 2W1S^{+} CD4 T cell pool were anticipated following TF deletion. However, given that later in the infection cells with a history of cytokine expression were disseminated in lymphoid tissue, I elected to test whether key TF deletion impacted the circulating Tcm cell pool. Therefore, CD62L expression was assessed in conjunction with IL-17A production history (tdRFP). Cells co-expressing CD62L and tdRFP were not observed in any of the tested mouse strains (Fig5.7a), possibly suggesting that TF deletion did not disrupt the divergence of Tcm and Teff cell fates. Preliminary data suggested that mice lacking ROR family TFs but not T-bet in established Th17 cells contained no recirculating antigen-specific CD4 T cells within the mLN (Fig5.7b-c). Conversely, 2W1S^{+} CD44^{hi} CD4 T cells harvested from the iLN of the TF-deficient mice appeared to harbour a higher proportion of CD62L^{+} cells (Fig5.7d). However, the total number of such cells within the iLN was low in all mouse strains tested (Fig5.7e). Taken together, these data raised the possibility

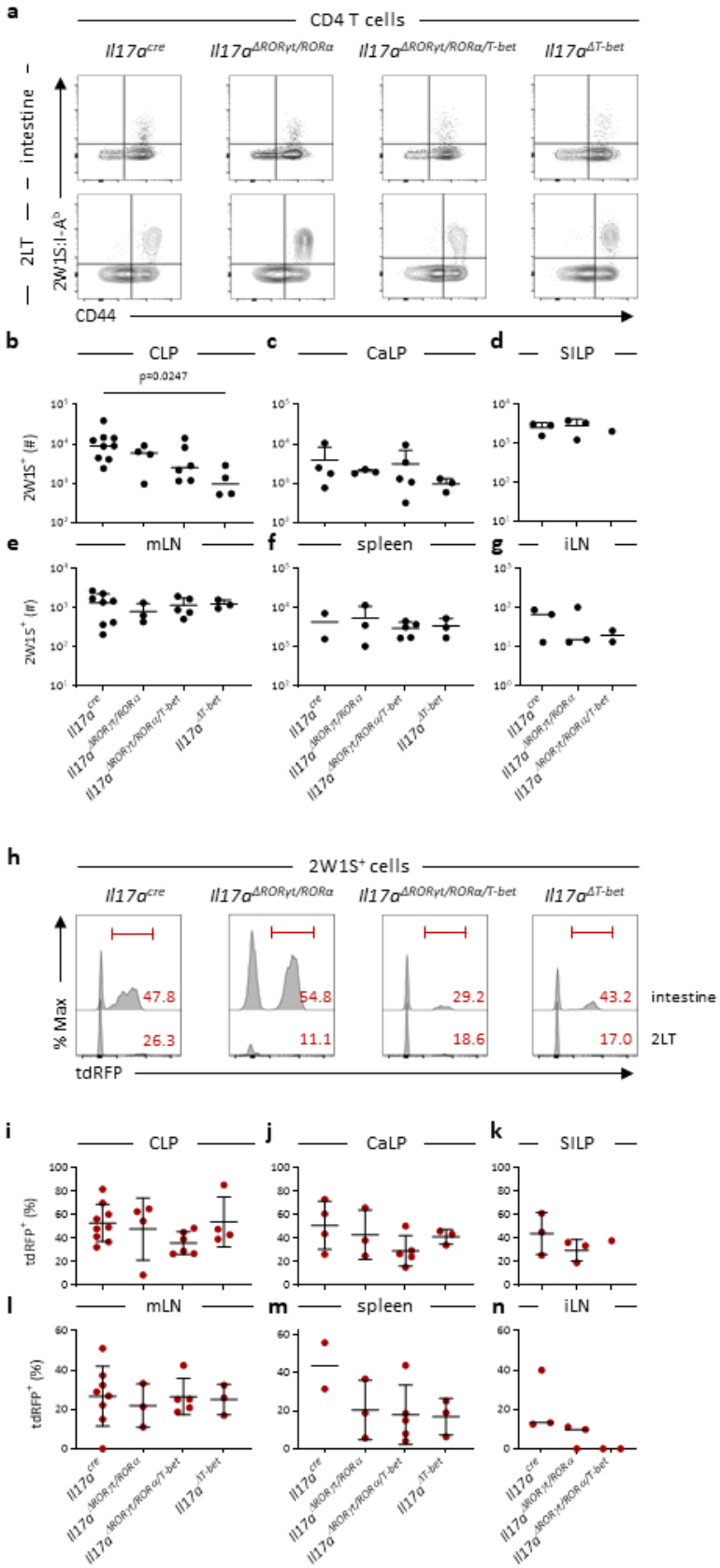
a
CD4 T cells
Il17a^cre
Il17a^ΔRORγt/RORα
Il17a^ΔRORγt/RORα/T-bet
Il17a^ΔT-bet
intestine
2LT
2W1S:I-A^b
CD44
b
CLP
c
CaLP
d
SILP
p=0.0247
2W1S^+ (#)
e
mLN
f
spleen
g
iLN
h
2W1S^+ cells
% Max
47.8
26.3
54.8
11.1
29.2
18.6
43.2
17.0
intestine
2LT
tdRFP
i
CLP
j
CaLP
k
SILP
tdRFP^+ (%)
l
mLN
m
spleen
n
iLN

Figure 5.6. Manipulation of ROR family TF and T-bet antagonism may impact the antigen-specific CD4 T cell population following *C.rodentium* infection

Il17a^{cre}, *Il17a*$^{\Delta ROR\gamma t/ROR\alpha}$, *Il17a*$^{\Delta ROR\gamma t/ROR\alpha/T\text{-}bet}$ and *Il17a*$^{\Delta T\text{-}bet}$ mice were infected with *C.rodentium-2W1S* to enable tracking of the consequences of perturbations in the Th17/exTh17 continuum.

a) Representative flow cytometry plots gated on CD4 T cells showing 2W1S:I-A^{b} tetramer and CD44 staining in the intestine and 2LT of *Il17a*^{cre}, *Il17a*$^{\Delta ROR\gamma t/ROR\alpha}$, *Il17a*$^{\Delta ROR\gamma t/ROR\alpha/T\text{-}bet}$ and *Il17a*$^{\Delta T\text{-}bet}$ mice on D35 following *C.rodentium-2W1S* infection.

b-g) Quantification of the total number of 2W1S^{+} CD4 T cells in the CLP (b), CaLP (c), SILP (d), mLN (e), spleen (f) and iLN (g) of *Il17a*^{cre}, *Il17a*$^{\Delta ROR\gamma t/ROR\alpha}$, *Il17a*$^{\Delta ROR\gamma t/ROR\alpha/T\text{-}bet}$ and *Il17a*$^{\Delta T\text{-}bet}$ mice on D35 following *C.rodentium-2W1S* infection. *Il17a*^{cre} CLP n=9, data pooled from 4 independent experiments, *Il17a*$^{\Delta ROR\gamma t/ROR\alpha}$ and *Il17a*$^{\Delta T\text{-}bet}$ CLP n=4, data pooled from 2 independent experiments, *Il17a*$^{\Delta ROR\gamma t/ROR\alpha/T\text{-}bet}$ CLP n=6, data pooled from 3 independent experiments, *Il17a*^{cre} CaLP n=4, data pooled from 2 independent experiments, *Il17a*$^{\Delta ROR\gamma t/ROR\alpha}$ and *Il17a*$^{\Delta T\text{-}bet}$ CaLP n=3, data from 1 experiment, *Il17a*$^{\Delta ROR\gamma t/ROR\alpha/T\text{-}bet}$ CaLP n=5, data pooled from 2 independent experiments, *Il17a*^{cre} and *Il17a*$^{\Delta ROR\gamma t/ROR\alpha}$ SILP n=3, data from 1 experiment, *Il17a*$^{\Delta ROR\gamma t/ROR\alpha/T\text{-}bet}$ SILP n=1, data from 1 experiment, *Il17a*^{cre} mLN n=8, data pooled from 3 independent experiments, *Il17a*$^{\Delta ROR\gamma t/ROR\alpha}$ and *Il17a*$^{\Delta T\text{-}bet}$ mLN n=3, data from 1 experiment, *Il17a*$^{\Delta ROR\gamma t/ROR\alpha/T\text{-}bet}$ mLN n=5, data pooled from 2 independent experiments, *Il17a*^{cre} spleen n=2, data pooled from 2 independent experiments, *Il17a*$^{\Delta ROR\gamma t/ROR\alpha}$ and *Il17a*$^{\Delta T\text{-}bet}$ spleen n=3, data from 1 experiment, *Il17a*$^{\Delta ROR\gamma t/ROR\alpha/T\text{-}bet}$ spleen n=5, data pooled from 2 independent experiments, *Il17a*^{cre} and *Il17a*$^{\Delta ROR\gamma t/ROR\alpha}$ iLN n=3, data from 1 experiment and *Il17a*$^{\Delta ROR\gamma t/ROR\alpha/T\text{-}bet}$ iLN n=2, data from 1 experiment.

h) Representative histograms showing tdRFP expression in 2W1S^{+} CD4 T cells in the intestine and 2LT of *Il17a*^{cre}, *Il17a*$^{\Delta ROR\gamma t/ROR\alpha}$, *Il17a*$^{\Delta ROR\gamma t/ROR\alpha/T\text{-}bet}$ and *Il17a*$^{\Delta T\text{-}bet}$ mice on D35 following *C.rodentium-2W1S* infection.

i-n) Quantification of the proportion of tdRFP^{+} 2W1S^{+} CD4 T cells in the CLP (i), CaLP (j), SILP (k), mLN (l), spleen (m) and iLN (n) of *Il17a*^{cre}, *Il17a*$^{\Delta ROR\gamma t/ROR\alpha}$, *Il17a*$^{\Delta ROR\gamma t/ROR\alpha/T\text{-}bet}$ and *Il17a*$^{\Delta T\text{-}bet}$ mice on D35 following *C.rodentium-2W1S* infection. *Il17a*^{cre} CLP n=9, data pooled from 4 independent experiments, *Il17a*$^{\Delta ROR\gamma t/ROR\alpha}$ and *Il17a*$^{\Delta T\text{-}bet}$ CLP n=4, data pooled from 2 independent experiments, *Il17a*$^{\Delta ROR\gamma t/ROR\alpha/T\text{-}bet}$ CLP n=6, data pooled from 3 independent experiments, *Il17a*^{cre} CaLP n=4, data pooled from 2 independent experiments, *Il17a*$^{\Delta ROR\gamma t/ROR\alpha}$ and *Il17a*$^{\Delta T\text{-}bet}$ CaLP n=3, data from 1 experiment, *Il17a*$^{\Delta ROR\gamma t/ROR\alpha/T\text{-}bet}$ CaLP n=5, data pooled from 2 independent experiments, *Il17a*^{cre} and *Il17a*$^{\Delta ROR\gamma t/ROR\alpha}$ SILP n=3, data from 1 experiment, *Il17a*$^{\Delta ROR\gamma t/ROR\alpha/T\text{-}bet}$ SILP n=1, data from 1 experiment, *Il17a*^{cre} mLN n=8, data pooled from 3 independent experiments, *Il17a*$^{\Delta ROR\gamma t/ROR\alpha}$ and *Il17a*$^{\Delta T\text{-}bet}$ mLN n=3, data from 1 experiment, *Il17a*$^{\Delta ROR\gamma t/ROR\alpha/T\text{-}bet}$ mLN n=5, data pooled from 2 independent experiments, *Il17a*^{cre} spleen n=2, data pooled from 2 independent experiments, *Il17a*$^{\Delta ROR\gamma t/ROR\alpha}$ and *Il17a*$^{\Delta T\text{-}bet}$ spleen n=3, data from 1 experiment, *Il17a*$^{\Delta ROR\gamma t/ROR\alpha/T\text{-}bet}$ spleen n=5, data pooled from 2 independent experiments, *Il17a*^{cre} and *Il17a*$^{\Delta ROR\gamma t/ROR\alpha}$ iLN n=3, data from 1 experiment and *Il17a*$^{\Delta ROR\gamma t/ROR\alpha/T\text{-}bet}$ iLN n=2, data from 1 experiment.

Values on histograms represent percentages. Normality was tested using Shapiro-Wilk test. Lines on graphs show mean+SD (c, d, e, f), mean±SD (i, j, k, l, m) or median (b, g, n). Significance was tested using One-Way ANOVA (c, d, e, f, i, j, l, m). Kruskal-Wallis test (b), unpaired t test (d, k) or Mann-Whitney U test (g, n).

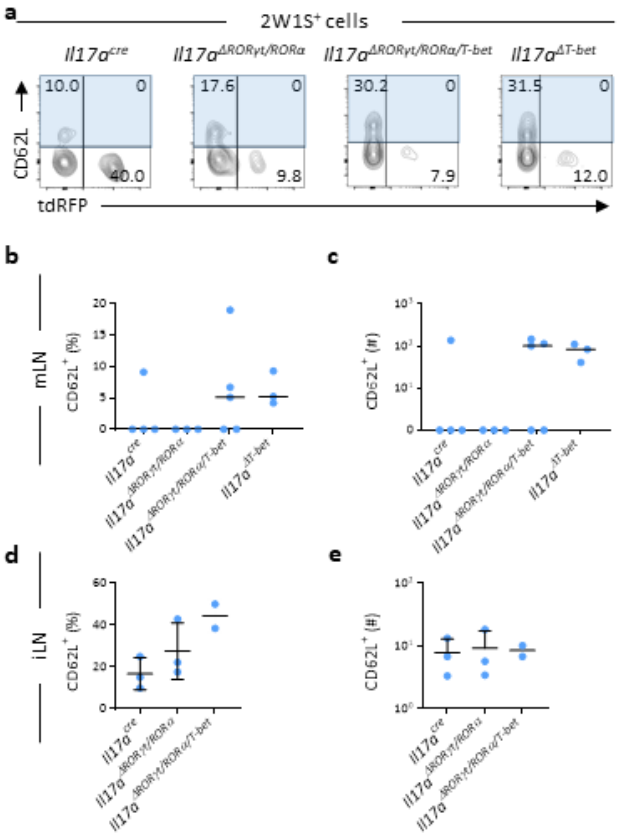
a
2W1S+ cells
Il17a^cre
Il17a^ΔRORγt/RORα
Il17a^ΔRORγt/RORα/T-bet
Il17a^ΔT-bet
10.0
0
40.0
17.6
0
9.8
30.2
0
7.9
31.5
0
12.0
CD62L
tdRFP
b
mLN
CD62L+ (%)
c
CD62L+ (#)
d
iLN
CD62L+ (%)
e
CD62L+ (#)

Figure 5.7. CD4 Tcm-like cell generation following manipulation of the Th17/exTh17 continuum

CD62L expression was assessed in *Il17a*^{cre}, *Il17a*$^{\Delta ROR\gamma t/ROR\alpha}$, *Il17a*$^{\Delta ROR\gamma t/ROR\alpha/T\text{-}bet}$ and *Il17a*$^{\Delta T\text{-}bet}$ mice to test the effects of ROR family TF and T-bet deletion on recirculating CD4 T cell generation following *C.rodentium-2W1S* infection.

a) Representative flow cytometry plots gated on 2W1S^{+} CD4 T cells showing CD62L and tdRFP expression in 2LT of *Il17a*^{cre}, *Il17a*$^{\Delta ROR\gamma t/ROR\alpha}$, *Il17a*$^{\Delta ROR\gamma t/ROR\alpha/T\text{-}bet}$ and *Il17a*$^{\Delta T\text{-}bet}$ mice on D35 following *C.rodentium-2W1S* infection.

b-e) Quantification of the proportion and total number of CD62L^{+} 2W1S^{+} CD4 T cells in mLN (b, c) and iLN (d, e) of *Il17a*^{cre}, *Il17a*$^{\Delta ROR\gamma t/ROR\alpha}$, *Il17a*$^{\Delta ROR\gamma t/ROR\alpha/T\text{-}bet}$ and *Il17a*$^{\Delta T\text{-}bet}$ mice on D35 following *C.rodentium-2W1S* infection. *Il17a*^{cre} mLN n=4, data pooled from 2 independent experiments, *Il17a*$^{\Delta ROR\gamma t/ROR\alpha}$ and *Il17a*$^{\Delta T\text{-}bet}$ mLN n=3, data from 1 experiment, *Il17a*$^{\Delta ROR\gamma t/ROR\alpha/T\text{-}bet}$ mLN n=5, data pooled from 2 independent experiments, *Il17a*^{cre} and *Il17a*$^{\Delta ROR\gamma t/ROR\alpha}$ iLN n=3, data from 1 experiment, *Il17a*$^{\Delta ROR\gamma t/ROR\alpha/T\text{-}bet}$ n=2, data from 1 experiment.

Values on flow cytometry plots represent percentages. Normality was tested using Shapiro-Wilk test. Lines on graphs show mean±SD (d), mean+SD (e) or median (b, c). Significance was tested using Kruskal-Wallis test (b, c) or unpaired t test (d, e).

that perturbations in exTh17 cell differentiation resulted in small differences in the size of the circulating *C.rodentium*-induced CD4 T cell population. Given the small absolute difference in the total numbers of such cells it is unclear whether this holds functional relevance.

Focusing on cells derived from the effector Th17 cell arm of the response, I began to assess TF-deletion-induced differences in the intestinal antigen-specific CD4 T cell compartment. A main described function of *C.rodentium*-induced Trm cells derived from Th17 cells is to produce large amounts of IL-22 upon re-infection and thus aid rapid control of the bacteria (Bishu, Hou, et al., 2019). However, in Chapter 4 I have shown that pushing cells into the exTh17 cell state significantly impaired their ability to produce this cytokine. Whether Th17 cells that never lost the ability to produce normal levels of IL-22 and cells that have differentiated into 'fully mature' exTh17 show differences in their ability to enter the mucosal Trm cell pool remains unknown. Therefore, the expression of CD69 and CD103 was tested on intestinal CD4 T cells at different stages of the Th17/exTh17 spectrum in preliminary experiments (Fig5.8a). The proportion of 2W1S-specific cells expressing CD69 was higher in the SILP and potentially the CaLP but not CLP of *Il17a*$^{\Delta ROR\gamma t/ROR\alpha}$ mice compared to controls (Fig5.8b-d). Similarly, CD103 expression appeared to increase in the only in the SILP and maybe CaLP of these mice (Fig5.8e-g). The increase in CD103 expression was largely due to upregulation of this marker on CD69^{+} cells, as shown by the changes in the proportion of cells expressing both markers (Fig5.8h-j). Whether phenotypic changes reflect crucial functional alterations remains untested, but these initial data suggested potential differences that should be explored in future experiments.

5.4 OX40L-DEFICIENCY PERTURBS NORMAL CD4 T CELL MEMORY GENERATION

Using *C.rodentium-2W1S* infection, I have established a tractable mucosal infection model and began to assess the CD4 T cell response over multiple timepoints while investigating tissue resident and circulating memory T cell formation. Through this work I have identified multiple 2W1S-specific CD4 T cell populations and provided preliminary data linking effector T cell states with memory populations formed. Finally, I aimed to being to explore the mechanisms that might influence the formation of

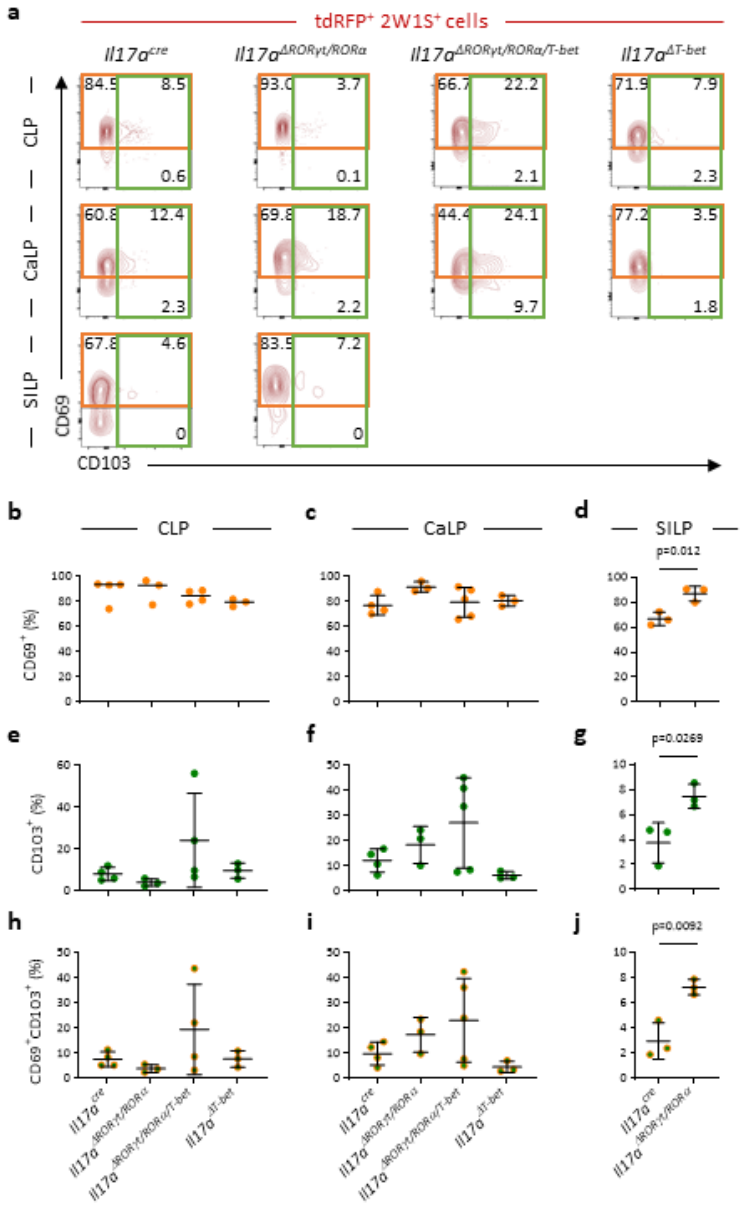
a
tdRFP+ 2W1S+ cells
Il17a^cre
Il17a^ΔRORγt/RORα
Il17a^ΔRORγt/RORα/T-bet
Il17a^ΔT-bet
CLP
CaLP
SILP
CD69
CD103
84.9
8.5
0.6
93.0
3.7
0.1
66.7
22.2
2.1
71.9
7.9
2.3
60.8
12.4
2.3
69.8
18.7
2.2
44.4
24.1
9.7
77.2
3.5
1.8
67.8
4.6
0
83.5
7.2
0
b
CLP
c
CaLP
d
SILP
p=0.012
CD69+ (%)
e
f
g
p=0.0269
CD103+ (%)
h
i
j
p=0.0092
CD69+CD103+ (%)
Il17a^cre
Il17a^ΔRORγt/RORα
Il17a^ΔRORγt/RORα/T-bet
Il17a^ΔT-bet

Figure 5.8. Manipulation of the Th17/exTh17 continuum may perturb CD4 Trm-like cell formation in response to *C.rodentium* infection

CD69 and CD103 expression were assessed in *Il17a*^{cre}, *Il17a*$^{\Delta ROR\gamma t/ROR\alpha}$, *Il17a*$^{\Delta ROR\gamma t/ROR\alpha/T\text{-}bet}$ and *Il17a*$^{\Delta T\text{-}bet}$ mice to test the effects of ROR family TF and T-bet deletion on intestinal CD4 Trm-like cell generation following *C.rodentium-2W1S* infection.

a) Representative flow cytometry plots gated on 2W1S^{+} CD4 T cells showing CD69 and CD103 expression in CLP, CaLP and SILP of *Il17a*^{cre}, *Il17a*$^{\Delta ROR\gamma t/ROR\alpha}$, *Il17a*$^{\Delta ROR\gamma t/ROR\alpha/T\text{-}bet}$ and *Il17a*$^{\Delta T\text{-}bet}$ mice on D35 following *C.rodentium-2W1S* infection.

b-j) Quantification of the proportion of CD69^{+} (b-d), CD103^{+} (e-g) or CD69^{+}CD103^{+} (h-j) 2W1S^{+} CD4 T cells in the CLP, CaLP and SILP of *Il17a*^{cre}, *Il17a*$^{\Delta ROR\gamma t/ROR\alpha}$, *Il17a*$^{\Delta ROR\gamma t/ROR\alpha/T\text{-}bet}$ and *Il17a*$^{\Delta T\text{-}bet}$ mice on D35 following *C.rodentium-2W1S* infection. *Il17a*^{cre} and *Il17a*$^{\Delta ROR\gamma t/ROR\alpha/T\text{-}bet}$ CLP n=4, data pooled from 2 independent experiments, *Il17a*$^{\Delta ROR\gamma t/ROR\alpha}$ and *Il17a*$^{\Delta T\text{-}bet}$ CLP n=3, data from 1 experiment, *Il17a*^{cre} CaLP n=4, data pooled from 2 independent experiments, *Il17a*$^{\Delta ROR\gamma t/ROR\alpha}$ and *Il17a*$^{\Delta T\text{-}bet}$ n=3, data from 1 experiment, *Il17a*$^{\Delta ROR\gamma t/ROR\alpha/T\text{-}bet}$ n=5, data pooled from 2 independent experiments, *Il17a*^{cre} and *Il17a*$^{\Delta ROR\gamma t/ROR\alpha}$ SILP n=3, data from 1 experiment.

Values on flow cytometry plots represent percentages. Normality was tested using Shapiro-Wilk test. Lines on graphs show mean±SD (c, d, e, f, g, h, i, j) or median (b). Significance was tested using One-Way ANOVA (c, e, f, h, i), Kruskal-Wallis test (b) or unpaired t test (d, g, j).

these populations by exploiting available mouse models and combining them with the tractable infection model.

Observations reported in Chapter 3 raised the possibility that OX40L deletion on both CD11c^{+} and RORγt^{+} APCs resulted in impaired *C.rodentium* clearance. Even though impaired clearance was not linked to a defect in effector function, recent work has shown that effector cells induced in distinct compartments, including the intestinal mucosa, interacted with different APCs but were all OX40L-reliant (Gajdasik et al., 2020). Therefore, I hypothesised that in *C.rodentium* infection OX40L may be required by distinct CD4 T cell populations, including those of an effector and recirculating Tcm cell-like phenotype, following *C.rodentium* infection. Conditional OX40L knockout strains were combined with the *C.rodentium-2W1S* infection model to enable testing of the costimulatory requirements of all cells responding to the infection. Here, conditional knockout mice were compared to their littermate controls with total OX40L$^{-/-}$ animals included as a further comparison.

Assessment of the size of the 2W1S-specific CD4 T cell compartment throughout the body of control, OX40L$^{-/-}$, *Itgax*$^{\Delta OX40L}$ and *Rorc*$^{\Delta OX40L}$ mice (Fig5.9a) revealed a decrease in the caecal and potentially colonic antigen specific population in both total and conditional *Itgax*$^{\Delta OX40L}$ knockouts (Fig5.9b-c). These data were consistent with a DC-specific role in OX40L-provision for the effector population that is likely to be enriched in the intestinal tissue but further repeats and functional tests are required to confirm this effect. In the 2LT, these observations pointed to an interesting potential difference in the size of the antigen-specific CD4 T cell population of OX40L$^{-/-}$ mice compared to controls (Fig5.9d-f). However, the mouse breeding strategy did not allow for the generation of littermate controls for total OX40L$^{-/-}$ animals and so microbiota-induced differences could not be excluded.

Similar patterns were observed when assessing the response in *Rorc*$^{\Delta OX40L}$ mice (Fig5.9g-k) but, as before, no robust conclusions could be drawn in the absence of further datapoints. Furthermore, future experiments would benefit for the inclusion of the SILP. Nonetheless, these results raised the possibility that the reduction in the size of the responding CD4 T cell pool was in itself the cause of

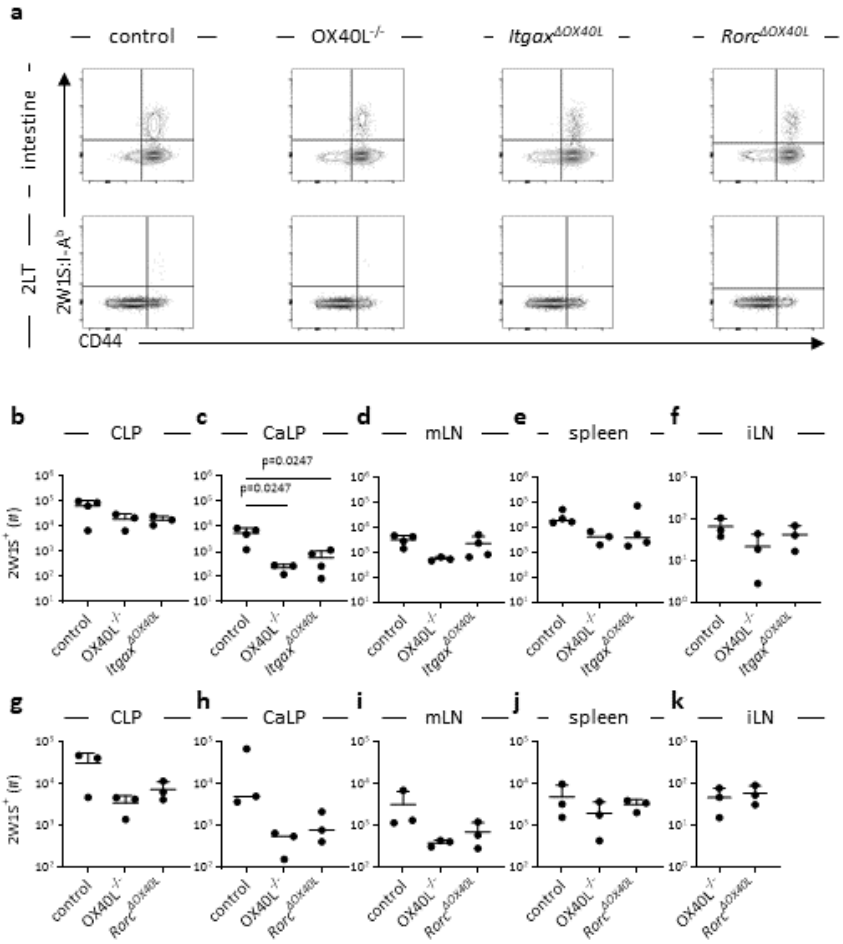
a
control
OX40L-/-
Itgax ΔOX40L
Rorc ΔOX40L
intestine
2LT
2W1S:I-Ab
CD44
b
CLP
c
CaLP
d
mLN
e
spleen
f
iLN
p=0.0247
p=0.0247
2W1S+ (#)
control
OX40L-/-
Itgax ΔOX40L
g
CLP
h
CaLP
i
mLN
j
spleen
k
iLN
2W1S+ (#)
control
OX40L-/-
Rorc ΔOX40L

Figure 5.9. OX40L-deficiency impacts the antigen-specific CD4 T cell population following *C.rodentium* infection

Control ($Cre^{-/-}$) , $OX40L^{-/-}$, $Itgax^{\Delta OX40L}$ and $Rorc^{\Delta OX40L}$ mice were infected with *C.rodentium-2W1S* to enable tracking of the consequences of OX40L-deficiency.

a) Representative flow cytometry plots gated on CD4 T cells showing 2W1S:I-A^b tetramer and CD44 staining in the intestine and 2LT of control, $OX40L^{-/-}$, $Itgax^{\Delta OX40L}$ and $Rorc^{\Delta OX40L}$ mice on D35 following *C.rodentium-2W1S* infection.

b-f) Quantification of the total number of $2W1S^+$ CD4 T cells in control, $OX40L^{-/-}$ and $Itgax^{\Delta OX40L}$ CLP (b), CaLP (c), mLN (d) spleen (e) and iLN (f). Controls are $Cre^{-/-}$ littermates of $Itgax^{\Delta OX40L}$ mice. CLP, CaLP, mLN and spleen control n=4, data pooled from 2 independent experiments, CLP, CaLP, mLN, spleen and iLN $OX40L^{-/-}$ n=3, data from 1 experiment, $Itgax^{\Delta OX40L}$ CLP and iLN n=3, data from 1 experiment, $Itgax^{\Delta OX40L}$ CaLP, mLN and spleen n=4, data pooled from 2 independent experiments.

g-k) Quantification of the total number of $2W1S^+$ CD4 T cells in control, $OX40L^{-/-}$ and $Rorc^{\Delta OX40L}$ CLP (g), CaLP (h), mLN (i), spleen (j) and iLN (k). Controls are $Cre^{-/-}$ littermates of $Rorc^{\Delta OX40L}$ mice. CLP, CaLP, mLN and spleen control n=3, data pooled from 2 independent experiments, CLP, CaLP, mLN, spleen and iLN $OX40L^{-/-}$ and $Rorc^{\Delta OX40L}$ n=3, data from 1 experiment.

Normality was tested using Shapiro-Wilk test. Lines on graphs show mean+SD (b, c, d, f, g, i, j, k) or median (e, h). Significance was tested using One-Way ANOVA (b, c, d, f, g, i, j), Kruskal-Wallis test (e, h) or unpaired t test (k).

delayed *C.rodentium* clearance. In addition, these initial data tentatively linked OX40L to the effector arm within the colon and suggested that these cells, like Th1 effectors cells, may be OX40L-dependent.

To further test mucosal infection-induced CD4 T cell OX40L-requirements, putative Tcm and Trm cell populations were assessed in $Cre^{-/-}$ control and $OX40L^{-/-}$ mice. Importantly, controls and $OX40L^{-/-}$ animals were not littermates. Surprisingly, assessment of CD62L expression in 2LT (Fig5.10a), revealed an increase in the proportion of $2W1S^{+}CD44^{hi}$ CD4 T cells expressing this marker in the mLN but not in the iLN. However, differences in the total numbers of these cells showed no evidence of an increase in either location (Fig5.10b-e). It is possible that a defect in the accumulation of effector cells within the mLN of $OX40L^{-/-}$ mice was behind the apparent increase in $CD62L^{+}$ Tcm-like cell frequency. Such changes were less likely to affect the iLN as effector cells induced by mucosal *C.rodentium* infection were not expected to be present in large numbers here.

Assessing CD69 and CD103 expression in the colon and caecum (Fig5.10f) did not reveal differences in the frequency of $CD69^{+}$ 2W1S-specific cells in either the colon or the caecum although both were reduced in numbers, owing to the reduction of the overall antigen-specific CD4 T cell population (Fig5.10g-j). CD103 expression, on the other hand, was detected on a larger proportion of caecal antigen-specific cells in OX40L-deficient mice than in controls but remained unchanged in the colon. Much like $CD69^{+}$ cells, the total number of $CD103^{+}$ cells appeared lower in knockout mice although this difference was not statistically significant (Fig5.10k-n). The apparent contradiction between the large increase in the proportion of CaLP $CD103^{+}$ cells but potential decrease in their numbers was likely the result of an overall decrease in the size of the antigen-specific population in $OX40L^{-/-}$ mice (Fig5.9).

Together, the differences observed between $OX40L^{-/-}$ and control animals pointed to the existence of as yet unidentified subsets of mucosal and mLN CD4 T cells induced by *C.rodentium* infection that show differential requirements for OX40L. One possible explanation is that these cells may occupy different niches within the mucosa and are affected by OX40L from distinct APC populations. In fact, compartmentalised provision of OX40L to Teff cells has been reported (Gajdasik et al., 2020). To test

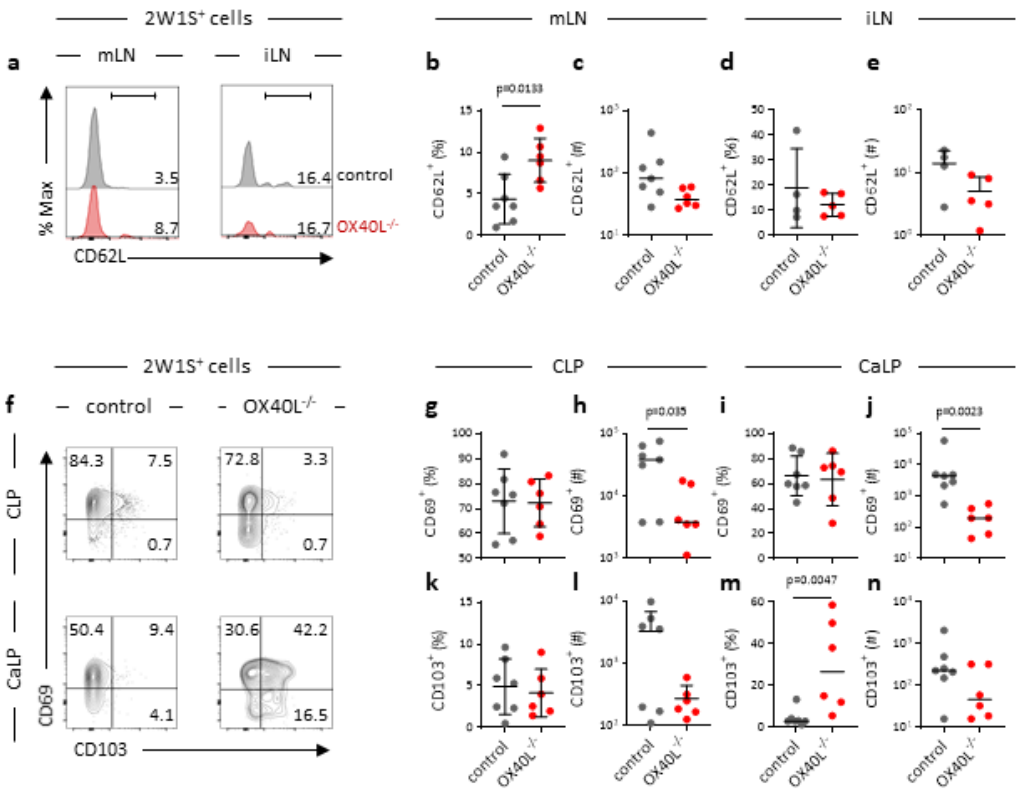
2W1S+ cells
mLN
iLN
a
% Max
CD62L
3.5
8.7
16.4
16.7
control
OX40L-/-
b
c
d
e
p=0.0133
CD62L+ (%)
CD62L+ (#)
control
OX40L-/-
2W1S+ cells
CLP
CaLP
f
control
OX40L-/-
CD69
CD103
84.3
7.5
0.7
72.8
3.3
0.7
50.4
9.4
4.1
30.6
42.2
16.5
g
h
i
j
k
l
m
n
p=0.035
p=0.0023
p=0.0047
CD69+ (%)
CD69+ (#)
CD103+ (%)
CD103+ (#)

Figure 5.10. OX40L-deficiency perturbs normal CD4 Tcm- and Trm-like cell generation in response to *C.rodentium* infection

CD62L, CD69 and CD103 expression were assessed in control and OX40L$^{-/-}$ mice to test the effects of OX40L-deficiency on recirculating and intestinal mucosa resident CD4 T cell generation following *C.rodentium-2W1S* infection.

a) Representative histograms showing CD62L expression in the 2W1S^{+} CD4 T cell population in mLN and iLN of control and OX40L$^{-/-}$ on D35 following *C.rodentium-2W1S* infection.

b-c) Quantification of the proportion (b) and total number (c) of CD62L^{+} 2W1S^{+} CD4 T cells in the mLN of control and OX40L$^{-/-}$ mice on D35 following *C.rodentium-2W1S* infection. Control n=7, data pooled from 4 independent experiments, OX40L$^{-/-}$ n=6, data pooled from 2 independent experiments.

d-e) Quantification of the proportion (d) and total number (e) of CD62L^{+} 2W1S^{+} CD4 T cells in the iLN of control and OX40L$^{-/-}$ mice on D35 following *C.rodentium-2W1S* infection. Control n=4, data pooled from 2 independent experiments, OX40L$^{-/-}$ n=5, data pooled from 2 independent experiments.

f) Representative flow cytometry plots gated on 2W1S^{+} CD4 T cells showing CD69 and CD103 expression in CLP and CaLP of control and OX40L$^{-/-}$ mice on D35 following *C.rodentium-2W1S* infection.

g-j) Quantification of the proportion and total number of CD69^{+} 2W1S^{+} CD4 T cells in the CLP (g-h) and CaLP (i-j) of control and OX40L$^{-/-}$ mice on D35 following *C.rodentium-2W1S* infection. Control n=7, data pooled from 4 independent experiments, OX40L$^{-/-}$ n=6, data pooled from 2 independent experiments.

k-n) Quantification of the proportion and total number of CD103^{+} 2W1S^{+} CD4 T cells in the CLP (k-l) and CaLP (m-n) of control and OX40L$^{-/-}$ mice on D35 following *C.rodentium-2W1S* infection. Control n=7, data pooled from 4 independent experiments, OX40L$^{-/-}$ n=6, data pooled from 2 independent experiments.

Values on histograms and flow cytometry plots represent percentages. Normality was tested using Shapiro-Wilk test. Lines on graphs show mean±SD (b, d, g, i, k), mean+SD (e, l) or median (c, h, j, m, n). Significance was tested using unpaired t test (b, d, e, g, i, k, l) or Mann-Whitney U test (c, h, j, m, n).

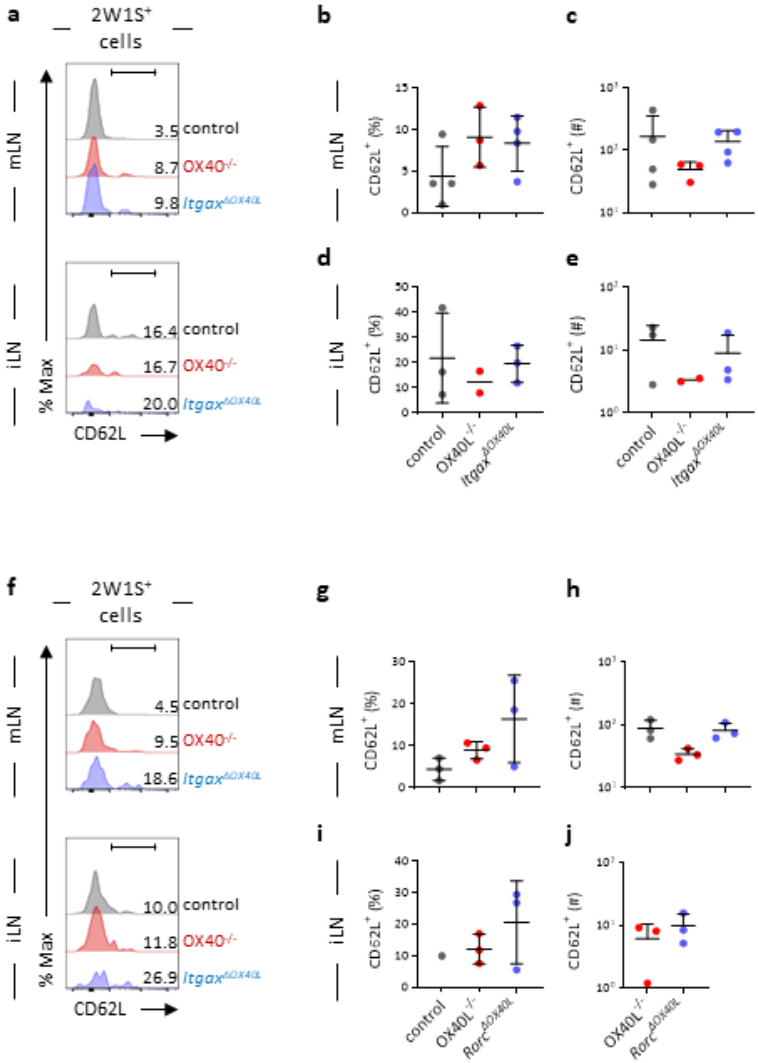
a
2W1S+ cells
mLN
iLN
% Max
CD62L
3.5 control
8.7 OX40-/-
9.8 Itgax ΔOX40L
16.4 control
16.7 OX40-/-
20.0 Itgax ΔOX40L
b
c
d
e
CD62L+ (%)
CD62L+ (#)
control
OX40L -/-
Itgax ΔOX40L
f
2W1S+ cells
4.5 control
9.5 OX40-/-
18.6 Itgax ΔOX40L
10.0 control
11.8 OX40-/-
26.9 Itgax ΔOX40L
g
h
i
j
OX40L -/-
Rorc ΔOX40L

Figure 5.11. Assessment of OX40L provision to CD4 Tcm-like cells generated in response to *C.rodentium* infection

CD62L expression was assessed in control, OX40L$^{-/-}$, *Itgax*$^{\Delta OX40L}$ and *Rorc*$^{\Delta OX40L}$ mice to test the effects of OX40L-deficiency on recirculating CD4 T cell generation following *C.rodentium-2W1S* infection.

a) Representative histograms showing CD62L expression in the 2W1S^{+} CD4 T cell population in mLN and iLN of control, OX40L$^{-/-}$ and *Itgax*$^{\Delta OX40L}$ mice on D35 following *C.rodentium-2W1S* infection.

b-e) Quantification of the proportion and total number of CD62L^{+} 2W1S^{+} CD4 T cells in mLN (b, c) and iLN (d, e) of control, OX40L$^{-/-}$ and *Itgax*$^{\Delta OX40L}$ mice on D35 following *C.rodentium-2W1S* infection. Controls are Cre$^{-/-}$ littermates of *Itgax*$^{\Delta OX40L}$ mice. OX40L$^{-/-}$ mice were inoculated with the same inoculum as control and *Itgax*$^{\Delta OX40L}$ mice. Control and *Itgax*$^{\Delta OX40L}$ mLN n=4, data pooled from 2 independent experiments, OX40L$^{-/-}$ mLN n=3, data from 1 experiment, control and *Itgax*$^{\Delta OX40L}$ iLN n=3, data from 1 experiment, OX40L$^{-/-}$ iLN n=2, data from 1 experiment.

f) Representative histograms showing CD62L expression in the 2W1S^{+} CD4 T cell population in mLN and iLN of control, OX40L$^{-/-}$ and *Rorc*$^{\Delta OX40L}$ mice on D35 following *C.rodentium-2W1S* infection.

g-j) Quantification of the proportion and total number of CD62L^{+} 2W1S^{+} CD4 T cells in mLN (g, h) and iLN (i, j) of control, OX40L$^{-/-}$ and *Rorc*$^{\Delta OX40L}$ mice on D35 following *C.rodentium-2W1S* infection. Controls are Cre$^{-/-}$ littermates of *Rorc*$^{\Delta OX40L}$ mice. OX40L$^{-/-}$ mice were inoculated with the same inoculum as control and *Rorc*$^{\Delta OX40L}$ mice. Control mLN n=3, data pooled from 2 independent experiments, OX40L$^{-/-}$ and *Rorc*$^{\Delta OX40L}$ mLN and iLN n=3, data from 1 experiment.

Values on histograms represent percentages. Normality was tested using Shapiro-Wilk test. Lines on graphs show mean±SD (b, d, g, i) or mean+SD (c, e, h, j). Significance was tested using One-Way ANOVA (b, c, g, h) or unpaired t test (d, e, i, j).

whether distinct systemic and mucosal CD4 T cell populations also relied on OX40L from different cellular sources, CD62L, CD69 and CD103 expression were also assessed in *Itgax*$^{\Delta OX40L}$ and *Rorc*$^{\Delta OX40L}$ mice.

Comparing CD62L expression on 2W1S-specific activated CD4 T cells in the mLN and iLN of *Itgax*$^{\Delta OX40L}$ mice to those of Cre^{-} littermate controls and OX40L$^{-/-}$ mice gavaged with the same inoculum (Fig5.11a) failed to identify any statistically significant changes in this population (Fig5.11b-e). Assessment of *Rorc*$^{\Delta OX40L}$ mice (Fig5.11f) yielded similar results (Fig5.11g-j). However, further experimental repeats are required to fully test the contribution of CD11c^{+} (DC) and RORγt^{+} (likely ILC3) APC to the regulation of *C.rodentium*-induced Tcm cells.

As expected, based on comparison of control and OX40L$^{-/-}$ mice, evaluation of CD69 and CD103 expression in control, OX40L$^{-/-}$ and *Itgax*$^{\Delta OX40L}$ or *Rorc*$^{\Delta OX40L}$ intestines (Fig5.12a-b) revealed no changes in the proportion of CD69^{+} 2W1S-specific CD4 T cells in either the colon or caecum (Fig5.12b-f). However, some evidence of a defect in these cells' normal accumulation was observed not only in OX40L$^{-/-}$ but also in conditional knockout intestines (Fig5.12g-j). The observed changes were likely caused by the overall reduction in the size of the antigen-specific population (Fig5.9) and were only statistically significant in the caecum. Since these experiments were not sufficiently powered to test these differences further datapoints are required. Assessment CD103 expression also failed to link CD11c- or RORγt-driven OX40L deficiency to a change in the frequency of the CD103^{+} antigen-specific T cell population, despite the increase in caecal CD103^{+} 2W1S-specific CD4 T cells in total OX40L knockout mice (Fig5.12k-n). The observed changes in the numbers of these cells across the different strains reflected the patterns seen when assessing the total 2W1S-specific CD4 T cell population (Fig5.12o-r). Comparison of the frequency of cells expressing both markers returned results similar results to those observed assessment of the total CD103^{+} antigen-specific CD4 T cell population (Fig5.12s-v). Taken together, these data pointed to the control of normal CD103 expression potentially

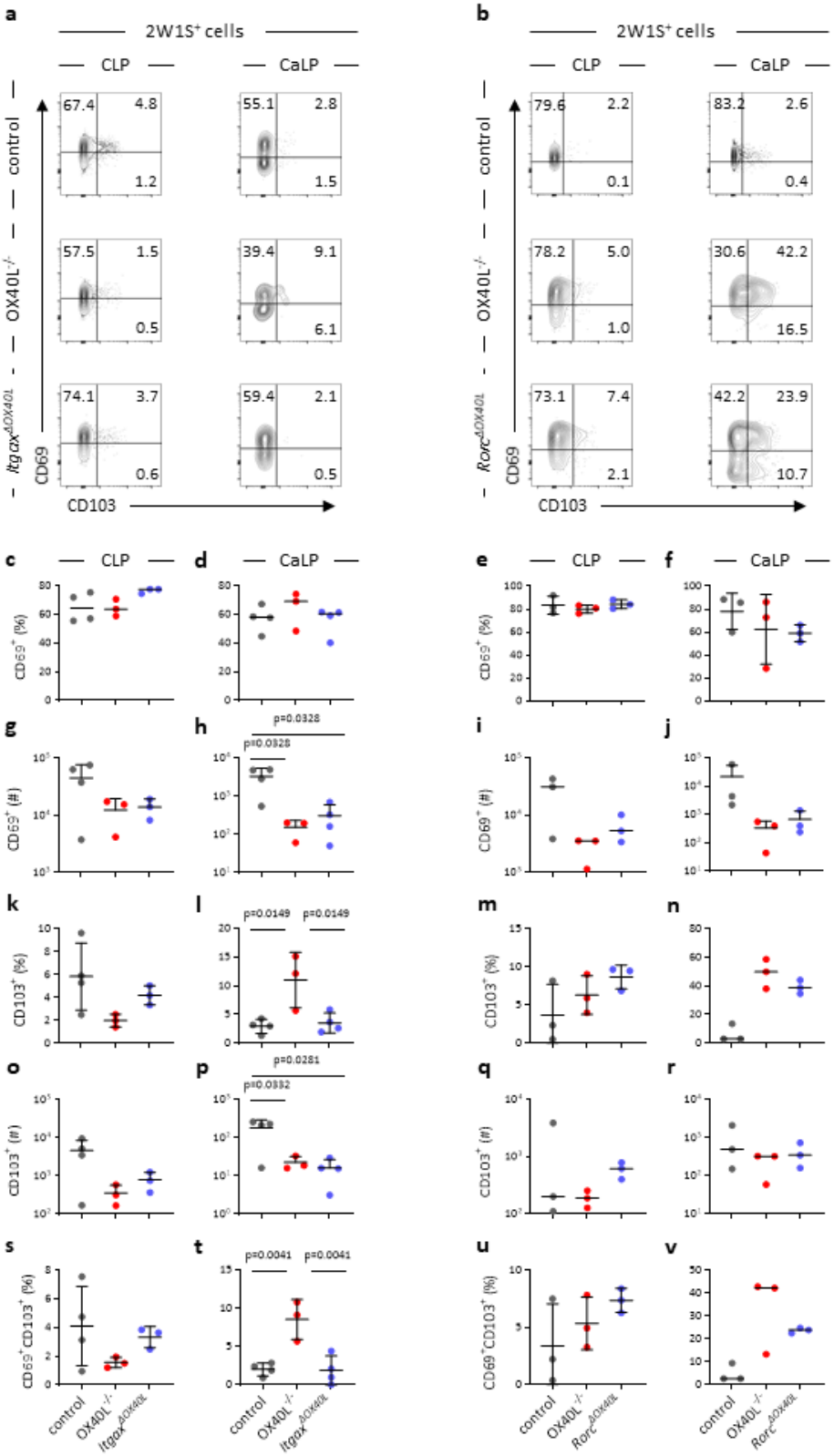
a
2W1S+ cells
CLP
CaLP
control
OX40L-/-
Itgax ΔOX40L
CD69
CD103
67.4
4.8
1.2
55.1
2.8
1.5
57.5
1.5
0.5
39.4
9.1
6.1
74.1
3.7
0.6
59.4
2.1
0.5
b
2W1S+ cells
CLP
CaLP
control
OX40L-/-
Rorc ΔOX40L
CD69
CD103
79.6
2.2
0.1
83.2
2.6
0.4
78.2
5.0
1.0
30.6
42.2
16.5
73.1
7.4
2.1
42.2
23.9
10.7
c
CLP
d
CaLP
e
CLP
f
CaLP
CD69+ (%)
g
h
i
j
CD69+ (#)
p=0.0328
k
l
m
n
CD103+ (%)
p=0.0149
p=0.0149
o
p
q
r
CD103+ (#)
p=0.0281
p=0.0332
s
t
u
v
CD69+CD103+ (%)
p=0.0041
p=0.0041
control
OX40L-/-
Itgax ΔOX40L
Rorc ΔOX40L

Figure 5.12. Assessment of OX40L provision to CD4 Trm-like cells generated in response to *C.rodentium* infection

CD69 and CD103 expression were assessed in control, OX40L$^{-/-}$, *Itgax*$^{\Delta OX40L}$ and *Rorc*$^{\Delta OX40L}$ mice to test the effects of OX40L-deficiency on intestinal CD4 Trm-like cell generation following *C.rodentium-2W1S* infection.

a-b) Representative flow cytometry plots gated on 2W1S^{+} CD4 T cells showing CD69 and CD103 expression in CLP and CaLP of control, OX40L$^{-/-}$ and *Itgax*$^{\Delta OX40L}$ (a) and *Rorc*$^{\Delta OX40L}$ (b) mice on D35 following *C.rodentium-2W1S* infection.

c-j) Quantification of the proportion and total number of CD69^{+} 2W1S^{+} CD4 T cells in the CLP and CaLP of control, OX40L$^{-/-}$ and *Itgax*$^{\Delta OX40L}$ (c-d, g-h) or *Rorc*$^{\Delta OX40L}$ (e-f, i-j) mice on D35 following *C.rodentium-2W1S* infection. Controls are Cre$^{-/-}$ littermates of *Itgax*$^{\Delta OX40L}$ or *Rorc*$^{\Delta OX40L}$ mice. OX40L$^{-/-}$ mice were inoculated with the same inoculum as control and *Itgax*$^{\Delta OX40L}$ mice. *Itgax*$^{\Delta OX40L}$ control CLP and CaLP n=4, data pooled from 2 independent experiments, *Rorc*$^{\Delta OX40L}$ control n=3, data pooled from 2 independent experiments, OX40L$^{-/-}$ CLP and CaLP n=3, data from 1 experiment, *Itgax*$^{\Delta OX40L}$ CLP n=3, data from 1 experiment, *Itgax*$^{\Delta OX40L}$ CaLP n=4, data pooled from 2 independent experiments, *Rorc*$^{\Delta OX40L}$ CLP and CaLP n=3, data from 1 experiment.

k-r) Quantification of the proportion and total number of CD103^{+} 2W1S^{+} CD4 T cells in the CLP and CaLP of control, OX40L$^{-/-}$ and *Itgax*$^{\Delta OX40L}$ (k-l, o-p) or *Rorc*$^{\Delta OX40L}$ (m-n, q-r) mice on D35 following *C.rodentium-2W1S* infection. Controls are Cre$^{-/-}$ littermates of *Itgax*$^{\Delta OX40L}$ or *Rorc*$^{\Delta OX40L}$ mice. OX40L$^{-/-}$ mice were inoculated with the same inoculum as control and *Itgax*$^{\Delta OX40L}$ mice. *Itgax*$^{\Delta OX40L}$ control CLP and CaLP n=4, data pooled from 2 independent experiments, *Rorc*$^{\Delta OX40L}$ control n=3, data pooled from 2 independent experiments, OX40L$^{-/-}$ CLP and CaLP n=3, data from 1 experiment, *Itgax*$^{\Delta OX40L}$ CLP n=3, data from 1 experiment, *Itgax*$^{\Delta OX40L}$ CaLP n=4, data pooled from 2 independent experiments, *Rorc*$^{\Delta OX40L}$ CLP and CaLP n=3, data from 1 experiment.

s-v) Quantification of the proportion of CD69^{+}CD103^{+} 2W1S^{+} CD4 T cells in the CLP and CaLP of control, OX40L$^{-/-}$ and *Itgax*$^{\Delta OX40L}$ (s-t) or *Rorc*$^{\Delta OX40L}$ (u-v) mice on D35 following *C.rodentium-2W1S* infection. Controls are Cre$^{-/-}$ littermates of *Itgax*$^{\Delta OX40L}$ or *Rorc*$^{\Delta OX40L}$ mice. OX40L$^{-/-}$ mice were inoculated with the same inoculum as control and *Itgax*$^{\Delta OX40L}$ mice. *Itgax*$^{\Delta OX40L}$ control CLP and CaLP n=4, data pooled from 2 independent experiments, *Rorc*$^{\Delta OX40L}$ control n=3, data pooled from 2 independent experiments, OX40L$^{-/-}$ CLP and CaLP n=3, data from 1 experiment, *Itgax*$^{\Delta OX40L}$ CLP n=3, data from 1 experiment, *Itgax*$^{\Delta OX40L}$ CaLP n=4, data pooled from 2 independent experiments, *Rorc*$^{\Delta OX40L}$ CLP and CaLP n=3, data from 1 experiment.

Values on flow cytometry plots represent percentages. Normality was tested using Shapiro-Wilk test. Lines on graphs show mean±SD (k, l, s, t, e, f, m, u), mean+SD (g, h, o, p, j) or median (c, d, i, n, q, r, v). Significance was tested using One-Way ANOVA (g, h, k, l, o, p, s, t, e, f, j, m, u) or Kruskal-Wallis test (c, d, i, n, q, r, v).

being linked to OX40L presentation. However, larger experimental groups are required to confirm or exclude the contributions of $CD11c^+$ or $ROR\gamma t^+$ APC.

5.5 SUMMARY

Here, I have shown that a tractable *C.rodentium* infection model enables the assessment of the whole CD4 T cell compartment responding to the infection. This model, in combination with genetically modified mouse strains, provides the first platform that enables comprehensive characterisation of the development and function of both mucosal and circulating CD4 T cells induced by an extracellular infection.

I have begun to assess the kinetics of the *C.rodentium*-induced CD4 T cell response by testing the antigen-specific population early in the infection and shortly after expected clearance. Published literature suggested that the antigen-specific CD4 T cell pool generated following mucosal infection diminished rapidly (Pepper et al., 2010). Surprisingly, the size of the colonic population responding to the *C.rodentium* was found to increase by day 35 of the infection. This discrepancy is likely the result of the different approaches taken to trigger a mucosal Th17 cell response. The earlier study mentioned above assessed Th17 cells generated in response to *L.monocytogenes-2W1S* administered nasally (Pepper et al., 2010). However, *L.monocytogenes-2W1S* is an attenuated pathogen that is not adapted to the intranasal environment it was placed in and is cleared rapidly by the innate immune system. Thus, the short duration of antigen exposure, and lack of reliance on adaptive immune cells for the control of bacteria, likely resulted in rapid contraction of the effector CD4 T cell response. *C.rodentium*, on the other hand, is a natural mouse pathogen evolved to not only survive in but also colonise the large intestine, driving a potent Th17 cell response (Silberger et al., 2017). Nonetheless, assessment of the anti-*C.rodentium-2W1S* CD4 T cell response kinetics would benefit from extended time course experiments. This would further ensure that a true memory phase, following contraction of the initial response, is studied. Furthermore, due to the low number of colonised mice it was not possible to

match the age, sex or bacterial load of mice assessed at the early and late timepoints introducing further confounding factors. Future experiments would benefit from consideration of these factors.

To account for the documented plasticity of *C.rodentium* infection-induced Th17 cells (Omenetti et al., 2019), tracking of antigen-specific populations was combined with cytokine expression fate mapping. Further conditional knockout models were included to enable assessment the effects of Th17/exTh17 continuum manipulation and OX40L provision on responding CD4 T cells. Together, these models revealed the existence of at least two phenotypically distinct populations. A circulating $CD62L^+$ Tcm cell precursor-like population that showed no developmental link to effector Th17 cells and IL-17A-producing cells that mainly occupied the mucosal effector sites. The exact functional relevance or mechanism underpinning the separation of these two cell fates is unclear but may reflect mutually antagonistic transcriptional programmes. Tcm cell formation following Th1 cell responses requires the expression of the transcription factor Bcl6 (Pepper et al., 2011). Effector cells, on the other hand, rely on Id2 and, in the case of Th1 cell responses, reciprocal inhibition between these two transcriptional repressors was shown to control CD4 T cell fate (Shaw et al., 2016). Given that differentiation of Th17 cells, both from naïve CD4 T cells and $FoxP3^+$ Treg cells, was reported to require Id2 (Hwang et al., 2018; Lin et al., 2012) the same mechanism may explain the observations outlined above. However, the existence of this relationship between Th17 and mucosal infection-induced Tcm cells remains to be tested. In addition, study of the exact mechanism underpinning Teff/Tcm cell fate decisions would require additional animal models. The upstream trigger of Bcl6 or Id2 expression is not known but has been reported to be linked to a lack of IL-2 receptor (IL-2R) stimulation. This may reflect asymmetric cell division-driven generation of high affinity IL-2Rα^+ ($CD25^+$) and $CD25^-$ populations following TCR ligation (Chang et al., 2007; Pepper et al., 2011). A further proposed mechanism is the local competition for IL-2 with other immune cells, potentially including ILC3 (Hepworth et al., 2015). Taken together, the observations outlined above are consistent with Bcl6/Id2 antagonism-driven divergence of Teff and Tcm cell fates being a fundamental feature of all CD4 T cell responses, not just those dominated by Th1 cells. Importantly, however, assessment of the antigen-

specific CD4 T cell compartment across multiple tissues provided some evidence that populations with a history of IL-17A production could enter peripheral lymph nodes later in the infection. A possible explanation is that Th17 cells were differentiating into Tcm-like cells. However, tdRFP$^+$ CD4 T cells within lymph nodes were not found to express CD62L, as would be expected of Tcm cells (Pepper & Jenkins, 2011). While these data are consistent with early bifurcation of mucosal infection induced Tcm and Th17 cell fates they do not explain how tdRFP$^+$ antigen-specific CD4 T cells entered the 2LT. CD62L shedding, the loss of CD62L from the cell membrane, is a known feature of T cell activation (Jung & Dailey, 1990). Therefore, cell surface CD62L assessment alone may have underestimated the size of the CD4 T cell population able to express this marker. However, why CD62L loss would occur on tdRFP$^+$ CD4 T cells at a seemingly higher rate than on tdRFP$^-$ populations is unexplained. On the other hand, should antigen-specific CD4 T cells with a history of *Il17a* expression truly lack CD62L expression in tissues such as peripheral LNs, it is unclear by what mechanism they would have been able to traffic there. Optimisation of the use of further Tcm cell markers with more stable expression or more reliable detection would greatly benefit future studies.

Assessing the effector arm of the response and focusing on the potential generation of mucosal Trm cells pointed to the existence of further tissue-specific CD4 T cell subsets generated in response to *C.rodentium* infection. In both the colon and the caecum the majority of *C.rodentium*-induced CD4 T cells were CD69$^+$ but only a small proportion expressed the integrin CD103. Interestingly, the main observed effect of both Th17/exTh17 continuum manipulation and OX40L deletion appeared to be an increase in CD103 expression on certain mucosal *C.rodentium*-induced CD4 T cell populations. The biggest such increase was observed in mice lacking both ROR family TFs and T-bet, and potentially representing a dysregulated Th17 cell phenotype. Coupled with the observations from OX40L-deficient mice, these data suggested that increase of CD103 expression on intestinal lamina propria CD4 T cells may be a marker of inappropriate Teff cell regulation. However, the biological relevance of this is unclear. CD103 could drive cell trafficking into the intraepithelial layer (Kilshaw & Baker, 1988) and the CD103$^+$ CD4 T cell population may have resulted from contamination of lamina propria

homogenates with intraepithelial lymphocytes. Therefore, testing of antigen-specific CD4 T cell localisation over time may prove informative. In addition, CD103 expression on lamina propria cells may have additional roles in supporting Th17 and exTh17 cells, as it does in aiding suppressive Treg cell function (Braun et al., 2015). Importantly, the large variation in the CD103 expression data highlighted the possibility that factors not considered here, such as antigen availability, were affecting the mucosal antigen-specific CD4 T cell population. Therefore, in future experiments matching of day 6-8 bacterial loads across mouse strains and confirmation of bacterial clearance prior to tissue harvest would be desirable.

While we have not carried out experiments to definitively assess tissue residency, such as FTY720 administration to block the egress of CD4 T cells from lymphoid tissues (Matloubian et al., 2004) or *in situ* labelling of cells (Tomura et al., 2008), the observed enrichment of $CD69^+$ antigen-specific cells in the colon is consistent with data reported by others on *C.rodentium*-induced CD4 T cell memory formation (Bishu, Hou, et al., 2019). However, even though the results presented here were consistent with Th17-derived Trm cell formation, there was no evidence that Th17 and exTh17 cells were more likely to enter the tissue resident memory pool than other local *C.rodentium*-induced CD4 T cells. Future work must assess the source of all *C.rodentium*-induced Trm cells to build a better understanding of mucosal CD4 T cell populations. These studies would likely benefit from further research into the anti-*C.rodentium* response kinetics with both earlier and much later time points. Moreover, as CD69 expression is required for presence in the intestinal lamina propria it is also possible that by looking simply at expression of these markers key differences were missed. It is conceivable that $tdRFP^+$ cells would be more likely to react to antigen re-encounter by cytokine production and this should be tested in future experiments.

Taken together, these data showed that the majority of *C.rodentium*-induced CD4 T cells expressed CD69 but lacked CD103 in both the colon and caecum. However, the existence of both $CD103^-$ and

CD103^{+} cells pointed to further heterogeneity within the Trm-like cell pool that may reflect adaptations to different niches within the mucosal microenvironment.

Interestingly, the data presented here suggested that both DC and ILC3 or T cell-derived OX40L were required for accumulation of normal numbers of *C.rodentium* responsive CD4 T cells. However, a clear role in the support of either Tcm or Teff/Trm cell populations was not evident. Assessment of TF-deficient mice pointed to a potential impairment in the generation of Tcm-like cells in mice lacking normal Th17cell responses. However, this observation was not broadly applicable to all lymphoid tissues assessed and was relatively small in terms of changes in total cellularity. OX40L deficiency appeared to have the opposite effect with an increase in the frequency of these cells in the same anatomical location. These observations leave open the possibility that interaction of CD4 T cell OX40 with OX40L present on APCs favoured Teff cell rather than Tcm cell precursor formation. However, the experimental models used were not suitable for the assessment of the causal relationship between Tcm/Teff cell bifurcation and OX40:OX40L interactions – it is unclear whether ligation of OX40 drives cell fate decisions or whether its expression is restricted to Teff cells where it is required for normal proliferation and survival. More clearly, I found no evidence that the fundamental pathways governing Tcm and effector Th17 cell fate bifrucation were perturbed by manipulation of Th17/exTh17 states. Crucially, however, the preliminary investigations presented here did test potential functional changes in memory populations generated following *C.rodentium* infection. A key role of CD4 T cell memory is to rapidly react upon secondary infection. Tcm cells proliferate to give rise to Tfh, Tcm and Teff cell populations (Pepper et al., 2011). Th17-derived Trm cells, on the other hand, have been shown to be the main sources of IL-22 following infection and upon re-challenge (Bishu, Hou, et al., 2019). Whether this response was perturbed by manipulation of costimulation or exTh17 cell differentiation would be of great interest. Moreover, given that mucosal Trm cells exhibiting both Th1 and Th17 cell-like characteristics are key drivers of human diseases (Annunziato et al., 2007; Bishu, El Zaatari, et al., 2019), assessment of their regulation, and differences compared to 'non-pathogenic' Th17 Trm cell counterparts would likely aid the identification of novel therapeutic

avenues. Available literature points to either a combination of IL-7 and IL-15 or IL-7 alone being involved in maintaining mucosal Th17 memory cells (Amezcua Vesely et al., 2019; Chen et al., 2017). The source of these survival factors is unclear but was reported not to include DC (Bishu, Hou, et al., 2019) raising the possibility that mucosal ILC3 may be important.

Having discussed Tcm and Trm cells at length, it is important to note that these studies failed to consider a further key CD4 T cell population. Tfh cells are also generated following *C.rodentium* infection and, given that protection against this pathogen is mediated by IgG responses, play important roles in the orchestration of the immune response (Bai et al., 2020). It is currently unclear whether Th17 and Tfh cells also represent entirely separate lineages following infection. Tfh cells rely on Bcl6 (Johnston et al., 2009; Nurieva et al., 2009; Yu et al., 2009), suggesting that they may not develop from $Id2^+$ Th17 cells. Indeed, studies focusing on Th1 cell responses reported that Tfh and Tcm cells formed from common $CD25^-$ precursors with their eventual fate likely decided by differential TCR affinity for their cognate p:MHCII complexes (Fazilleau et al., 2009; Pepper et al., 2011). However, Th17 cell-derived Tfh cells have been described using IL-17A fate mapper mice (Hirota et al., 2013). Therefore, assessment of antigen-specific *C.rodentium*-induced Tfh cells, along with Id2 and Bcl6 expression cells would be of great interest. As previously mentioned, reagents to identify cells expressing Bcl6 and CXCR5 did not function reliably in the experiments outlined here. Given that these are key Tfh cell markers this is a technical limitation that precluded the identification of 2W1S-specific Tfh cells within these studies.

In conclusion, the use of *C.rodentium-2W1S* shows great potential in aiding the comprehensive assessment of extracellular mucosal infection induced CD4 T cell responses. However, further work is required to confirm the initial observations presented here and to establish methods that enable testing of CD4 Tcm and Trm cell function over time.

CHAPTER 6: DISCUSSION

In this thesis I have presented an integrated investigation of the origin and fate of CD4 T cell populations in the intestine, taking into account cellular plasticity, costimulatory requirements and the role of distinct transcriptional programmes. Through studying the extensive functional plasticity of this CD4 T cell subset I assessed the relationship between mucosal Th17 and Treg cell populations at steady state and in the presence of inflammation, and further tested the regulation of fate decisions through the provision of costimulation. Moreover, I provide a framework for the detailed characterisation of the requirement for key TFs in regulating Th1-like exTh17 differentiation. Finally, through the use of a novel tractable intestinal infection model that enables the study of inflammatory Th17 cells I have started to assess the formation of mucosal pathogen-induced memory CD4 T cell populations.

6.1 TH17 CELLS ARE A PROMINENT BUT HIGHLY PLASTIC MUCOSAL CD4 T CELL POPULATION

In line with published observations, my analyses confirmed that CD4 T cells expressing RORγt were enriched in the intestinal mucosa and its draining mLN compared to the systemic compartment in healthy animals (Ivanov et al., 2006; X. O. Yang, B. P. Pappu, et al., 2008). However, assessment of Th17 cells by IL-17A rather than TF expression returned tissue-specific differences. Even though RORγt is a key Th17 cell lineage-defining TF, production of IL-17A, the canonical Th17 cell cytokine (Harrington et al., 2005; Veldhoen et al., 2006), did not appear to follow the same pattern as TF expression – a high proportion of small intestinal CD4 T cells were found to produce this cytokine compared to a very small percentage in the colon. SFB, a poorly defined class of commensal bacteria known to induce stable homeostatic Th17 populations, reside in the terminal ileum but are excluded from the colon (Ivanov et al., 2009). The SFB colonisation status of the mouse colonies housed at BMSU is unknown, but should it be confirmed, it may explain the high concordance of IL-17A and RORγt expression in the small intestine. Furthermore, other as yet undefined microbial species

inducing stable homeostatic Th17 cell populations may also exist in the mucosal flora of mouse colonies used in the work presented in this thesis. Potential explanations for the low expression of IL-17A in large intestinal RORγt+ CD4 T cells are discussed below.

6.1.1 Th17 cells have lost their ability to produce IL-17A

Development of the different T helper cell subsets is driven by distinct transcriptional pathways (Harrington et al., 2005). In Th17 cells, these are associated with epigenetic modifications resulting in the silencing of Th1- and Th2 cell-associated genes but permissive remodelling Th17 cell-associated cytokine gene loci. However, rather than resulting in stable expression of type 3 cytokines, these fail to prevent post-developmental plasticity, the best-described of which is the acquisition of Th1 cell-like effector functions (Hirota et al., 2011; Lee et al., 2009). Certain Th17 cell populations appeared to exhibit a comparatively low stability with chromatin remodelling rapidly reversed in response to Th1 cell-polarising signals and T-bet- and STAT4-mediated silencing of *Rorc*-driven gene expession (Mukasa et al., 2010). Therefore, I hypothesised that colonic RORγt^{+} cells may have lost IL-17A production due to such environmental signals. However, use of the *Il17a*^{cre}*Ros26*^{tdRFP} fate reporter mice (Hirota et al., 2011) to assess the history of *Il17a* expression revealed only a very small population of colonic CD4 T cells that may at some point have been committed Th17 cells. Furthermore, the expression of IFNγ, a key Th1-associated cytokine, was limited, although not absent, in both colonic and small intestinal CD4 T cells with a history of IL-17A production. Together, *Il17a* mapping and staining for RORγt and IL-17A suggest that, at steady state, Th17 cell transdifferentiation into Th1-like exTh17 cells is not behind the limited IL-17A production in colonic RORγt^{+} CD4 T cells.

Importantly, a small number of Th1-like exTh17 cells, identified as cells with a history of *Il17a* expression but IFNγ production in addition to or instead of IL-17A, were found in both the small intestinal and colonic mucosa. Pathogen invasion is known to be a robust driver of Th1-like exTh17 cell differentiation (Omenetti et al., 2019). The role of Th17 reprogramming towards a Th1 cell-like phenotype at steady state, on the other hand, is not widely studied with most work focusing on the

role of this process in driving disease. The regulation and functional consequences of pathogen-induced exTh17 cell differentiation are discussed later.

6.1.2 RORγt expression in non-Th17 CD4 T cells

Il17a fate mapping established that the vast majority of colonic RORγt$^+$ CD4 T cells were unlikely to be Th17 cell-derived. Importantly, while it is true that RORγt is important in the development of Th17 cells (Ivanov et al., 2006; X. O. Yang, B. P. Pappu, et al., 2008) its expression is not restricted to these but can also mark mucosal pTreg cells. These RORγt$^+$ cells are largely induced in response to harmless commensal microbes and serve to dampen inflammation, such as allergic reactions driven by overactive Th2 cells (Ohnmacht et al., 2015; Sefik et al., 2015). The exact mechanism by which the Th17 cell master TF aids suppressive function is unclear but RORγt-mediated antagonism of T-bet and type 1 effector functions may be a key mechanism (Bhaumik et al., 2021). However, whether this is universal or a mechanism limited to Treg cells present in Th1 cell-polarising environments is unresolved. My data confirming that CD4 T cells expressing the Treg cell lineage-defining TF FoxP3 were highly abundant in the colon but less so in the SILP is consistent with RORγt being expressed predominantly by Treg rather than Th17 cells here in the absence of inflammation. However, a small population of Treg cells with a history of cytokine expression were observed and, in the colon, formed the majority of the tdRFP$^+$ CD4 T cell population. These observations can be explained either by the production of IL-17A by Treg cells or Th17 cell transdifferentiation into exTh17 pTreg cells.

RORγt$^+$ Treg cells are not normally linked to Th17 cell effector cytokine production. In fact, acquisition of a Th17 cell programme is predominantly associated with disease. Skin Treg cells producing IL-17A are reported to lead to increased inflammation and, in humans, are associated with psoriasis and other skin conditions (Remedios et al., 2018). IL-17$^+$ Treg cells were similarly reported to be present in the intestinal mucosa of Crohn's disease patients but not healthy controls (Hovhannisyan et al., 2011), although, given that the suppressive capacity of Treg cells was not affected by IL-17A production, it is unclear whether these cells contribute to pathogenesis. In addition, aberrant Th17 cells effector

programme-driven diseases are not limited to barrier sites. In an animal model of ovarian cancer Treg cells making IL-17A were found to be central to generating a microenvironment permissive of tumour progression (Downs-Canner et al., 2017). Importantly, the IL-17A-producing Treg cells in the tumour were generated not through the activation of the type 3 effector programme in established Treg cells but by Th17-to-Treg cell transdifferentiation. In addition, tumour-associated exTh17 Treg cells were found to be a mixed population with some producing IL-17A but others no longer making this cytokine. In physiological responses Th17-to-Treg cell differentiation, mediated by TGFβ signalling and AhR activation, is a key component of the resolution of acute inflammation (Gagliani et al., 2015).

Given that Th17-derived Treg cells are a normal part of the mucosal CD4 T cell compartment while IL-17A$^+$ Treg cells are mostly linked to pathology, our data identifying intestinal Treg cells with a history of IL-17A expression was consistent with Th17 cell transdifferentiation into Treg cells and a loss of Th17 cell function. However, assessment of active cytokine production revealed the existence of a small population of IL-17A$^+$ Treg cells. Surprisingly, IL-17A production within Treg cells fate reporting *Il17a* expression was lower than in non-Treg (FoxP3$^-$) CD4 T cells with a similar cytokine expression history. These data raised the possibility that I was observing homeostatic Th17-to-Treg cell transdifferentiation. However, in the absence of tracking these cells over time I could not confirm this. Instead, I also assessed Treg cell fate by fate mapping expression of the TF FoxP3. My data suggested that mucosal Treg cells are a highly stable population but the increased turnover of IL-17A-producing Treg cells was consistent with the hypothesis that small numbers of exTh17 pTreg cells were constantly generated. Moreover, combination of *Foxp3* fate mapping with the *C.rodentium* infection model, to induce acute intestinal inflammation, did not reveal Treg-to-Th17 cell differentiation. On balance, my data support a model of low level Th17-to-Treg cell conversion even at steady state while I failed to observe compelling evidence of Treg cells forming Th17 cells (Fig6.1). Importantly, I cannot confirm this in the absence of more sophisticated systems, that enable the tracking of *de novo* generated commensal microbe-derived peptide specific CD4 T cells over time.

6.2 TH17/EXTH17 CONTINUUM

As discussed above, Th1-like exTh17 cell populations were present in the intestine at steady state but only in very small numbers. In fact, expansion of these populations is associated with both mucosal and systemic pathology, making this process and cytokines associated with it key targets of therapeutic interventions.

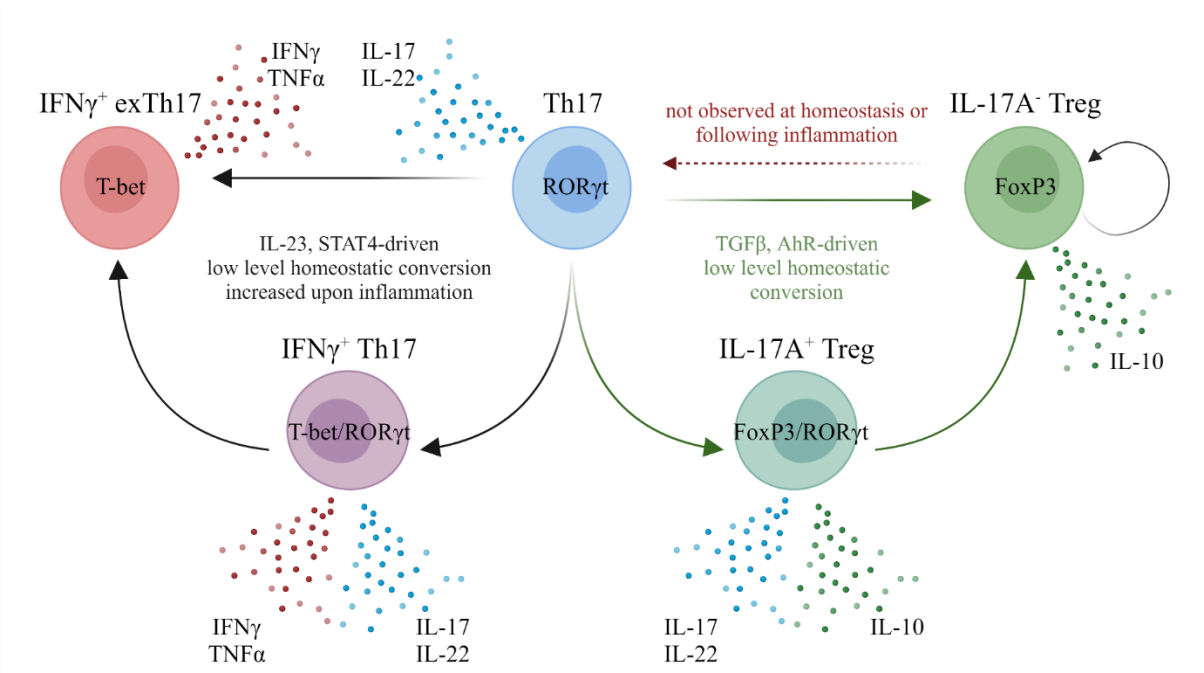

Figure 6.1. Colonic Th17 cell plasticity.
Colonic Th17 cells differentiate into pTreg cells at a low but constant rate while IL-17A$^-$ mucosal Treg form a stable self-renewing population at homeostasis. Minimal Th17 cell acquisition of type 1 effector functions is increased in response to infection giving rise to a spectrum Th1-like exTh17 cells. Images generated with BioRender.com.

6.2.1 Th1-like exTh17 cells in disease

Elevated frequencies of intestinal CD4 T cell co-producing IL-17A and IFNγ or IL-17A and TNFα are associated with increased Crohn's disease severity in humans and shown to be potent drivers of inflammation in animal models of colitis (Annunziato et al., 2007; Bishu, El Zaatari, et al., 2019; Lee et al., 2009). In addition, in a model of periodontitis, IFNγ-producing Th17 cells were found predominantly in CD4 T cell populations isolated from diseased and not from control mice (Dutzan et al., 2018). Furthermore, Th1-like exTh17 cells present away from barrier sites have also been identified as causative agents of diseases previously linked only to the Th1 cell subset (Hirota et al., 2011). The

acquisition of a Th1 cell effector programme is linked to signalling through the IL-23 receptor, although this pathway likely also has important roles in supporting Th17 cell stability (Ahern et al., 2010; Lee et al., 2009; McGeachy et al., 2009). Nonetheless, IL-23 is associated with a range of inflammatory diseases known to involve Th17 and exTh17 cells (Cua et al., 2003; Dutzan et al., 2018; Langrish et al., 2005) and can also aid tumour formation. Whether this occurs in a Th17 cell-mediated manner is unclear (Langowski et al., 2006). These observations identified IL-23 along with both Th17 and Th1 cell-associated cytokines and their receptors as important targets of immunomodulation in a range of autoimmune and inflammatory diseases. However, Th17 and Th1-like exTh17 cell differentiation also form part of normal immune responses. Extracellular mucosal infection-induced Th17 cells occupy the whole Th17/Th1-like exTh17 cell spectrum of phenotypes (Amezcua Vesely et al., 2019; Omenetti et al., 2019). Therefore, targeting Th17 or exTh17 cell functions to treat disease returned mixed results. Blocking IL-23 and IL-17 function was beneficial in the treatment of psoriasis (Bilal et al., 2018). However targeting IL-17A or IL-17R in Crohn's disease had such serious adverse effects that clinical trials were halted early (Hueber et al., 2012; Targan et al., 2016), likely reflecting inadvertent inhibition of pathways central to the control of commensal bacteria (Ivanov et al., 2009; Liang et al., 2006). Instead, TNF antagonists have become the mainstay of inflammatory bowel disease treatment. However, these fail in over a third of patients with non-responders less likely to ever achieve remission even with alternative therapies (Hyams et al., 2007; Papamichael et al., 2015; Singh et al., 2018).

Partly underlying the difficulty in developing appropriate treatments, the regulation of Th1-like exTh17 cell differentiation appears to be highly context-specific and the exact differences between pathogenic and homeostatic Th17 and exTh17 cell populations are incompletely understood. T-bet is crucial for Th1 cell development (Szabo et al., 2000) and is upregulated in Th17 cells upon acquisition of Th1 cell-like function in a STAT4- and potentially IL-23-dependent manner (Lee et al., 2009). However, the requirement for this TF in the emergence of disease-associated IFNγ^{+} Th17/exTh17 cells is mixed. Transfer models of diabetes showed rapid upregulation of both T-bet and IFNγ in Th17 cells (Bending et al., 2009) and pointed to complete loss of IL-17A production and conversion into fully

mature Th1-like exTh17 cells being required for progression from inflammation to disease (Martin-Orozco et al., 2009). Similarly, T-bet deletion in T cells prevented the induction of experimental autoimmune encephalomyelitis (EAE) in animal models of multiple sclerosis in one study (Bettelli et al., 2004). A potential explanation for this protective effect is the reported inability of Th17 cells to acquire any IFNγ expression in the absence of T-bet (Brucklacher-Waldert et al., 2016). Interestingly, however, a distinct study assessing the same process returned conflicting results with the induction of both IFNγ^{+} Th17 cells and disease despite T-bet deletion (Duhen et al., 2013). Importantly, these studies differed in their method of T-bet ablation with the latter targeting a wider set of immune cells. Nonetheless, these reports highlighted the importance of potential environmental cues in the regulation of Th1-like exTh17 cell generation. Strengthening this observation, mice that were unable to generate IFNγ^{+} Th17 cells in EAE did not show the same defect in response to pathobiont colonisation, a different proinflammatory stimulus (Brucklacher-Waldert et al., 2016). Furthermore, as the observation reported in this thesis that TNFα and IFNγ expression may be regulated differently, with TNFα co-expressed with IL-17A even at steady state, demonstrated, even populations within the currently defined stages of the Th17/exTh17 spectrum exhibit considerable and unexplored heterogeneity. Building on previous work assessing the regulation of ILC3 and exILC3 regulation, I sought to establish models that could help develop a better understanding of transcriptional networks controlling Th1-like exTh17 cell differentiation and function.

First, I assessed the spectrum of Th17 cells arising from *C.rodentium* infection. Splitting the Th17/exTh17 continuum into 3 stages based on IL-17A and IFNγ or RORγt and T-bet expression, I and others have found that the infection gave rise to CD4 T cells of all three phenotypes (Fig6.1). Importantly, as reported in the case of ILC3 plasticity, further TFs may play key roles in supporting the balance between type 3 and type 1 effector functions (Fiancette et al., 2021). The potential contribution of other TFs to Th17/exTh17 cell function is understudied. Given this lack of clarity in post-developmental requirement for TF expression, I assessed the response following combinatorial deletion of ROR family TFs and T-bet.

6.2.2 Reciprocal ROR family TF/T-bet antagonism regulates Th17 cell fate and function

My results have shown that in addition to playing key roles in Th17 cell development (Ivanov et al., 2006; X. O. Yang, B. P. Pappu, et al., 2008), RORγt and RORα also actively support Th17 cell function. Type 3 cytokine expression was impaired following RORγt deletion but recovered when T-bet was also absent, consistent with antagonism between and the balance of the two TFs being a key determinant of Th17 cell function (Lazarevic et al., 2011). However, added loss of RORα abrogated this effect. Together, these data confirmed, for the first time, that RORα is capable of supporting Th17 cell function, not just development. However, whether this represents functional redundancy or synergy is unclear and cannot be resolved in the absence of mouse models lacking RORα only in Th17 cells. The investigations presented in this thesis would have benefited from the additional generation of mouse strains deleting RORα but not RORγt or T-bet upon Th17 cell induction.

In addition to establishing a role for RORα and demonstrating that RORγt represses T-bet activity, my data suggest that ROR family TFs also directly activate Th17 cell-associated gene expression. Should this not be the case, deletion of all three TFs would have been expected to result in a return to normal type 3 cytokine production. These results are consistent with reported roles for the RORγt/RORα/T-bet transcription factor networks in the regulation of other CD4 T cell and innate lymphoid cell populations (Bhaumik et al., 2021; Fiancette et al., 2021; Stehle et al., 2021).

Upon assessing the effects of T-bet deletion on the ability of Th17 cells to produce IFNγ, I observed no overall impairment but an apparent arrest in the 'intermediate' IFNγ$^+$ Th17 cell phase and an inability to completely switch off IL-17A production. Importantly, this work was carried out using similar models to studies reporting comparison of EAE- and microbe-induced exTh17 cell T-bet dependence and is therefore directly comparable (Brucklacher-Waldert et al., 2016). Together, these observations suggest that in the context of intestinal inflammation induced by a broader range of bacteria, some Th17 cells are primed to produce IFNγ in a T-bet-independent manner but rely on this TF for differentiation into 'fully mature' IL-17A$^-$ INFγ$^+$ exTh17 (Fig6.2). A potential interpretation of my data

is that subpopulations of Th17 cells are programmed to switch on both Th17 and Th1 cell effector programmes and can do this independently of post-developmental TF expression. However, in these cells T-bet expression above a certain threshold can result in inhibition of ROR family TF-mediated *Il17a* expression. Alternatively, it is possible that T-bet can directly drive remodelling of Th17 cell-associated gene loci and thus promoting downregulation of the Th17 cell effector programme (Fig6.2). Overall, my data are consistent with reported T-bet mediated suppression of type 3 function (Intlekofer et al., 2008; Lazarevic et al., 2011).

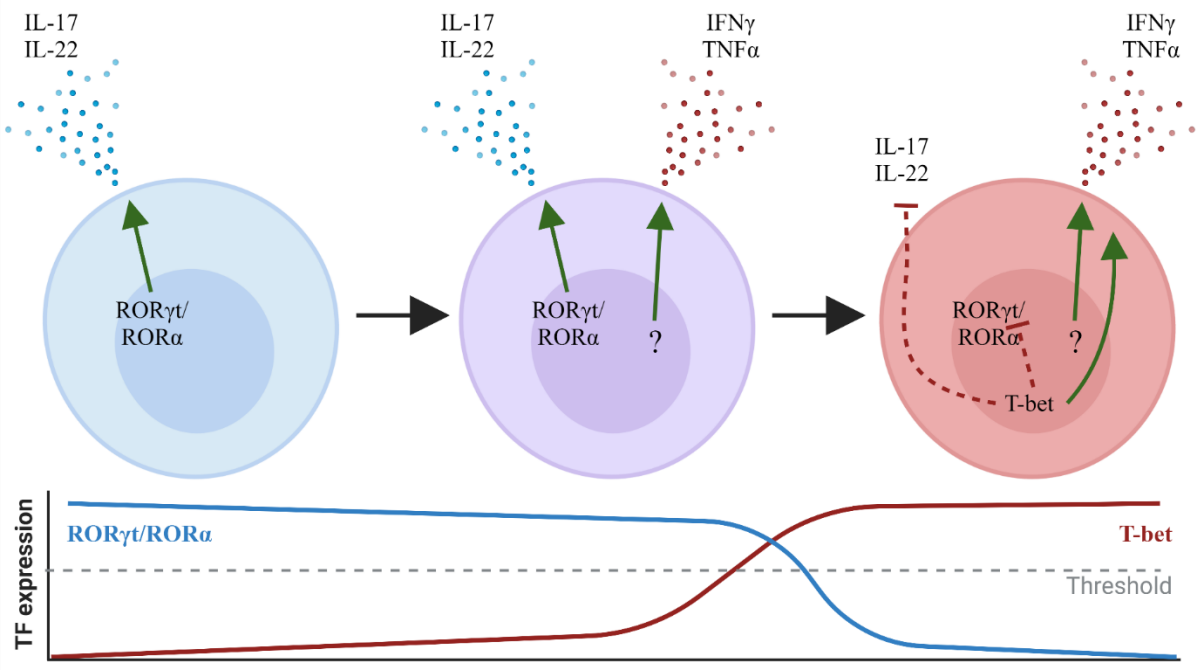

Figure 6.2. The interplay of ROR family TFs and T-bet guide Th1-like exTh17 cell differentiation. ROR family TF-driven Th17-associated cytokine expression is replaced by Th1 cell effector functions, partly supported by unidentified mechanisms. Gradually increasing T-bet expression levels may reach a threshold above which inhibition of Th17 cell TFs and effector functions facilitates the differentiation of fully mature exTh17 cells. Images generated with BioRender.com.

Importantly, the signals that maintain Th17 cells in the intermediate stage or push them towards fully mature exTh17 cells are not well-defined. In addition, my data leave open the possibility that functional redundancy exists between Th1 cell-associated TFs, such as T-bet and Eomes, and results in unperturbed IFNγ expression in T-bet-deficient Th17 cells. To specifically address the potential redundancy between T-bet and Eomes, conditional deletion of both in Th17 would be an important

further line of investigation (Y. Yang et al., 2008). Mouse models that would enable conditional Cre-mediated deletion of Eomes are available (Intlekofer et al., 2008; Y. Zhu et al., 2010) but the COVID-19 pandemic-related facility closure prevented their within our animal colonies. Furthermore, the availability of mice fate mapping IFNγ production, models that produce Cre under the control of the *Ifng* promoter, may enable targeting of the later stages of the Th17/exTh17 spectrum and thus allow specific assessment of key TFs' contribution to the regulation of IFNγ$^+$ Th17 and exTh17 cells. However, this approach would lose *Il17a* fate mapping, a key tool in the analyses presented here. Given that we observed induction of Th17 and potentially Th1 cell populations in response to *C.rodentium* infection, this is a key issue that must be resolved if IFNγ-driven TF deletion is to be assessed. Experimental systems that enable parallel and specific fate mapping of multiple targets have been described but their efficiency has not been tested extensively *in vivo* (Anastassiadis et al., 2009; Karimova et al., 2018).

The exact role IFNγ production, either in conjunction with or in the absence of IL-17A, has not yet been teased apart in Th17 cell-skewed responses. Possibly, IFNγ may simply serve to aid the clearance of recruited innate lymphoid cells following pathogen expulsion. Th17 cells efficiently recruit large numbers of neutrophils to the site of infection following their induction in a process that is crucial to appropriate pathogen control (Liang et al., 2007; Ye et al., 2001). Neutrophil recruitment, function and clearance are tightly regulated processes, as prolonged presence of apoptosing cells is highly damaging to the surrounding tissue (Fadok et al., 2001). Neutrophils are cleared by phagocytic macrophages, the function of which is improved in the presence of IFNγ (MacMicking, 2012). This process was shown to be important in *C.rodentium* infection but mice unable to produce IFNγ in any immune cells showed further impairments in resistance to and clearance of bacteria (Shiomi et al., 2010). Moreover, IFNγ was found to be crucial for the production of protective IgG responses (Shiomi et al., 2010), although the cellular source of IFNγ was not identified. Crucially, my early observations using the *C.rodentium* infection model do not exclude the induction of Th1 cells in addition to Th17

cells. Since no TF deletion I tested here resulted in a loss of IFNγ production in Th17 cells I am currently unable to test the contributions of Th17/exTh17 cell-derived IFNγ and *bona fide* Th1 cell IFNγ.

In summary, through this body of work, I evaluated a novel set of mouse models and established that these can serve to force or block exTh17 cell differentiation. I anticipate that these models will prove a key resource in better understanding not only the regulation of this process but also the functional heterogeneity within each currently defined stage of the spectrum. However, the work presented in this thesis focused on infection-induced colonic Th17 cells, ignoring key homeostatic populations. Results revealed identified striking differences in the composition of the microbiome even in the absence of infection, likely contributing to strain-specific changes in susceptibility to and clearance of *C.rodentium* infection. Small intestinal Th17 cells are induced in response to commensal microbes and are crucial to their control. Importantly, IL-17A production is not limited to Th17 cells. Subpopulations of ILC3s produce IL-17A in the intestine and play important roles in shaping the mucosal microbiome (Aparicio-Domingo et al., 2015; Satoh-Takayama et al., 2008). ILC3 regulation shares many features of Th17 cell biology described in this thesis (Fiancette et al., 2021) and alterations of ILC3 phenotype driven by TF deletion may contribute to dysbiosis. Therefore, my preliminary observations on strain-specific differences in the composition of the microbiota likely reflect a combined effect perturbed homeostatic Th17 cell and ILC3 function. These changes could have significant implications on human health – interactions with the microbiome can determine whether a pathogen is able to colonise its host (Curtis et al., 2014; Ghosh et al., 2011; Ivanov et al., 2009; Mullineaux-Sanders et al., 2017) and how fast it is then cleared (Kamada et al., 2012; Kamada et al., 2015). In addition, these interactions drive resistance or susceptibility to inflammation (Dutzan et al., 2018; Neumann et al., 2019). Assessment of intestinal inflammation through pharmacologically induced colitis models would complement the study of responses to pathogens and potentially pinpoint currently unidentified homeostatic Th17 cell-targeted effects.

Should future work using these models yield any therapeutic targets, it is imperative that the effects of any modifications are assessed across multiple barrier sites and immune cell populations to limit the potential of adverse effects such as dysbiosis or opportunistic pathogen invasion.

6.3 CD4 T CELL MEMORY IN THE INTESTINAL MUCOSA

My and others' assessment of intestinal cytokine production following *C.rodentium* infection revealed that a heterogeneous Th17 cell response associated with a spectrum of Th1 cell-like functions is generated. However, Th17 cell-derived tissue resident memory is understudied compared CD8 T cell or even Th1 cell memory. Elegant studies have recently shown that *Klebsiella pneumoniae* infection of the lung resulted in the formation of Th17 Trm cells with a small but not negligible population of IFNγ-producing cells also retained in the lungs (Amezcua Vesely et al., 2019). In addition, mixed Th17/Th1-like CD4 T cells are present in humans (Annunziato et al., 2007) where they are associated with intestinal and systemic inflammation. Importantly, chronic intestinal inflammation was shown to be driven by Trm rather than alternative T cell populations (Zundler et al., 2019). Together, these reports suggest that *C.rodentium*-induced Th17 and exTh17 cells have the capacity to enter the tissue resident memory pool regardless of their effector profile. Indeed, recent work has shown that *C.rodentium* does drive Trm cell formation but, surprisingly, identified IL-22 expression as the primary function of antigen-specific cells retained in the intestine (Bishu, Hou, et al., 2019). However, the work presented here showed that fully mature exTh17 cells had only a limited ability to make this cytokine. How these observations tie into exTh17 Trm cell formation and the presence of IFNγ or $TNF\alpha^{+}$ Th17 Trm cells in disease is highly relevant to human health but has not yet been addressed in detail. The study assessing *C.rodentium* infection-induced Trm cell formation presented preliminary functional findings only while assessment of lung Trm cells following *K.pneumoniae* would have benefitted from identification of cells responding to pathogen-derived antigens. The work presented in this thesis provides the first initial characterisation of a tractable natural intestinal infection model that has the potential to greatly accelerate the study of mucosal CD4 Trm cell formation and function.

6.3.1 *C.rodentium*-induced Trm cells form a heterogeneous population

Basic phenotyping revealed that CD4 T cells retained in the intestine for up to 5 weeks were heterogeneous for IL-17A expression history. Interestingly, I failed to identify a link between residency marker and cytokine expression, whether assessed using lineage tracing mouse models or through *ex vivo* restimulation for active IL-17A and IFNγ production. A potential explanation of this observation is that *C.rodentium*-induced Trm cells are derived from multiple CD4 T cell subsets rather than only Th17 cells. As previously mentioned, I have not directly tested whether Th1 cells that never go through a Th17 cell phase are also generated and populate the intestine in response to infection. Early reports assessing this infection model attributed the majority of *C.rodentium*-induced CD4 T cell function to Th1 cells (Higgins et al., 1999) but this was prior to the identification of Th17 cells as a separate lineage and did not take into account Th17 cell conversion into Th1 cells, now a known feature of this model (Omenetti et al., 2019). Combined use of our *Il17a* and *Ifng* fate reporter mouse strains with the tractable infection model has the potential to greatly increase our understanding of the contribution of distinct Teff cell populations to the *C.rodentium*-induced Trm cell pool. A further possibility is that my method of assessing residency was simply too crude. Even though CD69 is a Trm cell marker on both CD4 and CD8 T cells it is also expressed on the majority of intestinal lymphocytes that are not retained long-term (Amezcua Vesely et al., 2019; Bishu, Hou, et al., 2019). In addition, it is important to note that in the absence of extended and detailed analysis of the kinetics of the antigen-specific CD4 T cell response to *C.rodentium* I cannot be certain that the endpoint (day 35) represented a true memory phase. Confirmation of contraction and stabilisation of antigen-specific cell numbers over time would aid this work. Therefore, functional testing of residency over time course studies is key to better understanding mucosal Teff cell entry into the Trm cell pool. Functional studies could include FTY720 treatment (Matloubian et al., 2004) to block LN-derived lymphocyte entry into the mucosa. In addition, photoactivated labelling of the intestine in Kaede animals would enable monitoring of lymphocyte trafficking *in vivo* by distinguishing cells originating in the intestine from those newly entering by the presence of a red dye (Tomura et al., 2008). A slight drawback of this approach is that

the label decays over the duration of up to 7 days, thus limiting the period over which residency can be assessed. Finally, parabiosis experiments are highly informative in the assessment of true tissue residency as well as the functional contributions of Trm cells to protection from reinfection (Amezcua Vesely et al., 2019). However, such experiments are technically challenging and not routinely carried out at institutes across the United Kingdom. Combined, our infection models, pharmacological inhibition of lymphocyte migration and photoconversion of the intestinal mucosa are powerful tools that will enable this response to be teased apart in great detail.

Trm cells, like all memory cells generated in response to pathogens, are primarily tasked with preventing re-infection. It was thought that these cells functioned as highly efficient Teff cells acting in a near-sentinel-like manner, rapidly responding to TCR stimulation not constrained by Treg cell-mediated suppression (Bartolome-Casado et al., 2019; Masopust et al., 2010). More recently, further roles have also been linked to Trm cells (Fonseca et al., 2020). Assessment of recall responses within our infection model would therefore be of great interest. However, anti-*C.rodentium* antibody responses generated following primary infection would likely confound simple reinfection studies (Bai et al., 2020). Adoptive transfer of Trm cells isolated from the intestine of infected mice into allotypically marked uninfected hosts could overcome this limitation. Importantly, intravenous transfer of cells may result in distribution of cells to microenvironments other than the intestinal mucosa. Therefore, direct transfer into the colon wall would be desirable. Endoscopically guided injection of cells intro the colon wall of mice is a novel tool that is currently predominantly used for the deposition colorectal tumour cells (Chen et al., 2020) but could in theory also aid immune cell transfer.

Isolation of Trm cells requires confident identification of antigen-specific CD4 T cells that were retained in the intestine. Interestingly, my data revealed additional phenotypic heterogeneity with at least two populations distinguished by residency marker expression. $CD69^{+}$ cells not expressing CD103 made up the majority of the antigen-specific intestinal CD4 T cell pool in mice generating unperturbed

responses but a small CD103$^+$ population was also identified. This was an unexpected observation as CD103 is associated with exit from the LP and entry into the IEL layer of the mucosa (Karecla et al., 1995; Kilshaw & Baker, 1988). Moreover, the small number of studies assessing mucosal CD4 Trm reported that these cells expressed CD69 but not CD103 (Amezcua Vesely et al., 2019; Bishu, Hou, et al., 2019). Given that no additional biological functions have been described for CD103, it is possible that different Trm cells occupy distinct niches with CD103$^+$ cells found in close contact with the epithelium. This is a hypothesis easily tested through immunohistochemistry. Strikingly, the data presented here tentatively suggested that perturbations of the Th17/exTh17 spectrum affected residency marker expression. Further analysis of Trm cell function is crucial in teasing apart the potential consequences of these observations.

6.3.2 Memory CD4 T cells also populate the lymphoid tissue

Using the novel *C.rodentium-2W1S* infection model I was able to show that the mucosa harbours large numbers of antigen-specific CD4 T cells even after the expected clearance of bacteria. In addition, I have begun to assess the formation of tissue resident memory cells and the effects of Th17 cell plasticity on this process. This work focused on the intestinal mucosa and therefore likely captured the effector arm of the response. However, antigen-specific CD4 T cells were also present in lymphoid tissue. Strikingly, early in the response IL-17A-production history appeared limited to the effector sites and it was practically absent in peripheral lymphoid tissue (2LT excluding the intestine-draining mLN), where CD62L$^+$ Tcm-like cells were enriched. These data were consistent with early divergence of Teff and Tcm cell fates and aligned with observations made in a systemic Th1 cell-skewed infection model (Pepper et al., 2011). Surprisingly, we found that over time, cells showing a history of IL-17A production became more widely distributed. Together, these data raised the possibility that recirculating Tcm-like cells could be generated from both non-Th17 and Th17 cells precursors at different points in the response to *C.rodentium* colonisation. However, CD62L expression did not support this hypothesis. Importantly, CD62L is a suboptimal marker of Tcm cells and future work must

focus on the development of alternative, more reliable methods such as lineage tracing or reporting of the TF Bcl6 and chemokine receptor CXCR5 (Pepper et al., 2011). Since both Bcl6 and CXCR5 are also expressed on Tfh cells, further phenotyping to distinguish this subset from true Tcm cells would also be needed. Furthermore, adoptive transfer via intravenous injection followed by *C.rodentium-2W1S* challenge would aid the study of recall responses.

Upon challenge, Tcm cells are able to generate further Tcm cells but also give rise to Tfh and Teff cells, thus linking the two arms of the response (Ciucci et al., 2019). Moreover, CD8 Trm cells have recently been found to also generate both effector and Tcm cells upon reactivation (Fonseca et al., 2020). The observation that tdRFP^{+} antigen-specific CD4 T cells (most likely Th17 or exTh17 cells) entered peripheral lymphoid tissues suggested that even within our model, effector and central memory cells may not form completely distinct populations. However, Trm cells were not reactivated, therefore, these observations are not necessarily comparable to those reporting the emergence of CD8 Trm cell-derived Tcm cells. Adoptive transfer of the two memory populations, as described above, would likely provide at least a partial answer as to their function and progeny upon challenge. Furthermore, transferring Trm and Tcm cells separately would also likely identify potential overlap in their functions. However, in unmanipulated animals both of these populations exist and their functions likely not only overlap but also synergize with one another. Therefore, co-transfer of Trm cells directly into the colon wall and Tcm cells into the circulation may prove a really exciting novel approach in assessing how Trm and Tcm cell functions integrate in a healthy mouse.

Should Teff cells that can enter the Tcm cell pool either during the primary response or via Trm cell differentiation in secondary infection be identified, the impact of manipulating exTh17 cell differentiation must be assessed. It is currently unclear whether Teff and Trm cells generated from distinct stages of the Th17/exTh17 spectrum show differential predisposition towards certain fates but could easily be addressed by combination of our TF-deleting models and the modified *C.rodentium*.

6.4 THE OX40:OX40L PATHWAY IN CONTROLLING MUCOSAL CD4 T CELL FATE AND FUNCTION

Combined use of Th17 and Treg cell linage tracing with a natural mucosal infection model enabled extensive characterisation of the intestinal CD4 T cell compartment both at steady state and during inflammation. Combinatorial TF deletion aided assessment of the requirement for continued expression of key lineage-defining TFs in supporting Th17 and Th1-like exTh17 cell function. Following initial characterisation of our mouse models, I have also established a platform, using *C.rodentium-2W1S*, that will enable detailed study of the CD4 T cell memory compartment generated in response to mucosal infection. Through this work, I have identified microenvironment-specific cell fate decisions, such as the dominance of homeostatic Th17 cells in the small intestine but Treg cells in the colon. As outlined earlier, appropriate regulation of fate decisions is imperative not only to the maintenance of the mucosal barrier but also the control of pro-inflammatory and suppressive functions of mucosal immune populations. Perturbations of this intricate balance are associated with a multitude of diseases but how cell fate decisions are controlled in the mucosa is incompletely understood.

The OX40:OX40L pathway plays key roles in the regulation of both Treg and Th17 responses. However, reported results are often contradictory. OX40 was found to be crucial in promoting both Treg cell function and survival in animal models of colitis (Griseri et al., 2010; Piconese et al., 2010). However, the same pathway was found to inhibit Treg cells in the tumour microenvironment (Piconese et al., 2008). Linking the two key CD4 T cell populations, OX40 signalling was reported to result in diminished IL-17A expression within skin-resident Treg cells (Remedios et al., 2018). On the other hand, OX40 was also specifically linked to the effector arm of pathogen-induced responses with previous work identifying compartmentalised provision of OX40L as a key difference between systemic and mucosal immune responses (Gajdasik et al., 2020). However, even in effector Th17 cell responses, OX40 signalling can have mixed effects – even though Th17 cell-driven inflammation was exacerbated in a

model of uveitis, EAE-associated Th17 cell function was inhibited by the activation of the OX40:OX40L pathway (Xiao et al., 2016; Zhang et al., 2010)

The work presented here revealed a small and likely microbiota-dependent defect in the accumulation of intestinal Treg cell in the absence of OX40. Even though the provision of costimulation is expected to occur in the context of antigen presentation, I found that OX40L expression on DCs, the 'professional' APCs, failed to phenocopy total OX40-deletion. However, my data were consistent with a non-redundant role for ILC3 OX40L in supporting mucosal Treg cell populations. Due to mouse breeding strategies these experiments lacked optimal control animals. Nonetheless, these observations aligned with previous reports showing that systemic and mucosal Th1 cells relied on DC and ILC3 OX40L, respectively (Gajdasik et al., 2020).

Whether thymic Treg or pTreg cells were more likely to be affected by OX40 deletion was not tested. In addition, the loss of a small but clear phenotype, possibly induced by responses to a changing microbiota (Al Nabhani et al., 2019; Miragaia et al., 2019), highlighted the fact that my approach did not take the heterogeneity of the mucosal Treg cell population into consideration. More sophisticated experimental systems may be better suited to further analysis of Treg OX40L requirements. *H.hepaticus* colonisation enables tracking of a newly generated pTreg cell population (Xu et al., 2018) and may prove useful in the assessment of the role the OX40:OX40L pathway plays in mucosal Treg cell regulation. However, it is currently unclear whether *H.hepaticus*-induced Treg cells form part of the OX40-dependent mucosal Treg cell population.

In summary, this costimulatory pathway has limited but clear effects on Treg cell persistence in the intestine. Conversely, my assessment of the effector Th17 cell responses was hampered by low sample sizes. Therefore, all conclusions presented here a tentative and require further confirmation. Nonetheless, I observed a potential defect in the clearance of bacteria in the absence of OX40L on either DCs or ILC3. Potential explanations for this are a diminished effector response, defective circulating Tcm-like or Tfh cell generation or a global defect in the activation or survival of *C.rodentium*-

induced CD4 T cells. Suboptimal generation of effector responses around the peak of the infection was consistent with a role for OX40 in supporting the effector arm of the response. Therefore, I hypothesised that OX40L provision may also be key to the regulation of CD4 Trm generated following infection. Making use of the *C.rodentium-2W1S* infection model to enable assessment of the memory response, I observed an overall reduction in the number of responding cells in mice lacking OX40L on either DC or ILC3. Interestingly, however, the proportion of Tcm-like cells within the mLN increased with OX40L deletion. These observations, if confirmed on further repeats, could be explained by a reduction in cells of an effector phenotype. Moreover, alteration of CD103 expression similar to that observed upon manipulation of ROR family TF and T-bet antagonism was evident in mice lacking OX40L. However, linking this to either DC or ILC3 OX40L with confidence is not currently possible. Taken together, these tentative observations are consistent with OX40L playing a role mainly in supporting the effector arm of the response to *C.rodentium*. Whether clear differences would be maintained even after contraction of the response remains untested. Furthermore, it is currently unclear whether the small drop in IFNγ production in response to *C.rodentium* infection in $OX40^{-/-}$ animals reflected a specific defect in Th1-like exTh17 cell differentiation or overall impairment of the effector response.

6.5 CONCLUDING REMARKS

The gastrointestinal tract is a key immune environment tasked with responding to a deluge of microbial, environmental and dietary antigens. Homeostasis is achieved by the dynamic interactions of the intestinal epithelium, commensal microbes and mucosal immune populations. Th17 cells are central to the maintenance of this balance and, when dysregulated, are associated with both mucosal and systemic inflammatory diseases. Despite their relevance to human health, little is understood about the regulation of Th17 cell fate and function long-term. Thus, the success of Th17 cell-targeted therapies is impeded. Through the investigations presented in this thesis we took multiple complementary approaches to begin to address this gap in our understanding and to establish a set

of novel experimental tools that, together, will enable the first detailed characterisation of Th17 cell regulation.

These investigations provide evidence that intestinal lamina propria Treg cells are a highly stable population with only negligible transdifferentiation into Th17 cells, if any. Conversely, Th17 cells exhibit a high degree of plasticity with some conversion into both Treg and Th1 cells even in the absence of infection. Here, I assessed the transcriptional regulation of Th17 cell conversion into Th1-like cells and identified post-developmental and integrated roles for three key TFs. Finally, I present an exciting new experimental model and show that it captures the entire CD4 memory compartment generated following a mucosal infection, enabling the assessment of costimulatory requirements and forced plasticity in the memory response.

Crucially, I anticipate that combination of our animal and infection models will provide a robust platform for the study of Th17 and exTh17 cell function and fate. Specifically, these models provide the opportunity to build a clear picture of the CD4 T cell memory populations arising from mucosal infection and enable detailed analysis of their regulation. These findings have the potential to not only advance our basic understanding of mucosal T cell biology but also improve human health through a better characterising disease pathogenesis.

LIST OF REFERENCES

Abreu, M. T. (2010). Toll-like receptor signalling in the intestinal epithelium: how bacterial recognition shapes intestinal function. *Nat Rev Immunol*, *10*(2), 131-144. https://doi.org/10.1038/nri2707

Adachi, O., Kawai, T., Takeda, K., Matsumoto, M., Tsutsui, H., Sakagami, M., Nakanishi, K., & Akira, S. (1998). Targeted disruption of the MyD88 gene results in loss of IL-1- and IL-18-mediated function. *Immunity*, *9*(1), 143-150. https://doi.org/10.1016/s1074-7613(00)80596-8

Afkarian, M., Sedy, J. R., Yang, J., Jacobson, N. G., Cereb, N., Yang, S. Y., Murphy, T. L., & Murphy, K. M. (2002). T-bet is a STAT1-induced regulator of IL-12R expression in naive CD4+ T cells. *Nat Immunol*, *3*(6), 549-557. https://doi.org/10.1038/ni794

Aggarwal, S., Xie, M. H., Maruoka, M., Foster, J., & Gurney, A. L. (2001). Acinar cells of the pancreas are a target of interleukin-22. *J Interferon Cytokine Res*, *21*(12), 1047-1053. https://doi.org/10.1089/107999001317205178

Ahern, P. P., Schiering, C., Buonocore, S., McGeachy, M. J., Cua, D. J., Maloy, K. J., & Powrie, F. (2010). Interleukin-23 drives intestinal inflammation through direct activity on T cells. *Immunity*, *33*(2), 279-288. https://doi.org/10.1016/j.immuni.2010.08.010

Ahmad-Nejad, P., Hacker, H., Rutz, M., Bauer, S., Vabulas, R. M., & Wagner, H. (2002). Bacterial CpG-DNA and lipopolysaccharides activate Toll-like receptors at distinct cellular compartments. *Eur J Immunol*, *32*(7), 1958-1968. https://doi.org/10.1002/1521-4141(200207)32:7<1958::AID-IMMU1958>3.0.CO;2-U

Akimzhanov, A. M., Yang, X. O., & Dong, C. (2007). Chromatin remodeling of interleukin-17 (IL-17)-IL-17F cytokine gene locus during inflammatory helper T cell differentiation. *J Biol Chem*, *282*(9), 5969-5972. https://doi.org/10.1074/jbc.C600322200

Akira, S., & Takeda, K. (2004). Toll-like receptor signalling. *Nat Rev Immunol*, *4*(7), 499-511. https://doi.org/10.1038/nri1391

Al Nabhani, Z., Dulauroy, S., Marques, R., Cousu, C., Al Bounny, S., Dejardin, F., Sparwasser, T., Berard, M., Cerf-Bensussan, N., & Eberl, G. (2019). A Weaning Reaction to Microbiota Is Required for Resistance to Immunopathologies in the Adult. *Immunity*, *50*(5), 1276-1288 e1275. https://doi.org/10.1016/j.immuni.2019.02.014

Amadi-Obi, A., Yu, C. R., Liu, X., Mahdi, R. M., Clarke, G. L., Nussenblatt, R. B., Gery, I., Lee, Y. S., & Egwuagu, C. E. (2007). TH17 cells contribute to uveitis and scleritis and are expanded by IL-2 and inhibited by IL-27/STAT1. *Nat Med*, *13*(6), 711-718. https://doi.org/10.1038/nm1585

Amakawa, R., Hakem, A., Kundig, T. M., Matsuyama, T., Simard, J. J., Timms, E., Wakeham, A., Mittruecker, H. W., Griesser, H., Takimoto, H., Schmits, R., Shahinian, A., Ohashi, P., Penninger, J. M., & Mak, T. W. (1996). Impaired negative selection of T cells in Hodgkin's disease antigen CD30-deficient mice. *Cell*, *84*(4), 551-562. https://doi.org/10.1016/s0092-8674(00)81031-4

Amezcua Vesely, M. C., Pallis, P., Bielecki, P., Low, J. S., Zhao, J., Harman, C. C. D., Kroehling, L., Jackson, R., Bailis, W., Licona-Limon, P., Xu, H., Iijima, N., Pillai, P. S., Kaplan, D. H., Weaver, C. T., Kluger, Y., Kowalczyk, M. S., Iwasaki, A., Pereira, J. P., Esplugues, E., Gagliani, N., & Flavell, R. A. (2019). Effector TH17 Cells Give Rise to Long-Lived TRM Cells that Are Essential for an Immediate Response against Bacterial Infection. *Cell*, *178*(5), 1176-1188 e1115. https://doi.org/10.1016/j.cell.2019.07.032

Anastassiadis, K., Fu, J., Patsch, C., Hu, S., Weidlich, S., Duerschke, K., Buchholz, F., Edenhofer, F., & Stewart, A. F. (2009). Dre recombinase, like Cre, is a highly efficient site-specific recombinase in E. coli, mammalian cells and mice. *Dis Model Mech*, *2*(9-10), 508-515. https://doi.org/10.1242/dmm.003087

Annunziato, F., Cosmi, L., Santarlasci, V., Maggi, L., Liotta, F., Mazzinghi, B., Parente, E., Fili, L., Ferri, S., Frosali, F., Giudici, F., Romagnani, P., Parronchi, P., Tonelli, F., Maggi, E., & Romagnani, S. (2007). Phenotypic and functional features of human Th17 cells. *J Exp Med*, *204*(8), 1849-1861. https://doi.org/10.1084/jem.20070663

Aparicio-Domingo, P., Romera-Hernandez, M., Karrich, J. J., Cornelissen, F., Papazian, N., Lindenbergh-Kortleve, D. J., Butler, J. A., Boon, L., Coles, M. C., Samsom, J. N., & Cupedo, T. (2015). Type 3 innate lymphoid cells maintain intestinal epithelial stem cells after tissue damage. *J Exp Med*, *212*(11), 1783-1791. https://doi.org/10.1084/jem.20150318

Archer, N. K., Adappa, N. D., Palmer, J. N., Cohen, N. A., Harro, J. M., Lee, S. K., Miller, L. S., & Shirtliff, M. E. (2016). Interleukin-17A (IL-17A) and IL-17F Are Critical for Antimicrobial Peptide Production and Clearance of Staphylococcus aureus Nasal Colonization. *Infect Immun*, *84*(12), 3575-3583. https://doi.org/10.1128/IAI.00596-16

Artis, D., Wang, M. L., Keilbaugh, S. A., He, W., Brenes, M., Swain, G. P., Knight, P. A., Donaldson, D. D., Lazar, M. A., Miller, H. R., Schad, G. A., Scott, P., & Wu, G. D. (2004). RELMbeta/FIZZ2 is a goblet cell-specific immune-effector molecule in the gastrointestinal tract. *Proc Natl Acad Sci U S A*, *101*(37), 13596-13600. https://doi.org/10.1073/pnas.0404034101

Atarashi, K., Tanoue, T., Ando, M., Kamada, N., Nagano, Y., Narushima, S., Suda, W., Imaoka, A., Setoyama, H., Nagamori, T., Ishikawa, E., Shima, T., Hara, T., Kado, S., Jinnohara, T., Ohno, H., Kondo, T., Toyooka, K., Watanabe, E., Yokoyama, S., Tokoro, S., Mori, H., Noguchi, Y., Morita, H., Ivanov, II, Sugiyama, T., Nunez, G., Camp, J. G., Hattori, M., Umesaki, Y., & Honda, K. (2015). Th17 Cell Induction by Adhesion of Microbes to Intestinal Epithelial Cells. *Cell*, *163*(2), 367-380. https://doi.org/10.1016/j.cell.2015.08.058

Baba, M., Imai, T., Nishimura, M., Kakizaki, M., Takagi, S., Hieshima, K., Nomiyama, H., & Yoshie, O. (1997). Identification of CCR6, the specific receptor for a novel lymphocyte-directed CC chemokine LARC. *J Biol Chem*, *272*(23), 14893-14898. https://doi.org/10.1074/jbc.272.23.14893

Bai, X., Chi, X., Qiao, Q., Xie, S., Wan, S., Ni, L., Wang, P., Jin, W., & Dong, C. (2020). T Follicular Helper Cells Regulate Humoral Response for Host Protection against Intestinal Citrobacter rodentium Infection. *J Immunol*, *204*(10), 2754-2761. https://doi.org/10.4049/jimmunol.2000046

Barker, N., van Es, J. H., Kuipers, J., Kujala, P., van den Born, M., Cozijnsen, M., Haegebarth, A., Korving, J., Begthel, H., Peters, P. J., & Clevers, H. (2007). Identification of stem cells in small intestine and colon by marker gene Lgr5. *Nature*, *449*(7165), 1003-1007. https://doi.org/10.1038/nature06196

Bartolome-Casado, R., Landsverk, O. J. B., Chauhan, S. K., Richter, L., Phung, D., Greiff, V., Risnes, L. F., Yao, Y., Neumann, R. S., Yaqub, S., Oyen, O., Horneland, R., Aandahl, E. M., Paulsen, V., Sollid, L. M., Qiao, S. W., Baekkevold, E. S., & Jahnsen, F. L. (2019). Resident memory CD8 T cells persist for years in human small intestine. *J Exp Med*, *216*(10), 2412-2426. https://doi.org/10.1084/jem.20190414

Basu, R., O'Quinn, D. B., Silberger, D. J., Schoeb, T. R., Fouser, L., Ouyang, W., Hatton, R. D., & Weaver, C. T. (2012). Th22 cells are an important source of IL-22 for host protection against enteropathogenic bacteria. *Immunity*, *37*(6), 1061-1075. https://doi.org/10.1016/j.immuni.2012.08.024

Becher, B., Durell, B. G., & Noelle, R. J. (2002). Experimental autoimmune encephalitis and inflammation in the absence of interleukin-12. *J Clin Invest*, *110*(4), 493-497. https://doi.org/10.1172/JCI15751

Bending, D., De la Pena, H., Veldhoen, M., Phillips, J. M., Uyttenhove, C., Stockinger, B., & Cooke, A. (2009). Highly purified Th17 cells from BDC2.5NOD mice convert into Th1-like cells in NOD/SCID recipient mice. *J Clin Invest*, *119*(3), 565-572. https://doi.org/10.1172/JCI37865

Bettelli, E., Carrier, Y., Gao, W., Korn, T., Strom, T. B., Oukka, M., Weiner, H. L., & Kuchroo, V. K. (2006). Reciprocal developmental pathways for the generation of pathogenic effector TH17 and regulatory T cells. *Nature*, *441*(7090), 235-238. https://doi.org/10.1038/nature04753

Bettelli, E., Sullivan, B., Szabo, S. J., Sobel, R. A., Glimcher, L. H., & Kuchroo, V. K. (2004). Loss of T-bet, but not STAT1, prevents the development of experimental autoimmune encephalomyelitis. *J Exp Med*, *200*(1), 79-87. https://doi.org/10.1084/jem.20031819

Bhaumik, S., Mickael, M. E., Moran, M., Spell, M., & Basu, R. (2021). RORgammat Promotes Foxp3 Expression by Antagonizing the Effector Program in Colonic Regulatory T Cells. *J Immunol*, *207*(8), 2027-2038. https://doi.org/10.4049/jimmunol.2100175

Bilal, J., Berlinberg, A., Bhattacharjee, S., Trost, J., Riaz, I. B., & Kurtzman, D. J. B. (2018). A systematic review and meta-analysis of the efficacy and safety of the interleukin (IL)-12/23 and IL-17 inhibitors ustekinumab, secukinumab, ixekizumab, brodalumab, guselkumab and tildrakizumab for the treatment of moderate to severe plaque psoriasis. *J Dermatolog Treat*, *29*(6), 569-578. https://doi.org/10.1080/09546634.2017.1422591

Birchenough, G. M., Nystrom, E. E., Johansson, M. E., & Hansson, G. C. (2016). A sentinel goblet cell guards the colonic crypt by triggering Nlrp6-dependent Muc2 secretion. *Science*, *352*(6293), 1535-1542. https://doi.org/10.1126/science.aaf7419

Bishu, S., El Zaatari, M., Hayashi, A., Hou, G., Bowers, N., Kinnucan, J., Manoogian, B., Muza-Moons, M., Zhang, M., Grasberger, H., Bourque, C., Zou, W., Higgins, P. D. R., Spence, J. R., Stidham, R. W., Kamada, N., & Kao, J. Y. (2019). CD4+ Tissue-resident Memory T Cells Expand and Are a Major Source of Mucosal Tumour Necrosis Factor alpha in Active Crohn's Disease. *J Crohns Colitis*, *13*(7), 905-915. https://doi.org/10.1093/ecco-jcc/jjz010

Bishu, S., Hou, G., El Zaatari, M., Bishu, S. R., Popke, D., Zhang, M., Grasberger, H., Zou, W., Stidham, R. W., Higgins, P. D. R., Spence, J. R., Kamada, N., & Kao, J. Y. (2019). Citrobacter rodentium Induces Tissue-Resident Memory CD4(+) T Cells. *Infect Immun*, *87*(7). https://doi.org/10.1128/IAI.00295-19

Bogdan, C., Moll, H., Solbach, W., & Rollinghoff, M. (1990). Tumor necrosis factor-alpha in combination with interferon-gamma, but not with interleukin 4 activates murine macrophages for elimination of Leishmania major amastigotes. *Eur J Immunol*, *20*(5), 1131-1135. https://doi.org/10.1002/eji.1830200528

Bouskra, D., Brezillon, C., Berard, M., Werts, C., Varona, R., Boneca, I. G., & Eberl, G. (2008). Lymphoid tissue genesis induced by commensals through NOD1 regulates intestinal homeostasis. *Nature*, *456*(7221), 507-510. https://doi.org/10.1038/nature07450

Brandl, K., Plitas, G., Schnabl, B., DeMatteo, R. P., & Pamer, E. G. (2007). MyD88-mediated signals induce the bactericidal lectin RegIII gamma and protect mice against intestinal Listeria monocytogenes infection. *J Exp Med*, *204*(8), 1891-1900. https://doi.org/10.1084/jem.20070563

Braun, A., Dewert, N., Brunnert, F., Schnabel, V., Hardenberg, J. H., Richter, B., Zachmann, K., Cording, S., Classen, A., Brans, R., Hamann, A., Huehn, J., & Schon, M. P. (2015). Integrin alphaE(CD103) Is Involved in Regulatory T-Cell Function in Allergic Contact Hypersensitivity. *J Invest Dermatol*, *135*(12), 2982-2991. https://doi.org/10.1038/jid.2015.287

Briney, B., Inderbitzin, A., Joyce, C., & Burton, D. R. (2019). Commonality despite exceptional diversity in the baseline human antibody repertoire. *Nature*, *566*(7744), 393-397. https://doi.org/10.1038/s41586-019-0879-y

Broz, P., & Dixit, V. M. (2016). Inflammasomes: mechanism of assembly, regulation and signalling. *Nat Rev Immunol*, *16*(7), 407-420. https://doi.org/10.1038/nri.2016.58

Brucklacher-Waldert, V., Ferreira, C., Innocentin, S., Kamdar, S., Withers, D. R., Kullberg, M. C., & Veldhoen, M. (2016). Tbet or Continued RORgammat Expression Is Not Required for Th17-Associated Immunopathology. *J Immunol*, *196*(12), 4893-4904. https://doi.org/10.4049/jimmunol.1600137

Burchill, M. A., Yang, J., Vogtenhuber, C., Blazar, B. R., & Farrar, M. A. (2007). IL-2 receptor beta-dependent STAT5 activation is required for the development of Foxp3+ regulatory T cells. *J Immunol*, *178*(1), 280-290. https://doi.org/10.4049/jimmunol.178.1.280

Cabeza-Cabrerizo, M., Cardoso, A., Minutti, C. M., Pereira da Costa, M., & Reis e Sousa, C. (2021). Dendritic Cells Revisited. *Annu Rev Immunol*, *39*, 131-166. https://doi.org/10.1146/annurev-immunol-061020-053707

Campbell, C., Dikiy, S., Bhattarai, S. K., Chinen, T., Matheis, F., Calafiore, M., Hoyos, B., Hanash, A., Mucida, D., Bucci, V., & Rudensky, A. Y. (2018). Extrathymically Generated Regulatory T Cells Establish a Niche for Intestinal Border-Dwelling Bacteria and Affect Physiologic Metabolite Balance. *Immunity*, *48*(6), 1245-1257 e1249. https://doi.org/10.1016/j.immuni.2018.04.013

Campbell, L., Hepworth, M. R., Whittingham-Dowd, J., Thompson, S., Bancroft, A. J., Hayes, K. S., Shaw, T. N., Dickey, B. F., Flamar, A. L., Artis, D., Schwartz, D. A., Evans, C. M., Roberts, I. S., Thornton, D. J., & Grencis, R. K. (2019). ILC2s mediate systemic innate protection by priming mucus production at distal mucosal sites. *J Exp Med*, *216*(12), 2714-2723. https://doi.org/10.1084/jem.20180610

Capaldo, C. T., Beeman, N., Hilgarth, R. S., Nava, P., Louis, N. A., Naschberger, E., Sturzl, M., Parkos, C. A., & Nusrat, A. (2012). IFN-gamma and TNF-alpha-induced GBP-1 inhibits epithelial cell proliferation through suppression of beta-catenin/TCF signaling. *Mucosal Immunol*, *5*(6), 681-690. https://doi.org/10.1038/mi.2012.41

Carter, P. B., & Collins, F. M. (1974). The route of enteric infection in normal mice. *J Exp Med*, *139*(5), 1189-1203. https://doi.org/10.1084/jem.139.5.1189

Cash, H. L., Whitham, C. V., Behrendt, C. L., & Hooper, L. V. (2006). Symbiotic bacteria direct expression of an intestinal bactericidal lectin. *Science*, *313*(5790), 1126-1130. https://doi.org/10.1126/science.1127119

Castellanos, J. G., Woo, V., Viladomiu, M., Putzel, G., Lima, S., Diehl, G. E., Marderstein, A. R., Gandara, J., Perez, A. R., Withers, D. R., Targan, S. R., Shih, D. Q., Scherl, E. J., & Longman, R. S. (2018). Microbiota-Induced TNF-like Ligand 1A Drives Group 3 Innate Lymphoid Cell-Mediated Barrier Protection and Intestinal T Cell Activation during Colitis. *Immunity*, *49*(6), 1077-1089 e1075. https://doi.org/10.1016/j.immuni.2018.10.014

Castro, G., Liu, X., Ngo, K., De Leon-Tabaldo, A., Zhao, S., Luna-Roman, R., Yu, J., Cao, T., Kuhn, R., Wilkinson, P., Herman, K., Nelen, M. I., Blevitt, J., Xue, X., Fourie, A., & Fung-Leung, W. P. (2017). RORgammat and RORalpha signature genes in human Th17 cells. *PLoS One*, *12*(8), e0181868. https://doi.org/10.1371/journal.pone.0181868

Caton, M. L., Smith-Raska, M. R., & Reizis, B. (2007). Notch-RBP-J signaling controls the homeostasis of CD8- dendritic cells in the spleen. *J Exp Med*, *204*(7), 1653-1664. https://doi.org/10.1084/jem.20062648

Chang, J. T., Palanivel, V. R., Kinjyo, I., Schambach, F., Intlekofer, A. M., Banerjee, A., Longworth, S. A., Vinup, K. E., Mrass, P., Oliaro, J., Killeen, N., Orange, J. S., Russell, S. M., Weninger, W., & Reiner, S. L. (2007). Asymmetric T lymphocyte division in the initiation of adaptive immune responses. *Science*, *315*(5819), 1687-1691. https://doi.org/10.1126/science.1139393

Chang, S. H., & Dong, C. (2007). A novel heterodimeric cytokine consisting of IL-17 and IL-17F regulates inflammatory responses. *Cell Res*, *17*(5), 435-440. https://doi.org/10.1038/cr.2007.35

Chen, C., Neumann, J., Kuhn, F., Lee, S. M. L., Drefs, M., Andrassy, J., Werner, J., Bazhin, A. V., & Schiergens, T. S. (2020). Establishment of an Endoscopy-Guided Minimally Invasive Orthotopic Mouse Model of Colorectal Cancer. *Cancers (Basel)*, *12*(10). https://doi.org/10.3390/cancers12103007

Chen, W., Jin, W., Hardegen, N., Lei, K. J., Li, L., Marinos, N., McGrady, G., & Wahl, S. M. (2003). Conversion of peripheral CD4+CD25- naive T cells to CD4+CD25+ regulatory T cells by TGF-beta induction of transcription factor Foxp3. *J Exp Med*, *198*(12), 1875-1886. https://doi.org/10.1084/jem.20030152

Chen, X., Cai, G., Liu, C., Zhao, J., Gu, C., Wu, L., Hamilton, T. A., Zhang, C. J., Ko, J., Zhu, L., Qin, J., Vidimos, A., Koyfman, S., Gastman, B. R., Jensen, K. B., & Li, X. (2019). IL-17R-EGFR axis links wound healing to tumorigenesis in Lrig1(+) stem cells. *J Exp Med*, *216*(1), 195-214. https://doi.org/10.1084/jem.20171849

Chen, Y., Chauhan, S. K., Tan, X., & Dana, R. (2017). Interleukin-7 and -15 maintain pathogenic memory Th17 cells in autoimmunity. *J Autoimmun*, *77*, 96-103. https://doi.org/10.1016/j.jaut.2016.11.003

Chen, Z., Laurence, A., Kanno, Y., Pacher-Zavisin, M., Zhu, B. M., Tato, C., Yoshimura, A., Hennighausen, L., & O'Shea, J. J. (2006). Selective regulatory function of Socs3 in the formation of IL-17-secreting T cells. *Proc Natl Acad Sci U S A*, *103*(21), 8137-8142. https://doi.org/10.1073/pnas.0600666103

Choi, G. B., Yim, Y. S., Wong, H., Kim, S., Kim, H., Kim, S. V., Hoeffer, C. A., Littman, D. R., & Huh, J. R. (2016). The maternal interleukin-17a pathway in mice promotes autism-like phenotypes in offspring. *Science*, *351*(6276), 933-939. https://doi.org/10.1126/science.aad0314

Christensen, D., Mortensen, R., Rosenkrands, I., Dietrich, J., & Andersen, P. (2017). Vaccine-induced Th17 cells are established as resident memory cells in the lung and promote local IgA responses. *Mucosal Immunol*, *10*(1), 260-270. https://doi.org/10.1038/mi.2016.28

Ciucci, T., Vacchio, M. S., Gao, Y., Tomassoni Ardori, F., Candia, J., Mehta, M., Zhao, Y., Tran, B., Pepper, M., Tessarollo, L., McGavern, D. B., & Bosselut, R. (2019). The Emergence and Functional Fitness of Memory CD4(+) T Cells Require the Transcription Factor Thpok. *Immunity*, *50*(1), 91-105 e104. https://doi.org/10.1016/j.immuni.2018.12.019

Clemens, M. J., & Elia, A. (1997). The double-stranded RNA-dependent protein kinase PKR: structure and function. *J Interferon Cytokine Res*, *17*(9), 503-524. https://doi.org/10.1089/jir.1997.17.503

Coffman, R. L., & Carty, J. (1986). A T cell activity that enhances polyclonal IgE production and its inhibition by interferon-gamma. *J Immunol*, *136*(3), 949-954. https://www.ncbi.nlm.nih.gov/pubmed/2934482

Conti, H. R., Bruno, V. M., Childs, E. E., Daugherty, S., Hunter, J. P., Mengesha, B. G., Saevig, D. L., Hendricks, M. R., Coleman, B. M., Brane, L., Solis, N., Cruz, J. A., Verma, A. H., Garg, A. V., Hise, A. G., Richardson, J. P., Naglik, J. R., Filler, S. G., Kolls, J. K., Sinha, S., & Gaffen, S. L. (2016). IL-17 Receptor Signaling in Oral Epithelial Cells Is Critical for Protection against Oropharyngeal Candidiasis. *Cell Host Microbe*, *20*(5), 606-617. https://doi.org/10.1016/j.chom.2016.10.001

Coombes, J. L., Siddiqui, K. R., Arancibia-Carcamo, C. V., Hall, J., Sun, C. M., Belkaid, Y., & Powrie, F. (2007). A functionally specialized population of mucosal CD103+ DCs induces Foxp3+ regulatory T cells via a TGF-beta and retinoic acid-dependent mechanism. *J Exp Med*, *204*(8), 1757-1764. https://doi.org/10.1084/jem.20070590

Cornes, J. S. (1965). Number, size, and distribution of Peyer's patches in the human small intestine: Part I The development of Peyer's patches. *Gut*, *6*(3), 225-229. https://doi.org/10.1136/gut.6.3.225

Cortini, A., Ellinghaus, U., Malik, T. H., Cunninghame Graham, D. S., Botto, M., & Vyse, T. J. (2017). B cell OX40L supports T follicular helper cell development and contributes to SLE pathogenesis. *Ann Rheum Dis*, *76*(12), 2095-2103. https://doi.org/10.1136/annrheumdis-2017-211499

Cua, D. J., Sherlock, J., Chen, Y., Murphy, C. A., Joyce, B., Seymour, B., Lucian, L., To, W., Kwan, S., Churakova, T., Zurawski, S., Wiekowski, M., Lira, S. A., Gorman, D., Kastelein, R. A., & Sedgwick, J. D. (2003). Interleukin-23 rather than interleukin-12 is the critical cytokine for autoimmune inflammation of the brain. *Nature*, *421*(6924), 744-748. https://doi.org/10.1038/nature01355

Cua, D. J., & Tato, C. M. (2010). Innate IL-17-producing cells: the sentinels of the immune system. *Nat Rev Immunol*, *10*(7), 479-489. https://doi.org/10.1038/nri2800

Curtis, M. M., Hu, Z., Klimko, C., Narayanan, S., Deberardinis, R., & Sperandio, V. (2014). The gut commensal Bacteroides thetaiotaomicron exacerbates enteric infection through modification of the metabolic landscape. *Cell Host Microbe*, *16*(6), 759-769. https://doi.org/10.1016/j.chom.2014.11.005

Cyster, J. G. (2005). Chemokines, sphingosine-1-phosphate, and cell migration in secondary lymphoid organs. *Annu Rev Immunol*, *23*, 127-159. https://doi.org/10.1146/annurev.immunol.23.021704.115628

Cyster, J. G., & Allen, C. D. C. (2019). B Cell Responses: Cell Interaction Dynamics and Decisions. *Cell*, *177*(3), 524-540. https://doi.org/10.1016/j.cell.2019.03.016

Darrah, P. A., Patel, D. T., De Luca, P. M., Lindsay, R. W., Davey, D. F., Flynn, B. J., Hoff, S. T., Andersen, P., Reed, S. G., Morris, S. L., Roederer, M., & Seder, R. A. (2007). Multifunctional TH1 cells define a correlate of vaccine-mediated protection against Leishmania major. *Nat Med*, *13*(7), 843-850. https://doi.org/10.1038/nm1592

de Leeuw, E., Li, C., Zeng, P., Li, C., Diepeveen-de Buin, M., Lu, W. Y., Breukink, E., & Lu, W. (2010). Functional interaction of human neutrophil peptide-1 with the cell wall precursor lipid II. *FEBS Lett*, *584*(8), 1543-1548. https://doi.org/10.1016/j.febslet.2010.03.004

Denning, T. L., Norris, B. A., Medina-Contreras, O., Manicassamy, S., Geem, D., Madan, R., Karp, C. L., & Pulendran, B. (2011). Functional specializations of intestinal dendritic cell and macrophage subsets that control Th17 and regulatory T cell responses are dependent on the T cell/APC ratio, source of mouse strain, and regional localization. *J Immunol*, *187*(2), 733-747. https://doi.org/10.4049/jimmunol.1002701

Dileepan, T., Linehan, J. L., Moon, J. J., Pepper, M., Jenkins, M. K., & Cleary, P. P. (2011). Robust antigen specific th17 T cell response to group A Streptococcus is dependent on IL-6 and intranasal route of infection. *PLoS Pathog*, *7*(9), e1002252. https://doi.org/10.1371/journal.ppat.1002252

Doherty, P. C., & Zinkernagel, R. M. (1975). A biological role for the major histocompatibility antigens. *Lancet*, *1*(7922), 1406-1409. https://doi.org/10.1016/s0140-6736(75)92610-0

Downs-Canner, S., Berkey, S., Delgoffe, G. M., Edwards, R. P., Curiel, T., Odunsi, K., Bartlett, D. L., & Obermajer, N. (2017). Suppressive IL-17A(+)Foxp3(+) and ex-Th17 IL-17A(neg)Foxp3(+) Treg cells are a source of tumour-associated Treg cells. *Nat Commun*, *8*, 14649. https://doi.org/10.1038/ncomms14649

Dudakov, J. A., Hanash, A. M., Jenq, R. R., Young, L. F., Ghosh, A., Singer, N. V., West, M. L., Smith, O. M., Holland, A. M., Tsai, J. J., Boyd, R. L., & van den Brink, M. R. (2012). Interleukin-22 drives endogenous thymic regeneration in mice. *Science*, *336*(6077), 91-95. https://doi.org/10.1126/science.1218004

Dudley, D. D., Chaudhuri, J., Bassing, C. H., & Alt, F. W. (2005). Mechanism and control of V(D)J recombination versus class switch recombination: similarities and differences. *Adv Immunol*, *86*, 43-112. https://doi.org/10.1016/S0065-2776(04)86002-4

Duhen, R., Glatigny, S., Arbelaez, C. A., Blair, T. C., Oukka, M., & Bettelli, E. (2013). Cutting edge: the pathogenicity of IFN-gamma-producing Th17 cells is independent of T-bet. *J Immunol*, *190*(9), 4478-4482. https://doi.org/10.4049/jimmunol.1203172

Dutzan, N., Kajikawa, T., Abusleme, L., Greenwell-Wild, T., Zuazo, C. E., Ikeuchi, T., Brenchley, L., Abe, T., Hurabielle, C., Martin, D., Morell, R. J., Freeman, A. F., Lazarevic, V., Trinchieri, G., Diaz, P. I., Holland, S. M., Belkaid, Y., Hajishengallis, G., & Moutsopoulos, N. M. (2018). A dysbiotic microbiome triggers TH17 cells to mediate oral mucosal immunopathology in mice and humans. *Sci Transl Med*, *10*(463). https://doi.org/10.1126/scitranslmed.aat0797

Eberl, G., & Littman, D. R. (2004). Thymic origin of intestinal alphabeta T cells revealed by fate mapping of RORgammat+ cells. *Science*, *305*(5681), 248-251. https://doi.org/10.1126/science.1096472

Eberl, G., Marmon, S., Sunshine, M. J., Rennert, P. D., Choi, Y., & Littman, D. R. (2004). An essential function for the nuclear receptor RORgamma(t) in the generation of fetal lymphoid tissue inducer cells. *Nat Immunol*, *5*(1), 64-73. https://doi.org/10.1038/ni1022

Elmentaite, R., Kumasaka, N., Roberts, K., Fleming, A., Dann, E., King, H. W., Kleshchevnikov, V., Dabrowska, M., Pritchard, S., Bolt, L., Vieira, S. F., Mamanova, L., Huang, N., Perrone, F., Goh Kai'En, I., Lisgo, S. N., Katan, M., Leonard, S., Oliver, T. R. W., Hook, C. E., Nayak, K., Campos, L. S., Dominguez Conde, C., Stephenson, E., Engelbert, J., Botting, R. A., Polanski, K., van Dongen, S., Patel, M., Morgan, M. D., Marioni, J. C., Bayraktar, O. A., Meyer, K. B., He, X., Barker, R. A., Uhlig, H. H., Mahbubani, K. T., Saeb-Parsy, K., Zilbauer, M., Clatworthy, M. R., Haniffa, M., James, K. R., & Teichmann, S. A. (2021). Cells of the human intestinal tract mapped across space and time. *Nature*, *597*(7875), 250-255. https://doi.org/10.1038/s41586-021-03852-1

Erlandsen, S. L., Parsons, J. A., & Taylor, T. D. (1974). Ultrastructural immunocytochemical localization of lysozyme in the Paneth cells of man. *J Histochem Cytochem*, *22*(6), 401-413. https://doi.org/10.1177/22.6.401

Ermund, A., Gustafsson, J. K., Hansson, G. C., & Keita, A. V. (2013). Mucus properties and goblet cell quantification in mouse, rat and human ileal Peyer's patches. *PLoS One*, *8*(12), e83688. https://doi.org/10.1371/journal.pone.0083688

Ermund, A., Schutte, A., Johansson, M. E., Gustafsson, J. K., & Hansson, G. C. (2013). Studies of mucus in mouse stomach, small intestine, and colon. I. Gastrointestinal mucus layers have different properties depending on location as well as over the Peyer's patches. *Am J Physiol Gastrointest Liver Physiol*, *305*(5), G341-347. https://doi.org/10.1152/ajpgi.00046.2013

Fadok, V. A., Bratton, D. L., Guthrie, L., & Henson, P. M. (2001). Differential effects of apoptotic versus lysed cells on macrophage production of cytokines: role of proteases. *J Immunol*, *166*(11), 6847-6854. https://doi.org/10.4049/jimmunol.166.11.6847

Fazilleau, N., McHeyzer-Williams, L. J., Rosen, H., & McHeyzer-Williams, M. G. (2009). The function of follicular helper T cells is regulated by the strength of T cell antigen receptor binding. *Nat Immunol*, *10*(4), 375-384. https://doi.org/10.1038/ni.1704

Fearon, D. T., & Locksley, R. M. (1996). The instructive role of innate immunity in the acquired immune response. *Science*, *272*(5258), 50-53. https://doi.org/10.1126/science.272.5258.50

Ferber, I. A., Brocke, S., Taylor-Edwards, C., Ridgway, W., Dinisco, C., Steinman, L., Dalton, D., & Fathman, C. G. (1996). Mice with a disrupted IFN-gamma gene are susceptible to the induction of experimental autoimmune encephalomyelitis (EAE). *J Immunol*, *156*(1), 5-7. https://www.ncbi.nlm.nih.gov/pubmed/8598493

Fiancette, R., Finlay, C. M., Willis, C., Bevington, S. L., Soley, J., Ng, S. T. H., Baker, S. M., Andrews, S., Hepworth, M. R., & Withers, D. R. (2021). Reciprocal transcription factor networks govern tissue-resident ILC3 subset function and identity. *Nat Immunol*, *22*(10), 1245-1255. https://doi.org/10.1038/s41590-021-01024-x

Fonseca, R., Beura, L. K., Quarnstrom, C. F., Ghoneim, H. E., Fan, Y., Zebley, C. C., Scott, M. C., Fares-Frederickson, N. J., Wijeyesinghe, S., Thompson, E. A., Borges da Silva, H., Vezys, V., Youngblood, B., & Masopust, D. (2020). Developmental plasticity allows outside-in immune responses by resident memory T cells. *Nat Immunol*, *21*(4), 412-421. https://doi.org/10.1038/s41590-020-0607-7

Fossiez, F., Djossou, O., Chomarat, P., Flores-Romo, L., Ait-Yahia, S., Maat, C., Pin, J. J., Garrone, P., Garcia, E., Saeland, S., Blanchard, D., Gaillard, C., Das Mahapatra, B., Rouvier, E., Golstein, P., Banchereau, J., & Lebecque, S. (1996). T cell interleukin-17 induces stromal cells to produce proinflammatory and hematopoietic cytokines. *J Exp Med*, *183*(6), 2593-2603. https://doi.org/10.1084/jem.183.6.2593

Franklin, C. L., & Ericsson, A. C. (2017). Microbiota and reproducibility of rodent models. *Lab Anim (NY)*, *46*(4), 114-122. https://doi.org/10.1038/laban.1222

Fu, S., Zhang, N., Yopp, A. C., Chen, D., Mao, M., Chen, D., Zhang, H., Ding, Y., & Bromberg, J. S. (2004). TGF-beta induces Foxp3 + T-regulatory cells from CD4 + CD25 - precursors. *Am J Transplant*, *4*(10), 1614-1627. https://doi.org/10.1111/j.1600-6143.2004.00566.x

Gaboriau-Routhiau, V., Rakotobe, S., Lecuyer, E., Mulder, I., Lan, A., Bridonneau, C., Rochet, V., Pisi, A., De Paepe, M., Brandi, G., Eberl, G., Snel, J., Kelly, D., & Cerf-Bensussan, N. (2009). The key role of segmented filamentous bacteria in the coordinated maturation of gut helper T cell responses. *Immunity*, *31*(4), 677-689. https://doi.org/10.1016/j.immuni.2009.08.020

Gagliani, N., Amezcua Vesely, M. C., Iseppon, A., Brockmann, L., Xu, H., Palm, N. W., de Zoete, M. R., Licona-Limon, P., Paiva, R. S., Ching, T., Weaver, C., Zi, X., Pan, X., Fan, R., Garmire, L. X., Cotton, M. J., Drier, Y., Bernstein, B., Geginat, J., Stockinger, B., Esplugues, E., Huber, S., & Flavell, R. A. (2015). Th17 cells transdifferentiate into regulatory T cells during resolution of inflammation. *Nature*, *523*(7559), 221-225. https://doi.org/10.1038/nature14452

Gajdasik, D. W., Gaspal, F., Halford, E. E., Fiancette, R., Dutton, E. E., Willis, C., Ruckert, T., Romagnani, C., Gerard, A., Bevington, S. L., MacDonald, A. S., Botto, M., Vyse, T., & Withers, D. R. (2020). Th1 responses in vivo require cell-specific provision of OX40L dictated by environmental cues. *Nat Commun*, *11*(1), 3421. https://doi.org/10.1038/s41467-020-17293-3

Ganz, T. (2003). Defensins: antimicrobial peptides of innate immunity. *Nat Rev Immunol*, *3*(9), 710-720. https://doi.org/10.1038/nri1180

Ganz, T., Gabayan, V., Liao, H. I., Liu, L., Oren, A., Graf, T., & Cole, A. M. (2003). Increased inflammation in lysozyme M-deficient mice in response to Micrococcus luteus and its peptidoglycan. *Blood*, *101*(6), 2388-2392. https://doi.org/10.1182/blood-2002-07-2319

Gaspal, F., Withers, D., Saini, M., Bekiaris, V., McConnell, F. M., White, A., Khan, M., Yagita, H., Walker, L. S., Anderson, G., & Lane, P. J. (2011). Abrogation of CD30 and OX40 signals prevents autoimmune disease in FoxP3-deficient mice. *J Exp Med*, *208*(8), 1579-1584. https://doi.org/10.1084/jem.20101484

Gerbe, F., Sidot, E., Smyth, D. J., Ohmoto, M., Matsumoto, I., Dardalhon, V., Cesses, P., Garnier, L., Pouzolles, M., Brulin, B., Bruschi, M., Harcus, Y., Zimmermann, V. S., Taylor, N., Maizels, R. M., & Jay, P. (2016). Intestinal epithelial tuft cells initiate type 2 mucosal immunity to helminth parasites. *Nature*, *529*(7585), 226-230. https://doi.org/10.1038/nature16527

Ghosh, S., Dai, C., Brown, K., Rajendiran, E., Makarenko, S., Baker, J., Ma, C., Halder, S., Montero, M., Ionescu, V. A., Klegeris, A., Vallance, B. A., & Gibson, D. L. (2011). Colonic microbiota alters host susceptibility to infectious colitis by modulating inflammation, redox status, and ion transporter gene expression. *Am J Physiol Gastrointest Liver Physiol*, *301*(1), G39-49. https://doi.org/10.1152/ajpgi.00509.2010

Gmunder, H., & Lesslauer, W. (1984). A 45-kDa human T-cell membrane glycoprotein functions in the regulation of cell proliferative responses. *Eur J Biochem*, *142*(1), 153-160. https://doi.org/10.1111/j.1432-1033.1984.tb08263.x

Godfrey, D. I., Uldrich, A. P., McCluskey, J., Rossjohn, J., & Moody, D. B. (2015). The burgeoning family of unconventional T cells. *Nat Immunol*, *16*(11), 1114-1123. https://doi.org/10.1038/ni.3298

Gramaglia, I., Weinberg, A. D., Lemon, M., & Croft, M. (1998). Ox-40 ligand: a potent costimulatory molecule for sustaining primary CD4 T cell responses. *J Immunol*, *161*(12), 6510-6517. https://www.ncbi.nlm.nih.gov/pubmed/9862675

Gribble, F. M., & Reimann, F. (2019). Function and mechanisms of enteroendocrine cells and gut hormones in metabolism. *Nat Rev Endocrinol*, *15*(4), 226-237. https://doi.org/10.1038/s41574-019-0168-8

Griseri, T., Asquith, M., Thompson, C., & Powrie, F. (2010). OX40 is required for regulatory T cell-mediated control of colitis. *J Exp Med*, *207*(4), 699-709. https://doi.org/10.1084/jem.20091618

Grivennikov, S., Karin, E., Terzic, J., Mucida, D., Yu, G. Y., Vallabhapurapu, S., Scheller, J., Rose-John, S., Cheroutre, H., Eckmann, L., & Karin, M. (2009). IL-6 and Stat3 are required for survival of intestinal epithelial cells and development of colitis-associated cancer. *Cancer Cell*, *15*(2), 103-113. https://doi.org/10.1016/j.ccr.2009.01.001

Grivennikov, S. I., & Karin, M. (2010). Dangerous liaisons: STAT3 and NF-kappaB collaboration and crosstalk in cancer. *Cytokine Growth Factor Rev*, *21*(1), 11-19. https://doi.org/10.1016/j.cytogfr.2009.11.005

Guo, Y., MacIsaac, K. D., Chen, Y., Miller, R. J., Jain, R., Joyce-Shaikh, B., Ferguson, H., Wang, I. M., Cristescu, R., Mudgett, J., Engstrom, L., Piers, K. J., Baltus, G. A., Barr, K., Zhang, H., Mehmet, H., Hegde, L. G., Hu, X., Carter, L. L., Aicher, T. D., Glick, G., Zaller, D., Hawwari, A., Correll, C. C., Jones, D. C., & Cua, D. J. (2016). Inhibition of RORgammaT Skews TCRalpha Gene Rearrangement and Limits T Cell Repertoire Diversity. *Cell Rep*, *17*(12), 3206-3218. https://doi.org/10.1016/j.celrep.2016.11.073

Ha, H. L., Wang, H., Pisitkun, P., Kim, J. C., Tassi, I., Tang, W., Morasso, M. I., Udey, M. C., & Siebenlist, U. (2014). IL-17 drives psoriatic inflammation via distinct, target cell-specific mechanisms. *Proc Natl Acad Sci U S A*, *111*(33), E3422-3431. https://doi.org/10.1073/pnas.1400513111

Hanash, A. M., Dudakov, J. A., Hua, G., O'Connor, M. H., Young, L. F., Singer, N. V., West, M. L., Jenq, R. R., Holland, A. M., Kappel, L. W., Ghosh, A., Tsai, J. J., Rao, U. K., Yim, N. L., Smith, O. M., Velardi, E., Hawryluk, E. B., Murphy, G. F., Liu, C., Fouser, L. A., Kolesnick, R., Blazar, B. R., & van den Brink, M. R. (2012). Interleukin-22 protects intestinal stem cells from immune-mediated tissue damage and regulates sensitivity to graft versus host disease. *Immunity*, *37*(2), 339-350. https://doi.org/10.1016/j.immuni.2012.05.028

Harding, F. A., McArthur, J. G., Gross, J. A., Raulet, D. H., & Allison, J. P. (1992). CD28-mediated signalling co-stimulates murine T cells and prevents induction of anergy in T-cell clones. *Nature*, *356*(6370), 607-609. https://doi.org/10.1038/356607a0

Harrington, L. E., Hatton, R. D., Mangan, P. R., Turner, H., Murphy, T. L., Murphy, K. M., & Weaver, C. T. (2005). Interleukin 17-producing CD4+ effector T cells develop via a lineage distinct from the T helper type 1 and 2 lineages. *Nat Immunol*, *6*(11), 1123-1132. https://doi.org/10.1038/ni1254

Harrington, L. E., Janowski, K. M., Oliver, J. R., Zajac, A. J., & Weaver, C. T. (2008). Memory CD4 T cells emerge from effector T-cell progenitors. *Nature*, *452*(7185), 356-360. https://doi.org/10.1038/nature06672

Harris, T. J., Grosso, J. F., Yen, H. R., Xin, H., Kortylewski, M., Albesiano, E., Hipkiss, E. L., Getnet, D., Goldberg, M. V., Maris, C. H., Housseau, F., Yu, H., Pardoll, D. M., & Drake, C. G. (2007). Cutting edge: An in vivo requirement for STAT3 signaling in TH17 development and TH17-dependent autoimmunity. *J Immunol*, *179*(7), 4313-4317. https://doi.org/10.4049/jimmunol.179.7.4313

Harrison, O. J., Linehan, J. L., Shih, H. Y., Bouladoux, N., Han, S. J., Smelkinson, M., Sen, S. K., Byrd, A. L., Enamorado, M., Yao, C., Tamoutounour, S., Van Laethem, F., Hurabielle, C., Collins, N., Paun, A., Salcedo, R., O'Shea, J. J., & Belkaid, Y. (2019). Commensal-specific T cell plasticity promotes rapid tissue adaptation to injury. *Science*, *363*(6422). https://doi.org/10.1126/science.aat6280

Hase, K., Kawano, K., Nochi, T., Pontes, G. S., Fukuda, S., Ebisawa, M., Kadokura, K., Tobe, T., Fujimura, Y., Kawano, S., Yabashi, A., Waguri, S., Nakato, G., Kimura, S., Murakami, T., Iimura, M., Hamura, K., Fukuoka, S., Lowe, A. W., Itoh, K., Kiyono, H., & Ohno, H. (2009). Uptake through glycoprotein 2 of FimH(+) bacteria by M cells initiates mucosal immune response. *Nature*, *462*(7270), 226-230. https://doi.org/10.1038/nature08529

Hase, K., Murakami, T., Takatsu, H., Shimaoka, T., Iimura, M., Hamura, K., Kawano, K., Ohshima, S., Chihara, R., Itoh, K., Yonehara, S., & Ohno, H. (2006). The membrane-bound chemokine CXCL16 expressed on follicle-associated epithelium and M cells mediates lympho-epithelial interaction in GALT. *J Immunol*, *176*(1), 43-51. https://doi.org/10.4049/jimmunol.176.1.43

Hataye, J., Moon, J. J., Khoruts, A., Reilly, C., & Jenkins, M. K. (2006). Naive and memory CD4+ T cell survival controlled by clonal abundance. *Science*, *312*(5770), 114-116. https://doi.org/10.1126/science.1124228

Hauet-Broere, F., Unger, W. W., Garssen, J., Hoijer, M. A., Kraal, G., & Samsom, J. N. (2003). Functional CD25- and CD25+ mucosal regulatory T cells are induced in gut-draining lymphoid tissue within 48 h after oral antigen application. *Eur J Immunol*, *33*(10), 2801-2810. https://doi.org/10.1002/eji.200324115

Henning, S. J. (1985). Ontogeny of enzymes in the small intestine. *Annu Rev Physiol*, *47*, 231-245. https://doi.org/10.1146/annurev.ph.47.030185.001311

Hepworth, M. R., Fung, T. C., Masur, S. H., Kelsen, J. R., McConnell, F. M., Dubrot, J., Withers, D. R., Hugues, S., Farrar, M. A., Reith, W., Eberl, G., Baldassano, R. N., Laufer, T. M., Elson, C. O., & Sonnenberg, G. F. (2015). Immune tolerance. Group 3 innate lymphoid cells mediate intestinal selection of commensal bacteria-specific CD4(+) T cells. *Science*, *348*(6238), 1031-1035. https://doi.org/10.1126/science.aaa4812

Hepworth, M. R., Monticelli, L. A., Fung, T. C., Ziegler, C. G., Grunberg, S., Sinha, R., Mantegazza, A. R., Ma, H. L., Crawford, A., Angelosanto, J. M., Wherry, E. J., Koni, P. A., Bushman, F. D., Elson, C. O., Eberl, G., Artis, D., & Sonnenberg, G. F. (2013). Innate lymphoid cells regulate CD4+ T-cell responses to intestinal commensal bacteria. *Nature*, *498*(7452), 113-117. https://doi.org/10.1038/nature12240

Herbrand, H., Bernhardt, G., Forster, R., & Pabst, O. (2008). Dynamics and function of solitary intestinal lymphoid tissue. *Crit Rev Immunol*, *28*(1), 1-13. https://doi.org/10.1615/critrevimmunol.v28.i1.10

Higgins, L. M., Frankel, G., Douce, G., Dougan, G., & MacDonald, T. T. (1999). Citrobacter rodentium infection in mice elicits a mucosal Th1 cytokine response and lesions similar to those in murine inflammatory bowel disease. *Infect Immun*, *67*(6), 3031-3039. https://doi.org/10.1128/IAI.67.6.3031-3039.1999

Hirota, K., Duarte, J. H., Veldhoen, M., Hornsby, E., Li, Y., Cua, D. J., Ahlfors, H., Wilhelm, C., Tolaini, M., Menzel, U., Garefalaki, A., Potocnik, A. J., & Stockinger, B. (2011). Fate mapping of IL-17-producing T cells in inflammatory responses. *Nat Immunol*, *12*(3), 255-263. https://doi.org/10.1038/ni.1993

Hirota, K., Turner, J. E., Villa, M., Duarte, J. H., Demengeot, J., Steinmetz, O. M., & Stockinger, B. (2013). Plasticity of Th17 cells in Peyer's patches is responsible for the induction of T cell-dependent IgA responses. *Nat Immunol*, *14*(4), 372-379. https://doi.org/10.1038/ni.2552

Hirota, K., Yoshitomi, H., Hashimoto, M., Maeda, S., Teradaira, S., Sugimoto, N., Yamaguchi, T., Nomura, T., Ito, H., Nakamura, T., Sakaguchi, N., & Sakaguchi, S. (2007). Preferential recruitment of CCR6-expressing Th17 cells to inflamed joints via CCL20 in rheumatoid arthritis and its animal model. *J Exp Med*, *204*(12), 2803-2812. https://doi.org/10.1084/jem.20071397

Hooper, L. V., Stappenbeck, T. S., Hong, C. V., & Gordon, J. I. (2003). Angiogenins: a new class of microbicidal proteins involved in innate immunity. *Nat Immunol*, *4*(3), 269-273. https://doi.org/10.1038/ni888

Hornef, M. W., Putsep, K., Karlsson, J., Refai, E., & Andersson, M. (2004). Increased diversity of intestinal antimicrobial peptides by covalent dimer formation. *Nat Immunol*, *5*(8), 836-843. https://doi.org/10.1038/ni1094

Horng, T., Barton, G. M., Flavell, R. A., & Medzhitov, R. (2002). The adaptor molecule TIRAP provides signalling specificity for Toll-like receptors. *Nature*, *420*(6913), 329-333. https://doi.org/10.1038/nature01180

Hovhannisyan, Z., Treatman, J., Littman, D. R., & Mayer, L. (2011). Characterization of interleukin-17-producing regulatory T cells in inflamed intestinal mucosa from patients with inflammatory bowel diseases. *Gastroenterology*, *140*(3), 957-965. https://doi.org/10.1053/j.gastro.2010.12.002

Hueber, W., Sands, B. E., Lewitzky, S., Vandemeulebroecke, M., Reinisch, W., Higgins, P. D., Wehkamp, J., Feagan, B. G., Yao, M. D., Karczewski, M., Karczewski, J., Pezous, N., Bek, S., Bruin, G., Mellgard, B., Berger, C., Londei, M., Bertolino, A. P., Tougas, G., Travis, S. P., & Secukinumab in Crohn's Disease Study, G. (2012). Secukinumab, a human anti-IL-17A monoclonal antibody, for moderate to severe Crohn's disease: unexpected results of a randomised, double-blind placebo-controlled trial. *Gut*, *61*(12), 1693-1700. https://doi.org/10.1136/gutjnl-2011-301668

Hwang, J. R., Byeon, Y., Kim, D., & Park, S. G. (2020). Recent insights of T cell receptor-mediated signaling pathways for T cell activation and development. *Exp Mol Med*, *52*(5), 750-761. https://doi.org/10.1038/s12276-020-0435-8

Hwang, S. M., Sharma, G., Verma, R., Byun, S., Rudra, D., & Im, S. H. (2018). Inflammation-induced Id2 promotes plasticity in regulatory T cells. *Nat Commun*, *9*(1), 4736. https://doi.org/10.1038/s41467-018-07254-2

Hyams, J., Crandall, W., Kugathasan, S., Griffiths, A., Olson, A., Johanns, J., Liu, G., Travers, S., Heuschkel, R., Markowitz, J., Cohen, S., Winter, H., Veereman-Wauters, G., Ferry, G., Baldassano, R., & Group, R. S. (2007). Induction and maintenance infliximab therapy for the

treatment of moderate-to-severe Crohn's disease in children. *Gastroenterology*, *132*(3), 863-873; quiz 1165-1166. https://doi.org/10.1053/j.gastro.2006.12.003

Imura, A., Hori, T., Imada, K., Ishikawa, T., Tanaka, Y., Maeda, M., Imamura, S., & Uchiyama, T. (1996). The human OX40/gp34 system directly mediates adhesion of activated T cells to vascular endothelial cells. *J Exp Med*, *183*(5), 2185-2195. https://doi.org/10.1084/jem.183.5.2185

Infante-Duarte, C., Horton, H. F., Byrne, M. C., & Kamradt, T. (2000). Microbial lipopeptides induce the production of IL-17 in Th cells. *J Immunol*, *165*(11), 6107-6115. https://doi.org/10.4049/jimmunol.165.11.6107

Intlekofer, A. M., Banerjee, A., Takemoto, N., Gordon, S. M., Dejong, C. S., Shin, H., Hunter, C. A., Wherry, E. J., Lindsten, T., & Reiner, S. L. (2008). Anomalous type 17 response to viral infection by CD8+ T cells lacking T-bet and eomesodermin. *Science*, *321*(5887), 408-411. https://doi.org/10.1126/science.1159806

Irvin, C., Zafar, I., Good, J., Rollins, D., Christianson, C., Gorska, M. M., Martin, R. J., & Alam, R. (2014). Increased frequency of dual-positive TH2/TH17 cells in bronchoalveolar lavage fluid characterizes a population of patients with severe asthma. *J Allergy Clin Immunol*, *134*(5), 1175-1186 e1177. https://doi.org/10.1016/j.jaci.2014.05.038

Ivanov, II, Atarashi, K., Manel, N., Brodie, E. L., Shima, T., Karaoz, U., Wei, D., Goldfarb, K. C., Santee, C. A., Lynch, S. V., Tanoue, T., Imaoka, A., Itoh, K., Takeda, K., Umesaki, Y., Honda, K., & Littman, D. R. (2009). Induction of intestinal Th17 cells by segmented filamentous bacteria. *Cell*, *139*(3), 485-498. https://doi.org/10.1016/j.cell.2009.09.033

Ivanov, II, McKenzie, B. S., Zhou, L., Tadokoro, C. E., Lepelley, A., Lafaille, J. J., Cua, D. J., & Littman, D. R. (2006). The orphan nuclear receptor RORgammat directs the differentiation program of proinflammatory IL-17+ T helper cells. *Cell*, *126*(6), 1121-1133. https://doi.org/10.1016/j.cell.2006.07.035

Iwata, M., Hirakiyama, A., Eshima, Y., Kagechika, H., Kato, C., & Song, S. Y. (2004). Retinoic acid imprints gut-homing specificity on T cells. *Immunity*, *21*(4), 527-538. https://doi.org/10.1016/j.immuni.2004.08.011

Jain, A., & Pasare, C. (2017). Innate Control of Adaptive Immunity: Beyond the Three-Signal Paradigm. *J Immunol*, *198*(10), 3791-3800. https://doi.org/10.4049/jimmunol.1602000

Janeway, C. A., Jr., & Medzhitov, R. (2002). Innate immune recognition. *Annu Rev Immunol*, *20*, 197-216. https://doi.org/10.1146/annurev.immunol.20.083001.084359

Jenkins, M. K., & Schwartz, R. H. (1987). Antigen presentation by chemically modified splenocytes induces antigen-specific T cell unresponsiveness in vitro and in vivo. *J Exp Med*, *165*(2), 302-319. https://doi.org/10.1084/jem.165.2.302

Jetten, A. M. (2009). Retinoid-related orphan receptors (RORs): critical roles in development, immunity, circadian rhythm, and cellular metabolism. *Nucl Recept Signal*, *7*, e003. https://doi.org/10.1621/nrs.07003

Jinnohara, T., Kanaya, T., Hase, K., Sakakibara, S., Kato, T., Tachibana, N., Sasaki, T., Hashimoto, Y., Sato, T., Watarai, H., Kunisawa, J., Shibata, N., Williams, I. R., Kiyono, H., & Ohno, H. (2017). IL-22BP dictates characteristics of Peyer's patch follicle-associated epithelium for antigen uptake. *J Exp Med*, *214*(6), 1607-1618. https://doi.org/10.1084/jem.20160770

Johansson-Lindbom, B., Svensson, M., Pabst, O., Palmqvist, C., Marquez, G., Forster, R., & Agace, W. W. (2005). Functional specialization of gut CD103+ dendritic cells in the regulation of tissue-selective T cell homing. *J Exp Med*, *202*(8), 1063-1073. https://doi.org/10.1084/jem.20051100

Johansson, M. E., Jakobsson, H. E., Holmen-Larsson, J., Schutte, A., Ermund, A., Rodriguez-Pineiro, A. M., Arike, L., Wising, C., Svensson, F., Backhed, F., & Hansson, G. C. (2015). Normalization of Host Intestinal Mucus Layers Requires Long-Term Microbial Colonization. *Cell Host Microbe*, *18*(5), 582-592. https://doi.org/10.1016/j.chom.2015.10.007

Johansson, M. E., Phillipson, M., Petersson, J., Velcich, A., Holm, L., & Hansson, G. C. (2008). The inner of the two Muc2 mucin-dependent mucus layers in colon is devoid of bacteria. *Proc Natl Acad Sci U S A*, *105*(39), 15064-15069. https://doi.org/10.1073/pnas.0803124105

Johnston, R. J., Poholek, A. C., DiToro, D., Yusuf, I., Eto, D., Barnett, B., Dent, A. L., Craft, J., & Crotty, S. (2009). Bcl6 and Blimp-1 are reciprocal and antagonistic regulators of T follicular helper cell differentiation. *Science*, *325*(5943), 1006-1010. https://doi.org/10.1126/science.1175870

Jones, C. E., & Chan, K. (2002). Interleukin-17 stimulates the expression of interleukin-8, growth-related oncogene-alpha, and granulocyte-colony-stimulating factor by human airway epithelial cells. *Am J Respir Cell Mol Biol*, *26*(6), 748-753. https://doi.org/10.1165/ajrcmb.26.6.4757

Jorgensen, I., Rayamajhi, M., & Miao, E. A. (2017). Programmed cell death as a defence against infection. *Nat Rev Immunol*, *17*(3), 151-164. https://doi.org/10.1038/nri.2016.147

Jung, T. M., & Dailey, M. O. (1990). Rapid modulation of homing receptors (gp90MEL-14) induced by activators of protein kinase C. Receptor shedding due to accelerated proteolytic cleavage at the cell surface. *J Immunol*, *144*(8), 3130-3136. https://www.ncbi.nlm.nih.gov/pubmed/2182714

Kalliolias, G. D., & Ivashkiv, L. B. (2016). TNF biology, pathogenic mechanisms and emerging therapeutic strategies. *Nat Rev Rheumatol*, *12*(1), 49-62. https://doi.org/10.1038/nrrheum.2015.169

Kamada, N., Kim, Y. G., Sham, H. P., Vallance, B. A., Puente, J. L., Martens, E. C., & Nunez, G. (2012). Regulated virulence controls the ability of a pathogen to compete with the gut microbiota. *Science*, *336*(6086), 1325-1329. https://doi.org/10.1126/science.1222195

Kamada, N., Sakamoto, K., Seo, S. U., Zeng, M. Y., Kim, Y. G., Cascalho, M., Vallance, B. A., Puente, J. L., & Nunez, G. (2015). Humoral Immunity in the Gut Selectively Targets Phenotypically Virulent Attaching-and-Effacing Bacteria for Intraluminal Elimination. *Cell Host Microbe*, *17*(5), 617-627. https://doi.org/10.1016/j.chom.2015.04.001

Kannanganat, S., Ibegbu, C., Chennareddi, L., Robinson, H. L., & Amara, R. R. (2007). Multiple-cytokine-producing antiviral CD4 T cells are functionally superior to single-cytokine-producing cells. *J Virol*, *81*(16), 8468-8476. https://doi.org/10.1128/JVI.00228-07

Kaplan, M. H., Schindler, U., Smiley, S. T., & Grusby, M. J. (1996). Stat6 is required for mediating responses to IL-4 and for development of Th2 cells. *Immunity*, *4*(3), 313-319. https://doi.org/10.1016/s1074-7613(00)80439-2

Karandikar, N. J., Vanderlugt, C. L., Walunas, T. L., Miller, S. D., & Bluestone, J. A. (1996). CTLA-4: a negative regulator of autoimmune disease. *J Exp Med*, *184*(2), 783-788. https://doi.org/10.1084/jem.184.2.783

Karecla, P. I., Bowden, S. J., Green, S. J., & Kilshaw, P. J. (1995). Recognition of E-cadherin on epithelial cells by the mucosal T cell integrin alpha M290 beta 7 (alpha E beta 7). *Eur J Immunol*, *25*(3), 852-856. https://doi.org/10.1002/eji.1830250333

Karimova, M., Baker, O., Camgoz, A., Naumann, R., Buchholz, F., & Anastassiadis, K. (2018). A single reporter mouse line for Vika, Flp, Dre, and Cre-recombination. *Sci Rep*, *8*(1), 14453. https://doi.org/10.1038/s41598-018-32802-7

Kayama, H., Ueda, Y., Sawa, Y., Jeon, S. G., Ma, J. S., Okumura, R., Kubo, A., Ishii, M., Okazaki, T., Murakami, M., Yamamoto, M., Yagita, H., & Takeda, K. (2012). Intestinal CX3C chemokine receptor 1(high) (CX3CR1(high)) myeloid cells prevent T-cell-dependent colitis. *Proc Natl Acad Sci U S A*, *109*(13), 5010-5015. https://doi.org/10.1073/pnas.1114931109

Kilshaw, P. J., & Baker, K. C. (1988). A unique surface antigen on intraepithelial lymphocytes in the mouse. *Immunol Lett*, *18*(2), 149-154. https://doi.org/10.1016/0165-2478(88)90056-9

Kim, C., Wilson, T., Fischer, K. F., & Williams, M. A. (2013). Sustained interactions between T cell receptors and antigens promote the differentiation of CD4(+) memory T cells. *Immunity*, *39*(3), 508-520. https://doi.org/10.1016/j.immuni.2013.08.033

Kim, K. S., Hong, S. W., Han, D., Yi, J., Jung, J., Yang, B. G., Lee, J. Y., Lee, M., & Surh, C. D. (2016). Dietary antigens limit mucosal immunity by inducing regulatory T cells in the small intestine. *Science*, *351*(6275), 858-863. https://doi.org/10.1126/science.aac5560

Kimura, A., Naka, T., Nohara, K., Fujii-Kuriyama, Y., & Kishimoto, T. (2008). Aryl hydrocarbon receptor regulates Stat1 activation and participates in the development of Th17 cells. *Proc Natl Acad Sci U S A*, *105*(28), 9721-9726. https://doi.org/10.1073/pnas.0804231105

Kitajima, S., Morimoto, M., Sagara, E., Shimizu, C., & Ikeda, Y. (2001). Dextran sodium sulfate-induced colitis in germ-free IQI/Jic mice. *Exp Anim*, *50*(5), 387-395. https://doi.org/10.1538/expanim.50.387

Kitoh, A., Ono, M., Naoe, Y., Ohkura, N., Yamaguchi, T., Yaguchi, H., Kitabayashi, I., Tsukada, T., Nomura, T., Miyachi, Y., Taniuchi, I., & Sakaguchi, S. (2009). Indispensable role of the Runx1-Cbfbeta transcription complex for in vivo-suppressive function of FoxP3+ regulatory T cells. *Immunity*, *31*(4), 609-620. https://doi.org/10.1016/j.immuni.2009.09.003

Knodler, L. A., Crowley, S. M., Sham, H. P., Yang, H., Wrande, M., Ma, C., Ernst, R. K., Steele-Mortimer, O., Celli, J., & Vallance, B. A. (2014). Noncanonical inflammasome activation of caspase-4/caspase-11 mediates epithelial defenses against enteric bacterial pathogens. *Cell Host Microbe*, *16*(2), 249-256. https://doi.org/10.1016/j.chom.2014.07.002

Kok, L., Masopust, D., & Schumacher, T. N. (2021). The precursors of CD8(+) tissue resident memory T cells: from lymphoid organs to infected tissues. *Nat Rev Immunol*. https://doi.org/10.1038/s41577-021-00590-3

Komatsu, N., Okamoto, K., Sawa, S., Nakashima, T., Oh-hora, M., Kodama, T., Tanaka, S., Bluestone, J. A., & Takayanagi, H. (2014). Pathogenic conversion of Foxp3+ T cells into TH17 cells in autoimmune arthritis. *Nat Med*, *20*(1), 62-68. https://doi.org/10.1038/nm.3432

Korn, T., Bettelli, E., Gao, W., Awasthi, A., Jager, A., Strom, T. B., Oukka, M., & Kuchroo, V. K. (2007). IL-21 initiates an alternative pathway to induce proinflammatory T(H)17 cells. *Nature*, *448*(7152), 484-487. https://doi.org/10.1038/nature05970

Krausgruber, T., Schiering, C., Adelmann, K., Harrison, O. J., Chomka, A., Pearson, C., Ahern, P. P., Shale, M., Oukka, M., & Powrie, F. (2016). T-bet is a key modulator of IL-23-driven pathogenic CD4(+) T cell responses in the intestine. *Nat Commun*, *7*, 11627. https://doi.org/10.1038/ncomms11627

Krebs, C. F., Reimers, D., Zhao, Y., Paust, H. J., Bartsch, P., Nunez, S., Rosemblatt, M. V., Hellmig, M., Kilian, C., Borchers, A., Enk, L. U. B., Zinke, M., Becker, M., Schmid, J., Klinge, S., Wong, M. N., Puelles, V. G., Schmidt, C., Bertram, T., Stumpf, N., Hoxha, E., Meyer-Schwesinger, C., Lindenmeyer, M. T., Cohen, C. D., Rink, M., Kurts, C., Franzenburg, S., Koch-Nolte, F., Turner, J. E., Riedel, J. H., Huber, S., Gagliani, N., Huber, T. B., Wiech, T., Rohde, H., Bono, M. R., Bonn, S., Panzer, U., & Mittrucker, H. W. (2020). Pathogen-induced tissue-resident memory TH17 (TRM17) cells amplify autoimmune kidney disease. *Sci Immunol*, *5*(50). https://doi.org/10.1126/sciimmunol.aba4163

Kruisbeek, A. M., Mond, J. J., Fowlkes, B. J., Carmen, J. A., Bridges, S., & Longo, D. L. (1985). Absence of the Lyt-2-,L3T4+ lineage of T cells in mice treated neonatally with anti-I-A correlates with absence of intrathymic I-A-bearing antigen-presenting cell function. *J Exp Med*, *161*(5), 1029-1047. https://doi.org/10.1084/jem.161.5.1029

Kumar, B. V., Connors, T. J., & Farber, D. L. (2018). Human T Cell Development, Localization, and Function throughout Life. *Immunity*, *48*(2), 202-213. https://doi.org/10.1016/j.immuni.2018.01.007

Kumar, M., & Carmichael, G. G. (1998). Antisense RNA: function and fate of duplex RNA in cells of higher eukaryotes. *Microbiol Mol Biol Rev*, *62*(4), 1415-1434. https://doi.org/10.1128/MMBR.62.4.1415-1434.1998

Lallemand, Y., Luria, V., Haffner-Krausz, R., & Lonai, P. (1998). Maternally expressed PGK-Cre transgene as a tool for early and uniform activation of the Cre site-specific recombinase. *Transgenic Res*, *7*(2), 105-112. https://doi.org/10.1023/a:1008868325009

Lamb, D., De Sousa, D., Quast, K., Fundel-Clemens, K., Erjefalt, J. S., Sanden, C., Hoffmann, H. J., Kastle, M., Schmid, R., Menden, K., & Delic, D. (2021). RORgammat inhibitors block both IL-17 and IL-

22 conferring a potential advantage over anti-IL-17 alone to treat severe asthma. *Respir Res*, *22*(1), 158. https://doi.org/10.1186/s12931-021-01743-7

Lamkanfi, M., & Dixit, V. M. (2014). Mechanisms and functions of inflammasomes. *Cell*, *157*(5), 1013-1022. https://doi.org/10.1016/j.cell.2014.04.007

Langowski, J. L., Zhang, X., Wu, L., Mattson, J. D., Chen, T., Smith, K., Basham, B., McClanahan, T., Kastelein, R. A., & Oft, M. (2006). IL-23 promotes tumour incidence and growth. *Nature*, *442*(7101), 461-465. https://doi.org/10.1038/nature04808

Langrish, C. L., Chen, Y., Blumenschein, W. M., Mattson, J., Basham, B., Sedgwick, J. D., McClanahan, T., Kastelein, R. A., & Cua, D. J. (2005). IL-23 drives a pathogenic T cell population that induces autoimmune inflammation. *J Exp Med*, *201*(2), 233-240. https://doi.org/10.1084/jem.20041257

Latz, E., Schoenemeyer, A., Visintin, A., Fitzgerald, K. A., Monks, B. G., Knetter, C. F., Lien, E., Nilsen, N. J., Espevik, T., & Golenbock, D. T. (2004). TLR9 signals after translocating from the ER to CpG DNA in the lysosome. *Nat Immunol*, *5*(2), 190-198. https://doi.org/10.1038/ni1028

Lazarevic, V., Chen, X., Shim, J. H., Hwang, E. S., Jang, E., Bolm, A. N., Oukka, M., Kuchroo, V. K., & Glimcher, L. H. (2011). T-bet represses T(H)17 differentiation by preventing Runx1-mediated activation of the gene encoding RORgammat. *Nat Immunol*, *12*(1), 96-104. https://doi.org/10.1038/ni.1969

Lecuyer, E., Rakotobe, S., Lengline-Garnier, H., Lebreton, C., Picard, M., Juste, C., Fritzen, R., Eberl, G., McCoy, K. D., Macpherson, A. J., Reynaud, C. A., Cerf-Bensussan, N., & Gaboriau-Routhiau, V. (2014). Segmented filamentous bacterium uses secondary and tertiary lymphoid tissues to induce gut IgA and specific T helper 17 cell responses. *Immunity*, *40*(4), 608-620. https://doi.org/10.1016/j.immuni.2014.03.009

Lee, A. Y., Chang, S. Y., Kim, J. I., Cha, H. R., Jang, M. H., Yamamoto, M., & Kweon, M. N. (2008). Dendritic cells in colonic patches and iliac lymph nodes are essential in mucosal IgA induction following intrarectal administration via CCR7 interaction. *Eur J Immunol*, *38*(4), 1127-1137. https://doi.org/10.1002/eji.200737442

Lee, J. S., Tato, C. M., Joyce-Shaikh, B., Gulen, M. F., Cayatte, C., Chen, Y., Blumenschein, W. M., Judo, M., Ayanoglu, G., McClanahan, T. K., Li, X., & Cua, D. J. (2015). Interleukin-23-Independent IL-17 Production Regulates Intestinal Epithelial Permeability. *Immunity*, *43*(4), 727-738. https://doi.org/10.1016/j.immuni.2015.09.003

Lee, P. P., Fitzpatrick, D. R., Beard, C., Jessup, H. K., Lehar, S., Makar, K. W., Perez-Melgosa, M., Sweetser, M. T., Schlissel, M. S., Nguyen, S., Cherry, S. R., Tsai, J. H., Tucker, S. M., Weaver, W. M., Kelso, A., Jaenisch, R., & Wilson, C. B. (2001). A critical role for Dnmt1 and DNA methylation in T cell development, function, and survival. *Immunity*, *15*(5), 763-774. https://doi.org/10.1016/s1074-7613(01)00227-8

Lee, Y. K., Turner, H., Maynard, C. L., Oliver, J. R., Chen, D., Elson, C. O., & Weaver, C. T. (2009). Late developmental plasticity in the T helper 17 lineage. *Immunity*, *30*(1), 92-107. https://doi.org/10.1016/j.immuni.2008.11.005

Lemaitre, B., Nicolas, E., Michaut, L., Reichhart, J. M., & Hoffmann, J. A. (1996). The dorsoventral regulatory gene cassette spatzle/Toll/cactus controls the potent antifungal response in Drosophila adults. *Cell*, *86*(6), 973-983. https://doi.org/10.1016/s0092-8674(00)80172-5

Levy, R., Okada, S., Beziat, V., Moriya, K., Liu, C., Chai, L. Y., Migaud, M., Hauck, F., Al Ali, A., Cyrus, C., Vatte, C., Patiroglu, T., Unal, E., Ferneiny, M., Hyakuna, N., Nepesov, S., Oleastro, M., Ikinciogullari, A., Dogu, F., Asano, T., Ohara, O., Yun, L., Della Mina, E., Bronnimann, D., Itan, Y., Gothe, F., Bustamante, J., Boisson-Dupuis, S., Tahuil, N., Aytekin, C., Salhi, A., Al Muhsen, S., Kobayashi, M., Toubiana, J., Abel, L., Li, X., Camcioglu, Y., Celmeli, F., Klein, C., AlKhater, S. A., Casanova, J. L., & Puel, A. (2016). Genetic, immunological, and clinical features of patients with bacterial and fungal infections due to inherited IL-17RA deficiency. *Proc Natl Acad Sci U S A*, *113*(51), E8277-E8285. https://doi.org/10.1073/pnas.1618300114

Liang, S. C., Long, A. J., Bennett, F., Whitters, M. J., Karim, R., Collins, M., Goldman, S. J., Dunussi-Joannopoulos, K., Williams, C. M., Wright, J. F., & Fouser, L. A. (2007). An IL-17F/A heterodimer protein is produced by mouse Th17 cells and induces airway neutrophil recruitment. *J Immunol*, *179*(11), 7791-7799. https://doi.org/10.4049/jimmunol.179.11.7791

Liang, S. C., Tan, X. Y., Luxenberg, D. P., Karim, R., Dunussi-Joannopoulos, K., Collins, M., & Fouser, L. A. (2006). Interleukin (IL)-22 and IL-17 are coexpressed by Th17 cells and cooperatively enhance expression of antimicrobial peptides. *J Exp Med*, *203*(10), 2271-2279. https://doi.org/10.1084/jem.20061308

Liao, F., Rabin, R. L., Smith, C. S., Sharma, G., Nutman, T. B., & Farber, J. M. (1999). CC-chemokine receptor 6 is expressed on diverse memory subsets of T cells and determines responsiveness to macrophage inflammatory protein 3 alpha. *J Immunol*, *162*(1), 186-194. https://www.ncbi.nlm.nih.gov/pubmed/9886385

Lin, Y. Y., Jones-Mason, M. E., Inoue, M., Lasorella, A., Iavarone, A., Li, Q. J., Shinohara, M. L., & Zhuang, Y. (2012). Transcriptional regulator Id2 is required for the CD4 T cell immune response in the development of experimental autoimmune encephalomyelitis. *J Immunol*, *189*(3), 1400-1405. https://doi.org/10.4049/jimmunol.1200491

Lindemans, C. A., Calafiore, M., Mertelsmann, A. M., O'Connor, M. H., Dudakov, J. A., Jenq, R. R., Velardi, E., Young, L. F., Smith, O. M., Lawrence, G., Ivanov, J. A., Fu, Y. Y., Takashima, S., Hua, G., Martin, M. L., O'Rourke, K. P., Lo, Y. H., Mokry, M., Romera-Hernandez, M., Cupedo, T., Dow, L., Nieuwenhuis, E. E., Shroyer, N. F., Liu, C., Kolesnick, R., van den Brink, M. R. M., & Hanash, A. M. (2015). Interleukin-22 promotes intestinal-stem-cell-mediated epithelial regeneration. *Nature*, *528*(7583), 560-564. https://doi.org/10.1038/nature16460

Luche, H., Weber, O., Nageswara Rao, T., Blum, C., & Fehling, H. J. (2007). Faithful activation of an extra-bright red fluorescent protein in "knock-in" Cre-reporter mice ideally suited for lineage tracing studies. *Eur J Immunol*, *37*(1), 43-53. https://doi.org/10.1002/eji.200636745

Luda, K. M., Joeris, T., Persson, E. K., Rivollier, A., Demiri, M., Sitnik, K. M., Pool, L., Holm, J. B., Melo-Gonzalez, F., Richter, L., Lambrecht, B. N., Kristiansen, K., Travis, M. A., Svensson-Frej, M., Kotarsky, K., & Agace, W. W. (2016). IRF8 Transcription-Factor-Dependent Classical Dendritic Cells Are Essential for Intestinal T Cell Homeostasis. *Immunity*, *44*(4), 860-874. https://doi.org/10.1016/j.immuni.2016.02.008

Lycke, N. Y., & Bemark, M. (2017). The regulation of gut mucosal IgA B-cell responses: recent developments. *Mucosal Immunol*, *10*(6), 1361-1374. https://doi.org/10.1038/mi.2017.62

MacMicking, J. D. (2012). Interferon-inducible effector mechanisms in cell-autonomous immunity. *Nat Rev Immunol*, *12*(5), 367-382. https://doi.org/10.1038/nri3210

Madisen, L., Zwingman, T. A., Sunkin, S. M., Oh, S. W., Zariwala, H. A., Gu, H., Ng, L. L., Palmiter, R. D., Hawrylycz, M. J., Jones, A. R., Lein, E. S., & Zeng, H. (2010). A robust and high-throughput Cre reporting and characterization system for the whole mouse brain. *Nat Neurosci*, *13*(1), 133-140. https://doi.org/10.1038/nn.2467

Madrenas, J., Chau, L. A., Smith, J., Bluestone, J. A., & Germain, R. N. (1997). The efficiency of CD4 recruitment to ligand-engaged TCR controls the agonist/partial agonist properties of peptide-MHC molecule ligands. *J Exp Med*, *185*(2), 219-229. https://doi.org/10.1084/jem.185.2.219

Mangan, P. R., Harrington, L. E., O'Quinn, D. B., Helms, W. S., Bullard, D. C., Elson, C. O., Hatton, R. D., Wahl, S. M., Schoeb, T. R., & Weaver, C. T. (2006). Transforming growth factor-beta induces development of the T(H)17 lineage. *Nature*, *441*(7090), 231-234. https://doi.org/10.1038/nature04754

Martin-Orozco, N., Chung, Y., Chang, S. H., Wang, Y. H., & Dong, C. (2009). Th17 cells promote pancreatic inflammation but only induce diabetes efficiently in lymphopenic hosts after conversion into Th1 cells. *Eur J Immunol*, *39*(1), 216-224. https://doi.org/10.1002/eji.200838475

Masahata, K., Umemoto, E., Kayama, H., Kotani, M., Nakamura, S., Kurakawa, T., Kikuta, J., Gotoh, K., Motooka, D., Sato, S., Higuchi, T., Baba, Y., Kurosaki, T., Kinoshita, M., Shimada, Y., Kimura, T.,

Okumura, R., Takeda, A., Tajima, M., Yoshie, O., Fukuzawa, M., Kiyono, H., Fagarasan, S., Iida, T., Ishii, M., & Takeda, K. (2014). Generation of colonic IgA-secreting cells in the caecal patch. *Nat Commun*, *5*, 3704. https://doi.org/10.1038/ncomms4704

Masopust, D., Choo, D., Vezys, V., Wherry, E. J., Duraiswamy, J., Akondy, R., Wang, J., Casey, K. A., Barber, D. L., Kawamura, K. S., Fraser, K. A., Webby, R. J., Brinkmann, V., Butcher, E. C., Newell, K. A., & Ahmed, R. (2010). Dynamic T cell migration program provides resident memory within intestinal epithelium. *J Exp Med*, *207*(3), 553-564. https://doi.org/10.1084/jem.20090858

Massoud, A. H., Charbonnier, L. M., Lopez, D., Pellegrini, M., Phipatanakul, W., & Chatila, T. A. (2016). An asthma-associated IL4R variant exacerbates airway inflammation by promoting conversion of regulatory T cells to TH17-like cells. *Nat Med*, *22*(9), 1013-1022. https://doi.org/10.1038/nm.4147

Mathur, A. N., Chang, H. C., Zisoulis, D. G., Stritesky, G. L., Yu, Q., O'Malley, J. T., Kapur, R., Levy, D. E., Kansas, G. S., & Kaplan, M. H. (2007). Stat3 and Stat4 direct development of IL-17-secreting Th cells. *J Immunol*, *178*(8), 4901-4907. https://doi.org/10.4049/jimmunol.178.8.4901

Matloubian, M., Lo, C. G., Cinamon, G., Lesneski, M. J., Xu, Y., Brinkmann, V., Allende, M. L., Proia, R. L., & Cyster, J. G. (2004). Lymphocyte egress from thymus and peripheral lymphoid organs is dependent on S1P receptor 1. *Nature*, *427*(6972), 355-360. https://doi.org/10.1038/nature02284

Matsumoto, M., Funami, K., Tanabe, M., Oshiumi, H., Shingai, M., Seto, Y., Yamamoto, A., & Seya, T. (2003). Subcellular localization of Toll-like receptor 3 in human dendritic cells. *J Immunol*, *171*(6), 3154-3162. https://doi.org/10.4049/jimmunol.171.6.3154

McAllister, F., Henry, A., Kreindler, J. L., Dubin, P. J., Ulrich, L., Steele, C., Finder, J. D., Pilewski, J. M., Carreno, B. M., Goldman, S. J., Pirhonen, J., & Kolls, J. K. (2005). Role of IL-17A, IL-17F, and the IL-17 receptor in regulating growth-related oncogene-alpha and granulocyte colony-stimulating factor in bronchial epithelium: implications for airway inflammation in cystic fibrosis. *J Immunol*, *175*(1), 404-412. https://doi.org/10.4049/jimmunol.175.1.404

McBlane, J. F., van Gent, D. C., Ramsden, D. A., Romeo, C., Cuomo, C. A., Gellert, M., & Oettinger, M. A. (1995). Cleavage at a V(D)J recombination signal requires only RAG1 and RAG2 proteins and occurs in two steps. *Cell*, *83*(3), 387-395. https://doi.org/10.1016/0092-8674(95)90116-7

McDole, J. R., Wheeler, L. W., McDonald, K. G., Wang, B., Konjufca, V., Knoop, K. A., Newberry, R. D., & Miller, M. J. (2012). Goblet cells deliver luminal antigen to CD103+ dendritic cells in the small intestine. *Nature*, *483*(7389), 345-349. https://doi.org/10.1038/nature10863

McGeachy, M. J., Bak-Jensen, K. S., Chen, Y., Tato, C. M., Blumenschein, W., McClanahan, T., & Cua, D. J. (2007). TGF-beta and IL-6 drive the production of IL-17 and IL-10 by T cells and restrain T(H)-17 cell-mediated pathology. *Nat Immunol*, *8*(12), 1390-1397. https://doi.org/10.1038/ni1539

McGeachy, M. J., Chen, Y., Tato, C. M., Laurence, A., Joyce-Shaikh, B., Blumenschein, W. M., McClanahan, T. K., O'Shea, J. J., & Cua, D. J. (2009). The interleukin 23 receptor is essential for the terminal differentiation of interleukin 17-producing effector T helper cells in vivo. *Nat Immunol*, *10*(3), 314-324. https://doi.org/10.1038/ni.1698

McGeachy, M. J., Cua, D. J., & Gaffen, S. L. (2019). The IL-17 Family of Cytokines in Health and Disease. *Immunity*, *50*(4), 892-906. https://doi.org/10.1016/j.immuni.2019.03.021

McSorley, S. J., Cookson, B. T., & Jenkins, M. K. (2000). Characterization of CD4+ T cell responses during natural infection with Salmonella typhimurium. *J Immunol*, *164*(2), 986-993. https://doi.org/10.4049/jimmunol.164.2.986

Milner, J. D., Brenchley, J. M., Laurence, A., Freeman, A. F., Hill, B. J., Elias, K. M., Kanno, Y., Spalding, C., Elloumi, H. Z., Paulson, M. L., Davis, J., Hsu, A., Asher, A. I., O'Shea, J., Holland, S. M., Paul, W. E., & Douek, D. C. (2008). Impaired T(H)17 cell differentiation in subjects with autosomal dominant hyper-IgE syndrome. *Nature*, *452*(7188), 773-776. https://doi.org/10.1038/nature06764

Miragaia, R. J., Gomes, T., Chomka, A., Jardine, L., Riedel, A., Hegazy, A. N., Whibley, N., Tucci, A., Chen, X., Lindeman, I., Emerton, G., Krausgruber, T., Shields, J., Haniffa, M., Powrie, F., & Teichmann,

S. A. (2019). Single-Cell Transcriptomics of Regulatory T Cells Reveals Trajectories of Tissue Adaptation. *Immunity*, *50*(2), 493-504 e497. https://doi.org/10.1016/j.immuni.2019.01.001

Moon, J. J., Chu, H. H., Pepper, M., McSorley, S. J., Jameson, S. C., Kedl, R. M., & Jenkins, M. K. (2007). Naive CD4(+) T cell frequency varies for different epitopes and predicts repertoire diversity and response magnitude. *Immunity*, *27*(2), 203-213. https://doi.org/10.1016/j.immuni.2007.07.007

Morishima, N., Mizoguchi, I., Takeda, K., Mizuguchi, J., & Yoshimoto, T. (2009). TGF-beta is necessary for induction of IL-23R and Th17 differentiation by IL-6 and IL-23. *Biochem Biophys Res Commun*, *386*(1), 105-110. https://doi.org/10.1016/j.bbrc.2009.05.140

Mosmann, T. R., Cherwinski, H., Bond, M. W., Giedlin, M. A., & Coffman, R. L. (1986). Two types of murine helper T cell clone. I. Definition according to profiles of lymphokine activities and secreted proteins. *J Immunol*, *136*(7), 2348-2357. https://www.ncbi.nlm.nih.gov/pubmed/2419430

Mowat, A. M., & Agace, W. W. (2014). Regional specialization within the intestinal immune system. *Nat Rev Immunol*, *14*(10), 667-685. https://doi.org/10.1038/nri3738

Mueller, S. N., & Mackay, L. K. (2016). Tissue-resident memory T cells: local specialists in immune defence. *Nat Rev Immunol*, *16*(2), 79-89. https://doi.org/10.1038/nri.2015.3

Mukasa, R., Balasubramani, A., Lee, Y. K., Whitley, S. K., Weaver, B. T., Shibata, Y., Crawford, G. E., Hatton, R. D., & Weaver, C. T. (2010). Epigenetic instability of cytokine and transcription factor gene loci underlies plasticity of the T helper 17 cell lineage. *Immunity*, *32*(5), 616-627. https://doi.org/10.1016/j.immuni.2010.04.016

Mullineaux-Sanders, C., Collins, J. W., Ruano-Gallego, D., Levy, M., Pevsner-Fischer, M., Glegola-Madejska, I. T., Sagfors, A. M., Wong, J. L. C., Elinav, E., Crepin, V. F., & Frankel, G. (2017). Citrobacter rodentium Relies on Commensals for Colonization of the Colonic Mucosa. *Cell Rep*, *21*(12), 3381-3389. https://doi.org/10.1016/j.celrep.2017.11.086

Munoz, M., Eidenschenk, C., Ota, N., Wong, K., Lohmann, U., Kuhl, A. A., Wang, X., Manzanillo, P., Li, Y., Rutz, S., Zheng, Y., Diehl, L., Kayagaki, N., van Lookeren-Campagne, M., Liesenfeld, O., Heimesaat, M., & Ouyang, W. (2015). Interleukin-22 induces interleukin-18 expression from epithelial cells during intestinal infection. *Immunity*, *42*(2), 321-331. https://doi.org/10.1016/j.immuni.2015.01.011

Nava, P., Koch, S., Laukoetter, M. G., Lee, W. Y., Kolegraff, K., Capaldo, C. T., Beeman, N., Addis, C., Gerner-Smidt, K., Neumaier, I., Skerra, A., Li, L., Parkos, C. A., & Nusrat, A. (2010). Interferon-gamma regulates intestinal epithelial homeostasis through converging beta-catenin signaling pathways. *Immunity*, *32*(3), 392-402. https://doi.org/10.1016/j.immuni.2010.03.001

Neumann, C., Blume, J., Roy, U., Teh, P. P., Vasanthakumar, A., Beller, A., Liao, Y., Heinrich, F., Arenzana, T. L., Hackney, J. A., Eidenschenk, C., Galvez, E. J. C., Stehle, C., Heinz, G. A., Maschmeyer, P., Sidwell, T., Hu, Y., Amsen, D., Romagnani, C., Chang, H. D., Kruglov, A., Mashreghi, M. F., Shi, W., Strowig, T., Rutz, S., Kallies, A., & Scheffold, A. (2019). c-Maf-dependent Treg cell control of intestinal TH17 cells and IgA establishes host-microbiota homeostasis. *Nat Immunol*, *20*(4), 471-481. https://doi.org/10.1038/s41590-019-0316-2

Nevalainen, T. J., Graham, G. G., & Scott, K. F. (2008). Antibacterial actions of secreted phospholipases A2. Review. *Biochim Biophys Acta*, *1781*(1-2), 1-9. https://doi.org/10.1016/j.bbalip.2007.12.001

Nurieva, R., Yang, X. O., Martinez, G., Zhang, Y., Panopoulos, A. D., Ma, L., Schluns, K., Tian, Q., Watowich, S. S., Jetten, A. M., & Dong, C. (2007). Essential autocrine regulation by IL-21 in the generation of inflammatory T cells. *Nature*, *448*(7152), 480-483. https://doi.org/10.1038/nature05969

Nurieva, R. I., Chung, Y., Martinez, G. J., Yang, X. O., Tanaka, S., Matskevitch, T. D., Wang, Y. H., & Dong, C. (2009). Bcl6 mediates the development of T follicular helper cells. *Science*, *325*(5943), 1001-1005. https://doi.org/10.1126/science.1176676

O'Keefe, S. J., Ou, J., Aufreiter, S., O'Connor, D., Sharma, S., Sepulveda, J., Fukuwatari, T., Shibata, K., & Mawhinney, T. (2009). Products of the colonic microbiota mediate the effects of diet on colon cancer risk. *J Nutr*, *139*(11), 2044-2048. https://doi.org/10.3945/jn.109.104380

Ohnmacht, C., Park, J. H., Cording, S., Wing, J. B., Atarashi, K., Obata, Y., Gaboriau-Routhiau, V., Marques, R., Dulauroy, S., Fedoseeva, M., Busslinger, M., Cerf-Bensussan, N., Boneca, I. G., Voehringer, D., Hase, K., Honda, K., Sakaguchi, S., & Eberl, G. (2015). MUCOSAL IMMUNOLOGY. The microbiota regulates type 2 immunity through RORgammat(+) T cells. *Science*, *349*(6251), 989-993. https://doi.org/10.1126/science.aac4263

Ohshima, Y., Tanaka, Y., Tozawa, H., Takahashi, Y., Maliszewski, C., & Delespesse, G. (1997). Expression and function of OX40 ligand on human dendritic cells. *J Immunol*, *159*(8), 3838-3848. https://www.ncbi.nlm.nih.gov/pubmed/9378971

Okada, S., Markle, J. G., Deenick, E. K., Mele, F., Averbuch, D., Lagos, M., Alzahrani, M., Al-Muhsen, S., Halwani, R., Ma, C. S., Wong, N., Soudais, C., Henderson, L. A., Marzouqa, H., Shamma, J., Gonzalez, M., Martinez-Barricarte, R., Okada, C., Avery, D. T., Latorre, D., Deswarte, C., Jabot-Hanin, F., Torrado, E., Fountain, J., Belkadi, A., Itan, Y., Boisson, B., Migaud, M., Arlehamn, C. S. L., Sette, A., Breton, S., McCluskey, J., Rossjohn, J., de Villartay, J. P., Moshous, D., Hambleton, S., Latour, S., Arkwright, P. D., Picard, C., Lantz, O., Engelhard, D., Kobayashi, M., Abel, L., Cooper, A. M., Notarangelo, L. D., Boisson-Dupuis, S., Puel, A., Sallusto, F., Bustamante, J., Tangye, S. G., & Casanova, J. L. (2015). IMMUNODEFICIENCIES. Impairment of immunity to Candida and Mycobacterium in humans with bi-allelic RORC mutations. *Science*, *349*(6248), 606-613. https://doi.org/10.1126/science.aaa4282

Oliphant, C. J., Hwang, Y. Y., Walker, J. A., Salimi, M., Wong, S. H., Brewer, J. M., Englezakis, A., Barlow, J. L., Hams, E., Scanlon, S. T., Ogg, G. S., Fallon, P. G., & McKenzie, A. N. (2014). MHCII-mediated dialog between group 2 innate lymphoid cells and CD4(+) T cells potentiates type 2 immunity and promotes parasitic helminth expulsion. *Immunity*, *41*(2), 283-295. https://doi.org/10.1016/j.immuni.2014.06.016

Omenetti, S., Bussi, C., Metidji, A., Iseppon, A., Lee, S., Tolaini, M., Li, Y., Kelly, G., Chakravarty, P., Shoaie, S., Gutierrez, M. G., & Stockinger, B. (2019). The Intestine Harbors Functionally Distinct Homeostatic Tissue-Resident and Inflammatory Th17 Cells. *Immunity*, *51*(1), 77-89 e76. https://doi.org/10.1016/j.immuni.2019.05.004

Oppmann, B., Lesley, R., Blom, B., Timans, J. C., Xu, Y., Hunte, B., Vega, F., Yu, N., Wang, J., Singh, K., Zonin, F., Vaisberg, E., Churakova, T., Liu, M., Gorman, D., Wagner, J., Zurawski, S., Liu, Y., Abrams, J. S., Moore, K. W., Rennick, D., de Waal-Malefyt, R., Hannum, C., Bazan, J. F., & Kastelein, R. A. (2000). Novel p19 protein engages IL-12p40 to form a cytokine, IL-23, with biological activities similar as well as distinct from IL-12. *Immunity*, *13*(5), 715-725. https://doi.org/10.1016/s1074-7613(00)00070-4

Owyang, A. M., Zaph, C., Wilson, E. H., Guild, K. J., McClanahan, T., Miller, H. R., Cua, D. J., Goldschmidt, M., Hunter, C. A., Kastelein, R. A., & Artis, D. (2006). Interleukin 25 regulates type 2 cytokine-dependent immunity and limits chronic inflammation in the gastrointestinal tract. *J Exp Med*, *203*(4), 843-849. https://doi.org/10.1084/jem.20051496

Pabst, O., & Mowat, A. M. (2012). Oral tolerance to food protein. *Mucosal Immunol*, *5*(3), 232-239. https://doi.org/10.1038/mi.2012.4

Pandiyan, P., Conti, H. R., Zheng, L., Peterson, A. C., Mathern, D. R., Hernandez-Santos, N., Edgerton, M., Gaffen, S. L., & Lenardo, M. J. (2011). CD4(+)CD25(+)Foxp3(+) regulatory T cells promote Th17 cells in vitro and enhance host resistance in mouse Candida albicans Th17 cell infection model. *Immunity*, *34*(3), 422-434. https://doi.org/10.1016/j.immuni.2011.03.002

Panzer, M., Sitte, S., Wirth, S., Drexler, I., Sparwasser, T., & Voehringer, D. (2012). Rapid in vivo conversion of effector T cells into Th2 cells during helminth infection. *J Immunol*, *188*(2), 615-623. https://doi.org/10.4049/jimmunol.1101164

Papamichael, K., Gils, A., Rutgeerts, P., Levesque, B. G., Vermeire, S., Sandborn, W. J., & Vande Casteele, N. (2015). Role for therapeutic drug monitoring during induction therapy with TNF

antagonists in IBD: evolution in the definition and management of primary nonresponse. *Inflamm Bowel Dis*, *21*(1), 182-197. https://doi.org/10.1097/MIB.0000000000000202

Parham, C., Chirica, M., Timans, J., Vaisberg, E., Travis, M., Cheung, J., Pflanz, S., Zhang, R., Singh, K. P., Vega, F., To, W., Wagner, J., O'Farrell, A. M., McClanahan, T., Zurawski, S., Hannum, C., Gorman, D., Rennick, D. M., Kastelein, R. A., de Waal Malefyt, R., & Moore, K. W. (2002). A receptor for the heterodimeric cytokine IL-23 is composed of IL-12Rbeta1 and a novel cytokine receptor subunit, IL-23R. *J Immunol*, *168*(11), 5699-5708. https://doi.org/10.4049/jimmunol.168.11.5699

Paterson, D. J., Jefferies, W. A., Green, J. R., Brandon, M. R., Corthesy, P., Puklavec, M., & Williams, A. F. (1987). Antigens of activated rat T lymphocytes including a molecule of 50,000 Mr detected only on CD4 positive T blasts. *Mol Immunol*, *24*(12), 1281-1290. https://doi.org/10.1016/0161-5890(87)90122-2

Pepper, M., & Jenkins, M. K. (2011). Origins of CD4(+) effector and central memory T cells. *Nat Immunol*, *12*(6), 467-471. https://doi.org/10.1038/ni.2038

Pepper, M., Linehan, J. L., Pagan, A. J., Zell, T., Dileepan, T., Cleary, P. P., & Jenkins, M. K. (2010). Different routes of bacterial infection induce long-lived TH1 memory cells and short-lived TH17 cells. *Nat Immunol*, *11*(1), 83-89. https://doi.org/10.1038/ni.1826

Pepper, M., Pagan, A. J., Igyarto, B. Z., Taylor, J. J., & Jenkins, M. K. (2011). Opposing signals from the Bcl6 transcription factor and the interleukin-2 receptor generate T helper 1 central and effector memory cells. *Immunity*, *35*(4), 583-595. https://doi.org/10.1016/j.immuni.2011.09.009

Persson, E. K., Uronen-Hansson, H., Semmrich, M., Rivollier, A., Hagerbrand, K., Marsal, J., Gudjonsson, S., Hakansson, U., Reizis, B., Kotarsky, K., & Agace, W. W. (2013). IRF4 transcription-factor-dependent CD103(+)CD11b(+) dendritic cells drive mucosal T helper 17 cell differentiation. *Immunity*, *38*(5), 958-969. https://doi.org/10.1016/j.immuni.2013.03.009

Peterson, L. W., & Artis, D. (2014). Intestinal epithelial cells: regulators of barrier function and immune homeostasis. *Nat Rev Immunol*, *14*(3), 141-153. https://doi.org/10.1038/nri3608

Petty, N. K., Bulgin, R., Crepin, V. F., Cerdeno-Tarraga, A. M., Schroeder, G. N., Quail, M. A., Lennard, N., Corton, C., Barron, A., Clark, L., Toribio, A. L., Parkhill, J., Dougan, G., Frankel, G., & Thomson, N. R. (2010). The Citrobacter rodentium genome sequence reveals convergent evolution with human pathogenic Escherichia coli. *J Bacteriol*, *192*(2), 525-538. https://doi.org/10.1128/JB.01144-09

Piconese, S., Pittoni, P., Burocchi, A., Gorzanelli, A., Care, A., Tripodo, C., & Colombo, M. P. (2010). A non-redundant role for OX40 in the competitive fitness of Treg in response to IL-2. *Eur J Immunol*, *40*(10), 2902-2913. https://doi.org/10.1002/eji.201040505

Piconese, S., Valzasina, B., & Colombo, M. P. (2008). OX40 triggering blocks suppression by regulatory T cells and facilitates tumor rejection. *J Exp Med*, *205*(4), 825-839. https://doi.org/10.1084/jem.20071341

Pippig, S. D., Pena-Rossi, C., Long, J., Godfrey, W. R., Fowell, D. J., Reiner, S. L., Birkeland, M. L., Locksley, R. M., Barclay, A. N., & Killeen, N. (1999). Robust B cell immunity but impaired T cell proliferation in the absence of CD134 (OX40). *J Immunol*, *163*(12), 6520-6529. https://www.ncbi.nlm.nih.gov/pubmed/10586044

Poltorak, A., He, X., Smirnova, I., Liu, M. Y., Van Huffel, C., Du, X., Birdwell, D., Alejos, E., Silva, M., Galanos, C., Freudenberg, M., Ricciardi-Castagnoli, P., Layton, B., & Beutler, B. (1998). Defective LPS signaling in C3H/HeJ and C57BL/10ScCr mice: mutations in Tlr4 gene. *Science*, *282*(5396), 2085-2088. https://doi.org/10.1126/science.282.5396.2085

Price, A. E., Reinhardt, R. L., Liang, H. E., & Locksley, R. M. (2012). Marking and quantifying IL-17A-producing cells in vivo. *PLoS One*, *7*(6), e39750. https://doi.org/10.1371/journal.pone.0039750

Propheter, D. C., Chara, A. L., Harris, T. A., Ruhn, K. A., & Hooper, L. V. (2017). Resistin-like molecule beta is a bactericidal protein that promotes spatial segregation of the microbiota and the

colonic epithelium. *Proc Natl Acad Sci U S A*, *114*(42), 11027-11033. https://doi.org/10.1073/pnas.1711395114

Qiu, J., Heller, J. J., Guo, X., Chen, Z. M., Fish, K., Fu, Y. X., & Zhou, L. (2012). The aryl hydrocarbon receptor regulates gut immunity through modulation of innate lymphoid cells. *Immunity*, *36*(1), 92-104. https://doi.org/10.1016/j.immuni.2011.11.011

Quintana, F. J., Basso, A. S., Iglesias, A. H., Korn, T., Farez, M. F., Bettelli, E., Caccamo, M., Oukka, M., & Weiner, H. L. (2008). Control of T(reg) and T(H)17 cell differentiation by the aryl hydrocarbon receptor. *Nature*, *453*(7191), 65-71. https://doi.org/10.1038/nature06880

Qureshi, O. S., Zheng, Y., Nakamura, K., Attridge, K., Manzotti, C., Schmidt, E. M., Baker, J., Jeffery, L. E., Kaur, S., Briggs, Z., Hou, T. Z., Futter, C. E., Anderson, G., Walker, L. S., & Sansom, D. M. (2011). Trans-endocytosis of CD80 and CD86: a molecular basis for the cell-extrinsic function of CTLA-4. *Science*, *332*(6029), 600-603. https://doi.org/10.1126/science.1202947

Ramirez-Carrozzi, V., Sambandam, A., Luis, E., Lin, Z., Jeet, S., Lesch, J., Hackney, J., Kim, J., Zhou, M., Lai, J., Modrusan, Z., Sai, T., Lee, W., Xu, M., Caplazi, P., Diehl, L., de Voss, J., Balazs, M., Gonzalez, L., Jr., Singh, H., Ouyang, W., & Pappu, R. (2011). IL-17C regulates the innate immune function of epithelial cells in an autocrine manner. *Nat Immunol*, *12*(12), 1159-1166. https://doi.org/10.1038/ni.2156

Raphael, I., Nalawade, S., Eagar, T. N., & Forsthuber, T. G. (2015). T cell subsets and their signature cytokines in autoimmune and inflammatory diseases. *Cytokine*, *74*(1), 5-17. https://doi.org/10.1016/j.cyto.2014.09.011

Rauch, I., Deets, K. A., Ji, D. X., von Moltke, J., Tenthorey, J. L., Lee, A. Y., Philip, N. H., Ayres, J. S., Brodsky, I. E., Gronert, K., & Vance, R. E. (2017). NAIP-NLRC4 Inflammasomes Coordinate Intestinal Epithelial Cell Expulsion with Eicosanoid and IL-18 Release via Activation of Caspase-1 and -8. *Immunity*, *46*(4), 649-659. https://doi.org/10.1016/j.immuni.2017.03.016

Rees, W., Bender, J., Teague, T. K., Kedl, R. M., Crawford, F., Marrack, P., & Kappler, J. (1999). An inverse relationship between T cell receptor affinity and antigen dose during CD4(+) T cell responses in vivo and in vitro. *Proc Natl Acad Sci U S A*, *96*(17), 9781-9786. https://doi.org/10.1073/pnas.96.17.9781

Reinhardt, R. L., Liang, H. E., & Locksley, R. M. (2009). Cytokine-secreting follicular T cells shape the antibody repertoire. *Nat Immunol*, *10*(4), 385-393. https://doi.org/10.1038/ni.1715

Remedios, K. A., Zirak, B., Sandoval, P. M., Lowe, M. M., Boda, D., Henley, E., Bhattrai, S., Scharschmidt, T. C., Liao, W., Naik, H. B., & Rosenblum, M. D. (2018). The TNFRSF members CD27 and OX40 coordinately limit TH17 differentiation in regulatory T cells. *Sci Immunol*, *3*(30). https://doi.org/10.1126/sciimmunol.aau2042

Rey, J., Garin, N., Spertini, F., & Corthesy, B. (2004). Targeting of secretory IgA to Peyer's patch dendritic and T cells after transport by intestinal M cells. *J Immunol*, *172*(5), 3026-3033. https://doi.org/10.4049/jimmunol.172.5.3026

Reynolds, J. M., Lee, Y. H., Shi, Y., Wang, X., Angkasekwinai, P., Nallaparaju, K. C., Flaherty, S., Chang, S. H., Watarai, H., & Dong, C. (2015). Interleukin-17B Antagonizes Interleukin-25-Mediated Mucosal Inflammation. *Immunity*, *42*(4), 692-703. https://doi.org/10.1016/j.immuni.2015.03.008

Rimoldi, M., Chieppa, M., Salucci, V., Avogadri, F., Sonzogni, A., Sampietro, G. M., Nespoli, A., Viale, G., Allavena, P., & Rescigno, M. (2005). Intestinal immune homeostasis is regulated by the crosstalk between epithelial cells and dendritic cells. *Nat Immunol*, *6*(5), 507-514. https://doi.org/10.1038/ni1192

Rochereau, N., Drocourt, D., Perouzel, E., Pavot, V., Redelinghuys, P., Brown, G. D., Tiraby, G., Roblin, X., Verrier, B., Genin, C., Corthesy, B., & Paul, S. (2013). Dectin-1 is essential for reverse transcytosis of glycosylated SIgA-antigen complexes by intestinal M cells. *PLoS Biol*, *11*(9), e1001658. https://doi.org/10.1371/journal.pbio.1001658

Rossi, D. L., Vicari, A. P., Franz-Bacon, K., McClanahan, T. K., & Zlotnik, A. (1997). Identification through bioinformatics of two new macrophage proinflammatory human chemokines: MIP-3alpha and MIP-3beta. *J Immunol*, *158*(3), 1033-1036. https://www.ncbi.nlm.nih.gov/pubmed/9013939

Rouvier, E., Luciani, M. F., Mattei, M. G., Denizot, F., & Golstein, P. (1993). CTLA-8, cloned from an activated T cell, bearing AU-rich messenger RNA instability sequences, and homologous to a herpesvirus saimiri gene. *J Immunol*, *150*(12), 5445-5456. https://www.ncbi.nlm.nih.gov/pubmed/8390535

Rubtsov, Y. P., Niec, R. E., Josefowicz, S., Li, L., Darce, J., Mathis, D., Benoist, C., & Rudensky, A. Y. (2010). Stability of the regulatory T cell lineage in vivo. *Science*, *329*(5999), 1667-1671. https://doi.org/10.1126/science.1191996

Rudensky, A., Rath, S., Preston-Hurlburt, P., Murphy, D. B., & Janeway, C. A., Jr. (1991). On the complexity of self. *Nature*, *353*(6345), 660-662. https://doi.org/10.1038/353660a0

Rudra, D., Egawa, T., Chong, M. M., Treuting, P., Littman, D. R., & Rudensky, A. Y. (2009). Runx-CBFbeta complexes control expression of the transcription factor Foxp3 in regulatory T cells. *Nat Immunol*, *10*(11), 1170-1177. https://doi.org/10.1038/ni.1795

Russell, J. H., & Ley, T. J. (2002). Lymphocyte-mediated cytotoxicity. *Annu Rev Immunol*, *20*, 323-370. https://doi.org/10.1146/annurev.immunol.20.100201.131730

Rutz, S., Noubade, R., Eidenschenk, C., Ota, N., Zeng, W., Zheng, Y., Hackney, J., Ding, J., Singh, H., & Ouyang, W. (2011). Transcription factor c-Maf mediates the TGF-beta-dependent suppression of IL-22 production in T(H)17 cells. *Nat Immunol*, *12*(12), 1238-1245. https://doi.org/10.1038/ni.2134

Saddawi-Konefka, R., Seelige, R., Gross, E. T., Levy, E., Searles, S. C., Washington, A., Jr., Santosa, E. K., Liu, B., O'Sullivan, T. E., Harismendy, O., & Bui, J. D. (2016). Nrf2 Induces IL-17D to Mediate Tumor and Virus Surveillance. *Cell Rep*, *16*(9), 2348-2358. https://doi.org/10.1016/j.celrep.2016.07.075

Sass, V., Schneider, T., Wilmes, M., Korner, C., Tossi, A., Novikova, N., Shamova, O., & Sahl, H. G. (2010). Human beta-defensin 3 inhibits cell wall biosynthesis in Staphylococci. *Infect Immun*, *78*(6), 2793-2800. https://doi.org/10.1128/IAI.00688-09

Sato, T., van Es, J. H., Snippert, H. J., Stange, D. E., Vries, R. G., van den Born, M., Barker, N., Shroyer, N. F., van de Wetering, M., & Clevers, H. (2011). Paneth cells constitute the niche for Lgr5 stem cells in intestinal crypts. *Nature*, *469*(7330), 415-418. https://doi.org/10.1038/nature09637

Satoh-Takayama, N., Vosshenrich, C. A., Lesjean-Pottier, S., Sawa, S., Lochner, M., Rattis, F., Mention, J. J., Thiam, K., Cerf-Bensussan, N., Mandelboim, O., Eberl, G., & Di Santo, J. P. (2008). Microbial flora drives interleukin 22 production in intestinal NKp46+ cells that provide innate mucosal immune defense. *Immunity*, *29*(6), 958-970. https://doi.org/10.1016/j.immuni.2008.11.001

Schatz, D. G., Oettinger, M. A., & Baltimore, D. (1989). The V(D)J recombination activating gene, RAG-1. *Cell*, *59*(6), 1035-1048. https://doi.org/10.1016/0092-8674(89)90760-5

Schenkel, J. M., & Masopust, D. (2014). Tissue-resident memory T cells. *Immunity*, *41*(6), 886-897. https://doi.org/10.1016/j.immuni.2014.12.007

Schnare, M., Barton, G. M., Holt, A. C., Takeda, K., Akira, S., & Medzhitov, R. (2001). Toll-like receptors control activation of adaptive immune responses. *Nat Immunol*, *2*(10), 947-950. https://doi.org/10.1038/ni712

Sefik, E., Geva-Zatorsky, N., Oh, S., Konnikova, L., Zemmour, D., McGuire, A. M., Burzyn, D., Ortiz-Lopez, A., Lobera, M., Yang, J., Ghosh, S., Earl, A., Snapper, S. B., Jupp, R., Kasper, D., Mathis, D., & Benoist, C. (2015). MUCOSAL IMMUNOLOGY. Individual intestinal symbionts induce a distinct population of RORgamma(+) regulatory T cells. *Science*, *349*(6251), 993-997. https://doi.org/10.1126/science.aaa9420

Sekimata, M., Yoshida, D., Araki, A., Asao, H., Iseki, K., & Murakami-Sekimata, A. (2019). Runx1 and RORgammat Cooperate to Upregulate IL-22 Expression in Th Cells through Its Distal Enhancer. *J Immunol*, *202*(11), 3198-3210. https://doi.org/10.4049/jimmunol.1800672

Sellin, M. E., Muller, A. A., Felmy, B., Dolowschiak, T., Diard, M., Tardivel, A., Maslowski, K. M., & Hardt, W. D. (2014). Epithelium-intrinsic NAIP/NLRC4 inflammasome drives infected enterocyte expulsion to restrict Salmonella replication in the intestinal mucosa. *Cell Host Microbe*, *16*(2), 237-248. https://doi.org/10.1016/j.chom.2014.07.001

Shaw, L. A., Belanger, S., Omilusik, K. D., Cho, S., Scott-Browne, J. P., Nance, J. P., Goulding, J., Lasorella, A., Lu, L. F., Crotty, S., & Goldrath, A. W. (2016). Id2 reinforces TH1 differentiation and inhibits E2A to repress TFH differentiation. *Nat Immunol*, *17*(7), 834-843. https://doi.org/10.1038/ni.3461

Shimoda, K., van Deursen, J., Sangster, M. Y., Sarawar, S. R., Carson, R. T., Tripp, R. A., Chu, C., Quelle, F. W., Nosaka, T., Vignali, D. A., Doherty, P. C., Grosveld, G., Paul, W. E., & Ihle, J. N. (1996). Lack of IL-4-induced Th2 response and IgE class switching in mice with disrupted Stat6 gene. *Nature*, *380*(6575), 630-633. https://doi.org/10.1038/380630a0

Shiomi, H., Masuda, A., Nishiumi, S., Nishida, M., Takagawa, T., Shiomi, Y., Kutsumi, H., Blumberg, R. S., Azuma, T., & Yoshida, M. (2010). Gamma interferon produced by antigen-specific CD4+ T cells regulates the mucosal immune responses to Citrobacter rodentium infection. *Infect Immun*, *78*(6), 2653-2666. https://doi.org/10.1128/IAI.01343-09

Silberger, D. J., Zindl, C. L., & Weaver, C. T. (2017). Citrobacter rodentium: a model enteropathogen for understanding the interplay of innate and adaptive components of type 3 immunity. *Mucosal Immunol*, *10*(5), 1108-1117. https://doi.org/10.1038/mi.2017.47

Singh, S., George, J., Boland, B. S., Vande Casteele, N., & Sandborn, W. J. (2018). Primary Non-Response to Tumor Necrosis Factor Antagonists is Associated with Inferior Response to Second-line Biologics in Patients with Inflammatory Bowel Diseases: A Systematic Review and Meta-analysis. *J Crohns Colitis*, *12*(6), 635-643. https://doi.org/10.1093/ecco-jcc/jjy004

Singh, S. P., Zhang, H. H., Foley, J. F., Hedrick, M. N., & Farber, J. M. (2008). Human T cells that are able to produce IL-17 express the chemokine receptor CCR6. *J Immunol*, *180*(1), 214-221. https://doi.org/10.4049/jimmunol.180.1.214

Songhet, P., Barthel, M., Stecher, B., Muller, A. J., Kremer, M., Hansson, G. C., & Hardt, W. D. (2011). Stromal IFN-gammaR-signaling modulates goblet cell function during Salmonella Typhimurium infection. *PLoS One*, *6*(7), e22459. https://doi.org/10.1371/journal.pone.0022459

Srinivasan, M., Wardrop, R. M., Gienapp, I. E., Stuckman, S. S., Whitacre, C. C., & Kaumaya, P. T. (2001). A retro-inverso peptide mimic of CD28 encompassing the MYPPPY motif adopts a polyproline type II helix and inhibits encephalitogenic T cells in vitro. *J Immunol*, *167*(1), 578-585. https://doi.org/10.4049/jimmunol.167.1.578

Starnes, T., Broxmeyer, H. E., Robertson, M. J., & Hromas, R. (2002). Cutting edge: IL-17D, a novel member of the IL-17 family, stimulates cytokine production and inhibits hemopoiesis. *J Immunol*, *169*(2), 642-646. https://doi.org/10.4049/jimmunol.169.2.642

Stehle, C., Ruckert, T., Fiancette, R., Gajdasik, D. W., Willis, C., Ulbricht, C., Durek, P., Mashreghi, M. F., Finke, D., Hauser, A. E., Withers, D. R., Chang, H. D., Zimmermann, J., & Romagnani, C. (2021). T-bet and RORalpha control lymph node formation by regulating embryonic innate lymphoid cell differentiation. *Nat Immunol*, *22*(10), 1231-1244. https://doi.org/10.1038/s41590-021-01029-6

Stuber, E., Neurath, M., Calderhead, D., Fell, H. P., & Strober, W. (1995). Cross-linking of OX40 ligand, a member of the TNF/NGF cytokine family, induces proliferation and differentiation in murine splenic B cells. *Immunity*, *2*(5), 507-521. https://doi.org/10.1016/1074-7613(95)90031-4

Sugimoto, K., Ogawa, A., Mizoguchi, E., Shimomura, Y., Andoh, A., Bhan, A. K., Blumberg, R. S., Xavier, R. J., & Mizoguchi, A. (2008). IL-22 ameliorates intestinal inflammation in a mouse model of ulcerative colitis. *J Clin Invest*, *118*(2), 534-544. https://doi.org/10.1172/JCI33194

Sujino, T., London, M., Hoytema van Konijnenburg, D. P., Rendon, T., Buch, T., Silva, H. M., Lafaille, J. J., Reis, B. S., & Mucida, D. (2016). Tissue adaptation of regulatory and intraepithelial CD4(+)

T cells controls gut inflammation. *Science*, *352*(6293), 1581-1586. https://doi.org/10.1126/science.aaf3892

Sun, C. M., Hall, J. A., Blank, R. B., Bouladoux, N., Oukka, M., Mora, J. R., & Belkaid, Y. (2007). Small intestine lamina propria dendritic cells promote de novo generation of Foxp3 T reg cells via retinoic acid. *J Exp Med*, *204*(8), 1775-1785. https://doi.org/10.1084/jem.20070602

Sun, L., Wu, J., Du, F., Chen, X., & Chen, Z. J. (2013). Cyclic GMP-AMP synthase is a cytosolic DNA sensor that activates the type I interferon pathway. *Science*, *339*(6121), 786-791. https://doi.org/10.1126/science.1232458

Szabo, S. J., Kim, S. T., Costa, G. L., Zhang, X., Fathman, C. G., & Glimcher, L. H. (2000). A novel transcription factor, T-bet, directs Th1 lineage commitment. *Cell*, *100*(6), 655-669. https://doi.org/10.1016/s0092-8674(00)80702-3

Takasawa, N., Ishii, N., Higashimura, N., Murata, K., Tanaka, Y., Nakamura, M., Sasaki, T., & Sugamura, K. (2001). Expression of gp34 (OX40 ligand) and OX40 on human T cell clones. *Jpn J Cancer Res*, *92*(4), 377-382. https://doi.org/10.1111/j.1349-7006.2001.tb01105.x

Takeda, K., Tanaka, T., Shi, W., Matsumoto, M., Minami, M., Kashiwamura, S., Nakanishi, K., Yoshida, N., Kishimoto, T., & Akira, S. (1996). Essential role of Stat6 in IL-4 signalling. *Nature*, *380*(6575), 627-630. https://doi.org/10.1038/380627a0

Targan, S. R., Feagan, B., Vermeire, S., Panaccione, R., Melmed, G. Y., Landers, C., Li, D., Russell, C., Newmark, R., Zhang, N., Chon, Y., Hsu, Y. H., Lin, S. L., & Klekotka, P. (2016). A Randomized, Double-Blind, Placebo-Controlled Phase 2 Study of Brodalumab in Patients With Moderate-to-Severe Crohn's Disease. *Am J Gastroenterol*, *111*(11), 1599-1607. https://doi.org/10.1038/ajg.2016.298

Taylor, B. C., Zaph, C., Troy, A. E., Du, Y., Guild, K. J., Comeau, M. R., & Artis, D. (2009). TSLP regulates intestinal immunity and inflammation in mouse models of helminth infection and colitis. *J Exp Med*, *206*(3), 655-667. https://doi.org/10.1084/jem.20081499

Teh, H. S., Kisielow, P., Scott, B., Kishi, H., Uematsu, Y., Bluthmann, H., & von Boehmer, H. (1988). Thymic major histocompatibility complex antigens and the alpha beta T-cell receptor determine the CD4/CD8 phenotype of T cells. *Nature*, *335*(6187), 229-233. https://doi.org/10.1038/335229a0

Thierfelder, W. E., van Deursen, J. M., Yamamoto, K., Tripp, R. A., Sarawar, S. R., Carson, R. T., Sangster, M. Y., Vignali, D. A., Doherty, P. C., Grosveld, G. C., & Ihle, J. N. (1996). Requirement for Stat4 in interleukin-12-mediated responses of natural killer and T cells. *Nature*, *382*(6587), 171-174. https://doi.org/10.1038/382171a0

Tomura, M., Yoshida, N., Tanaka, J., Karasawa, S., Miwa, Y., Miyawaki, A., & Kanagawa, O. (2008). Monitoring cellular movement in vivo with photoconvertible fluorescence protein "Kaede" transgenic mice. *Proc Natl Acad Sci U S A*, *105*(31), 10871-10876. https://doi.org/10.1073/pnas.0802278105

Torchinsky, M. B., Garaude, J., Martin, A. P., & Blander, J. M. (2009). Innate immune recognition of infected apoptotic cells directs T(H)17 cell differentiation. *Nature*, *458*(7234), 78-82. https://doi.org/10.1038/nature07781

Tran, D. Q., Ramsey, H., & Shevach, E. M. (2007). Induction of FOXP3 expression in naive human CD4+FOXP3 T cells by T-cell receptor stimulation is transforming growth factor-beta dependent but does not confer a regulatory phenotype. *Blood*, *110*(8), 2983-2990. https://doi.org/10.1182/blood-2007-06-094656

Trevejo-Nunez, G., Elsegeiny, W., Conboy, P., Chen, K., & Kolls, J. K. (2016). Critical Role of IL-22/IL22-RA1 Signaling in Pneumococcal Pneumonia. *J Immunol*, *197*(5), 1877-1883. https://doi.org/10.4049/jimmunol.1600528

Tsai, P. Y., Zhang, B., He, W. Q., Zha, J. M., Odenwald, M. A., Singh, G., Tamura, A., Shen, L., Sailer, A., Yeruva, S., Kuo, W. T., Fu, Y. X., Tsukita, S., & Turner, J. R. (2017). IL-22 Upregulates Epithelial Claudin-2 to Drive Diarrhea and Enteric Pathogen Clearance. *Cell Host Microbe*, *21*(6), 671-681 e674. https://doi.org/10.1016/j.chom.2017.05.009

Turner, J. E., Stockinger, B., & Helmby, H. (2013). IL-22 mediates goblet cell hyperplasia and worm expulsion in intestinal helminth infection. *PLoS Pathog*, *9*(10), e1003698. https://doi.org/10.1371/journal.ppat.1003698

Vaishnava, S., Behrendt, C. L., Ismail, A. S., Eckmann, L., & Hooper, L. V. (2008). Paneth cells directly sense gut commensals and maintain homeostasis at the intestinal host-microbial interface. *Proc Natl Acad Sci U S A*, *105*(52), 20858-20863. https://doi.org/10.1073/pnas.0808723105

van der Waaij, L. A., Harmsen, H. J., Madjipour, M., Kroese, F. G., Zwiers, M., van Dullemen, H. M., de Boer, N. K., Welling, G. W., & Jansen, P. L. (2005). Bacterial population analysis of human colon and terminal ileum biopsies with 16S rRNA-based fluorescent probes: commensal bacteria live in suspension and have no direct contact with epithelial cells. *Inflamm Bowel Dis*, *11*(10), 865-871. https://doi.org/10.1097/01.mib.0000179212.80778.d3

van Loosdregt, J., Fleskens, V., Tiemessen, M. M., Mokry, M., van Boxtel, R., Meerding, J., Pals, C. E., Kurek, D., Baert, M. R., Delemarre, E. M., Grone, A., Koerkamp, M. J., Sijts, A. J., Nieuwenhuis, E. E., Maurice, M. M., van Es, J. H., Ten Berge, D., Holstege, F. C., Staal, F. J., Zaiss, D. M., Prakken, B. J., & Coffer, P. J. (2013). Canonical Wnt signaling negatively modulates regulatory T cell function. *Immunity*, *39*(2), 298-310. https://doi.org/10.1016/j.immuni.2013.07.019

Velaga, S., Herbrand, H., Friedrichsen, M., Jiong, T., Dorsch, M., Hoffmann, M. W., Forster, R., & Pabst, O. (2009). Chemokine receptor CXCR5 supports solitary intestinal lymphoid tissue formation, B cell homing, and induction of intestinal IgA responses. *J Immunol*, *182*(5), 2610-2619. https://doi.org/10.4049/jimmunol.0801141

Veldhoen, M., Hirota, K., Christensen, J., O'Garra, A., & Stockinger, B. (2009). Natural agonists for aryl hydrocarbon receptor in culture medium are essential for optimal differentiation of Th17 T cells. *J Exp Med*, *206*(1), 43-49. https://doi.org/10.1084/jem.20081438

Veldhoen, M., Hirota, K., Westendorf, A. M., Buer, J., Dumoutier, L., Renauld, J. C., & Stockinger, B. (2008). The aryl hydrocarbon receptor links TH17-cell-mediated autoimmunity to environmental toxins. *Nature*, *453*(7191), 106-109. https://doi.org/10.1038/nature06881

Veldhoen, M., Hocking, R. J., Atkins, C. J., Locksley, R. M., & Stockinger, B. (2006). TGFbeta in the context of an inflammatory cytokine milieu supports de novo differentiation of IL-17 producing T cells. *Immunity*, *24*(2), 179-189. https://doi.org/10.1016/j.immuni.2006.01.001

Vernia, P., Caprilli, R., Latella, G., Barbetti, F., Magliocca, F. M., & Cittadini, M. (1988). Fecal lactate and ulcerative colitis. *Gastroenterology*, *95*(6), 1564-1568. https://doi.org/10.1016/s0016-5085(88)80078-7

von Moltke, J., Ji, M., Liang, H. E., & Locksley, R. M. (2016). Tuft-cell-derived IL-25 regulates an intestinal ILC2-epithelial response circuit. *Nature*, *529*(7585), 221-225. https://doi.org/10.1038/nature16161

Voo, K. S., Wang, Y. H., Santori, F. R., Boggiano, C., Wang, Y. H., Arima, K., Bover, L., Hanabuchi, S., Khalili, J., Marinova, E., Zheng, B., Littman, D. R., & Liu, Y. J. (2009). Identification of IL-17-producing FOXP3+ regulatory T cells in humans. *Proc Natl Acad Sci U S A*, *106*(12), 4793-4798. https://doi.org/10.1073/pnas.0900408106

Vu, M. D., Xiao, X., Gao, W., Degauque, N., Chen, M., Kroemer, A., Killeen, N., Ishii, N., & Li, X. C. (2007). OX40 costimulation turns off Foxp3+ Tregs. *Blood*, *110*(7), 2501-2510. https://doi.org/10.1182/blood-2007-01-070748

Wang, Y., Mumm, J. B., Herbst, R., Kolbeck, R., & Wang, Y. (2017). IL-22 Increases Permeability of Intestinal Epithelial Tight Junctions by Enhancing Claudin-2 Expression. *J Immunol*, *199*(9), 3316-3325. https://doi.org/10.4049/jimmunol.1700152

Wang, Y. H., Voo, K. S., Liu, B., Chen, C. Y., Uygungil, B., Spoede, W., Bernstein, J. A., Huston, D. P., & Liu, Y. J. (2010). A novel subset of CD4(+) T(H)2 memory/effector cells that produce inflammatory IL-17 cytokine and promote the exacerbation of chronic allergic asthma. *J Exp Med*, *207*(11), 2479-2491. https://doi.org/10.1084/jem.20101376

Wei, L., Laurence, A., Elias, K. M., & O'Shea, J. J. (2007). IL-21 is produced by Th17 cells and drives IL-17 production in a STAT3-dependent manner. *J Biol Chem*, *282*(48), 34605-34610. https://doi.org/10.1074/jbc.M705100200

Welty, N. E., Staley, C., Ghilardi, N., Sadowsky, M. J., Igyarto, B. Z., & Kaplan, D. H. (2013). Intestinal lamina propria dendritic cells maintain T cell homeostasis but do not affect commensalism. *J Exp Med*, *210*(10), 2011-2024. https://doi.org/10.1084/jem.20130728

Wiles, S., Clare, S., Harker, J., Huett, A., Young, D., Dougan, G., & Frankel, G. (2004). Organ specificity, colonization and clearance dynamics in vivo following oral challenges with the murine pathogen Citrobacter rodentium. *Cell Microbiol*, *6*(10), 963-972. https://doi.org/10.1111/j.1462-5822.2004.00414.x

Wiles, S., Dougan, G., & Frankel, G. (2005). Emergence of a 'hyperinfectious' bacterial state after passage of Citrobacter rodentium through the host gastrointestinal tract. *Cell Microbiol*, *7*(8), 1163-1172. https://doi.org/10.1111/j.1462-5822.2005.00544.x

Wiles, S., Pickard, K. M., Peng, K., MacDonald, T. T., & Frankel, G. (2006). In vivo bioluminescence imaging of the murine pathogen Citrobacter rodentium. *Infect Immun*, *74*(9), 5391-5396. https://doi.org/10.1128/IAI.00848-06

Williams, B. R. (1999). PKR; a sentinel kinase for cellular stress. *Oncogene*, *18*(45), 6112-6120. https://doi.org/10.1038/sj.onc.1203127

Wilson, N. J., Boniface, K., Chan, J. R., McKenzie, B. S., Blumenschein, W. M., Mattson, J. D., Basham, B., Smith, K., Chen, T., Morel, F., Lecron, J. C., Kastelein, R. A., Cua, D. J., McClanahan, T. K., Bowman, E. P., & de Waal Malefyt, R. (2007). Development, cytokine profile and function of human interleukin 17-producing helper T cells. *Nat Immunol*, *8*(9), 950-957. https://doi.org/10.1038/ni1497

Withers, D. R., Gaspal, F. M., Bekiaris, V., McConnell, F. M., Kim, M., Anderson, G., & Lane, P. J. (2011). OX40 and CD30 signals in CD4(+) T-cell effector and memory function: a distinct role for lymphoid tissue inducer cells in maintaining CD4(+) T-cell memory but not effector function. *Immunol Rev*, *244*(1), 134-148. https://doi.org/10.1111/j.1600-065X.2011.01057.x

Withers, D. R., Hepworth, M. R., Wang, X., Mackley, E. C., Halford, E. E., Dutton, E. E., Marriott, C. L., Brucklacher-Waldert, V., Veldhoen, M., Kelsen, J., Baldassano, R. N., & Sonnenberg, G. F. (2016). Transient inhibition of ROR-gammat therapeutically limits intestinal inflammation by reducing TH17 cells and preserving group 3 innate lymphoid cells. *Nat Med*, *22*(3), 319-323. https://doi.org/10.1038/nm.4046

Wolk, K., Witte, E., Wallace, E., Docke, W. D., Kunz, S., Asadullah, K., Volk, H. D., Sterry, W., & Sabat, R. (2006). IL-22 regulates the expression of genes responsible for antimicrobial defense, cellular differentiation, and mobility in keratinocytes: a potential role in psoriasis. *Eur J Immunol*, *36*(5), 1309-1323. https://doi.org/10.1002/eji.200535503

Wood, D. E., & Salzberg, S. L. (2014). Kraken: ultrafast metagenomic sequence classification using exact alignments. *Genome Biol*, *15*(3), R46. https://doi.org/10.1186/gb-2014-15-3-r46

Worbs, T., Bode, U., Yan, S., Hoffmann, M. W., Hintzen, G., Bernhardt, G., Forster, R., & Pabst, O. (2006). Oral tolerance originates in the intestinal immune system and relies on antigen carriage by dendritic cells. *J Exp Med*, *203*(3), 519-527. https://doi.org/10.1084/jem.20052016

Wright, J. F., Guo, Y., Quazi, A., Luxenberg, D. P., Bennett, F., Ross, J. F., Qiu, Y., Whitters, M. J., Tomkinson, K. N., Dunussi-Joannopoulos, K., Carreno, B. M., Collins, M., & Wolfman, N. M. (2007). Identification of an interleukin 17F/17A heterodimer in activated human CD4+ T cells. *J Biol Chem*, *282*(18), 13447-13455. https://doi.org/10.1074/jbc.M700499200

Wucherpfennig, K. W., Gagnon, E., Call, M. J., Huseby, E. S., & Call, M. E. (2010). Structural biology of the T-cell receptor: insights into receptor assembly, ligand recognition, and initiation of signaling. *Cold Spring Harb Perspect Biol*, *2*(4), a005140. https://doi.org/10.1101/cshperspect.a005140

Xiao, X., Shi, X., Fan, Y., Wu, C., Zhang, X., Minze, L., Liu, W., Ghobrial, R. M., Lan, P., & Li, X. C. (2016). The Costimulatory Receptor OX40 Inhibits Interleukin-17 Expression through Activation of

Repressive Chromatin Remodeling Pathways. *Immunity*, *44*(6), 1271-1283. https://doi.org/10.1016/j.immuni.2016.05.013

Xu, M., Pokrovskii, M., Ding, Y., Yi, R., Au, C., Harrison, O. J., Galan, C., Belkaid, Y., Bonneau, R., & Littman, D. R. (2018). c-MAF-dependent regulatory T cells mediate immunological tolerance to a gut pathobiont. *Nature*, *554*(7692), 373-377. https://doi.org/10.1038/nature25500

Yamamoto, M., Sato, S., Hemmi, H., Sanjo, H., Uematsu, S., Kaisho, T., Hoshino, K., Takeuchi, O., Kobayashi, M., Fujita, T., Takeda, K., & Akira, S. (2002). Essential role for TIRAP in activation of the signalling cascade shared by TLR2 and TLR4. *Nature*, *420*(6913), 324-329. https://doi.org/10.1038/nature01182

Yan, K. S., Chia, L. A., Li, X., Ootani, A., Su, J., Lee, J. Y., Su, N., Luo, Y., Heilshorn, S. C., Amieva, M. R., Sangiorgi, E., Capecchi, M. R., & Kuo, C. J. (2012). The intestinal stem cell markers Bmi1 and Lgr5 identify two functionally distinct populations. *Proc Natl Acad Sci U S A*, *109*(2), 466-471. https://doi.org/10.1073/pnas.1118857109

Yang, D., Chertov, O., Bykovskaia, S. N., Chen, Q., Buffo, M. J., Shogan, J., Anderson, M., Schroder, J. M., Wang, J. M., Howard, O. M., & Oppenheim, J. J. (1999). Beta-defensins: linking innate and adaptive immunity through dendritic and T cell CCR6. *Science*, *286*(5439), 525-528. https://doi.org/10.1126/science.286.5439.525

Yang, L., Anderson, D. E., Baecher-Allan, C., Hastings, W. D., Bettelli, E., Oukka, M., Kuchroo, V. K., & Hafler, D. A. (2008). IL-21 and TGF-beta are required for differentiation of human T(H)17 cells. *Nature*, *454*(7202), 350-352. https://doi.org/10.1038/nature07021

Yang, X. O., Chang, S. H., Park, H., Nurieva, R., Shah, B., Acero, L., Wang, Y. H., Schluns, K. S., Broaddus, R. R., Zhu, Z., & Dong, C. (2008). Regulation of inflammatory responses by IL-17F. *J Exp Med*, *205*(5), 1063-1075. https://doi.org/10.1084/jem.20071978

Yang, X. O., Panopoulos, A. D., Nurieva, R., Chang, S. H., Wang, D., Watowich, S. S., & Dong, C. (2007). STAT3 regulates cytokine-mediated generation of inflammatory helper T cells. *J Biol Chem*, *282*(13), 9358-9363. https://doi.org/10.1074/jbc.C600321200

Yang, X. O., Pappu, B. P., Nurieva, R., Akimzhanov, A., Kang, H. S., Chung, Y., Ma, L., Shah, B., Panopoulos, A. D., Schluns, K. S., Watowich, S. S., Tian, Q., Jetten, A. M., & Dong, C. (2008). T helper 17 lineage differentiation is programmed by orphan nuclear receptors ROR alpha and ROR gamma. *Immunity*, *28*(1), 29-39. https://doi.org/10.1016/j.immuni.2007.11.016

Yang, Y., Xu, J., Niu, Y., Bromberg, J. S., & Ding, Y. (2008). T-bet and eomesodermin play critical roles in directing T cell differentiation to Th1 versus Th17. *J Immunol*, *181*(12), 8700-8710. https://doi.org/10.4049/jimmunol.181.12.8700

Yao, Z., Fanslow, W. C., Seldin, M. F., Rousseau, A. M., Painter, S. L., Comeau, M. R., Cohen, J. I., & Spriggs, M. K. (1995). Herpesvirus Saimiri encodes a new cytokine, IL-17, which binds to a novel cytokine receptor. *Immunity*, *3*(6), 811-821. https://doi.org/10.1016/1074-7613(95)90070-5

Ye, P., Rodriguez, F. H., Kanaly, S., Stocking, K. L., Schurr, J., Schwarzenberger, P., Oliver, P., Huang, W., Zhang, P., Zhang, J., Shellito, J. E., Bagby, G. J., Nelson, S., Charrier, K., Peschon, J. J., & Kolls, J. K. (2001). Requirement of interleukin 17 receptor signaling for lung CXC chemokine and granulocyte colony-stimulating factor expression, neutrophil recruitment, and host defense. *J Exp Med*, *194*(4), 519-527. https://doi.org/10.1084/jem.194.4.519

Yoshimura, T., Sonoda, K. H., Ohguro, N., Ohsugi, Y., Ishibashi, T., Cua, D. J., Kobayashi, T., Yoshida, H., & Yoshimura, A. (2009). Involvement of Th17 cells and the effect of anti-IL-6 therapy in autoimmune uveitis. *Rheumatology (Oxford)*, *48*(4), 347-354. https://doi.org/10.1093/rheumatology/ken489

Yu, D., Rao, S., Tsai, L. M., Lee, S. K., He, Y., Sutcliffe, E. L., Srivastava, M., Linterman, M., Zheng, L., Simpson, N., Ellyard, J. I., Parish, I. A., Ma, C. S., Li, Q. J., Parish, C. R., Mackay, C. R., & Vinuesa, C. G. (2009). The transcriptional repressor Bcl-6 directs T follicular helper cell lineage commitment. *Immunity*, *31*(3), 457-468. https://doi.org/10.1016/j.immuni.2009.07.002

Zeuthen, L. H., Fink, L. N., & Frokiaer, H. (2008). Epithelial cells prime the immune response to an array of gut-derived commensals towards a tolerogenic phenotype through distinct actions of thymic stromal lymphopoietin and transforming growth factor-beta. *Immunology*, *123*(2), 197-208. https://doi.org/10.1111/j.1365-2567.2007.02687.x

Zhang, D. H., Cohn, L., Ray, P., Bottomly, K., & Ray, A. (1997). Transcription factor GATA-3 is differentially expressed in murine Th1 and Th2 cells and controls Th2-specific expression of the interleukin-5 gene. *J Biol Chem*, *272*(34), 21597-21603. https://doi.org/10.1074/jbc.272.34.21597

Zhang, F., Meng, G., & Strober, W. (2008). Interactions among the transcription factors Runx1, RORgammat and Foxp3 regulate the differentiation of interleukin 17-producing T cells. *Nat Immunol*, *9*(11), 1297-1306. https://doi.org/10.1038/ni.1663

Zhang, G. X., Gran, B., Yu, S., Li, J., Siglienti, I., Chen, X., Kamoun, M., & Rostami, A. (2003). Induction of experimental autoimmune encephalomyelitis in IL-12 receptor-beta 2-deficient mice: IL-12 responsiveness is not required in the pathogenesis of inflammatory demyelination in the central nervous system. *J Immunol*, *170*(4), 2153-2160. https://doi.org/10.4049/jimmunol.170.4.2153

Zhang, Z., Zhong, W., Hinrichs, D., Wu, X., Weinberg, A., Hall, M., Spencer, D., Wegmann, K., & Rosenbaum, J. T. (2010). Activation of OX40 augments Th17 cytokine expression and antigen-specific uveitis. *Am J Pathol*, *177*(6), 2912-2920. https://doi.org/10.2353/ajpath.2010.100353

Zhao, X., Sato, A., Dela Cruz, C. S., Linehan, M., Luegering, A., Kucharzik, T., Shirakawa, A. K., Marquez, G., Farber, J. M., Williams, I., & Iwasaki, A. (2003). CCL9 is secreted by the follicle-associated epithelium and recruits dome region Peyer's patch CD11b+ dendritic cells. *J Immunol*, *171*(6), 2797-2803. https://doi.org/10.4049/jimmunol.171.6.2797

Zheng, W., & Flavell, R. A. (1997). The transcription factor GATA-3 is necessary and sufficient for Th2 cytokine gene expression in CD4 T cells. *Cell*, *89*(4), 587-596. https://doi.org/10.1016/s0092-8674(00)80240-8

Zheng, Y., Valdez, P. A., Danilenko, D. M., Hu, Y., Sa, S. M., Gong, Q., Abbas, A. R., Modrusan, Z., Ghilardi, N., de Sauvage, F. J., & Ouyang, W. (2008). Interleukin-22 mediates early host defense against attaching and effacing bacterial pathogens. *Nat Med*, *14*(3), 282-289. https://doi.org/10.1038/nm1720

Zhou, L., Ivanov, II, Spolski, R., Min, R., Shenderov, K., Egawa, T., Levy, D. E., Leonard, W. J., & Littman, D. R. (2007). IL-6 programs T(H)-17 cell differentiation by promoting sequential engagement of the IL-21 and IL-23 pathways. *Nat Immunol*, *8*(9), 967-974. https://doi.org/10.1038/ni1488

Zhou, L., Lopes, J. E., Chong, M. M., Ivanov, II, Min, R., Victora, G. D., Shen, Y., Du, J., Rubtsov, Y. P., Rudensky, A. Y., Ziegler, S. F., & Littman, D. R. (2008). TGF-beta-induced Foxp3 inhibits T(H)17 cell differentiation by antagonizing RORgammat function. *Nature*, *453*(7192), 236-240. https://doi.org/10.1038/nature06878

Zhu, J., Yamane, H., & Paul, W. E. (2010). Differentiation of effector CD4 T cell populations (*). *Annu Rev Immunol*, *28*, 445-489. https://doi.org/10.1146/annurev-immunol-030409-101212

Zhu, Y., Ju, S., Chen, E., Dai, S., Li, C., Morel, P., Liu, L., Zhang, X., & Lu, B. (2010). T-bet and eomesodermin are required for T cell-mediated antitumor immune responses. *J Immunol*, *185*(6), 3174-3183. https://doi.org/10.4049/jimmunol.1000749

Zundler, S., Becker, E., Spocinska, M., Slawik, M., Parga-Vidal, L., Stark, R., Wiendl, M., Atreya, R., Rath, T., Leppkes, M., Hildner, K., Lopez-Posadas, R., Lukassen, S., Ekici, A. B., Neufert, C., Atreya, I., van Gisbergen, K., & Neurath, M. F. (2019). Hobit- and Blimp-1-driven CD4(+) tissue-resident memory T cells control chronic intestinal inflammation. *Nat Immunol*, *20*(3), 288-300. https://doi.org/10.1038/s41590-018-0298-5